DYNAMIC BEHAVIOUR

OF

ROTARY MECHANICAL SEALS

Robin Theodore Rowles

Thesis submitted for the degree of
Doctor of Philosophy of the
University of Aston in Birmingham

January 1980

Summary

'Dynamic Behaviour of Rotary Mechanical Seals'

Robin Theodore Rowles

Thesis submitted for the degree of Doctor of Philosophy 1980

This thesis covers both experimental and computer investigations into the dynamic behaviour of mechanical seals. The literature survey shows no investigations on the effect of vibration on mechanical seals of the type common in the various process industries. Typical seal designs are discussed.

A form of Reynolds' equation has been developed that permits the calculation of stiffnesses and damping coefficients for the fluid film. The dynamics of the mechanical seal floating ring have been investigated using approximate formulae, and it has been shown that the floating ring will behave as a rigid body. Some elements, such as the radial damping due to the fluid film, are small and may be neglected. The equations of motion of the floating ring have been developed utilising the significant elements, and a solution technique described.

The stiffness and damping coefficients of nitrile rubber o-rings have been obtained. These show a wide variation, with a constant stiffness up to 60 Hz. The importance of the effect of temperature on the properties is discussed. An unsuccessful test rig is described in the appendices.

The dynamic behaviour of a mechanical seal has been investigated experimentally, including the effect of changes of speed, sealed pressure and seal geometry. The results, as expected, show that high vibration levels result in both high leakage and seal temperatures.

Computer programs have been developed to solve Reynolds' Equation and the equations of motion. Two solution techniques for the latter program were developed, the unsuccessful technique is described in the appendices. Some stability problems were encountered, but despite these the solution shows good agreement with some of the experimental conditions. Possible reasons for the discrepancies are discussed.

Various suggestions for future work in this field are given. These include the combining of the programs and more extensive experimental and computer modelling.

KEYWORDS

MECHANICAL SEALS, VIBRATION, O-RINGS, REYNOLDS' EQUATION

Acknowledgements

I would like to thank Mr. G.F.W. Adler, Director of Research, and the directors of BHRA Fluid Engineering for allowing me to carry out the work described herein and to submit it for the award of a degree of Doctor of Philosophy of the University of Aston in Birmingham. The work has been carried out under MEMTRB Contract No. KA72C/343.

I would like to thank my supervisors, Dr. G.K. Lewis, Main Academic Supervisor, Mr. M.R. Mudge, Associate Supervisor, Dr. B.S. Nau, Industrial Supervisor, and Mr. G.A. Montgomerie, I.H.D. Tutor, for all their help, advice and encouragement.

I would also like to thank Mrs. M.E. Barker for carefully typing the manuscript, Mrs Linda Malins for typing the equations and Mrs. Alison Mills for tracing a number of figures.

I would also like to thank my colleagues at work for putting up with me and for their helpful advice. In particular I would like to thank Mr. R.M. Austin for help and advice on the mechanical seal test rig and Mrs. K.A. Smith for help with debugging the computer programs.

Finally, I would like to thank my wife Sandy for her help and support during the years of this research. Without her help, support and tolerance this thesis would never have come to fruition.

This work is dedicated as a humble gesture to the glory of God and the advancement of engineering science.

List of Contents

List of Tables

List of Figures

G-1 Scattergraph leakage and interface fluid Viscosity
G-2 Scattergraph leakage and seal pressure
G-3 Scattergraph leakage and shaft speed
G-4 Scattergraph leakage and mean film thickness
G-5 Scattergraph leakage and shaft vibration
G-6 Scattergraph leakage and separation of O-ring and centroid
G-7 Scattergraph leakage and radial floating ring vibration
G-8 Scattergraph leakage and axial vibration
G-9 Scattergraph leakage and angular vibration
G-10 Scattergraph radial vibration and interface fluid viscosity
G-11 Scattergraph radial vibration and sealed pressure
G-12 Scattergraph radial vibration and shaft speed
G-13 Scattergraph radial vibration and mean film thickness
G-14 Scattergraph radial and shaft vibration
G-15 Scattergraph radial vibration and separation of O-ring and centroid
G-16 Scattergraph axial vibration and interface fluid viscosity
G-17 Scattergraph axial vibration and sealed pressure
G-18 Scattergraph axial vibration and shaft speed
G-19 Scattergraph axial vibration and mean film thickness
G-20 Scattergraph axial vibration and shaft vibration
G-21 Scattergraph axial vibration and separation of O-ring and centroid
G-22 Scattergraph axial vibration and radial vibration
G-23 Scattergraph angular vibration and interface fluid viscosity
G-24 Scattergraph angular vibration and sealed pressure
G-25 Scattergraph angular vibration and rpm
G-26 Scattergraph angular vibration and mean film thickness
G-27 Scattergraph angular vibration and shaft vibration
G-28 Scattergraph angular vibration and separation of O-ring and centroid
G-29 Scattergraph angular vibration and radial vibration
G-30 Scattergraph angular vibration and axial vibration

Nomenclature

A	Mechanical seal face area
A	Matrices used in first solution of equations of motion
C	Capacitance
C	Damping coefficient
$[C]$	Matric of damping coefficients
$C_{f\ell 1}$	Force damping coefficient due to axial velocity
$C_{f\ell 2}$	Moment damping coefficient about OX due to axial velocity
$C_{f\ell 3}$	Moment damping coefficient about OY due to axial velocity
C_{fr1}	Force damping coefficient due to angular velocity about OX
C_{fr2}	Force damping coefficient due to angular velocity about OY
C_{fr3}	Moment damping coefficient about OY due to angular velocity about OX
C_{fr4}	Moment damping coefficient about OX due to angular velocity about OX
C_{fr5}	Moment damping coefficient about OY due to angular velocity about OY
C_{fr6}	Moment damping coefficient about OX due to angular velocity about OY
C_{rc}	O-ring damping coefficient in compression
C_{rs}	O-ring damping coefficient in shear
C_1	Coefficient of I_1 in Reynolds' Equation
C_2	Coefficient of I_2 in Reynolds' Equation
C_1^o	Factor in WLF transform
C_1^g	Factor in WLF transform
C_2^o	Factor in WLF transform
C_2^g	Factor in WLF transform
D	Differential operator $\partial/\partial t$
D_A	Floating ring movement measured by transducers
D_B	Floating ring movement measured by transducers

E	Youngs' Modulus
G''	Imaginery part of complex modulus
H_1	Distance of stator from reference plane
H_2	Distance of rotor from reference plane
I	Second moment of area
	Moment of inertia of floating ring cylinders
I_P	Polar second moment of area
I_T	Total moment of inertia of floating ring
I_X	Second moment of area about OX
I_1	Reynolds equation integral
I_2	Reynolds equation integral
I_3	Reynolds equation integral
K	Dielectric constant
K_1	Constant of integration - Reynolds' equation
K_2	Constant of integration - Reynolds' equation
L_p	Axial force on floating ring due to sealed pressure and drive spring
L_w	Axial force on floating ring due to fluid film load capacity
M	Mass
$[M]$	Mass matrix
M_i	Floating ring cylinder mass
M_t	Moment
P	Right hand side of equations of motion
$\dot{P}$	Differential of P with respect to time
Q	Amplitude ratio a_m/a_r
R	Mechanical seal interface diameter ratio ID/OD

R_i	Seal interface inner radius
R_m	Seal interface mean radius
R_o	Seal interface outer radius
S	Stiffness
[S]	Stiffness matrix
$S_{f\ell 1}$	Force stiffness due to axial displacement
$S_{f\ell 2}$	Moment stiffness about OY due to axial displacement
$S_{f\ell 3}$	Moment stiffness about OX due to axial displacement
S_{fr1}	Force stiffness due to angular displacement about OX
S_{fr2}	Force stiffness due to angular displacement about OY
S_{fr3}	Moment stiffness about OY due to angular displacement about OX
S_{fr4}	Moment stiffness about OX due to angular displacement about OX
S_{fr5}	Moment stiffness about OY due to angular displacement about OY
S_{fr6}	Moment stiffness about OX due to angular displacement about OY
S_{rc}	O-ring stiffness in compression
S_{rs}	O-ring stiffness in shear
S_{sp}	Spring stiffness
S_T	Surface tension
T	Experimental temperature, WLF transform
T_o	Reference temperature, WLF transform
T_i	Auxiliary function used in first solution of equations of motion
$T_{i+1,i}$	Auxiliary function used in first solution of equations of motion
$T_{1,2}$	Auxiliary function used in first solution of equations of motion
U	Sliding velocity
V	Sliding velocity
V_m	Mean velocity

V_{r1}	Stator radial velocity
V_{r2}	Rotor radial velocity
V_{z1}	Stator axial velocity
V_{z2}	Rotor axial velocity
$V_{\theta 1}$	Stator velocity about shaft axis
$V_{\theta 2}$	Rotor velocity about shaft axis
W	Load
X	Forcing function displacements
X_o	Floating ring displacements vector
a	Factor controlling whether surface profile is on rotor or stator
a_m	Acceleration at experimental point
a_r	Acceleration ar resonance
a_T	WLF transform shift factor
b	Factor in expression for ϕ
d_i	Separation of floating ring and constituent cylinder centroids
d_r	Distance between O-ring and floating ring centroid
f	Forcing function
h	Film thickness
$\bar{h}$	Non-dimensional film thickness
h_a	Film profile wave peak amplitude
h_c	Central film thickness (Fig. 2-1)
$\bar{h}_c$	Non-dimensional central film thickness
h_i	Film thickness at inner diameter
h_m	Mean film thickness
h max	Maximum film thickness
h min	Minimum film thickness

h_n	Initial mean film thickness
h_o	Film thickness at outer diameter
i	Number of waves around circumference of a vibrating ring
ℓ	Floating ring length
	Floating ring cylinder length
n	Number of waves in fluid film surface profile
p	Pressure
$\bar{p}$	Non-dimensional pressure
p_e	Pressure at outer diameter
p_i	Pressure at inner diameter
r	Radial co-ordinate
	Radius
$\bar{r}$	Non-dimensional radius
r_i	Inner radius
r_m	Mean radius
r_o	Outer radius
r_r	Radius of line of action of O-ring
r_s	Radius of line of action of spring
t	Time
$\bar{t}$	Non-dimensional time
t_i	Time, present timestep
t_{i-1}	Time, previous timestep
t_{i+1}	Time, following timestep
v	Axial velocity ($-\partial h_c/\partial t$)
w	Width

x	Displacement of floating ring along OX
	Experimental separation of floating ring transducers
	Variable in differentiation of Reynolds' equation
	Variable in vibration equation
x_x	Input vibration displacement along OX
x_y	Input vibration displacement along OY
x_z	Input vibration displacement along OZ
x_i	Displacement at time t_i
x_{i-1}	Displacement at time t_{i-1}
x_{i-2}	Displacement at time t_{i-2}
y	Displacement of floating ring along OY
y_1	Simpsons' rules integration factor
y_2	Simpsons' rules integration factor
y_3	Simpsons' rules integration factor
z	Displacement of floating ring along OZ
	Vertical co-ordinate (in film thickness direction)

β	Factor in sliding velocity formula
Δ	Difference
ϵ_o	Dielectric constant
ϵ_1	Seal runout
ϵ_2	Seal eccentricity (the ratio h max/ h min)
ζ	Damping ratio
η	Absolute viscosity
θ	Angular co-ordinate or position
ν_f	Specific volume water
ν_g	Specific volume saturated steam
ρ	Density
τ	Shear stress
ϕ	Phase angle
ψ	Misalignment, angular position
$\overline{\psi}$	Non-dimensional misalignment
$\dot{\psi}$	Misalignment velocity
ψ_x	Angular position about OX
ψ_y	Angular position about OY
Ω	Frequency ratio ω_m/ω_r
ω	Angular velocity
ω_m	Experimental angular frequency
ω_r	Resonance angular frequency
ω_v	Angular velocity in sliding velocity formula
ω_x	Shaft angular vibration frequency axis OX
ω_y	Shaft angular vibration frequency axis OY
ω_z	Shaft angular vibration frequency axis OZ

CHAPTER 1

INTRODUCTION AND BACKGROUND TO PROJECT

1.1 Design and Operation of Mechanical Seals

This chapter is an introduction to the project. It consists of details of the design of mechanical seals, a review of relevant literature in the fields of mechanical seals, elastomers and vibration. The background to the project is reviewed and the problem is defined. In the first section typical mechanical seal design features are discussed and the mode of operation of such seals is outlined.

There are many ways of sealing between a stationary housing and a rotating shaft so that the fluid within the housing cannot leak out around the shaft. The type of seal used will depend on the pressure to be sealed, the speed of rotation of the shaft, the maximum leakage that can be tolerated, the space available for the seal, the requirements of simplicity of design and ease of assembly, and very often, the cost. This thesis is a study of the type of seal known as a "mechanical seal" or "face seal" or "radial face seal".

The mechanical seal is used for a wide range of duties. For instance it may be used for sealing high pressure or for vacuums. It may be a simple low cost seal such as is used for car engine water pumps, central heating pumps and washing machines, or it may be a very large or expensive seal such as those used in the process and aerospace industries where leakage cannot be tolerated.

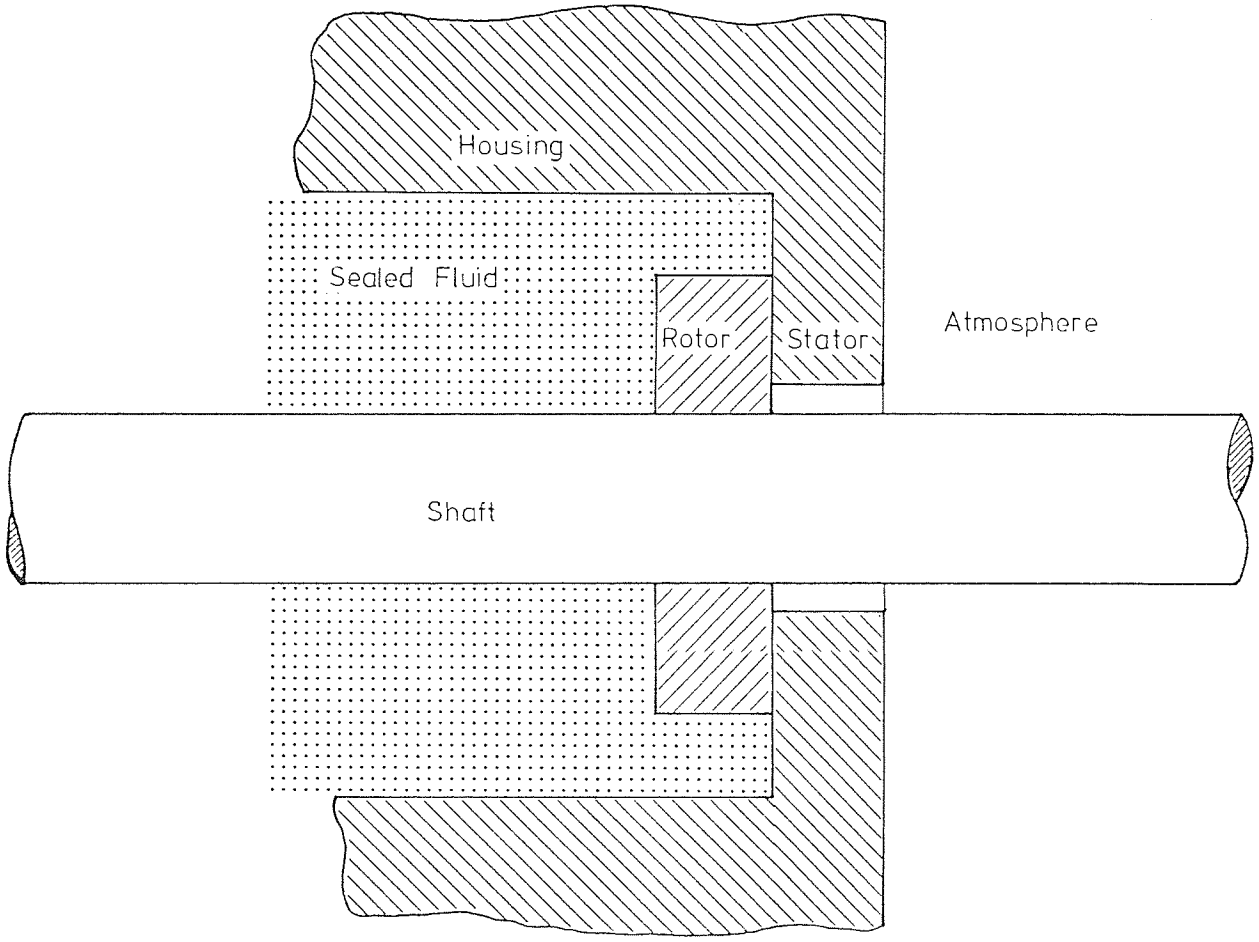

Fig 1-1 The Mechanical Seal Concept

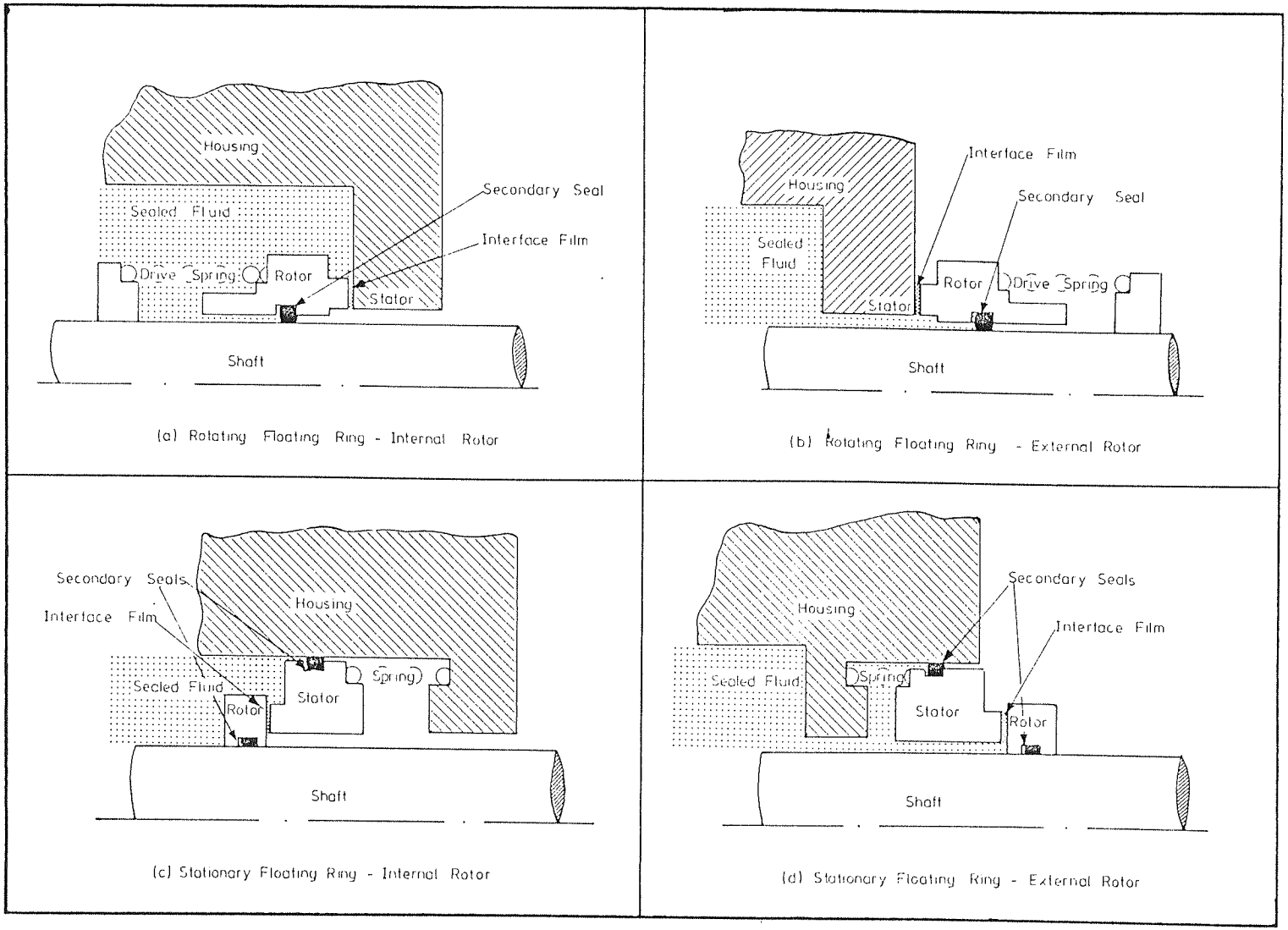

Fig. 1-2 Mechanical Seal Arrangements

The mechanical seal depends for its operation on the generation of pressure within the thin fluid film at the sliding interface. Fig.1 - 1 shows the basic principle of the mechanical seal, a rotating collar on a shaft sliding against a stationary housing. Such a design would not be used in practice as it would require very accurate and positive location in order to maintain its sealing ability. The mechanism of the operation will be discussed in more detail in the literature review.

In any mechanical seal design, four main elements may be identified:-

1) a stationary seal ring
2) a rotating seal ring
3) spring loading devices
4) static or pseudo-static seals.

Fig 1 - 2 shows various arrangements of the main elements. In fig 1 - 2a the rotating ring is sealed to the shaft by an o-ring secondary seal. Such a seal is usually referred to as a "pseudo-static" seal. It is loaded against the stationary seal ring by a spring driven by a collar fixed to the shaft. The pressurized fluid is on the outside diameter of the sliding interface. Fig 1 - 2b shows a different arrangement of the same basic elements, with the rotating ring outside the housing and the pressurized fluid on the inside diameter of the sliding interface. It is claimed that, because the seal is outside the housing, this design is easier to dismantle; and further that there is improved heat transfer from the rotating ring in this case (156). This would depend on how freely the liquid surrounding an internal rotor is exchanged with the process fluid.

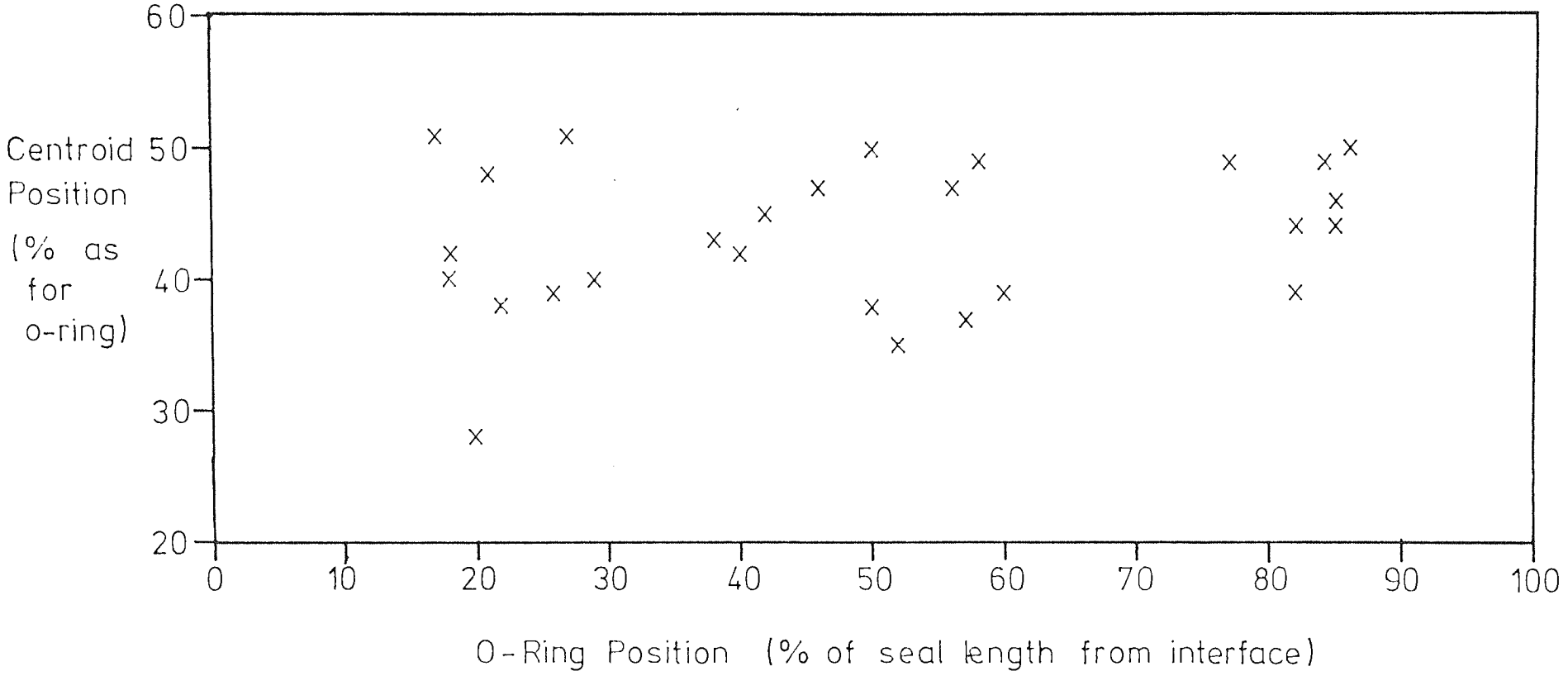

Fig 1-3 Mechanical Seal Floating Ring - Centroid Position vs O-Ring Position

The arrangements shown in figs 1 - 2a and b are generally used for process pumps. In the aerospace industry where shaft speeds in excess of 3,000 radians/sec may be encountered, it is more usual for the springs to load the stationary face. This is shown in figs 1 - 2c and d. If the rotating face is spring loaded then, for high speed operation the springs must be carefully balanced. Dynamic instability of the springs may lead to catastrophic seal failure at high speeds.

The stationary seal ring on figs 1 - 2a and b has been shown as an integral part of the housing. This is a typical arrangement for the cheap mass-produced seals used in the domestic market. The stationary face of aerospace and process industry mechanical seals is normally separate from the housing. It is then sealed against the housing by a suitable secondary seal.

The design of the floating ring itself has many variations, both in the cross-section and position of the o-ring secondary seal and in the cross-section design of the floating ring itself. Fig 1 - 3 shows a plot of the o-ring position against that of the axial co-ordinate of the centroid of the floating ring for various mechanical seals. Both positions are expressed as a percentage of the total length of the floating ring and are measured from the sliding interface. Although there is a wide variation of the o-ring position, the floating ring centroid position shows only a small variation.

Not all manufacturers use o-rings as the secondary seal. A description of the various types of secondary seal used may be found in reference (94). An investigation of the behaviour of mechanical seals fitted with secondary seals other than

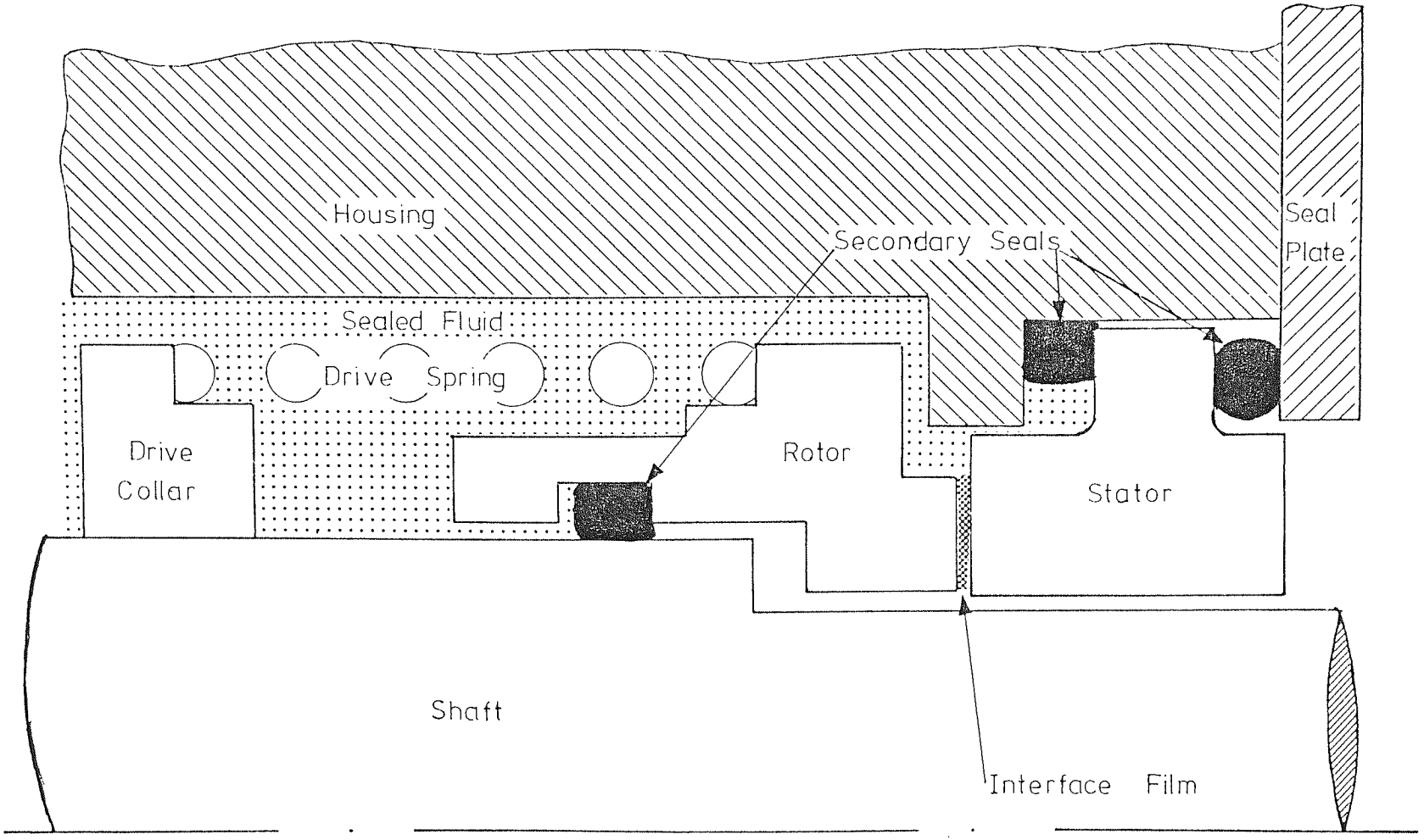

Fig 1-4 Balanced Mechanical Seal Design

o-rings is outside the scope of the present study. In some cases, particularly aerospace applications, the springs and secondary seal are replaced by a bellows arrangement. The bellows may be metal or elastomeric (94). Some work has been carried out into the dynamic behaviour of such a seal, and this will be reviewed in section 1.2.

The seals shown in fig 1 - 2 are suitable for low pressure applications from 0 - 1 MPa (gauge) (94). For higher pressures it is usual to step the shaft as shown in fig 1 - 4 in order to off-load some of the axial force on the sliding interface due to the sealed pressure.

A shaft sleeve is often used to provide the step, so that special machining of the shaft is not required. A shaft sleeve may also be used on the low pressure mechanical seals in order to prevent damage being caused to the shaft by the o-ring. The o-ring can cause fretting damage to the shaft although it is nominally static. If a sleeve is fitted then when damage does occur, only the sleeve needs replacing or refurbishing, which is much cheaper than replacing or refurbishing the shaft. Also the sleeve may be made of a harder material than the shaft providing longer life at less cost.

For some fluids additional equipment is needed in order to give reasonable seal life or a low leakage rate. This usually occurs when the fluid being sealed has a high solids content or a high temperature. In the former case, fluid is taken from the pump discharge, cleaned and then piped back into the seal housing to flush solids away from the seal. In the latter case the fluid is cooled before being recirculated as before. Where seals are operating at high temperatures a

completely separate cooling supply may be used to cool the stationary face. Details of this equipment, and more complicated systems are beyond the scope of this thesis but may be found elsewhere in the literature (3, 13, 25, 40, 44).

For many years after the introduction of the mechanical seal in the 1880s (113) it was thought that dry rubbing occurred between the rotating and stationary faces.

There was little research carried out into the operation of mechanical seals until they came into more general use after the Second World War. Various investigators were able to prove the existence of a very thin fluid film between the sliding parts (section 1.2) with pressures within the film that were much greater than would be expected for leakage flow across the annulus. Various theories have been put forward to explain this pressure generation, and it is now generally accepted (142) that the pressure generation is due to a combination of misalignment of the mating faces and residual waviness of the mating surfaces of the order of 1 μm wave amplitude. The pressure field generated is such that not only can the film support the load due to the sealed pressure but also leakage is minimal or zero.

1.2 Review of Mechanical Seal Literature

Several extensive reviews of mechanical seal research have already been published (3, 7, 16, 24, 39, 43, 44, 136, 137). In addition there have been eight conferences organised by BHRA Fluid Engineering (31-33, 42, 52-54, 60) and several books published (13, 40, 61, 94) covering the field of fluid sealing.

In the field of polymer and elastomer research, many studies have been carried out. However most of these have been concerned with the behaviour during processing. The use of elastomers as anti-vibration mounts has generated research interest, but even this is not directly relevant to the present project because of the special problems of the effect of shape and initial squeeze of the o-ring. Vibration, its diagnosis and cure, has been widely discussed. There is, however, little practical information on the vibration levels present at the seal housing.

Mechanical seals first came into use in the late 1880s when a Swedish company, Cederwall, developed a seal with a white metal face running against a spring loaded cast iron ring. This was mainly used as an oil seal on the stern shaft of ships (115). At first it was thought that these seals operated with dry rubbing between the rotating and stationary faces. After the Second World War, the use of mechanical seals on ships and pumps increased considerably. At this stage investigations started into the mechanism by which the seal operated. Many theories have been put forward to explain the operation of mechanical seals, and these include pressure generation due to residual distortion or surface profile, two-phase flow and non-Newtonian effects, surface tension and dry rubbing including interaction of the micro-profile of the surface.

1.2.1 Early Experimental Studies

The first indication that a fluid film might exist at the sliding interface came as a result of experiments on plane parallel thrust bearings (25). These experiments

showed that plane parallel annular rings could support a thrust load at least under partial film conditions. This work was discontinued in favour of thrust bearings with radial grooves.

In the early 1950s Denny (19, 85, 86) commenced an investigation into the behaviour of mechanical seals. This work was carried out at BHRA Fluid Engineering, and the work has been continued by other workers to the present day. The work of Denny, and others working independently during the same period have been reviewed elsewhere (137). Denny's main finding was that a fluid film existed at the sliding interface of a mechanical seal. The film was about 1 μm thick and the measured pressures within it were considerably in excess of the expected hydrostatic pressures. Measurements showed that the film thickness varied with a frequency twice that of the shaft rotation (138). Other workers at this time (57, 114) were also able to show the existence of a fluid film by considering the friction at the sliding interface. The results of these investigations included measurement of load and friction and confirmed that surface waviness and surface roughness could be the mechanism that generated the hydrodynamic pressures.

These results were countered by work carried out by Mayer (130, 131). He measured the film pressure over a long period and concluded that no film existed. This was despite a pressure build up occurring during the experiments. These conclusions are suspect because of the type of instrumentation used (bourden tube pressure gauges). Mayer concluded that the measured pressure generation was due to the effect of the pressure tappings. Later work (67) showed that the pressure

generated by such pressure tappings was small, much smaller than that measured by Mayer. It is probable that the pressure generation observed was due to the seal itself. The reason for the slow build up could be that the system has a long time constant due to the small volume of the interface film compared with that of the pressure gauges.

An effect known as "inward pumping" was also noted during this period. This occurs in seals where the pressurised fluid is on the inside of the seal. Under certain operating conditions, if the outside of the seal is flooded with a liquid it is pumped across to the inside against the pressure gradient. Non-Newtonian effects within the fluid film were first proposed as the cause of this (48, 49). However the magnitudes of likely non-Newtonian effects are too small to account for inward pumping (58, 59). Later work (21, 41, 51, 160) showed that it occurred with suitable combinations of radial run-out, surface waviness and angular misalignment, and that the flow could occur in either direction.

1.2.2 Surface Tension Theories

An early theory to take account both of the existence of a fluid film and low leakage rate of the mechanical seal considered surface tension as the mechanism responsible (12). This theory did not include any experimental evidence and was discounted by later work (10). Despite this, papers occur occasionally (35, 46, 47) that describe surface tension as the sealing mechanism. Although experimental evidence has been quoted in these papers, the hypothesis has never been developed into a viable theory for the operation of the mechanical seal. It seems unlikely (136) that surface tension alone is

the mechanism responsible for the sealing capability of the mechanical seal. This is because the interface pressure differentials are higher than those that could be resisted by surface tension alone. Recently however it has been suggested that this is not the case. Because the film is very thin, the fluid film acts as a highly viscous fluid and the surface tension forces are capable of preventing leakage (66). The theory has been developed as a result of observations of seals that have been operating satisfactorily. The seal faces exhibited a typical banded appearance but its cause is postulated to be the vaporisation and recondensation of the sealed fluid. It is claimed that the fluid reaches the critical point over a narrow band at the centre of the interface and that this is born out by the different appearance of the wear track. The wear profiles presented show evidence of high pressures within the interface causing compression of the soft face and thus less material removal, which supports the theory.

The theory is in its infancy, but from the work presented so far it appears to have only a limited application. The operating film thicknesses quoted are in the boundary lubrication regime and are a similar magnitude to surface roughness. It also seems unlikely the fluid would condense again within the interface as heat is continually being supplied due to the sliding of the contact. In addition the distortion likely when water is being sealed, if the critical point is reached, would cause distortions of the carbon seal face far in excess of the film thickness (152). There is evidence of compression of the carbon face on the seal ring profiles but it is difficult to quantify. The theory is likely to be

applicable only to heavily loaded seals.

1.2.3. Micro-profile Theories

The surface profile of the sliding interface of a mechanical seal exhibits two main features. First a macro-profile normally referred to as surface waviness, and secondly a micro-profile referred to as surface roughness, micro-asperities or micro-irregularities. This micro-profile has been proposed as the pressure generation mechanism in mechanical seals. Roughness was considered by several authors at the first International Conference on Fluid Sealing in 1961 (60). It had been observed that the roughness asperities become polished and much smoother during operation (57). However it was also proposed, theoretically, that the micro-profile could generate hydrodynamic lift by acting as micro thrust pads (18). Later workers actually observed cavitation streamers within the seal interface that appeared to develop downstream of micro-asperities. These micro-asperities were carefully manufactured onto the seals faces under test, and great care was taken to ensure that there was no residual surface waviness on the seals, despite the practical observations of other workers to the contrary (120). This theory was developed and experimental studies undertaken which showed that a mechanical seal could operate with the micro-profile generating the interface pressure (1, 2, 27, 34). Unfortunately although great care was taken to ensure that the micro-profile was the same as that used in the theory, there was no attempt to compare the effect of the micro-profile with that of the macro-profile. Thus although there can be no doubt that the micro-profile will, under suitable conditions, generate hydrodynamic pressures,

this work did not show that this was the mechanism by which seals operate.

Recently however the theory has been reconsidered. Mechanical seals that operate with the faces completely separated by a fluid film should not wear. But, although the wear rate is low under ideal conditions all seal faces do wear. A study of used seals with carbon faces (118) showed evidence of wear. The faces of these seals were found to have a circumferential wavy profile. It was postulated that the seal operates in a combined hydrodynamic and asperity contact regime. A statistical distribution was used to define the micro-profile and it was assumed that there would be some region of the seal where the asperity height exceeded the film thickness, and contact and wear occurred. In the initial work it was assumed that the micro-profile was of the form of circumferential grooves, with no side leakage in the contact regions (118, 120, 123). This model was clearly inadequate, both because of the lack of side leakage and also because the micro-profile had been observed to consist of peaks rather than grooves (154). In addition, an initial wave amplitude of 4 μm was used, which would be expected to cause excessive leakage. This theory is still being developed, and the latest work (36, 121) has resulted in the two dimensional problem being solved. The work however, remains theoretical with no correlation with experimental studies running under the same conditions.

1.2.4 Thermoelastic Instability

Another recent theory based on contact during sliding in seals is that of thermoelastic instability (4, 14, 15, 20, 64, 68, 70, 71, 119). This is a theory of the way in which

breakdown in sliding can occur. The hypothesis is that local heating due to the friction pair causes deformation of the surfaces in contact. Under certain circumstances the deformation can grow and this will result in an instability occurring that will cause failure of the contact. The work originated in England in a general form (4) but has since been the subject of detailed investigations in the U.S.A. The theory was originally developed as part of a Wankel engine research programme and early papers are concerned with line contact on semi-infinite plates (20). The model has been extended to a seal-like configuration (14, 15, 64, 119) but the work is concerned mostly with dry rubbing.

It is difficult to assess the practical implications of this work because there are few papers applying it to mechanical seals. The configurations used (64) have a much narrower contact width and thinner interface film than might be expected in a typical process pump mechanical seal. The results obtained are valid for a 'narrow lip' configuration, but this term is undefined. The results given suggest that a mechanical seal on a typical medium to large process pump (100 mm diameter shaft running at 3,000 rpm) would be subject to this type of instability. Although this instability may occur it is likely to be a low frequency effect, and thus the material of the seal would be able to deform sufficiently to allow stable operation (119, 122). Recent experimental studies have shown that although these operating conditions were predicted by the theory, instabilities did not occur (65). These studies were carried out for hydrodynamically lubricated seals. It seems likely that the instabilities will only occur with high face loadings. These are normally avoided by pressure balancing

the seal (section 1.1).

1.2.5 Surface Waviness Theories

The investigations into the behaviour of mechanical seals that have proved most fruitful have been studies of the effects of surface waviness and distortion. Waviness of the surface of either of the faces of the mechanical seal can lead to the generation of hydrodynamic pressures within the interface. The flatness of a seal face is normally quoted in terms of the half-wavelength of monochromatic light, such as sodium. A glass proof plane, or "optical flat", is placed on the surface of the seal and sodium light is shone onto it. The contours of the surface show up as a series of light and dark bands, usually referred to as "lightbands". These lightbands represent contours of the surface, and between each band the surface height changes by 0.295 μm when sodium light is used. Seal manufacturers usually lap the seal faces flat to within three lightbands (17, 94) which gives a residual surface profile of one (or more) waves around the circumference whose peak to peak amplitude is 1 μm or less. This profile has a much smaller amplitude than would be expected for a hydrodynamic journal bearing, but as the minimum film thickness is also much less, it is reasonable to assume that hydrodynamic pressure generation occurs. The initial experimental work that showed the generation of pressure and the periodic variation of the film profile has already been mentioned. It was also shown (136) by running a mechanical seal against a glass face, that cavitation could occur within the film and that, unlike oil bearings that have an oil feed, the cavitation region extended around 60 - 80% of the circumference. A

combined experimental and theoretical investigation was carried out by the Central Electricity Generating Board. This showed waviness to be the cause of pressure generation within the interface, and a theory was developed to predict design parameters for mechanical seals (5, 6, 29, 30, 55).

The theory utilised the Reynolds' lubrication equation since the assumptions made in deriving this equation (74) will apply to the mechanical seal configuration. Unfortunately in this, and other theories, approximations have been made that are not always justified, in order to achieve an analytical result. These approximations are known as "Reynolds Conditions" (76) and the "short-bearing approximation" (75). The first of these delineates the cavity region by assuming that within the region:-

$$p = \frac{\partial p}{\partial \theta} = 0$$

The start and end of the cavity being defined as the points at which:-

$$p = \frac{\partial p}{\partial \theta} = 0 \qquad \text{and} \quad \theta = 2\pi \qquad \text{respectively,}$$

where the maximum film thickness is located at $\theta = 0$ and 2π and the film profile is a sine wave.

These conditions only apply to a journal bearing with an oil feed at maximum film thickness (115). For a mechanical seal the end condition is an arbitrary one and these conditions will grossly underestimate the length of the cavity region (98, 148).

The second approximation assumes that the circumferential pressure gradient is small compared with the radial one and may therefore be neglected. This is usually a justifiable assumption because the seal face width is usually 10%, or less,

of the seal outside diameter. It may not be justified for wide face seals. However, unless flow conservation techniques are used to calculate the extent of the cavity region, the assumption will also lead to an overestimation of both the load capacity of the interface film and its leakage. With the advent of modern digital computers it has been possible to use numerical techniques to solve the two dimensional form of Reynolds' equation directly (36, 45, 142, 148). Flow conservation techniques are used to delineate the cavity and thus these two approximations are redundant. However such methods are not always appropriate, and approximate methods still have a place in the early stages of design and when it is necessary to solve Reynolds' equation a large number of times as a subsidiary part of a larger calculation (26, 37, 38, 106). The main problem with such methods is the inaccurate prediction of leakage, since the error in the load capacity is usually acceptable.

1.2.6 Seal Face Distortion

The effects of distortion have been investigated in Canada by Atomic Energy of Canada Ltd. Distortion has been considered as the reason for the existence of a fluid film in the sliding interface between the two rings of a mechanical seal (165). A pressure profile may be calculated from considerations of the radial flow within the interface. When the distortion of the seal ring is such as to open the interface to the sealed pressure, this will increase the hydrostatic component of the pressure field in the interface. This hydrostatic component will partly off-load the axial pressure on the seal due to the pressure of the fluid being sealed. This effect has been considered to be the operating mechanism of

high pressure mechanical seals (170).

Studies have been carried out considering hydrostatic effects (132, 133, 169) whilst neglecting any hydrodynamic effects due to the surface profile. Comparisons of the experimental and theoretical results published so far show poor agreement between them (133). However, this may be due to the high static leakage recorded in the experiments, since the theoretical results predict zero leakage at zero speed. The authors claim that this static leakage accounts fully for the discrepancies. The source of the static leakage is not explained, however its magnitude suggests that it is due to the surface profile that has been neglected.

The type of seal considered in this theory is used in the primary coolant system of a nuclear reactor (134) where the main criteria is reliability. A higher leakage rate is acceptable and thus the seals may operate in a different mode with a thicker interface fluid film than would be acceptable for a process pump handling chemicals. The computed temperatures quoted (132) support this as other workers (112, 146) have shown vaporisation occurring in the sliding interface that could not occur at the temperatures and pressures quoted. In later published work (134) it has been shown that hydrodynamics in the interface film have little effect on the behaviour of the seal, and that cavitation of the fluid does not occur. However it seems likely that this is a misinterpretation of the results (152), the hydrodynamic effect being small because cavitation does occur due to vaporization of the sealed fluid.

This theory obviously has a specialised application,

however the poor correlation between theoretical and practical results clearly shows the need to include other aspects of seal behaviour. The inclusion of surface waviness effects may improve these predictions.

1.2.7 Misalignment Theories

Although the mechanical seal rings may have residual waviness on the faces, and may distort due to the operating conditions, it is also possible that the mechanical seal may be installed incorrectly and hence for this or other reasons the two rings may be inclined to one another. If only one of the faces is perpendicular to the axis of rotation a hydrodynamic pressure field will be generated, similar to that due to a surface profile of one circumferential wave (126). Such a misalignment would be very small and it has been suggested that the mating face would track it (80) and thus cancel the defect. If the mating face does not track the misaligned face, and also is itself misaligned, axial vibration of the floating ring will occur (26, 37, 38, 106).

Although the misalignment could give rise to a fluid film with a single circumferential wave profile, it could not give the two-wave profile observed by other experimental workers. Thus the misalignment needs to be combined with other phenomena such as distortion or waviness but this has not been considered. The theory, however, utilises a concept that has a wider use than just analysing the effects of misalignment. The film profile is defined by considering the faces to be two planes each inclined relative to a third fixed plane that is perpendicular to the axis of rotation. This concept leads to a slight modification of Reynolds' Equation, but allows easy manipulation

of the misalignment of each ring. It thus has considerable use when considering vibrating seal rings.

A further analysis of the effect of misalignment considers the balance of forces and moments due to friction, the drive spring, o-ring friction, and hydrodynamic friction (127). The analysis uses a very simple model in order to achieve an analytical result. A 'low pressure' seal is considered that has no pressure drop across the face (and thus has no hydrostatic component) and circumferential waviness is not considered. Results are obtained by considering forces and moments about a radial axis in the direction of the minimum film thickness only. The calculated values of film thickness are stated to be in the 'expected range' although no measured values are given. Clearly further development of the theory is needed before it can be considered as a model of seal behaviour.

Recently the behaviour of a misaligned seal has been investigated with regard to the stability of the operating mode. A series of papers have been published on the subject (90-93, 125).

The first of these papers (90) considers nonaxisymmetric effects due to the hydrostatic pressure within the sliding interfaces. Hydrostatic effects are discussed initially as the author had not managed to find any work on this subject (despite a paper published in 1961 (22)). It is concluded that in high pressure seals, cavitation does not occur. The hydrodynamic effects will therefore cancel, and may be ignored. This is based on an unproven comment made by Sneck (160). By totally ignoring the hydrodynamic effects the paper concludes that hydrostatic effects are largely responsible for the proper

operation of seals. The paper shows that if the sealed pressure is on the outside diameter the operating mode will be unstable, but no attempt is made to show how such seals operate successfully in practice.

In order to assess the importance of the hydrodynamic pressure within the seal interface, the accuracy of approximate solutions of Reynolds' equation are considered (91) and then the various hydrodynamic stiffnesses are calculated (92). It is shown that there is good agreement between the narrow seal approximation and a full solution of the Reynolds' Equation. This however is not surprising as the only difference between the two solution methods is that negligble seal curvature has been assumed for the narrow bearing case. The difference in the solutions appears to be due to neglecting terms of the order of R^2 and higher in the expansion of lnR. No attempt has been made to include the effect of the circumferential pressure gradients.

It is also clear that the author does not understand the concept of pressure balancing of seals (91). A lack of appreciation of seal operating conditions is apparent when the hydrodynamic effects are calculated (92). Again the author limits the extent of the cavity to the half Sommerfeld condition for 'high pressure' seals. Computer calculations at BHRA Fluid Engineering (142) predict cavity lengths in excess of the half Sommerfeld cavity for pressures of 3MPa, hardly a low pressure seal! In addition the narrow bearing approximation and the half Sommerfeld pressure boundary conditions are muddled when developing the Reynolds' equation solution.

The author does concede that the half Sommerfeld condition

is not entirely satisfactory, but clearly does not appreciate the difference in the mode of hydrodynamic operation between 'short' bearings and 'narrow' seals. Also in this paper (92) details are given for a worked example, comparing hydrodynamic and hydrostatic effects. The film thickness used in the example is at least an order of magnitude larger than that normally found to cause catastrophic leakage in seals (147). Using the quoted formulae it can be shown that for a 1 μm film thickness, hydrostatic effects are negligible compared to hydrodynamic ones.

Radial forces have been considered (93). This is a useful contribution and the author concludes that the radial forces may be partly responsible for inward pumping. Again the paper uses a large film thickness and assumes no cavitation within the film (at a pressure of 1 MPa). By reworking the calculations using a film thickness of 1 μm instead of 25 μm it can be shown that hydrodynamics again are the predominant effect.

Finally a seal design, based on this theory, has been proposed (125). This design would always have positive (hydrostatic) stiffness and hence be stable in operation. Unfortunately the authors have not considered the practical application of the design. For a 50 mm outside diameter seal on a 40 mm shaft the optimum clearance between the (rotating) shaft and the (stationary) seal ring for stable operation is 2 μm, hardly a practical design. For a more practical clearance of 25 μm, a clearance bush 20 m long would be required! The papers represent an attempt to quantify the operation of a mechanical seal that could lead to a dynamic theory. Unfortunately the assumptions made have simplified the problem to

such an extent that the results no longer have a direct practical application.

1.2.8 Dynamic Behaviour

The misalignment theory predicts the dynamic response of a seal ring to a fixed misalignment. Although this is clearly a possible operating mode, it does not predict the behaviour of the floating ring when it is subjected to vibration of the shaft or housing. In a practical situation, where the floating ring is free to rock, it is likely that the pressure forces generated would oppose the misalignment and try to return the floating ring to a position perpendicular to the axis of rotation. However the forces set up also have a component at right angles to the misalignment, so it is not possible to consider just one mode in isolation. A dynamic theory must take account of the response to externally applied vibrations. An attempt to predict unstable behaviour of seals has been made (110). This considered the possibility of separation occurring between the mating faces and was a development of a similar theory for cam follower systems. The contact was represented by a series of springs. Separation was assumed to occur when the 'feet' of the springs lost contact with the mating surface. No attempt was made to include the behaviour of a fluid film. By assuming the contact elasticity to be that of the fluid film and using the graphs in the paper, it can be shown that separation will not occur for normal operating conditions. The application of this theory to mechanical seals is limited because the damping of the fluid film cannot be modelled.

Recently the effect of vibration on seal leakage has

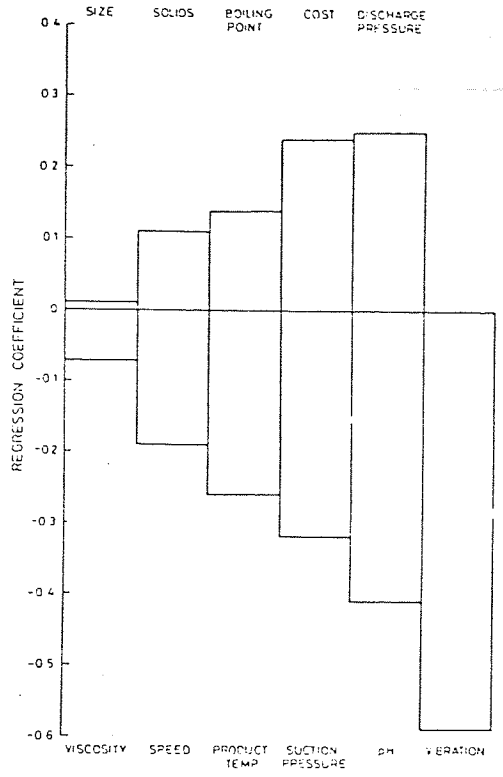

Fig 1-5 Relative Importance of Parameters Affecting the Performance of Mechnical Seals (from ref. 99)

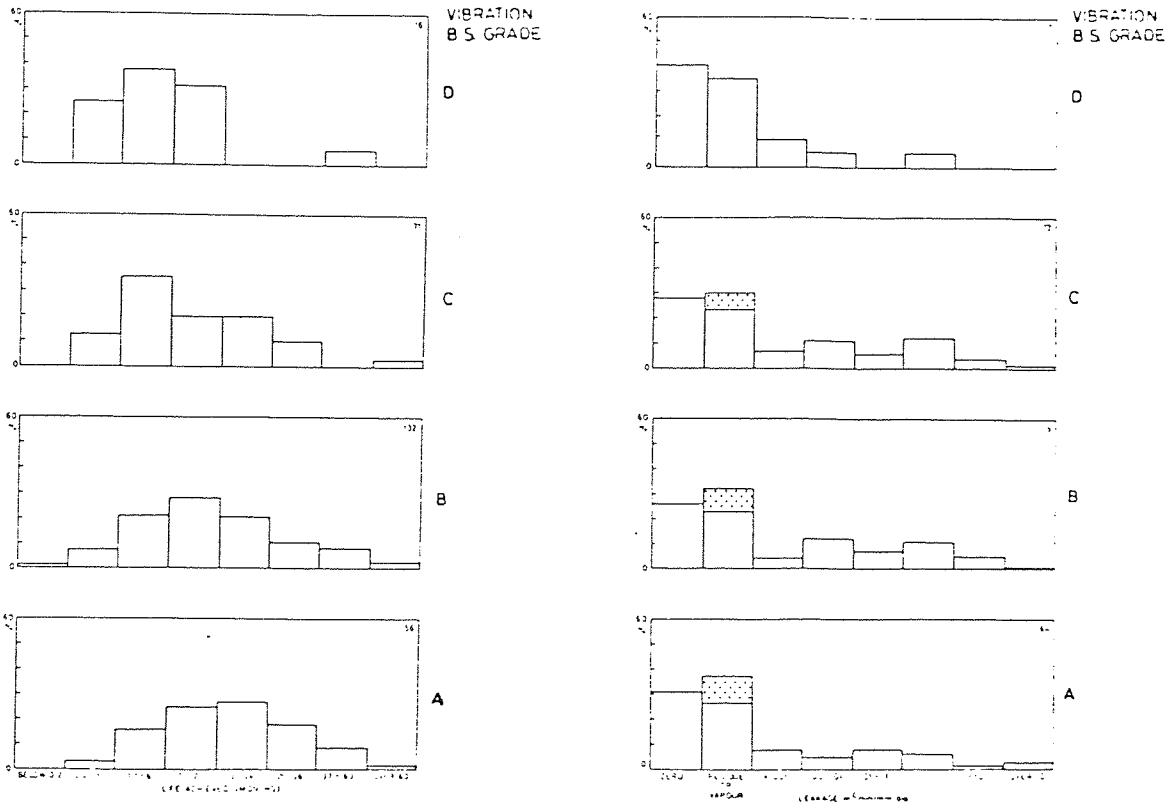

Fig 1-6 Effect of Vibration on Mechanical Seal Life and Leakage (from ref. 99)

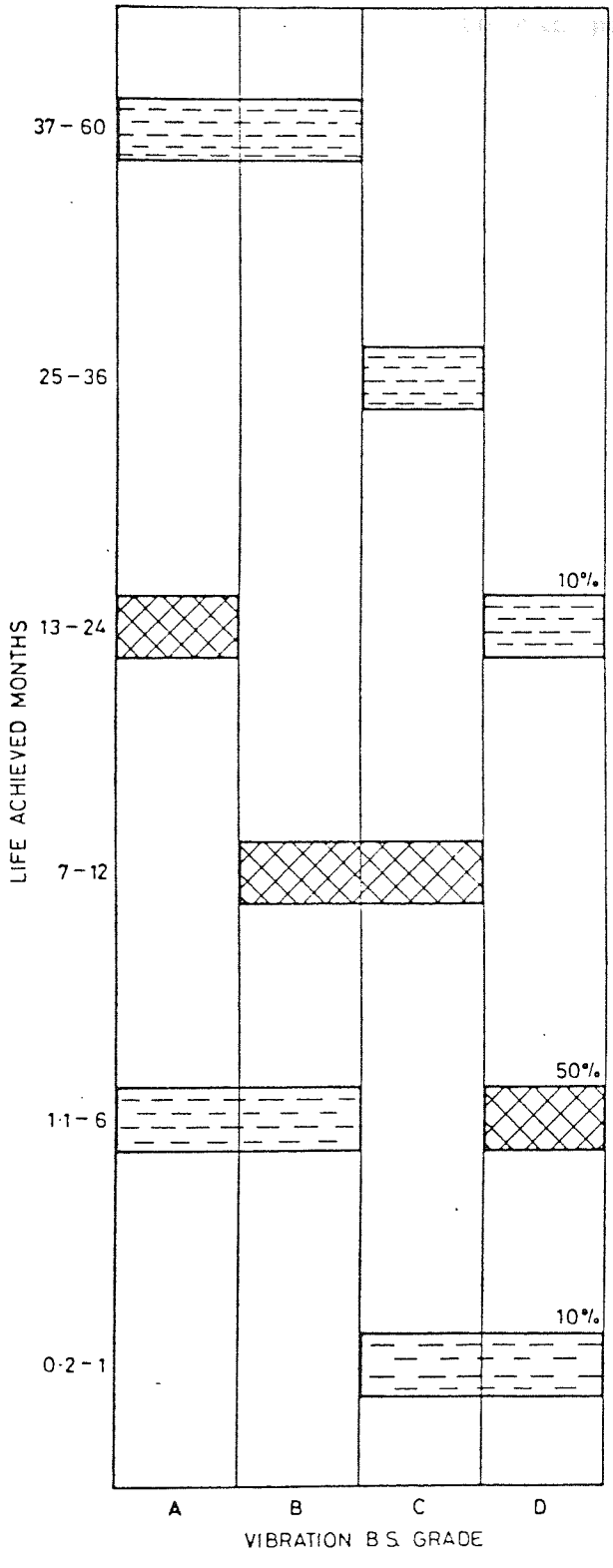

Fig 1-7 Cross-plot of Vibration and Life (from ref. 99)

been investigated (116). It was noted that perfect (sic) sealing only occurred when a complete gas path existed around the circumference of the sliding interface, and, the axial vibration frequency was the same as the shaft rotation frequency. The observations on leakage and inward pumping are similar to those of earlier workers (141).

It is useful to consider field observations on seal vibration and seal performance, in view of the lack of experimental or theoretical laboratory studies. A recent survey (99) has shown the relevance of various parameters to poor seal performance. Fig 1 - 5 is taken from the survey results and shows the regression coefficients for these parameters. The largest negative regression coefficient is for vibration, the survey showing that high vibration levels are most likely to result in poor seal performance. Fig 1 - 6a and b shows the effect found in the survey of various vibration levels on seal life and leakage. Fig 1 - 7, also taken fron the survey results, shows the 50 percentile and upper and lower deciles for seal failures, and clearly shows the effect of high vibration levels. The vibration grades are taken from BS 4675.

The dynamic behaviour of the non-contacting type of seal, which has much thicker interface films than mechanical seals, has been studied (81). The method of analysis used is similar to that used in this thesis (Chapter 3) and includes flexural vibration. The analysis considers undamped vibrations caused by coning, axial pulsation, wobbling and initial waviness. It was found that the ring vibrated elastically when excited by a wavy surface profile with a large number of circumferential waves. Such a profile is possible for the large diameter

seals considered in the study but is unlikely for the mechanical seals considered here. The stiffness of the cross-section of a typical process pump mechanical seal is too large for the seal to vibrate in a distortion mode (Chapter 3).

A further study of seal dynamics (102, 103, 157) has been carried out on seals used in the drilling industry. The type of seal is not fully described but the film thicknesses quoted are too large for a mechanical seal. It is likely that the seals are some form of clearance type. The work contains many sweeping assumptions which are not fully justified. A typical such assumption is that the o-ring has damping but no stiffness. Even more unsatisfactory than these assumptions is the use of two undefined coefficients. One of these is used to allow for squeeze film effects due to axial vibration of the floating ring and the other is used to allow for the difference between the theoretical predictions and experimental results. These coefficients make it impossible to give an assessment of the value of this work and make it impossible to apply the theory to other problems.

1.2.9 Inertia Effects

The effects of inertia on the performance of a mechanical seal have been considered (50, 51, 160) for both misaligned and wavy seals. Although the author (160) considers that inertia effects must be taken into account in order to accurately model the flow regime correctly, cavitation is dealt with by arbitrary boundary conditions. It is likely that a more accurate model could be obtained by a satisfactory solution of Reynolds' equation rather than by this method.

1.2.10 Phase Change Theories

Mechanical seals, particularly those operating on water, occasionally emit short bursts of leakage, a phenomenum normally referred to as puffing or popping. Most of the time these seals operate with no visible leakage. This has been explained by postulating that a boiling interface exists within the fluid film (146). Experimental studies had shown that the interface exhibited a circumferential band of fluid next to the pressurised edge, with a band of gas on the unpressurised edge. The exact position of the interface depended on the operating conditions.

These particular studies were carried out with water as the sealed liquid. The measured temperatures approached the saturation temperature for the sealed pressure, but leakage only occurred when the saturation temperature was reached, suggesting that boiling was occurring for some conditions. Similar gas and liquid films have been observed when sealing oil, but in this case the temperature was well below saturation, and cavitation is a more likely explanation for the gas band (141).

Theoretical studies have shown that most seals operating with mean film thicknesses of the order of 1 μm are unlikely to operate in this regime (112). These studies have however shown a particularly significant result of this hypothesis. That is, if a seal is operating in this regime, the leakage rate will be much less than for a similar seal with a liquid film. For a given leakage path and pressure gradient the mass flow rate is given by (142)

$$\dot{m}_{gas} = \left[\frac{\pi h^3 (p_i - p_o)}{6 \ell n (1/R)}\right] \quad \frac{p_i + p_o}{2 p_i} \cdot \frac{1}{\nu f} \cdot \pi D$$

$$\dot{m}_{liquid} = \left[\frac{\pi h^3 (p_i - p_o)}{6 \ell n (1/R)}\right] \cdot \frac{1}{\nu f} \pi D \ Kg.s^{-1}$$

Now for water νg is about two orders of magnitude greater than νf, and hence the mass flow rate of the steam will be less than that of water. The leakage across the seal is therefore controlled by the mass flow rate across the gas band, and the condensed volume of leakage will be considerably less than for a full fluid film.

These operating conditions are similar to those observed by other workers (66), described in the discussions of surface tension theories. Unlike the phase change theories described above, this theory resulted from observations which showed a third band on the low pressure side of the gas band suggesting the vapour was recondensing. In view of the rate of heat generation across the entire sliding interface, this seems a little unlikely, and suggests that the central gas band was due to cavitation.

1.2.11 Leakage

All seals are required to operate satisfactorily with the minimum possible leakage. It is therefore important that any theory used is capable of predicting the leakage rate accurately. Only the theories predicting extensive cavitation or some other form of gas band within the interface are capable of predicting the low leakage rates observed for most process pump mechanical seals.

Recently it has been suggested that, because of the thin film, the interface acts as a porous medium and not a clear leakage path (87). It can be shown that the theory predicts

reasonable leakage rates. However the accuracy will depend on an accurate knowledge of the permeability of the interface. This may limit the application of the theory.

1.3 Review of Elastomer Literature

Many of the studies considered above have been the result of observations of one or more facets of the performance of mechanical seals in general, or one design in particular. Nevertheless the results are generally applicable to any design of mechanical seal. However, for the dynamic performance, the overall design of the mechanical seal must be considered. The behaviour of the secondary seal influences the dynamic performance of the floating ring, but little research has been carried out into this facet.

In aerospace applications the metal bellows type of secondary seal is often used. This does not have the inherent damping properties of an elastomer and seal failures have occurred that can be traced to this. Dynamic instabilities can develop and these may lead to fatigue failure of the bellows. This problem has been investigated experimentally (28, 56) and overcome by utilising cylindrical particulate dampers acting on the bellows. Although this work is not relevant directly to the mechanical seal with an elastomeric secondary seal, it indicates that the damping properties of the secondary seal may be important for the stable operation of mechanical seals.

Various designs of secondary seals are used for mechanical seals (section 1.1). The o-ring secondary seal is the most common type but is difficult to analyse because of its shape and initial compression on fitting. This initial compression

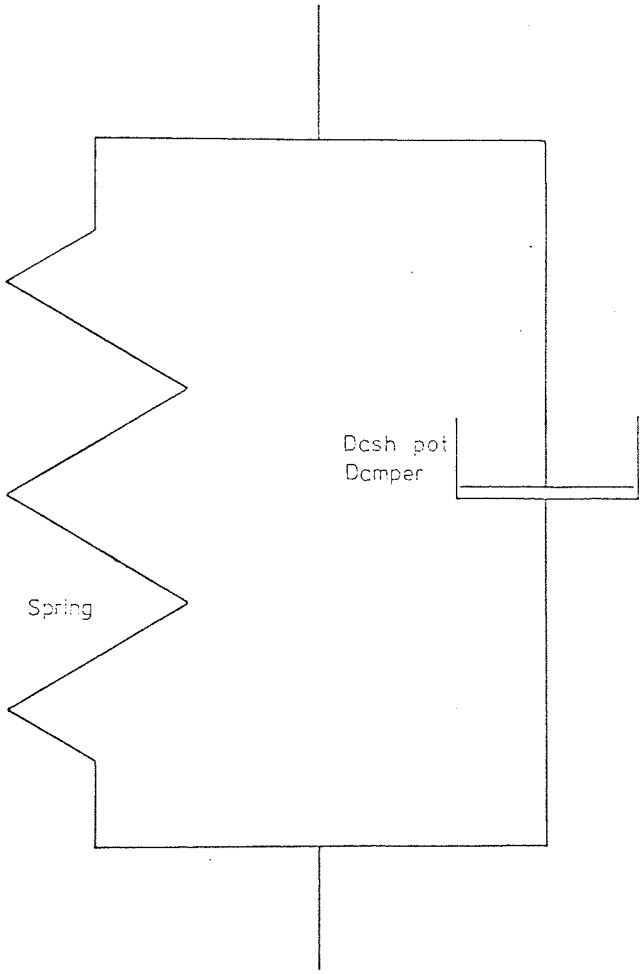

Fig 1-8 Kelvin Element

means that the o-ring is subject to a varying compression force, or in extreme cases a force that varies between compression and tension. The sealed fluid complicates the problem even more by forcing the o-ring against its groove and increasing its distortion. Few studies have been carried out to determine the dynamic properties of o-rings, although many papers are available on the dynamic properties of polymers in general. O-rings are only a small part of the total cost of a mechanical seal and it is difficult to justify expensive research into their dynamic properties.

The simplest model of the behaviour of an elastomer is the Kelvin or Voight element shown in fig 1 - 8 (95). Whilst this is easy to analyse, it does not represent the behaviour accurately. If the model is loaded and unloaded it does not have an elastic response. In addition, the creep and set properties are not accurately modelled and the creep rate approaches zero for long duration loading. Increasing the complexity of the model will improve its accuracy at the expense of ease of analysis. However, most models have some drawbacks (8). The complexity necessary to model an elastomer accurately makes the analysis of the behaviour of the o-ring and the floating ring of the mechanical seal very difficult. However for the frequency range being considered, the Kelvin element may be used to model the seal behaviour with reasonable accuracy.

In the general field of polymer research many studies have been carried out. The usual instrument used to obtain the complex modulus of the polymer in solid form is the Fitzgerald Transducer (23). For this method the specimens are discs of the polymer to be tested. Other methods (110) use rectangular

blocks of material. Many of the polymers tested are not elastomers, and the main interest has been their behaviour during the various manufacturing processes that they may undergo. Elastomers are used in the tyre industry of course, and for vibration isolation as well as in sealing applications. The behaviour of such elastomers may be used as a general guide to the behaviour of elastomeric o-rings, although it must be remembered that the shape, initial compression and pressure distortion of o-rings may modify their behaviour.

For most elastomers the modulus varies with frequency. Both the complex modulus and the damping factor (ratio of the out of phase modulus to the in phase modulus) increase with frequency. The exact form of the variation will depend on the type of polymer and the additives, processing and degree of cure. The 'low damping' rubbers have a peak value of damping factor and maximum rate of change of complex modulus at about 10^8 Hz (161). This frequency falls as the damping increases to a value of 10^3 Hz for 'high damping' rubbers. Thus if the properties of the rubber change due to ageing or absorbtion of sealed fluid the behaviour of the seal may change completely. At low frequencies (< 50 Hz) both properties were found to be constant.

When measuring the properties of polymers, the effects of temperature and frequency are interchangeable (96). Thus properties may be measured over a small frequency range (for instance 1 decade) at various temperatures, and a composite curve of the dynamic properties of the polymer at a constant temperature may be obtained. Similarly the properties may be measured at constant temperature, but over a wide frequency range. By using the inverse transform the temperature behaviour at a constant frequency may be obtained. It is thus important that both the

temperature and frequency at which measurements are made is accurately recorded (108).

It is also important to keep the deflection amplitude constant when temperature or frequency is being varied. The variation of the moduli with strain is complex (128, 158). In particular the out of phase modulus (damping) may exhibit two maxima when plotted against strain. For carbon black reinforced vulcanizates the in phase modulus has a maximum at low strain values (10^{-4}) whilst the out of phase modulus exhibits maxima at low strain values (10^{-4}) and at higher values (158). If the specimen is initially in compression, when a vibrating force is applied, the stress may be a varying compressive one or may oscillate between compression and tension. This will also affect the measured values of the rubber's characteristics, in general the moduli have different values at the same strain in tension and compression.

The effects of initial compression have been investigated (89). However this paper is unsatisfactory. It is a translation from German and from the graphs and equations given it appears that the German "Dampfung" has been incorrectly translated as "Damping" rather than "transmission loss".

In general increasing the filler content of a rubber will increase the moduli (62, 117, 129, 149, 158, 167). The exact effect will depend on the base polymer (117, 158) the degree of cure (117) and the type and quantity of filler (62, 110, 129, 149, 167). When carbon black is used as the filler, increasing the quantity of filler has a greater effect on the in-phase modulus (stiffness) than on the out-of-phase modulus (damping) (149).

Different base polymers have different modulii and much work has been carried out investigating their behaviour. This has mainly been with regard to polymers melts and the moulding and extruding process and is thus not directly relevant to elastomers. However investigations have shown that of the elastomers, viton (176), ethylene-propylene (77, 176) and neoprene (175) have good damping characteristics and may find an application in vibrating conditions. It will be appreciated that in general for mechanical and secondary seals, vibration characteristics have not been considered to be of much importance compared with fluid compatibility. Clearly the seal must be compatible with the fluid being sealed, and only if a choice then exists are the other properties considered. A discussion of fluid compatibility is outside the scope of this thesis, and has been dealt with in considerable depth elsewhere (9, 11).

As has already been stated, o-rings themselves have received little attention with regard to their dynamic properties. The static behaviour has been investigated (84) with the behaviour modelled by plane strain contact. A linear solution to the visco-elastic equations was obtained for a fixed deflection of the o-ring. The solution gives static properties only, and in addition assumes the o-ring is constrained only by the direct compressive force applied. In the case of the secondary seal of a mechanical seal this is not an adequate model since the pressurised fluid will force the o-ring into contact with its groove. This extra distortion will affect the results obtained.

The use of o-rings as static seals has led to an investigation into the load required to achieve certain deflections (166). Various conditions of loading were considered and the

results presented as graphs and a nomograph from which the required loads can be calculated for a given deflection for various elastomers and ring sections. None of this work is on the dynamic behaviour and only loads are given. However, from these results the static stiffness may be calculated, and this may be compared with the experimental results presented in this thesis.

A more recent investigation was carried out to develop a test rig and analysis technique to determine the properties of elastomers in terms of their stiffness and viscous damping coefficient, instead of the more usual complex modulii. The test rig is controlled by a computer which carries out the control of the rig and analyses the measurements. The rig utilises the resonance mass technique, the carrier mass being adjusted to obtain the range 30 - 1000 Hz (82, 104). The method has been 'verified' by comparing theoretical predictions based on the analysis and experimental measurements. However there is no correlation with other test methods such as measurements made with a Fitzgerald transducer. The comparison of the theoretical and experimental measurements suggests that the method is not as accurate as measurements of modulii using a Fitzgerald transducer.

This rig has been used to obtain the stiffness and damping coefficient of o-rings (159). A number of different parameters have been investigated, which enable the properties for a number of different conditions to be obtained. However the results are presented merely as trend lines, which again suggests that the spread of the results is large. The results are presented in an interesting manner as they are all for two o-rings, and hence

the values are twice those for a single o-ring. This is presumably because the original work was for a damper arrangement consisting of two o-rings. There is however a problem in carrying out any comparison as details of the formulation of the elastomer compounds used are not given. This limits the use of the results to little more than qualitative comparisons.

1.4 Review of Vibration Literature

The measurement of the levels of vibration present in machinery is becoming more important. This is because vibration levels are used to monitor the condition of the machinery and hence decide when maintenance is necessary. Damage to impellors and bearings of pumps for instance can be detected before catastrophic failure occurs with the attendant losses if a large process has to be shut down (101). However little attention is paid to vibration levels with respect to seal performance, although it is known to reduce the life of the seal or increase the leakage from it (151).

Vibration level measurement was first proposed by Rathbone (150) who suggested that condition monitoring could be carried out by measuring the vibration level and comparing it with a chart. This chart is known as a "Vibration Severity Chart" or "Rathbone" chart and is the basis of vibration standards such as BS 4675 (69). However, it has been realised that this is too general an approach for condition monitoring. Present monitoring systems involve the "baseline" measurement, that is the vibration levels are measured when the unit concerned is new or has just been overhauled. These levels then represent the minimum vibration levels attainable. All subsequent measurements are compared with these baseline values, and any degradation of the

condition of the unit is shown up (78).

1.5 Background to and Definition of the Project

In 1974 and 1975 BHRA carried out a survey of 330 mechanical seals in operation in various process industries throughout the U.K. This survey clearly showed that vibration was the most important single factor leading to short seal life or high seal leakage rates (section 1.2) This confirmed the observations of many plant operators (151). Fig 1 - 6a shows the effect of vibration levels present on the pump housing on leakage rates and Fig 1 - 6b shows its effect on seal life.

When expensive or toxic fluids are being pumped it is most important that leakage is kept to a minimum. It is also important to ensure that the seals do not fail catastrophically in the middle of a process run resulting in the loss of large sums of money. However it is difficult to maintain low vibration levels on pumps on continuous duties because of the effects of wear on the pump impellor and bearings. A pump also may be running at an off-design condition which may lead to higher than expected vibration levels.

Various theories have been proposed to explain the operation of mechanical seals. However it will have been seen from the previous section that there are none that adequately describe its behaviour in a vibrating environment. As this is an important operating regime this behaviour should be quantified. The dynamic performance of a mechanical seal will depend on a number of factors. Firstly the level of vibration and the manner in which it is transmitted to the mechanical seal. This itself depends on the arrangement of the mechanical seal, the drive

mechanism and the type of secondary seal. It also depends on the fluid film at the sliding interface. Here the major factors are the fluid type, viscosity and pressure, the shaft speed and the film profile. The sealed pressure will also affect the constant load applied axially to the seal. Finally the behaviour is modified by the mass and inertia of the floating ring, which in turn depends on its design. There are thus a number of dependent and independent variables that affect the way in which a mechanical seal behaves in a vibrating environment.

The purpose of the present project is to develop and verify a viable theory for the operation of a mechanical seal in a vibrating environment. In order to prove such a theory the effects of the various factors outlined above must be predicted and verified by comparison with measurements made experimentally. Some of these factors are easier to vary than others. For instance fluid pressure and shaft speed are easily varied experimentally, whereas the design and arrangement of the mechanical seal are difficult to vary. A more detailed discussion of the various factors and the experimental values used will be found in Chapter 5.

In particular the present project is concerned with the type of mechanical seal to be found on general purpose process pumps. These pumps have shafts between 25 and 100 mm diameter. Process pumps normally run at synchronous speed (approximately 2900 rpm) although a number run at 1450 rpm and around 900 rpm. Their discharge pressures are above ambient, but generally not more than 1 MPa, and utilise rubber o-rings as the secondary seal (99).

To predict the performance of this type of mechanical seal

it is necessary to know the properties of the secondary seal, which for this project is an o-ring. It has been seen in the previous section that no suitable information about the dynamic properties of o-rings is available. The project thus also includes the measurement of the dynamic properties of o-rings and further details of this part of the project are given in chapter 4 and appendix C. The mechanical seal is loaded and driven by a single coil spring. A positive drive is obtained by using drive pins at each end of the seal.

To predict the performance of the mechanical seal theoretically, computer programs have been developed. A special form of Reynolds' equation is utilised for the fluid film that takes account of the time dependent nature of the profile of the sliding interface. (Chapter 2). An order of magnitude analysis of factors affecting the ring dynamics is given in chapter 3. Details of the solution strategy are included in the appropriate chapters and the computer programs are described in Chapter 6.

The project thus consists of two major segments. An experimental program to measure the behaviour of the floating ring of a mechanical seal for different vibrating conditions and operating conditions. Secondly the development of a computer program based on a viable theory of the dynamic behaviour of a mechanical seal that will predict the seal behaviour under the same conditions as those used in the experimental programme. The project also has a secondary part, but one that is vital to both of the major segments. This is the measurement of the dynamic properties of o-rings of various sizes and materials.

CHAPTER 2

FLUID FILM DYNAMICS

2.1 Development of a Suitable Form of Reynolds' Equation

This chapter deals with the solution of the fluid film dynamics, using a dynamic form of Reynolds' Equation due to Haardt (106). In the first section the problem will be discussed and a model of the film profile developed. Haardt's form of Reynolds' Equation will be modified and extended to model the present problem. In the second section the solution technique, also due to Haardt, will be described.

In order to solve Reynolds' Equation for the interface of a vibrating mechanical seal it is necessary to use a technique that makes optimum use of computer time and storage capacity. The technique must be relatively simple and quick because the equation will be solved a large number of times. It will also be necessary to model the dynamic film profile in a manner that is compatible with both the Reynolds' Equation solution and the solution of the ring dynamics.

To solve for the interface conditions accurately it is necessary to consider the two dimensional form of Reynolds' Equation. In addition a flow conservation technique must be used to determine the extent of the cavity that has been observed in the interface fluid film. However, such a method requires a numerical solution technique and in consequence uses considerable computer time. If an analytical solution is used, the time taken for one calculation is considerably reduced.

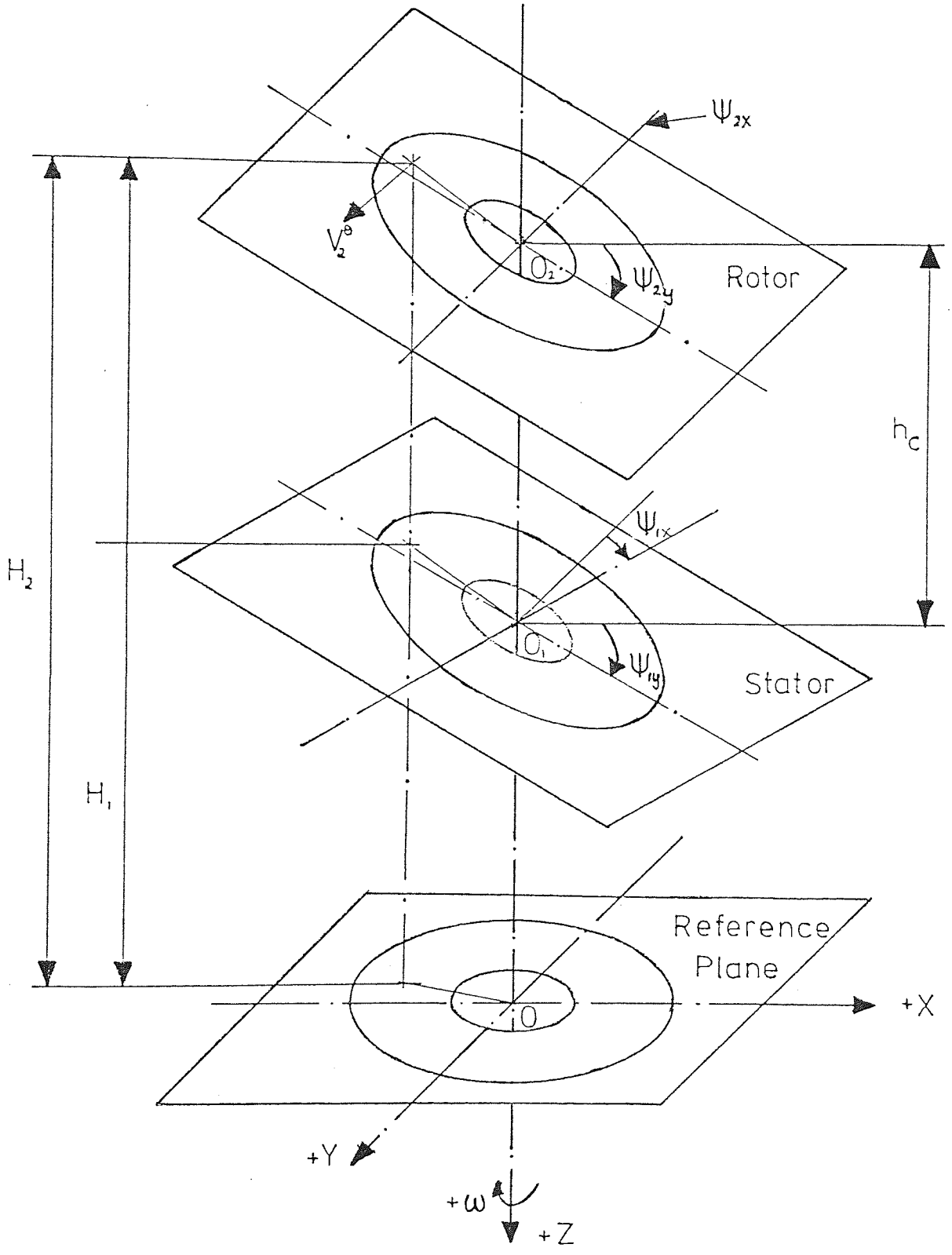

Fig 2-1 Theoretical Model of the Seal Interface

However such a technique is usually used in conjunction with arbitrarily applied cavity boundary conditions that are not justified for a mechanical seal (chapter 6). In order to overcome this problem, a flow conservation solution method could be adopted, or else arbitrary conditions applied, but ones that more accurately model the practical situation.

Fig 2 - 1 shows a diagrammatic representation of the sliding interface of a mechanical seal (106). Both the rotating and stationary faces are described relative to a reference plane which is perpendicular to the axis of rotation. It will be assumed that for each time step the position of the rotor is fixed relative to the reference plane. All the changes in the position of the rotor occur between the instantaneous calculation of the properties of the fluid film. The effects of the vibration history are thus to be neglected.

In order to utilise this model several assumptions will be made. Firstly it will be assumed that the centre of the reference plane coincides with the centre of the stationary plane. Thus H_1 only contains terms due to the misalignment of the stator and its surface profile, and H_2 contains terms due to the surface profile and misalignment of the rotor and the separation of the centre of the stator and rotor plane.

It is assumed that the position of the axes in space does not affect the problem. Their position will be chosen such that the positive X-axis coincides with a point at which the film thickness is a maximum due to the surface profile waviness. If the rotor surface is profiled this occurs at time zero only. This simplifies the calculation of the film profile since no phase angle is needed between the profile and the axes. In

addition the misalignments will be applied to the stator plane H_1 since they are fixed relative to the axes.

It is possible that both the rotor and the stator will have a wavy surface profile. However, since in practice a large number of seals are made with one hard member and the other relatively soft, for instance carbon against cast iron as in the test seal (chapter 5) it is convenient to model the interface assuming only one surface is profiled. If the surface profile is modelled by an expression of the form:-

$$h = h_a \cos(n\theta - at)$$

then if a = o the expression models the case of a profiled stator only, whereas if a = 1 the case of a profiled rotor is modelled.

In either case it will be assumed that no wear occurs. The profile will thus maintain a constant amplitude throughout the calculations.

The form of Reynolds' Equation for the condition described above has already been derived elsewhere (106). However this was concerned only with the effect of fixed misalignment angles and thus the basic equation could be simplified much further than the present problem will allow. The full form of Reynolds' Equation in two dimensions is:-

$$\frac{\partial}{\partial r}\left(\frac{r(H_2 - H_1)^3}{\eta}\frac{\partial p}{\partial r}\right) + \frac{\partial}{\partial \theta}\left(\frac{(H_2 - H_1)^3}{\eta r}\frac{\partial p}{\partial \theta}\right) =$$

$$6(H_2-H_1)\frac{\partial}{\partial r}\left(rV_{r_1} + V_{r_2}\right) + 6r\left(V_{r_1} - V_{r_2}\right)\frac{\partial(H_1+H_2)}{\partial r} \qquad 2.1\text{-}1$$

$$+ 6(H_2 - H_1)\frac{\partial}{\partial \theta}\left(V_{\theta_1} + V_{\theta_2}\right) + 6\left(V_{\theta_1} - V_{\theta_2}\right)\frac{\partial(H_1+H_2)}{\partial \theta} + 12r\left(V_{z_2} - V_{z_1}\right)$$

Suffixes 1 and 2 refer to the stationary and rotating faces respectively and hence:-

$$V_{r_1} = V_{\theta_1} = V_{z_1} = 0$$

In chapter 3 it is shown that the effects of the radial velocity are sufficiently small that they can be neglected. Then:-

$$V_{r_2} = 0$$

and the remaining velocities may be written:-

$$V_{\theta_2} = rw \qquad\qquad V_{z_2} = \frac{\partial h}{\partial t}$$

Utilising the assumptions described above expressions for H_1 and H_2 may be obtained:-

$$H_1 = -h_a \cos(n\theta - a\omega t) - r\psi_y \cos\theta + r\psi_x \sin\theta$$

$$H_2 = h_c$$

The film thickness at any point:-

$$h = H_2 - H_1$$

$$= h_c + h_a \cos(n\theta - a\omega\ell) + r(\psi_y \cos\theta - \psi_x \sin\theta)$$

The axial velocity Vz2:-

$$Vz_2 = \frac{\partial h_c}{\partial t}$$

$$= \frac{dh_c}{dt} + r\left(\frac{d\psi_y}{dt}\cos\theta - \frac{d\psi_x}{dt}\sin\theta\right) + a\omega h_a \sin(n\theta - a\omega t)$$

Substituting the above into Reynolds' Equation and rearranging gives the two dimensional form for the problem being considered. Note that $\frac{dhc}{dt} = -\frac{dz}{dt}$.

$$\frac{\partial}{\partial r}\left(\frac{rh^3}{\eta}\frac{\partial p}{\partial r}\right) + \frac{\partial}{\partial \theta}\left(\frac{h^3}{\eta r}\frac{\partial p}{\partial \theta}\right) =$$

$$-6r\left[(n-2a)\omega h_a \sin(n\theta - a\omega t) - 2\frac{dh_c}{dt}\right]$$

$$-6r^2\left[\omega\psi_x\cos\theta + \omega\psi_y\sin\theta - 2\left(\frac{d\psi_y}{dt}\cos\theta - \frac{d\psi_x}{dt}\sin\theta\right)\right] \qquad 2.1\text{-}2$$

The terms in this equation cover a wide range of orders of magnitude from the maximum pressure which may be of the order of

500 kPa to the film thickness which will be of the order of 1×10^{-6} m. For computer manipulation it is convenient to use numbers of similar orders of magnitude, reducing the effect of round-off errors. In the solution of Reynolds' equation Haardt uses the misalignment of the stationary face as one of the non-dimensionalising factors. This is not possible in our case since this misalignment varies with each time step. Similarly it is not convenient to use the mean film thickness. However by using the input value of the film thickness, and utilising the scheme set out below all the variables on the right hand side of the equation may be brought to a similar magnitude:-

$$\bar{h} = \frac{h}{h_n}$$

$$\bar{r} = \frac{r}{R_o}$$

$$\bar{h}_c = \frac{h_c}{h_n}$$

$$\bar{\psi} = \frac{R_o \psi}{h_n}$$

$$\bar{p} = \frac{h_n^2}{6\eta\omega R_o^2} p$$

$$\bar{t} = \omega t$$

The magnitudes of $\bar{p}$ and $\bar{h}$ on the left hand side will be different since $\frac{h_n^2}{6\eta\omega R_o^2} \simeq 10^{-10}$ but this is not important since they are multiplied together. The remaining non-dimensionalising coefficients are given in chapter 6.

Reynolds' Equation may now be written in non-dimensional form:-

$$\frac{\partial}{\partial \bar{r}}\left(\bar{r}\bar{h}^3 \frac{\partial \bar{p}}{\partial \bar{r}}\right) + \frac{\partial}{\partial \theta}\left(\frac{\bar{h}^3}{\bar{r}} \frac{\partial p}{\partial \theta}\right) = \bar{r}\left[-(n-2a)\bar{h}_a \sin(n\theta - at) + 2\frac{dh_c}{d\bar{t}}\right]$$

$$- \bar{r}^2\left[\bar{\psi}_x \cos\theta + \bar{\psi}_y \sin\theta - 2\left(\frac{\partial \bar{\psi}}{\partial \bar{t}} y\cos\theta - \frac{\partial \psi_x}{\partial \bar{t}} \sin\theta\right)\right] \qquad 2.1\text{-}3$$

For the sake of simplicity the bars on the non-dimensional terms will be omitted for the rest of this chapter and in the relevant parts of chapter 6. Whilst this equation is more complex than that derived by Haardt, the same solution technique may be used.

Haardt also derived the axial stiffness of the fluid film. He assumed that since the problem is a practical one and the mathematical model models it accurately, it is well posed. Thus the processes of integration and differentiation may be interchanged:-

$$\frac{\partial W}{\partial h_c} = \frac{\partial}{\partial h_c}\iint pr\ dr\ d\theta = \int\int \frac{\partial p}{\partial h_c} r dr\ d\theta$$

The problem being considered here is similar to Haardt's and the same assumption will be used.

The ring dynamics require the calculation not only of the axial stiffness of the fluid film, but also the axial damping and the stiffness and damping in the rocking modes. Each of these coefficients may be obtained in the same way by differentiating the pressure function with respect to the appropriate co-ordinate, then integrating over the surface of the fluid film. To obtain the values of the elements of the fluid film coefficients described in chapter 3 the integrations are carried out between the appropriate limits.

2.2 Solution of Reynolds' Equation

The full form of Reynolds' Equation for the problem being considered is:-

$$\frac{\partial}{\partial r}\left(rh^3\frac{\partial p}{\partial r}\right)+\frac{\partial}{\partial\theta}\left(\frac{h^3\partial p}{r\,\partial\theta}\right)=r\left[-(n-2a)ha\sin(n\theta-at)+2\frac{dh_c}{dt}\right]$$

$$-r^2\left[\psi_x\cos\theta+\psi_y\sin\theta-2\left(\frac{\partial\psi_y}{\partial t}\cos\theta-\frac{\partial\psi_x}{\partial}\sin\theta\right)\right] \qquad 2.2\text{-}1$$

Since the diameter ratio of most seals is close to one (the diameter ratio of the mechanical seal used in the experiments is approximately 0.9) the short bearing approximation discussed previously (chapter 1) may be utilised. Only the use of arbitrary positions for the cavity boundaries invalidates this approach. The equation may be rewritten:-

$$\frac{\partial}{\partial r}\left(rh^3\frac{\partial p}{\partial r}\right)=r\left[-(n-2a)\,h_a\sin(n\theta-at)+2\frac{dh_c}{dt}\right]$$

$$-r^2\left[\psi_x\cos\theta+\psi_y\sin\theta-2\left(\frac{d\psi_y}{dt}\cos\theta-\frac{d\psi_x}{dt}\sin\theta\right)\right] \qquad 2.2\text{-}2$$

This equation expresses the pressure in terms of the single variable r. This may be integrated twice to give the pressure distribution:-

$$P=\tfrac{1}{2}C_1I_1+\tfrac{1}{3}C_2I_2+K_1I_3+K_2 \qquad 2.2\text{-}3$$

where K_1 and K_2 are constants of integration and C_1, C_2, I_1, I_2 and I_3 are defined as follows:-

$$C_1=-(n-2a)\,h_a\sin(n\theta-at)+2\frac{dh_c}{dt}$$

$$C_2=-\psi_x\cos\theta-\psi_y\sin\theta-2\left(\frac{d\psi_x}{dt}\sin\theta-\frac{d\psi_y}{dt}\cos\theta\right) \qquad 2.2\text{-}4$$

$$I_1=\int\frac{r\,dr}{h^3}$$

$$I_2=\int\frac{r^2dr}{h^3}$$

$$I_3=\int\frac{dr}{rh^3}$$

where $h=h_c+h_a\cos(n\theta-at)-r(\psi_x\sin\theta-\psi_y\cos\theta)$

The constants of integration may be evaluated by considering the

pressures at the inside and outside edges of the seal. Thus:-

$$K_1 = \frac{pe-pi-\frac{1}{2}C_1(I_{1(e)}-I_{1(i)})-\frac{1}{3}C_2(I_{2(e)}-I_{2(i)}}{I_{3(e)}-I_{3(i)}}$$

$$K_2 = p_i - \tfrac{1}{2}C_1 I_{1(i)} - \tfrac{1}{3}C_2 I_{2(i)} - K_1 I_{3(i)}$$

The exact form of the integrals I_1, I_2 and I_3 will depend on whether $(\psi_x \sin\theta - \psi_y \cos\theta)$ is zero or not, since if it is the denominator of each integral becomes a constant. There are thus two cases:-

1. The general case when:-

$$h = h_c + h_a \cos(n\theta - at) - r(\psi_x \sin\theta - \psi_y \cos\theta)$$

2. the special case when $h = h_c + h_a \cos(n\theta - at)$

The total load capacity of the interface film may be obtained by integrating the pressure field:-

$$W = \int_0^{2\pi} \int_R^1 pr\,dr\,d\theta$$

The change in the axial capacity is due to changes in the position and velocity of the rotor. The total change is given by:-

$$dW = \frac{\partial W}{\partial h_c} dh_c + \frac{\partial w}{\partial v} dv + \frac{\partial w}{\partial \psi_x} d\psi_x + \frac{\partial w}{\partial \dot{\psi}_x} d\dot{\psi}_x$$

$$+ \frac{\partial w}{\partial \psi_y} d\psi_y + \frac{\partial w}{\partial \dot{\psi}_y} d\dot{\psi}_y$$

where $$v = -\frac{dh_c}{dt}$$

This is the axial resistance to motion. Each of the differential coefficients in this equation is either a stiffness or damping coefficient and may be used as such to determine the dynamics of the rotor.

The resistance to tilting is obtained by considering moments:-

$$dM_t = \frac{\partial M_t}{\partial h_c} dh_c + \frac{\partial M_t}{\partial v} dv + \frac{\partial M_t}{\partial \psi_x} d\psi_x + \frac{\partial M_t}{\partial \dot{\psi}_x} d\dot{\psi}_x + \frac{\partial M_t}{\partial \psi_y} d\psi_y + \frac{\partial M_t}{\partial \dot{\psi}_y} d\dot{\psi}_y$$

Again each differential coefficient in this equation is either a stiffness or damping coefficient and may be used as such to determine the dynamics of the rotor.

Each of the differential coefficients may be obtained as follows:-

$$\frac{\partial W}{\partial x} = \int_S \frac{\partial p}{\partial x} r \, dr \, d\theta$$

and

$$\frac{\partial M_t}{\partial x} = \int_S \frac{\partial p}{\partial x} r^2 dr \, d\theta$$

where

$$\frac{\partial p}{\partial x} = \tfrac{1}{2} C_1 \frac{\partial I_1}{\partial x} + \tfrac{1}{2} I_1 \frac{\partial C_1}{\partial x} + \tfrac{1}{3} C_2 \frac{\partial I_2}{\partial x} + \tfrac{1}{3} I_2 \frac{\partial C_2}{\partial x}$$

$$+ K_1 \frac{\partial I_3}{\partial x} + I_3 \frac{\partial K_1}{\partial x} + \frac{\partial K_2}{\partial x}$$

and x is any of the variables h_c, v, ψ_x, $\dot{\psi}_x$, ψ_y and $\dot{\psi}_y$
The forms of the expressions for the pressure differential coefficients are given in the table 2 - 1.

Finally it is necessary to consider the leakage from the seal. In order to calculate this accurately it would be necessary to solve Reynolds' equation taking full account of flow conservation. Since in this case, arbitrary boundary conditions will be used, an approximate formula must be developed. Since the cavity is a region of uniform pressure, all the flow within it will be circumferential shear flow, and the flow

$P = \frac{1}{2}C_1 I_1 + \frac{1}{3}C_2 I_2 + K_1 I_3 + K_2$
$\frac{\partial p}{\partial h_c} = \frac{1}{2}C_1\frac{\partial I_1}{\partial h_c} + \frac{1}{3}C_2\frac{\partial I_2}{\partial h_c} + K_1\frac{\partial I_3}{\partial h_c} + I_3\frac{\partial K_1}{\partial h_c} + \frac{\partial K_2}{\partial h_c}$
$\frac{\partial p}{\partial v} = \frac{1}{2} I_1\frac{dC}{dv} + I_3\frac{\partial K_1}{\partial v} + \frac{\partial K_2}{\partial v}$
$\frac{\partial p}{\partial \psi_x} = \frac{1}{2}C_1\frac{\partial I_1}{\partial \psi_x} + \frac{1}{3}I_2\frac{\partial C_2}{\partial \psi_x} + \frac{1}{3}C_2\frac{\partial I_2}{\partial \psi_x} + K_1\frac{\partial I_3}{\partial \psi_x} + I_3\frac{\partial K_1}{\partial \psi_x} + \frac{\partial K_2}{\partial \psi_x}$
$\frac{\partial p}{\partial \psi_y} = \frac{1}{2}C_1\frac{\partial I_1}{\partial \psi_y} + \frac{1}{3}I_2\frac{\partial C_2}{\partial \psi_y} + \frac{1}{3}C_2\frac{\partial I_2}{\partial \psi_y} + K_1\frac{\partial I_3}{\partial \psi_y} + I_3\frac{\partial K_1}{\partial \psi y} + \frac{\partial K_2}{\partial \psi_y}$
$\frac{\partial p}{\partial \dot{\psi}_x} = \frac{1}{3} I_2\frac{\partial C_2}{\partial \dot{\psi}_x} + I_3\frac{\partial K_1}{\partial \dot{\psi}_x} + \frac{\partial K_2}{\partial \dot{\psi}_x}$
$\frac{\partial p}{\partial \dot{\psi}_y} = \frac{1}{3}I_2\frac{\partial C_2}{\partial \dot{\psi}_y} + I_3\frac{\partial K_1}{\partial \dot{\psi} y} + \frac{\partial K_2}{\partial \dot{\psi}_y}$

Table 2-1 Expressions for Pressure Differential Coefficients

entering the cavity at the upstream end must leave across the downstream boundary. Radial flow only occurs outside the cavity. The leakage from the seal may thus be calculated from the pressure flow across the seal between the end and start of the cavity.

It can be shown that the flow rate, due to the pressure gradient, through converging or diverging annular space is given by:-

$$Q = \frac{pe-pi}{F}\left(\frac{h_i - Rh_o}{2(1-R)}\right)^3$$

where $F = \dfrac{\left(\frac{h_i}{h_c} - 1\right)\left(1 - \frac{Rh_o}{h_i}\right)}{1 - R}\left(2 + \dfrac{\left(\frac{h_i}{h_o} - 1\right)\left(1 - \left(R\frac{h_o}{h_i}\right)^2\right)}{2(1-R)\left(1-\frac{Rh_o}{h_i}\right)}\right) + \ell n \frac{h_i}{Rh_o}$

This formula may be applied to the leakage path between each cavity.

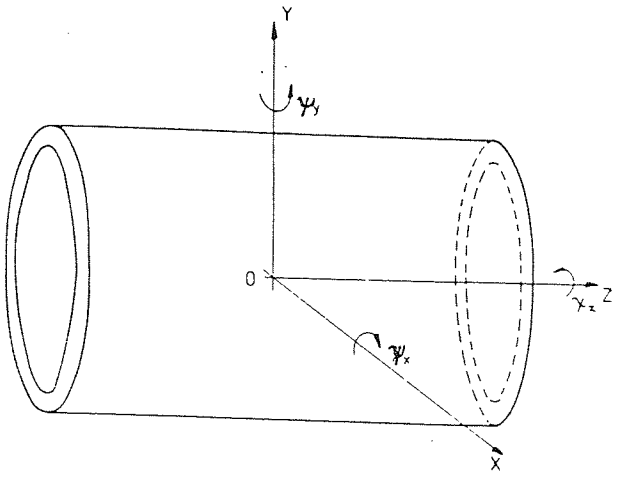

Fig 3-1 The Six Degrees of Freedom of a Rigid Body

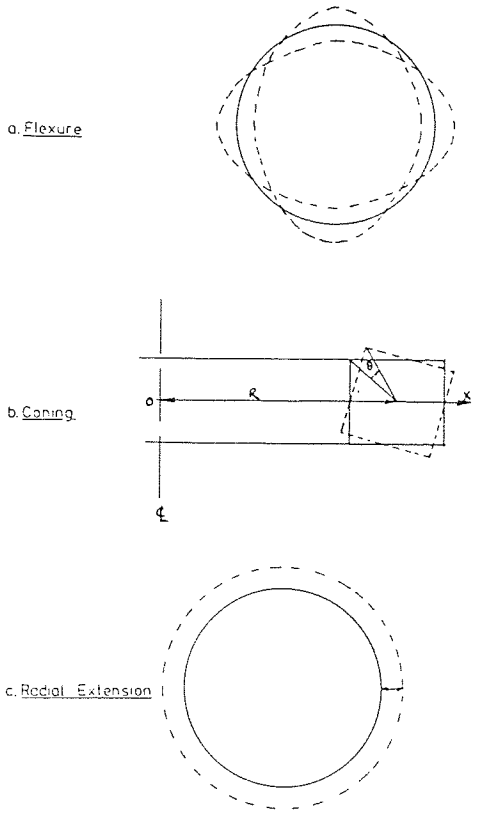

Fig 3-2 Seal Ring Distortion Modes

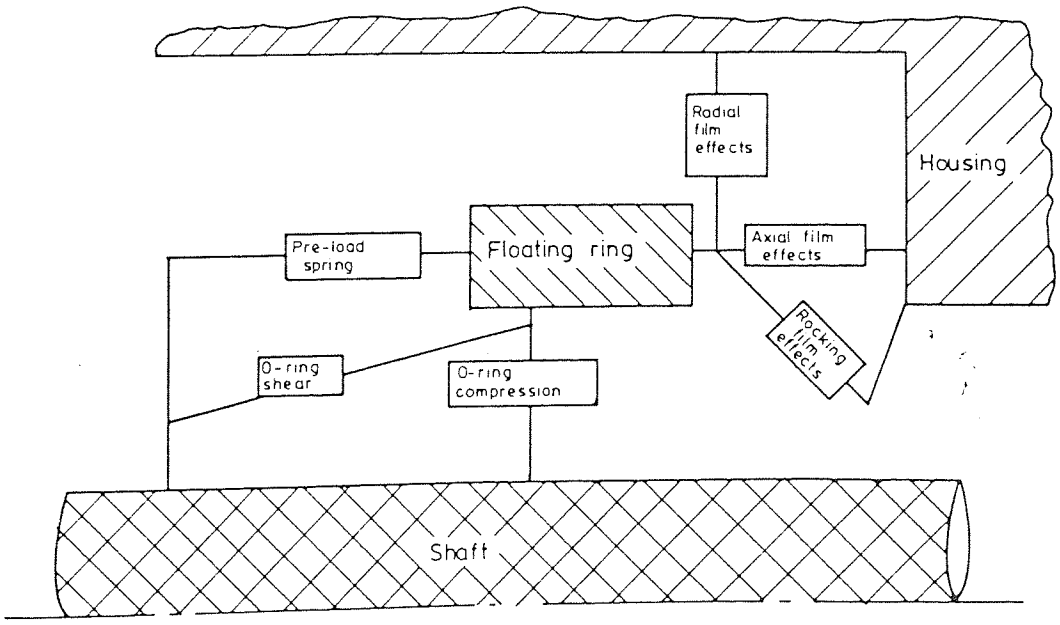

Fig 3-3 Stiffness and Damping Elements Acting on the Floating Ring

CHAPTER 3

THE DYNAMICS OF THE FLOATING RING

3.1 Approximate Analysis

The floating ring of a mechanical seal may be considered to be a rigid body. It would thus have six degrees of freedom; translation of, and rotation about the centroid for each of three mutually perpendicular axes (fig 3 - 1). However as the ring has a small wall thickness compared to its diameter it may also deform in flexure (fig 3 - 2a), torsion (fig 3 - 2b) or circumferential extension (fig 3 - 2c). There are thus nine possible degrees of freedom. By comparing the magnitude of the stiffness for each mode, it may be possible to eliminate some of these and hence only consider those most likely to occur in practice. Fig 3 - 3 shows the stiffness and damping elements acting on the ring in the rigid body mode. The magnitudes of these elements will now be calculated.

3.1.1 Ring Distortion Modes

Timoshenko (164) gives the following equation of motion for the flexural vibration of a ring:-

$$\pi r \rho A\left(1+\frac{1}{i^2}\right)\ddot{x} + \frac{EI\,\pi}{r^3}\left(1 - i^2\right)^2 x = 0$$

which may be compared with the general equation for Simple Harmonic Motion:-

$$\ddot{x} + \omega^2 x = 0$$

$$\text{where} \quad \omega^2 = \frac{\text{Stiffness}}{\text{Mass}}$$

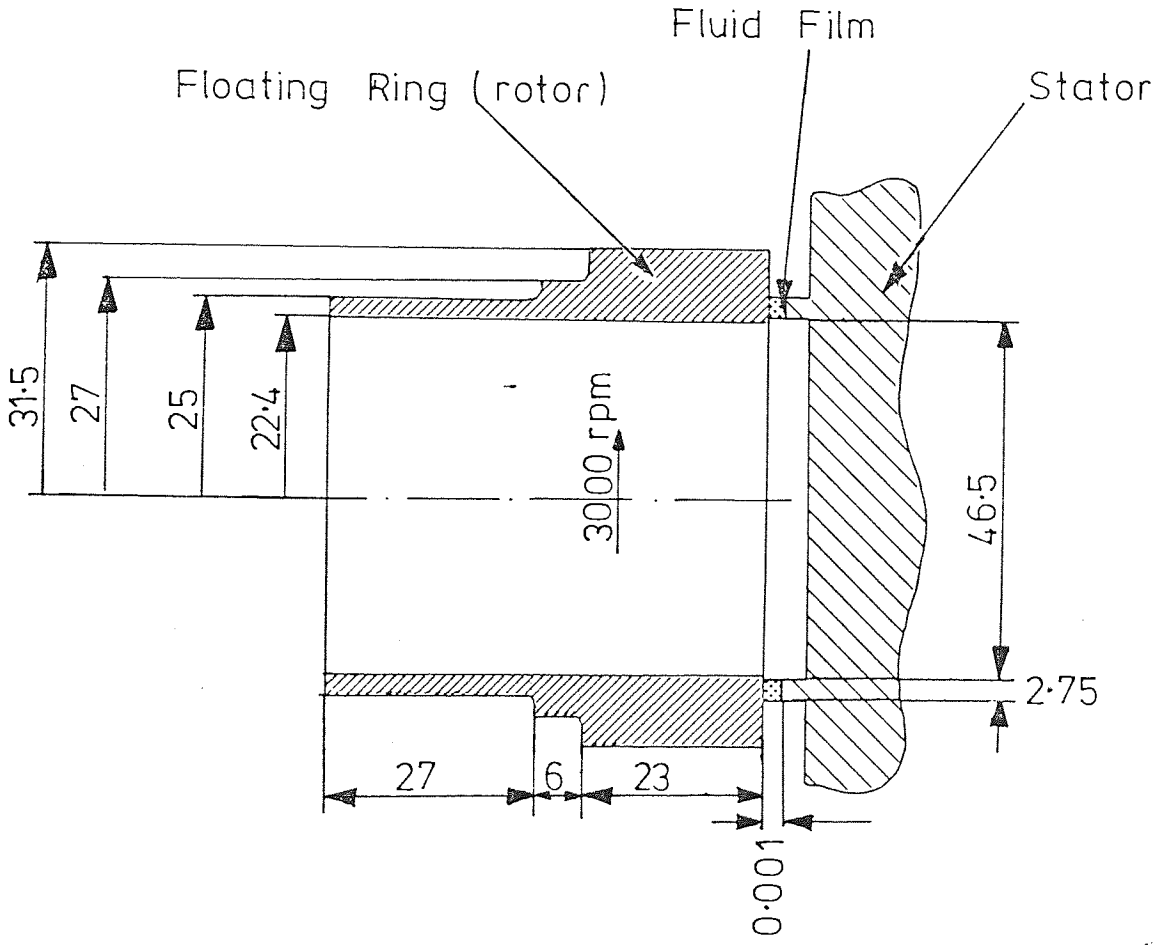

Fluid Viscosity 0·00316 N.s.m^{-2}

Fig 3-4 Details of the Floating Ring used in the Calculations with dimensions in mm

By comparing coefficients

$$\text{stiffness} = \frac{EI\,\pi}{r^3}(1 - i^2)^2 \qquad 3.1\text{-}1$$

Consider the floating ring of a mechanical seal as shown in fig 3 - 4 made of cast iron (Young's Modulus 128 GPa). For the fundamental mode i = 2, thus:-

$$\text{Stiffness} = 4.1 \times 10^{13} \text{N.m}^{-1}$$

For extension, (164):-

$$\omega^2 = \frac{E}{\rho r^2}$$

and hence:-

$$\text{Stiffness} = \frac{EM}{\rho r^2} \qquad 3.1\text{-}2$$

This gives for the ring shown in fig 3 - 4:-

$$\text{Stiffness} = 1 \times 10^{10} \text{N.m}^{-1}$$

For vibration of the section in the torsional mode (164):-

$$\frac{\omega_{torsion}}{\omega_{radial}} = \frac{Ix}{Ip}$$

Thus the stiffness in torsion is:-

$$\text{Stiffness} = \frac{EM}{\rho r^2} \qquad 3.1\text{-}3$$

$$= 1 \times 10^{10} \text{N.m}^{-1}$$

3.1.2. O-Ring and Spring Properties

From the tests on a nitrile rubber o-ring, of hardness 72 IRHD (chapter 4) the following data is obtained:-

$$\text{Stiffness} = 1.5 \times 10^{6} \text{N.m}^{-1}$$

$$\text{Damping Coefficient} = 2.1 \times 10^{3} \text{ Nsm}^{-1} \text{ at 50Hz}$$

For the spring a force of 7×10^{4}N per unit area of sealing interface may be used (94). For the seal ring considered this gives a force of 55N. It may be necessary to compress the spring 4 mm to achieve this force in a typical mechanical seal, giving:-

$$\text{Stiffness} = 1.0 \times 10^{4} \text{ N.m}^{-1}$$

3.1.3 Fluid Film - Axial Elements

To calculate the stiffness of the fluid film it is necessary first to consider what approximations may be made to the governing equation, as it is too complicated in its complete form for the present purposes. It has been shown (106), by comparing different solution methods, that the 'short bearing' approximation (75) may be applied to the fluid film at the sliding interface. This approximation assumes that the pressure gradients are small circumferentially compared to the radial pressure gradients, and that they may be ignored for the purposes of calculating the pressure field. The stiffness of the fluid film is given by (55):-

$$\text{Stiffness} = \frac{3\eta\omega}{4h^3}\left[\frac{(Ro^4 - Ri^4)\ln\left(\frac{Ro}{Ri}\right) - (Ro^2 - Ri^2)^2}{\ln\frac{Ro}{Ri}}\right]\left[\frac{64\varepsilon_2^3}{(4\varepsilon_2^2 - \varepsilon_1^2)^3} - \frac{(1+\varepsilon_2)\left[(1+\varepsilon_2)^2 - 3\varepsilon_1^2\right]}{\left[(1+\varepsilon_2)^2 - \varepsilon_1^2\right]^3}\right]$$

ε_1 defines the seal run out and may be set to zero. By defining $R = \frac{Ri}{Ro}$ the equation becomes:-

$$\text{Stiffness} = \frac{3\eta\omega\, Ro^4}{4h^3}\left[\frac{(1-R^4)\ln R + (1-R^2)^2}{\ln R}\right]\left[1 - \frac{1}{(1+\varepsilon_2)^3}\right] \qquad 3.1\text{-}4$$

For this, and all subsequent approximate calculations, the details of fig. 3-4 are used giving axial stiffness $2.8 \times 10^8 Nm^{-1}$

The circumferential extensional degree of freedom may be compared with the radial rigid body mode, in which case there will be no corresponding stiffness of the fluid film. The change in radius caused by this mode will have an effect on the load capacity of the fluid film. The following expression gives the load capacity of a fluid film of a mechanical seal with the sealed fluid on the outer periphery (30):-

$$\text{Load} = W = \frac{1}{4\ln\frac{Ro}{Ri}}\left[\pi p\left(2R_o^2 \ln\frac{Ro}{Ri} + Ri^2 - Ro^2\right) + \frac{3\eta\omega X}{2h^2}\left(\left[Ro^4 - Ri^4\right]\ln\frac{Ro}{Ri} - \left[Ro^2 - Ri^2\right]^2\right)\right]$$

$$\text{Where } X = 1 - \frac{1}{(1+\varepsilon_2)^2} = \frac{3}{4} \text{ for } \varepsilon_2 = 1 \qquad 3.1\text{-}5$$

Substituting $R_i = R_o - w$:-

$$W = \frac{1}{4}\left[\pi p\left(2R_o^2 + \frac{(Ro-w)^2-Ro^2}{\ell n\frac{Ro}{Ro-w}}\right) + \frac{9\eta\omega}{8h^2}\left(\left[Ro^4-(Ro-w)^4\right]-\frac{\left[Ro^2-(Ro-w)^2\right]^2}{\ell n\frac{Ro}{Ro-w}}\right)\right]$$

The axial stiffness of the interface film due to a small change in R_o is given by:-

$$\frac{\partial w}{\partial Ro} = \frac{1}{4}\left[\pi p\left(4Ro + \frac{2w}{\ell nR} + \frac{(R_1^2-Ro^2)w}{R_1Ro(\ell nR)^2}\right) + \frac{9\eta\omega}{8h^2}\left(4R_0^3-4R_1^3\right.\right.$$

$$\left.\left. + \frac{4(R_0^2-R_1^2)w}{\ell nR} - \frac{(R_0^2-R_1^2)^2 w}{R_0R_1(\ell nR)^2}\right)\right] \qquad 3.1\text{-}6$$

For the seal we have been considering sealing 7×10^5 Pa:-

$$\text{change in load per unit change in radius} = 1.1 \times 10^4 \text{ Nm}^{-1}$$

Although the ring will have six rigid body degrees of freedom there will only be four sources of input vibration. The remaining two degrees of freedom will be excited by the moments due to the input vibration. Axial vibration of the shaft relative to the housing will be the first source of input vibration, and will be transmitted to the floating ring by the drive spring and axial shearing of the O-ring. The second source will be speed variations, which will be transmitted through the drive spring (or drive peg if the ring is positively driven) and by circumferential shearing of the O-ring.

Finally, radial forces in the pump, shaft whip or whirl or other radial effects, will excite the ring in the two radial modes. Any of these effects that are not applied either through, or symmetrically about, the centroid of the seal ring will have a moment about the centroid. These moments will excite the floating ring in the two rocking modes about the radial axes.

If the floating ring is not positively driven than sliding could occur between the floating ring and the O-ring or the O-ring and the shaft. This may be observed on mechanical seals where friction at the sliding interface is very high (63). For the purposes of this investigation it will be assumed that the floating ring is positively driven and thus follows exactly any change in the speed of the shaft. This is not a rigorous treatment, and consideration of the effect of sliding may merit further consideration in the future. The effect of variations in the speed of rotation will be to cause a change in the load capacity of the fluid film, since:-

$$W = f(\omega)$$

The sliding velocity may be modelled with an equation of the form:-

$$V = V_m(1+\beta \sin\omega_v t)$$

By substituting this expression into equation 3.1 - 5 the effect of a small change in velocity about the mean value is obtained:-

$$\frac{\partial W}{\partial V} = \frac{9\eta R_o^4(1-R^2)}{8h^3 \ell nR}\left[(1+R^2)\,\ell nR + 1-R^2\right] \qquad 3.1\text{-}7$$

For the seal considered this gives a value:-

$$\frac{\partial W}{\partial V} = 2.4 \times 10^6 \text{Nsm}^{-1}$$

The damping of the fluid film for radial sliding may be calculated by considering the shear stress:-

$$\tau = \eta\frac{\partial V}{\partial z}$$

For laminar flow, there is a uniform velocity gradient in the fluid film and the shear force for a sliding annulus is given by:-

$$F = \frac{2R_o w \pi \eta}{h} V$$

Thus a damping coefficient can be defined:-

$$\text{Damping Coefficient} = \frac{2\eta\pi R_o w}{h} \qquad 3.1\text{-}8$$

$$\text{Damping Coefficient} = 1.4 \text{ N.s.m}^{-1}$$

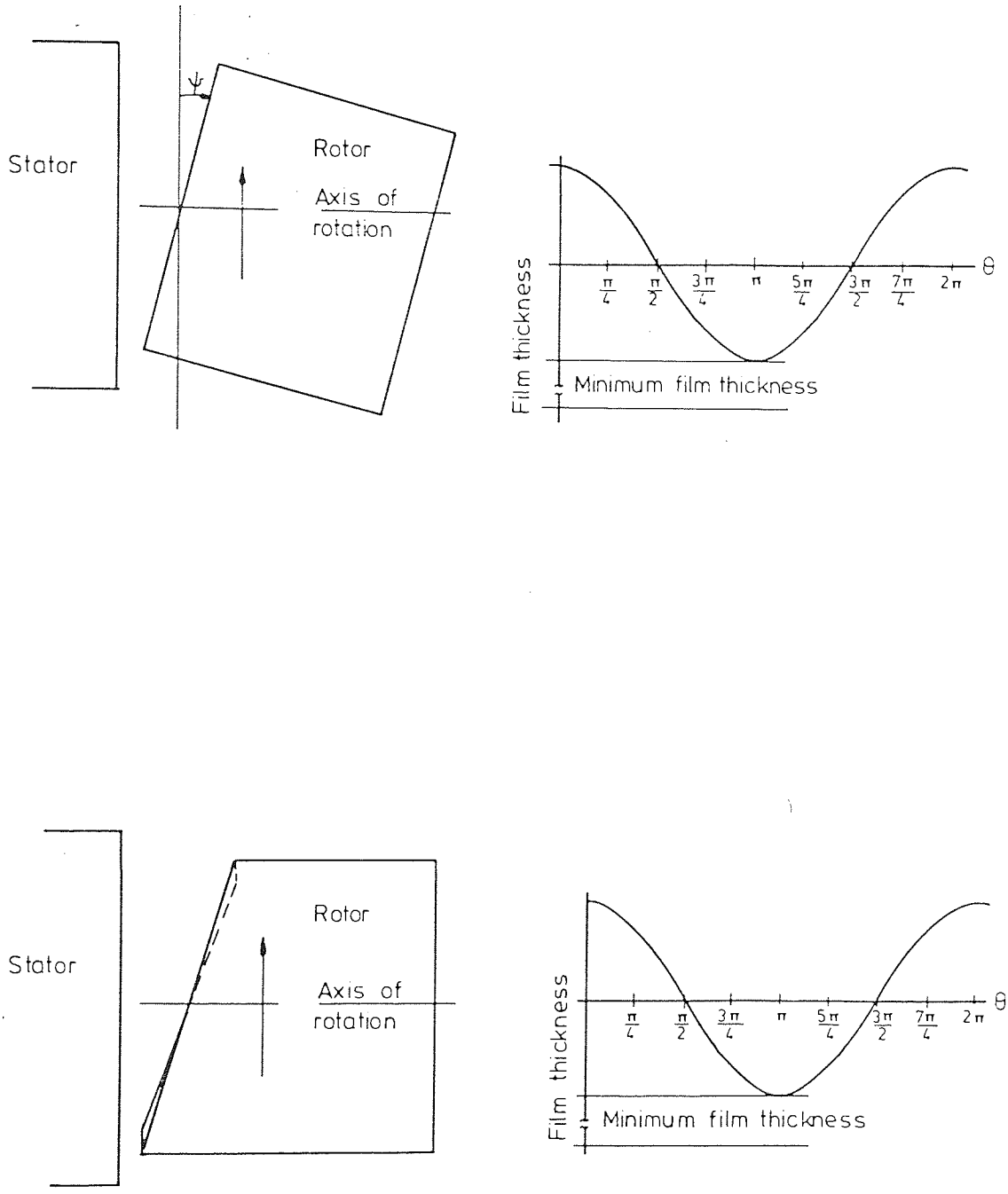

Fig 3-5 Comparison of Film Profiles

Published sources do not give formulae for axial damping coefficients or for damping or stiffness for the rocking mode. It will be appreciated that if the rotor face is misaligned by a fixed angle relative to the perpendicular to the shaft axis, and the mating face is flat, then the film thickness profile will be given, approximately, by:-

$$h = h_m + R_m \psi \cos\theta$$

(fig 3 - 5) provided that the width of the sealing interface is small compared with its diameter. This may be compared with the expression used in developing equation 3.1 - 5

$$h = h_m(1 + \varepsilon_2 \cos\theta)$$

The misaligned film thickness can be modelled by this expression if:-

$$\varepsilon_2 = \frac{R_m \psi}{h_m} \qquad 3.1\text{-}9$$

Now the stiffness due to a small change in the misalignment angle is given by:-

$$\text{Stiffness} = \frac{\partial W}{\partial \psi}$$

Substituting equation 3.1 - 9 into equation 3.1 - 5 and differentiating gives:-

$$\frac{\partial W}{\partial \psi} = \frac{3\eta\omega R_m R_o^4}{8h_m^3 \ell n \bar{R}} (1-\bar{R}^2)\left[(1+\bar{R}^2)\ell n R + 1 - \bar{R}^2\right] \frac{2}{\left(1+\frac{R_m\psi}{h_m}\right)^3} \qquad 3.1\text{-}10$$

This expression gives the axial stiffness for changes in misalignment angle. For the seal being considered assume $R_m \psi = 0.1 h_m$ and hence:-

$$\text{Stiffness} = 9.4 \times 10^6 \ \text{N.rad}^{-1}$$

To calculate a damping coefficient, which is change in load capacity due to a small change in velocity we require a time dependent term in the Reynolds' equation, and hence the derivation of the pressure distribution and load capacity. Reynolds'

equation, using the 'short bearing ' approximation (75) may be written

$$\frac{\partial}{\partial r}\left(rh\frac{\partial p}{\partial r}\right) = 6\eta r\omega\frac{\partial h}{\partial \theta} + 12r\eta\frac{\partial h}{\partial t} \qquad 3.1\text{-}11$$

And thus:-

$$P = \frac{3\eta\omega\frac{\partial h}{\partial \theta} + 6\eta\frac{\partial h}{\partial t}}{2h^3 \ell nR}\left[(r^2-Ri^2)\ell nR+(Ro^2-Ri^2)\ \ell n\ \frac{r}{Ri}\right] - ps\ \frac{\ell n\frac{r}{R}}{\ell nR} \qquad 3.1\text{-}12$$

Assuming that there is no misalignment angle or velocity the damping coefficient may be derived from the expression for the pressure. Assuming that the cavity extends over three quarters of the film (142), then:-

$$\frac{\partial W}{\partial V} = \int_{Ri}^{Ro}\int_{\frac{\pi}{2}}^{\pi}\frac{\partial p}{\partial V}\, r\, dr d\theta$$

and hence:-

$$\frac{\partial W}{\partial V} = \frac{3\eta\ Ro^4(1-R^2)}{4\ h_m{}^3 \ell nR}\left[(1+R^2)\ell nR+1-R^2\right]\ \left(\frac{\pi}{2}+\frac{3ha}{hm}\right) \qquad 3.1\text{-}13$$

giving a damping coefficient:-

$$\frac{\partial W}{\partial V} = 4.0 \times 10^6\ N.s.m^{-1}$$

The damping coefficient due to a misalignment velocity may be derived in a similar manner. In this case for simplicity assume that there is no circumferential surface profile. The pressure field is given by equation 3.1 - 12 with:-

$$h = h_m + R_m\ \psi \cos\theta$$

The damping coefficient is given by:-

$$\frac{\partial W}{\partial \dot{\psi}} = \int_{Ri}^{Ro}\int_{\frac{\pi}{2}}^{\pi}\frac{\partial p}{\partial \dot{\psi}}\, r\ dr\ d\theta$$

which gives:-

$$\frac{\partial w}{\partial \dot{\psi}} = \frac{-3\eta R_o{}^4 R_m}{4h^3{}_m \ell nR}\left(1-\frac{3\pi R_m\psi}{4h_m}\right)\left[(1+R^2)\ell nR+1-R^2\right]\ (1-R^2) \qquad 3.1\text{-}14$$

which may be evaluated to give:-

$$\frac{\partial W}{\partial \psi} = 1.2 \times 10^5\ N.s.rad^{-1}$$

3.1.4 Fluid Film - Moment Elements

In addition to the axial force due to the various displacements and velocities, each displacement and velocity will have a related moment stiffness or damping coefficient. A representative value for each of these will be obtained by calculating moments about an axis at right angles to that passing through the point of minimum film thickness. These elements differ from the axial elements only in the form of the integral. Thus for the stiffness related to the axial displacement:-

$$\frac{\partial m}{\partial h_m} = \int_{\frac{\pi}{2}}^{\pi}\int_{Ri}^{Ro} \frac{\partial p}{\partial h_m} r\cos\theta \; r \; dr d\theta$$

giving:-

$$\frac{\partial m}{\partial h_m} = \frac{9\eta\omega R_o^5 h_a}{2h_m^4 \ell nR}\left[\frac{1}{2} + \frac{4h_a}{3h_m} + \frac{3h_a^2}{3h_m^2}\right]\left[\frac{2}{15}(1-R^5)\ell nR + \frac{1}{9}(1-R^2)(1-R^3)\right] \quad 3.1\text{-}15$$

Which gives a stiffness:-

$$\frac{\partial M}{\partial h_m} = -5.9 \times 10^6 \; N.m.m^{-1}$$

Similarly the moment stiffness related to a misalignment angle is given by:-

$$\frac{\partial M}{\partial \psi} = \int_{\frac{\pi}{2}}^{\pi}\int_{Ri}^{Ro} \frac{\partial p}{\partial \psi} r\cos\theta \; r \; dr \; d\theta$$

$$= \frac{-3\eta\omega R_m R_o^5}{2h_m^3 \ell nR}\left[\frac{2}{15}(1-R^5)\ell nR + \frac{1}{9}(1-R^2)(1-R^3)\right]\left(\frac{1}{2} - \frac{2R_m\psi}{h_m} + \frac{2R_m^2\psi^2}{h_m^2}\right) \quad 3.1\text{-}16$$

Which gives a stiffness:-

$$\frac{\partial M}{\partial \psi} = -4.9 \times 10^4 \; Nm.\; rad^{-1}$$

The moment damping coefficient relating to an axial velocity is given by:-

$$\frac{\partial M}{\partial V} = \int_{\frac{\pi}{2}}^{\pi}\int_{Ri}^{Ro} \frac{\partial p}{\partial V} r\cos\theta \; r dr d\theta$$

ELEMENT	MODE	STIFFNESS	DAMPING COEFFICIENT
FLUID FILM			
Axial	FORCE	$2.8\times10^{8}\,Nm^{-1}$	$4.0\times10^{6}\,Nsm^{-1}$
Radial	"	-	$1.4Nsm^{-1}$
Change in Radius	"	$1.1\times10^{4}Nm^{-1}$	-
Misalignment	"	$9.4\times10^{6}Nrad^{-1}$	$1.2\times10^{5}Nsrad^{-1}$
Change in Speed	"	-	$2.4\times10^{6}Nsm^{-1}$
Axial	MOMENT	$-5.9\times10^{6}Nmm^{-1}$	$-6.8\times10^{4}Nmsm^{-1}$
Misalignment	MOMENT	$-4.9\times10^{4}Nm\,rad^{-1}$	$-5.7\times10^{2}Nmsrad^{-1}$
DRIVE SPRING	FORCE	$1\times10^{4}Nm^{-1}$	-
O-RING (50 Hz)	COMPRESSION	$1.5\times10^{6}Nm^{-1}$	$2.1\times10^{3}Nsm^{-1}$
FLOATING RING			
Distortion	RADIAL	$1\times10^{10}Nm^{-1}$	-
"	TORSION	$1\times10^{10}Nm^{-1}$	-
"	FLEXURE	$4.1\times10^{13}Nm^{-1}$	-

Table 3 - 1 Stiffness and Damping Elements

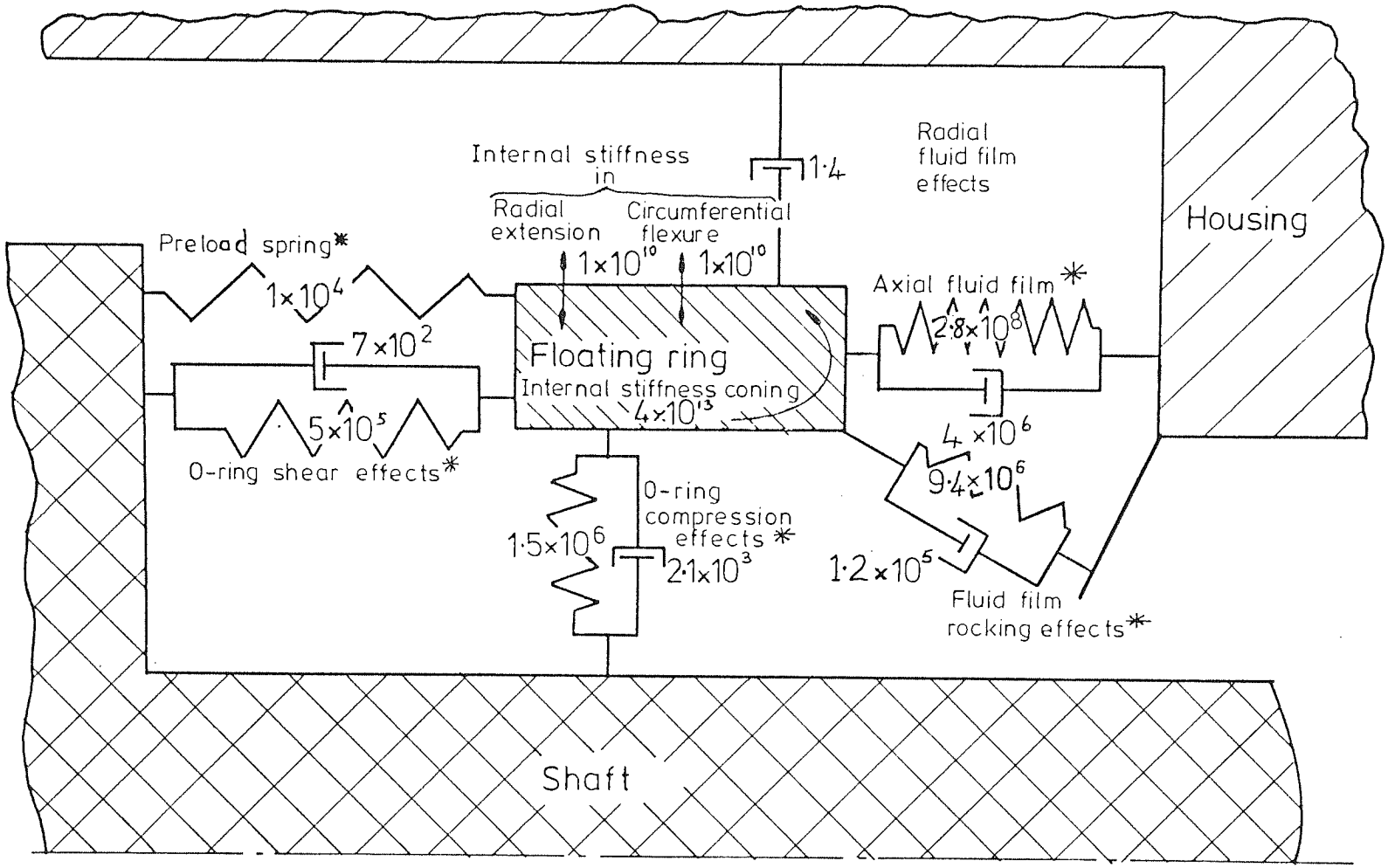

Fig 3-6 Approximate Values of Stiffness and Damping Elements Affecting the Floating Ring

$$= \frac{3\eta\ Ro^5}{hm^3\ lnR}\left(1+\frac{3\pi\ ha}{4h_m}\right)\left[\frac{2}{15}\ (1-R^5)\ lnR+\frac{1}{9}\ (1-R^2)(1-R^3)\right]$$

Which gives a damping coefficient:- 3.1-17

$$\frac{\partial m}{\partial V} = -\ 6.8\ \times\ 10^4 N.m.s.m^{-1}$$

Finally the moment damping coefficient related to a misalignment angular velocity is given by:-

$$\frac{\partial m}{\partial \dot{\psi}} = \int_{\frac{\pi}{2}}^{\pi}\int_{R_i}^{R_o} \frac{\partial p}{\partial \dot{\psi}}\ r\ \cos\theta dr dr d\theta$$

$$= -\frac{3\eta Ro^5 Rm}{hm^3 \ell nR}\left[\frac{2}{15}\ (1-R^5)\ \ell nR + \frac{1}{9}\ (1-R^2)(1-R^3)\right]\left(\frac{\pi}{4}-\frac{2Rm\psi}{hm}\right) \qquad 3.1\text{-}18$$

Which gives a damping coefficient:-

$$\frac{\partial m}{\partial \dot{\psi}} = -5.7\ \times\ 10^2\ N.m.s.rad^{-1}$$

A more detailed derivation of the expressions not taken directly from published sources will be found in Appendix A.

3.1.5 Conclusions

The elements acting on the floating ring in the rigid body mode and the stiffness in the distortion modes are summarised in Table 3 - 1. Some of these elements are represented diagrammatically on fig 3 - 6. It is obvious that the ring distortion stiffnesses are very much larger then the other elements. For the seal being considered here they may be ignored. The floating ring may thus be treated as a rigid body as far as the ring dynamics are concerned. Seals with much larger diameters, and hence a smaller width to radius ratio,(δ1) would have a lower section modulus and would thus be less stiff. The approximate equations used here will indicate when it is necessary to consider the distortion modes.

Three further elements will also be neglected. Firstly,

as it is assumed that the ring does not distort, the fluid film stiffness related to changes in the radius may be neglected. Secondly the damping coefficient related to radial motion is small and may be neglected. Finally it will be assumed that the floating ring is positively driven at a uniform speed, and the damping coefficient relating to changes in shaft speed will be neglected.

3.2 The Equations of Motion

In this section the equations of motion for the floating ring will be developed. These equations will utilise the elements shown in the previous section to be significant. Five degrees of freedom will be considered, linear translation along the axes OX, OY and OZ and rotation about OX and OY.

Figures 3 - 7a and b show the elements acting on the floating ring in the XOZ and YOZ planes respectively. The fluid film has three linear stiffness and damping elements, and three moment elements in each plane making nine stiffness and nine damping coefficients altogether. The spring force and the unbalanced axial force due to the sealed pressure are shown as a combined force acting on the end of the seal ring. Clearly this force is balanced about the shaft axis and only affects the axial translation along OZ.

To set up the equations of motion Newton's Laws will be used. It will be assumed that the axes are fixed in space and the positive OX direction coincides with a maximum film thickness due to the stator surface profile or a maximum film thickness at timestep zero due to the rotor surface profile

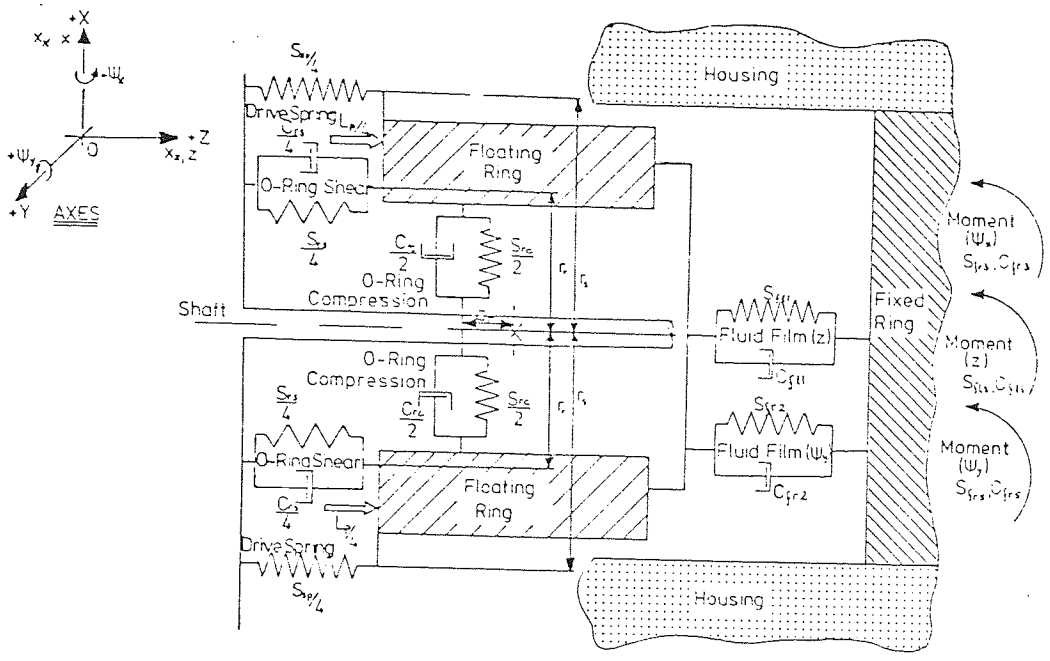

(a) Plane XOZ

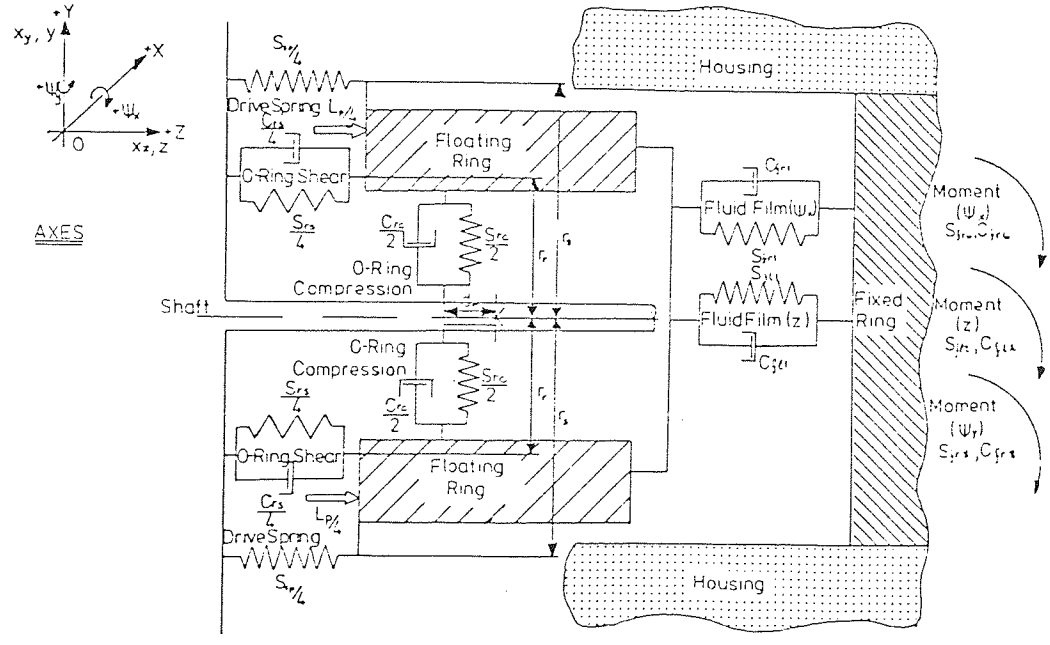

(b) Plane YOZ

Fig 3-7 Elements Acting on the Floating Ring.

(chapter 2). It will also be assumed that because the movements of the floating ring are small, no force acting on the ring will have a component at right angles to its original line of action. A typical misalignment angle would give a film thickness similar to that due to residual surface waviness. For a 50 mm diameter seal this would require a misalignment angle of 0.5×10^{-6} radians. Because of this, the usual assumptions with regard to the sines and cosines of the misalignment angles will be made. In the analysis the differential operator $D \left(\equiv \frac{\partial}{\partial t} \right)$ will be used. The motion variables are tabulated in table 3 - 2.

TABLE 3 - 2 MOTION VARIABLES

AXIS	MOTION	VARIABLE	
		MOTION OF CENTROID	MOTION OF SHAFT
OX	TRANSLATION	x	x_x
	ROTATION	ψ_x	
OY	TRANSLATION	y	x_y
	ROTATION	ψ_y	
OZ	TRANSLATION	z	x_z

For lateral translation along OX, the force equation (from fig 3 - 7a) is:-

$$\frac{Src}{2}(x_x - x - d_r\psi_y) + \frac{Crc}{2} D\,(x_x - x - d_r\psi_y)$$

$$+ \frac{Src}{2}(x_x - x - d_r\psi_y) + \frac{Crc}{2} D\,(x_x - x - d_r\psi_y) = MD^2x$$

Rearranging this equation gives the equation of motion for this mode of vibration:-

$$\left[MD^2 + CrcD + Src\right]x + \left[C_{rc}d_rD + S_{rc}d_r\right]\psi_y = \left[C_{rc}D + Src\right]x_x \qquad 3.2\text{-}1$$

Similarly for lateral translation along OY, the equation of motion is:-

$$\left[MD^2 + C_{rc}D + S_{rc}\right]y - \left[C_{rc}d_rD + S_{rc}d_r\right]\psi_x = \left[C_{rc}D + S_{rc}\right]x_y \qquad 3.2\text{-}2$$

From figures 3 - 7a and b, noting that the axial fluid film elements are shown on both figures, the force equation for this mode is:-

$$L_p - L_w + Srs(x_z - z) + C_{rs}D(x_z - z) - S_{fl_1}z - C_{fl_1}Dz$$

$$-S_{fr1}\psi_x - C_{fr_1}D\psi_x - S_{fr_2}\psi_y - C_{fr_2}D\psi_y + S_{sp}(x_z - z) = MD^2z$$

Collecting terms and rearranging gives the equation of motion for this mode:-

$$\left[MD^2 + (C_{rs} + C_{fl_1})D + S_{rs} + S_{fl_1} + S_{sp}\right]z + (C_{fr_1}D + S_{fr_1})\psi_x + (C_{fr_2}D + S_{fr_2})\psi_y$$

$$= (C_{rs}D + S_{rs} + S_{sp})x_z + L_p - L_W \qquad 3.2\text{-}3$$

To develop the equations of motion for the angular mode it is necessary to take moments about the centre of gravity of the floating ring. For these modes only the o-ring compression, spring and the fluid film moments need to be considered as the other elements are balanced about the centre of gravity.

For rotation about OX, the elements on the YOZ plane are considered:-

$$\left(-\frac{S_{sp}}{2}r_s^2 - \frac{S_{rs}}{2}r_r^2\right)\psi_x - C_{rs}r_r^2D\psi_x - Src(x_y - y + d_r\psi_x)d_r$$

$$-C_{rc}D(\psi_y - y + d_r\psi_x)d_r + S_{fr_4}\psi_x + C_{fr_4}D\psi_x + S_{fl_2}z + C_{fl_2}Dz$$

$$+S_{fr_6}\psi_y + C_{fr_6}D\psi_y = ID^2\psi_x$$

Rearranging this equation gives the equation of motion for this mode:-

$$\left[ID^2 + \left(\frac{Crs}{2} r_r^2 + C_{rc}d_r^2 - C_{fr4}\right)D + \frac{Ssp}{2} r_s^2 + \frac{Srs}{2}r_r^2 + Srcd_r^2 - S_{fr_4}\right]\psi_x$$

$$- (C_{rc}d_rD + S_{rc}d_r)y - (C_{fl2} + S_{fl2})z - (C_{fr6}D + S_{fr6})\psi_y$$

$$= - (C_{rc}d_rD + S_{rc})\, x_y \qquad 3.2\text{-}4$$

Similarly for rotation about OY:-

$$\left[ID^2 + \left(\frac{Crs}{2} r_r^2 - C_{rc}d_r^2 - C_{fr_5}\right)D + \frac{Ssp}{2} r_s^2 + \frac{Srs}{2}r_r^2 - S_{rc}d_r^2 - S_{fr_5}\right]$$

$$+ (C_{rc}d_rD + S_{rc}d_r)\, x - (C_{f\ell_3}D + S_{f\ell_3})z - (C_{fr_3}D + S_{fr_3})\,\psi_x$$

$$= (C_{rc}d_rD + S_{rc}d_r)\, x_x \qquad 3.2\text{-}5$$

It will be seen from equations 3.2 - 3, 3.2 - 4 and 3.2 -5 that there is coupling between all five degrees of freedom.

These equations of motion may be written in matrix form:-

$$([M]D^2 + [C]D + [S])\,[X_0] = [P] \qquad 3.2\text{-}6$$

where:-

$$[M] = \begin{vmatrix} M & & & & \\ & M & & & \\ & & I & & \\ & & & I & \\ & & & & I \end{vmatrix}$$

$$X_0 = \begin{Bmatrix} x \\ y \\ z \\ \psi_x \\ \psi_y \end{Bmatrix}$$

$$[S] = \begin{vmatrix} S_{rc} & 0 & 0 & 0 & C_{rc}d_r \\ 0 & S_{rc} & 0 & -S_{rc}d_r & 0 \\ 0 & 0 & S_{rs}+S_{fl1}+S_{sp} & S_{fr1} & S_{fr2} \\ 0 & -S_{rc}d_r & -S_{fl2} & \frac{S_{rs}r_r^2}{r} + S_{rc}d_r^2 + \frac{S_{sp}r_s^2}{2} - S_{fr4} & -S_{fr6} \\ S_{rc}d_r & 0 & -S_{fl3} & -S_{fr3} & \frac{S_{rs}r_r^2}{2} + S_{rc}d_r^2 + \frac{S_{sp}r_s^2}{2} - S_{fr5} \end{vmatrix}$$

$$[C] = \begin{vmatrix} C_{rc} & 0 & 0 & 0 & C_{rc}d_r \\ 0 & C_{rc} & 0 & -C_{rc}d_r & 0 \\ 0 & 0 & C_{rs}+C_{fl1} & C_{fr1} & C_{fr2} \\ 0 & -C_{rc}d_r & -C_{fl2} & \frac{C_{rs}}{2}r_r^2 + C_{rc}d_r^2 - C_{fr4} & -C_{fr6} \\ C_{rc}d_r & 0 & -C_{fl3} & -C_{fr3} & \frac{C_{rs}r_r^2}{2} + C_{rc}d_r^2 - C_{fr5} \end{vmatrix}$$

$$[F] = \begin{vmatrix} (C_{rc}D+S_{rc})X_x \\ (C_{rc}D+S_{rc})X_y \\ (C_{rs}D+S_{rs}+S_{sp})X_z + L_p - L_w \\ -(C_{rc}D+S_{rc})d_rX_y \\ (C_{rc}D+S_{rc})d_rX_x \end{vmatrix}$$

3.3 Solution of the Equations of Motion

Several methods of analysis are available for solving the equations of motion in the form of equation 3.2 - 6. A normal modes analysis could be carried out (163) or the problem solved as an eigenvector problem. However these methods do not give the displacements directly and are best suited to problems with constant coefficients. Although the results obtained (chapter 6) are for constant coefficients the present work is intended to lead to a more comprehensive computer program in which the present separate programs are combined. The solution technique must therefore handle time varying coefficients and recalculate the displacements (and velocities) directly at each time step.

Two techniques have been used. Firstly, in order to reduce possible errors a modified finite difference scheme was used (73). This technique has a truncation error of the order of Δt^6, compared with truncation errors of the order of Δt^3 for backward differencing. However this method proved to be unstable when tested on the problem data and on the simple spring-mass-damping model used for testing the program (chapter 6). This solution technique is described more fully in Appendix B.

It is not certain why the method is unstable. At very small timesteps (values of Δt less than 0.001, equivalent to $\frac{1}{10}$ th^{o} Arc) the

displacements calculation is stable, but not the velocity calculation. The method utilises the second (acceleration) and third differentials at the timestep, and any error in the starting values quickly results in an instability. The technique is used for calculating the response of buildings to earth tremors. It is essentially a central difference technique in which the position at the next timestep is predicted from the forcing function, velocity, acceleration and third differential at the present timestep and the displacement at the previous timestep. It seems that this is the probable reason for its instability. Whilst the next displacement is predicted (explicitly) there is no correction applied as in, for instance the Runge-Kutta integration, and small errors may build rapidly into an instability. The method is not being applied strictly as a solution for the position of the floating ring at any timestep as a result of the forces acting on the ring at that timestep.

A standard Taylor's Series expansion was therefore applied in order to obtain the difference equations from the second order differential equations developed above. The backward difference scheme was used in order to calculate the present position of the floating ring as a function of the forces acting on the ring and the previous displacements.

The differential coefficients are thus:-

$$D^2x_o = \frac{x_i - 2x_{i-1} + x_{i-2}}{\Delta t^2} \qquad Dx_o = \frac{3x_i - 4x_{i-1} + x_{i-2}}{2\Delta t}$$

And equation 3.2 - 6 becomes:-

$$([M]\frac{[X_o]_i - 2[Xo]_{i-1} + [Xo]_{i-2}}{\Delta t^2} + [C]\frac{3[Xo]_i - 4[Xo]_{i-1} + [Xo]_{i-2}}{2\Delta t} + [S][Xo]_i) = [P]_i$$

Rearranging this gives the five simultaneous equations in matrix form which may be solved for the displacements by a Gaussian Elimination technique.

$$\left(\frac{[M]}{\Delta t^2} + \frac{3[C]}{2\Delta t} + [S]\right)[Xo]_i = [P]_i + \left(\frac{2[M]}{\Delta t^2} + \frac{2[C]}{\Delta t}\right)[Xo]_{i-1} - \left(\frac{\{M\}}{\Delta t^2} + \frac{[C]}{2\Delta t}\right)[Xo]_{i-2}$$

This may be applied for each timestep except the first. At the first timestep ($t = \Delta t$), $[X]_{i-2}$ is undefined. However by considering the starting conditions its value may be defined. For instance, if it is assumed that the calculations start at a time when the displacement in any given mode is a maximum then the undefined displacement $x_{t=-\Delta t}$ is:-

$$x_{t=-\Delta t} = x_{t=\Delta t}$$

for simple harmonic motion. If the initial displacement is zero or at any other point between the maximum and minimum values then the undefined displacement $x_{t=-\Delta t}$ is given by:-

$$x_{t=-\Delta t} = x_{t=o} - (x_{t=\Delta t} - x_{t-o})$$

$$= 2x_{t=o} - x_{t=\Delta t}$$

Both of these conditions could be used as appropriate, however it would be more satisfactory to program only one condition and accepting a small error when the other condition applies.

The initial position of the floating ring is not easy to define since it will depend on the equilibrium of the various forces acting on it. By assuming static equilibrium an initial condition may be calculated. These values may then be used as $[X_o]_{i-1}$ at $t = \Delta t$ and $[X_o]_{i-2}$ at $t = 2\Delta t$.

Radially, the initial position may be defined as:-

$$X = 0$$

$$y = y_{max} \hat{=} X_y$$

For the axial and angular positions three equilibrium equations may be obtained by resolving axially and taking moments about the centre of gravity for the planes XOZ and YOZ:-

$$(S_{sp} + S_{rs} + S_{fl1})z + S_{fr1}\psi_x + S_{fr2}\psi_y = L_p - L_W$$

$$- S_{fl2}z + \left(\frac{S_{sp}r_s^2}{2} + \frac{S_{rs}r_r^2}{2} + S_{rc}d_r^2 - S_{fr4}\right)\psi_x - S_{fr6}\psi_y = S_{rc}d_r y$$

$$- S_{fl3}z - S_{fr3}\psi_x + \left(\frac{S_{sp}r_s^2}{2} + \frac{S_{rs}r_r^2}{2} - S_{fr5} - S_{rc}d_r^2\right)\psi_x = S_{rc}d_r x$$

These may be rearranged in matrix form:-

$$[A][X] = [B]$$

where

$$[A] = \begin{vmatrix} (S_{sp}+S_{rs}+S_{fl1}) & S_{fr1} & S_{fr2} \\ -S_{fl2} & \left(\frac{S_{sp}r_s^2}{2} + \frac{S_{rs}r_r^2}{2} + S_{rc}d_r^2 - S_{fr4}\right) & -S_{fr6} \\ -S_{fl3} & -S_{fr3} & \left(\frac{S_{sp}r_s^2}{2} + \frac{S_{rs}r_r^2}{2} - S_{fr5} - S_{rc}d_r^2\right) \end{vmatrix}$$

$$[B] = \begin{vmatrix} L_p - L_W \\ S_{rc}d_r y \\ -S_{rc}d_r x \end{vmatrix}$$

$$[X] = \begin{vmatrix} z \\ \psi_x \\ \psi_y \end{vmatrix}$$

These equations may be solved to give the initial position.

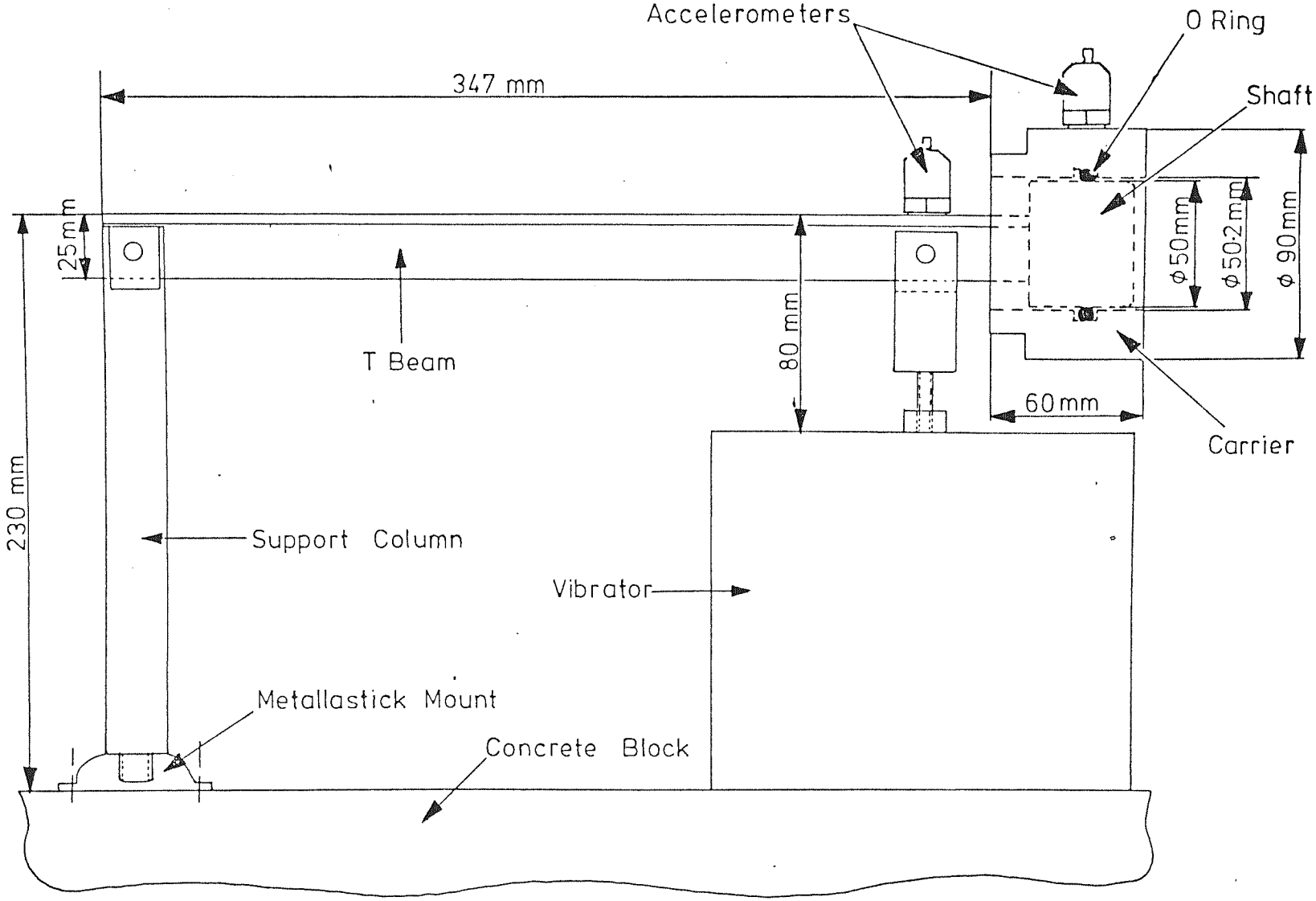

Fig 4-1 First O-Ring Test Rig Design

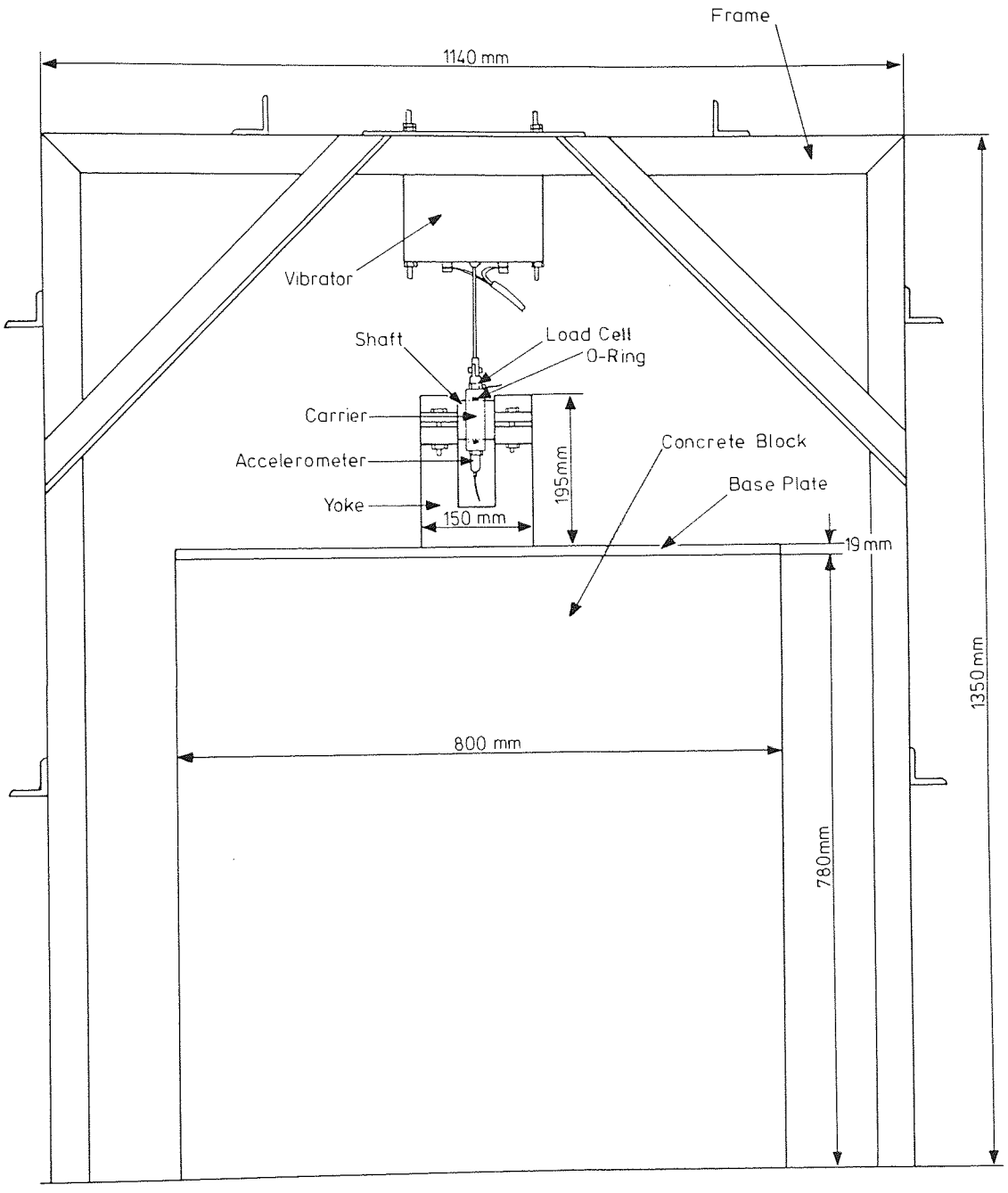

Fig. 4-2 Second O-Ring Test Rig-Basic Design

CHAPTER 4

O-RING EXPERIMENTS

4.1 Test Rig Design

In this chapter the o-ring stiffness and damping experiments will be discussed. In this first section the design of the test rig will be described. In subsequent sections the experimental programme, analysis and results will be discussed.

4.1.1 Design Criteria

Two test rigs were built for the o-ring experiments. The first design was based on an overhung shaft supported partially by the vibrator (Fig 4 - 1), and carrying the floating ring of a mechanical seal. It was intended to utilise the rig to investigate the effects of a fluid film by running a rotating disc against the floating ring with a fluid film between them. However, the proving tests on this rig showed that resonance of the T-Beam was occurring within the test frequency range. The rig and proving tests are described in Appendix C.

The second rig was designed purely for the o-ring tests, and was constructed to be as stiff as possible to avoid any resonances within the test frequency range. This resulted in a rig that was too heavy to be supported by the vibrator. Therefore the yoke supporting the shaft was bolted to a base-plate and the vibrator carried by a frame as shown in fig 4 - 2 . The main criterion in designing this rig was that it should be adequately stiff for the experiments. The rig was also to be suitable for measuring the properties of the o-rings

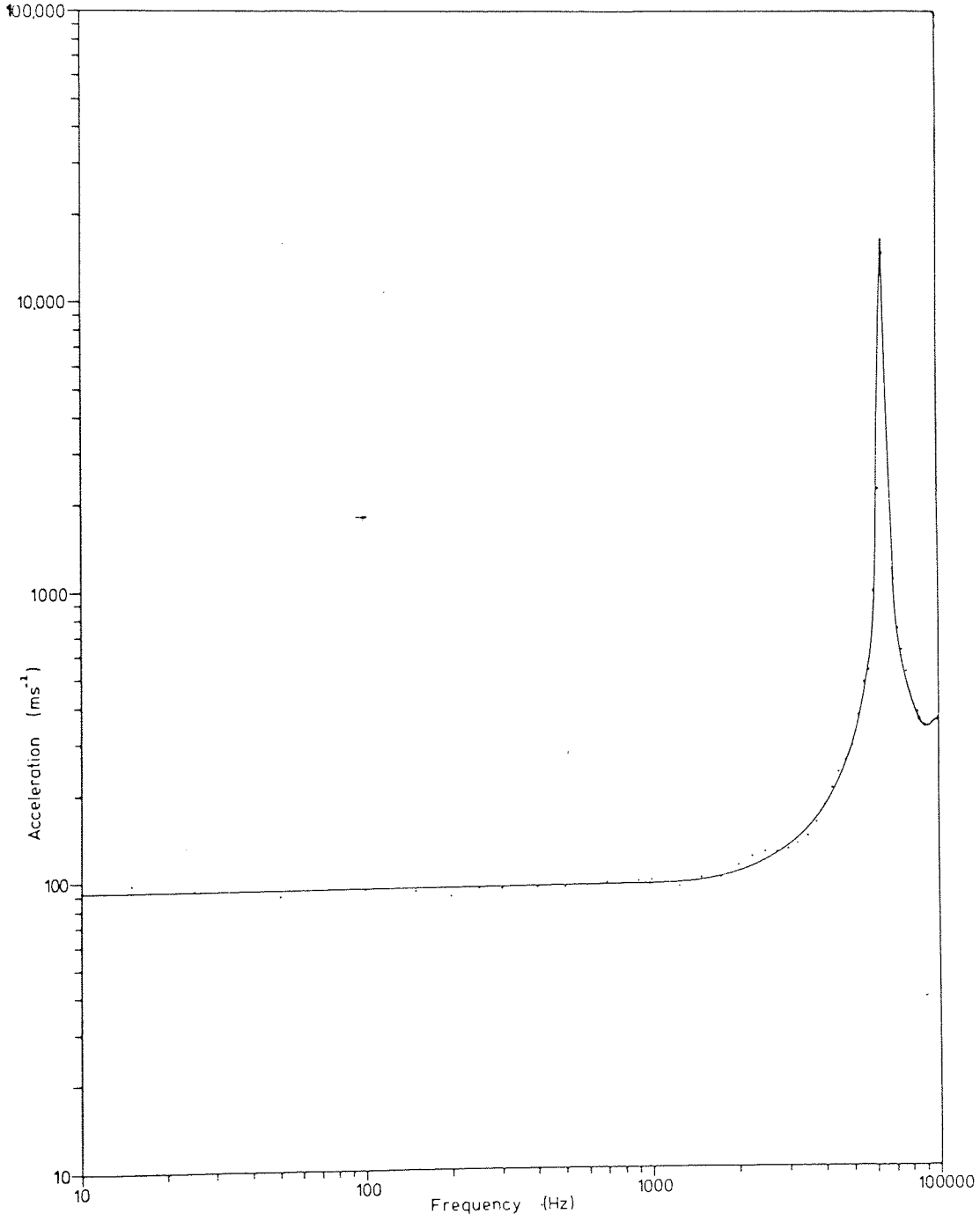

Fig. 4-3 Resonance Curve for Load-Cell Mass System

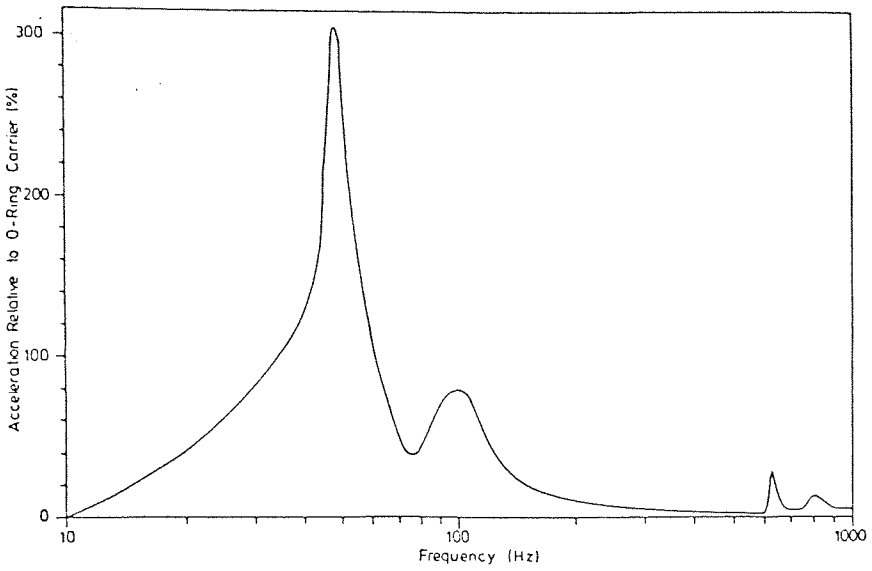

Fig. 4-4 Vibration of Vibrator Mounting Plate

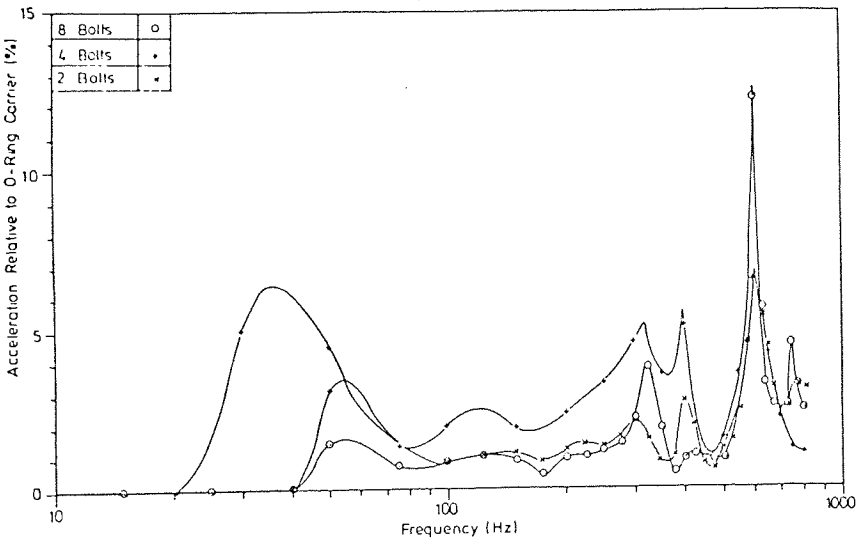

Fig. 4-5 Vibration of 19mm Base Plate - Effect of Clamping

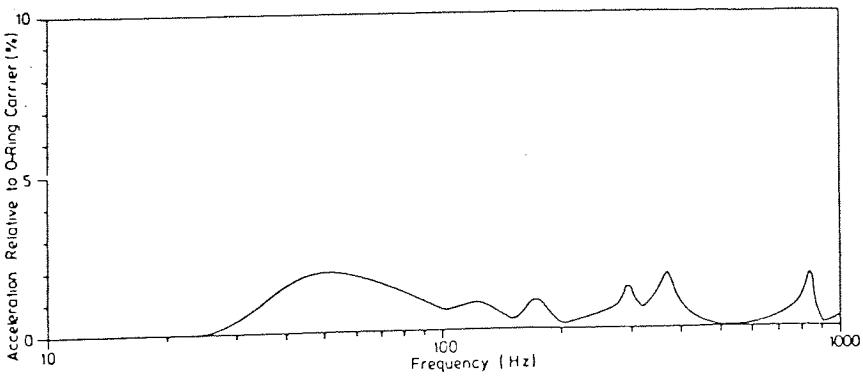

Fig. 4-6 Vibration of 100 mm Base Plate

used in the mechanical seal rig, as well as the o-rings obtained for the experiments described in this chapter.

4.1.2 Final Rig Design

The basis of the second rig design is shown in fig 4 - 2. However, the design was not finished until various proving tests were carried out. The first test was to discover the resonance of a load cell-mass system. The total mass vibrated was 0.2189 Kg and, from the load cell manufacturer's data, the expected resonance frequency was 6880 Hz. The measured resonance curve is given in fig 4 - 3. The measured resonance frequency is 6450 Hz. The o-ring carrier has a mass of 0.564 Kg and the resonance frequency of the load cell-carrier system would be 4020 Hz.

The second tests were designed to discover whether any part of the rig exhibited resonances that might affect the experimental results. Fig 4 - 4 shows the vibration of the vibrator mounting plate. The results indicate that measurements around 50, 100, 625 and 800 Hz could be in error due to resonance of the vibrator mounting plate. Fig 4 - 5 shows the vibration of the base plate, and indicates resonant vibration about 600 Hz. Further tests showed that this resonance could be varied by varying the clamping method as shown by the other curves of fig 4 - 5. The base plate was replaced by a thicker plate, 100 mm thick, and the mounting of the yoke changed. Fig 4 - 6 shows that there was no significant vibration of the new base plate.

Fig 4 - 7 shows the final design of the test rig. The

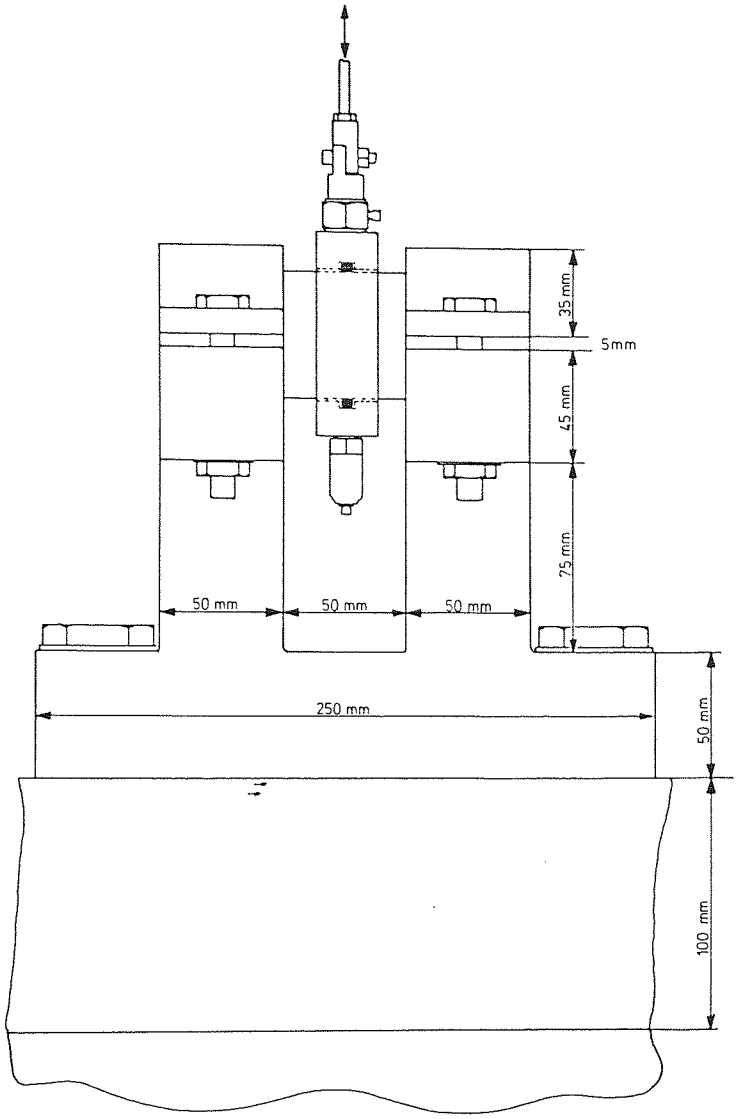

Fig 4-7 Second O-Ring Test Rig-Final Design of Base Plate and Yoke

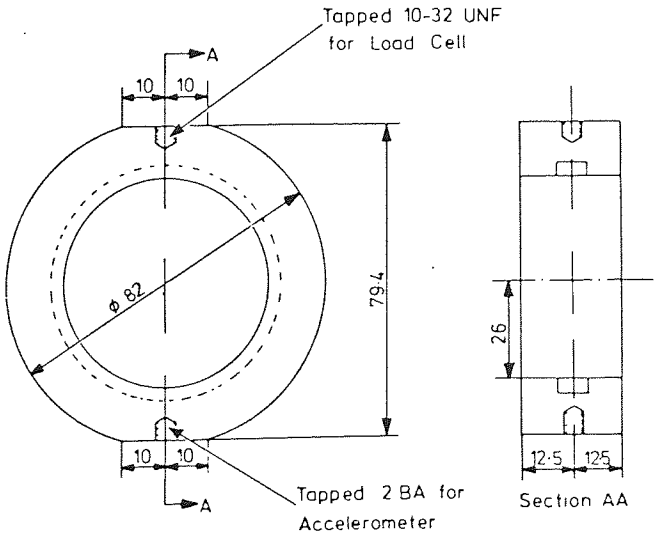

Fig. 4-8 O-Ring Carrier Details- Dimensions in mm

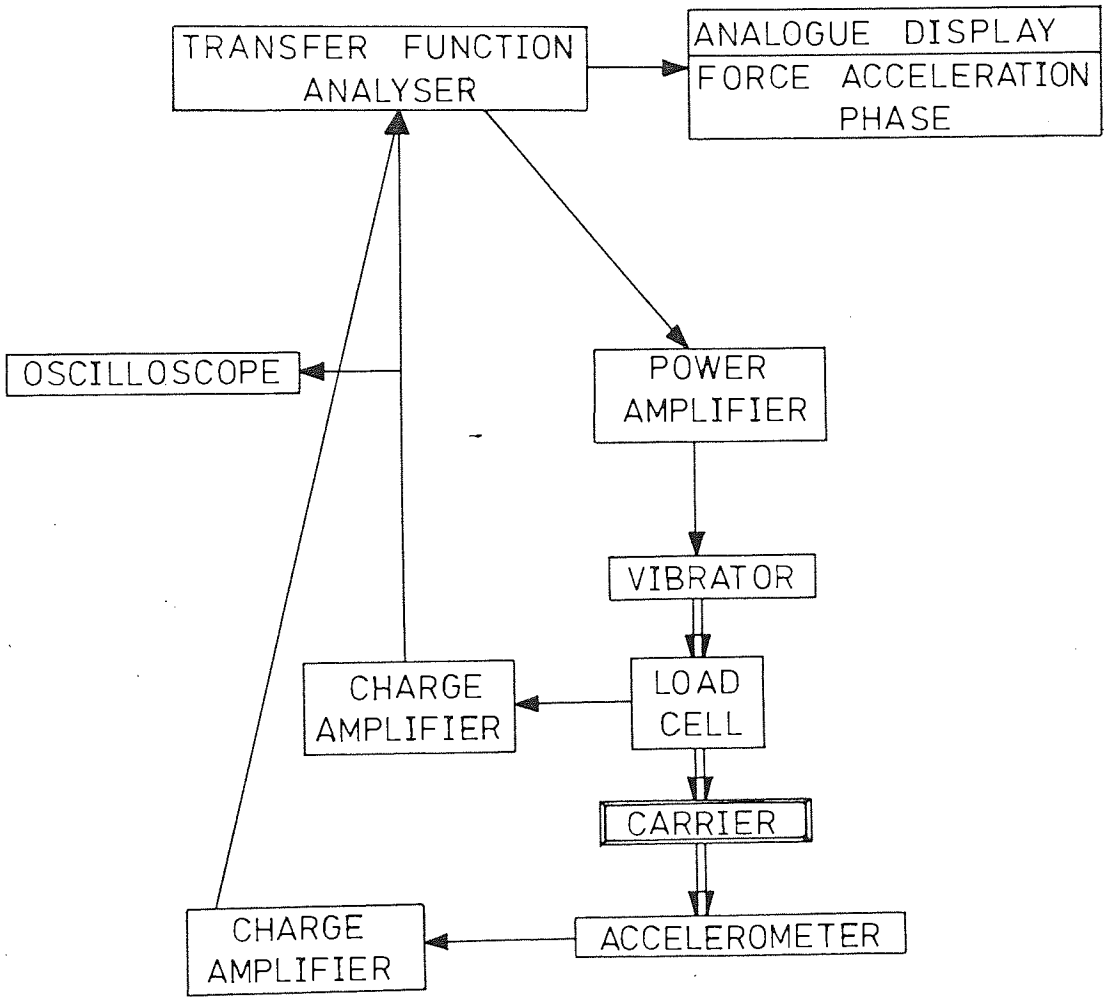

Fig. 4-9 Electronic Circuit Block Diagram

APPARATUS	MAKE	DETAILS
VIBRATOR	Goodmans Model 390A	100N Maximum force at 1kHz: frequency range DC to 4kHz (nominal)
FREQUENCY RESPONSE ANALYSER	Solartron 310 Frequency Response Analyser	Frequency Range 0.02Hz to 20kHz Output 10mV to 10V rms Accuracy: Frequency ±1% Amplitude ±1% Phase ±1°(at FSD)
CHARGE AMPLIFIERS	Vibro-meter Type TA-2/C	
LOAD CELL	Bruel and Kjaer 8200	0-1kN Tension 0-5kN Compression Linearity ±1% FS Resonance frequency 36kHz
ACCELEROMETER	Electromechanisms Type QZE	Frequency range 4Hz to 20kHz Resonance frequency 115kHz

Table 4 - 1 Experimental Apparatus

main dimensions of the test rig are given on the diagram. Details of the o-ring carrier are given in fig 4 - 8.

The signals from the load cell and accelerometer are analysed by a Frequency Response Analyser, which also produces the excitation signal for the vibrator. The analyser displays the transducer signal as an rms amplitude in mV and a phase angle relative to the phase of the oscillator signal. The electronic circuit block diagram is shown on fig 4 - 9, and a list of the apparatus in table 4 - 1.

4.2 The Experimental Programme

4.2.1. Programme Design Criteria

The purpose of the experimental programme was to determine the effect of various parameters on the stiffness and damping coefficient of o-rings. The programme design must ensure that only the required parameters have an effect on the properties for a given test run. The o-rings to be used for these tests were specially obtained from the manufacturer to ensure uniform properties.

O-rings may be moulded from various polymers, and the properties will depend on the base polymer. In addition to this the compounding, such as the use of oil extenders and fillers such as carbon black, will also affect the properties (chapter 1). For this reason the o-rings obtained were of the same compound. Despite this, the o-ring may exhibit different properties due to being moulded in different cavities of a multicavity mould or in different moulds because the heat cycle it is subjected to may vary, thus affecting the curing process. In

addition variations in a compound from batch to batch may also have an effect.

The properties of an o-ring of a given size will thus be affected by:-

(1) the compound

(2) the batch of compound

(3) the mould in which the o-rings are moulded

(4) the number of times the mould cavity has been charged (which is a measure of wear of the cavity in use)

(5) the cavity in which the ring is moulded, for o-rings moulded in a multi-cavity mould.

It is reasonable to expect that the minimum variation of properties will be obtained for rings moulded from the same compound, batch, mould, and if appropriate the same cavity. Only small changes are likely to occur with successive charges of the cavity. This variation is the baseline against which the significance of variations in the properties would be measured.

The object of the test programme is to quantify the variation, if significant, between o-rings resulting from changes in the above parameters. Initially the minimum variation will be measured by testing rings from a given cavity. Having ascertained this, the variation resulting from changing the cavity, the batch of compound and finally the mould will be measured. By comparing the results it should be possible to determine the likely spread of properties for o-rings whose moulding history is unknown. This information can be used when considering the properties of the o-rings used in the mechanical seal test rig, as these o-rings have not been specially purchased, a situation

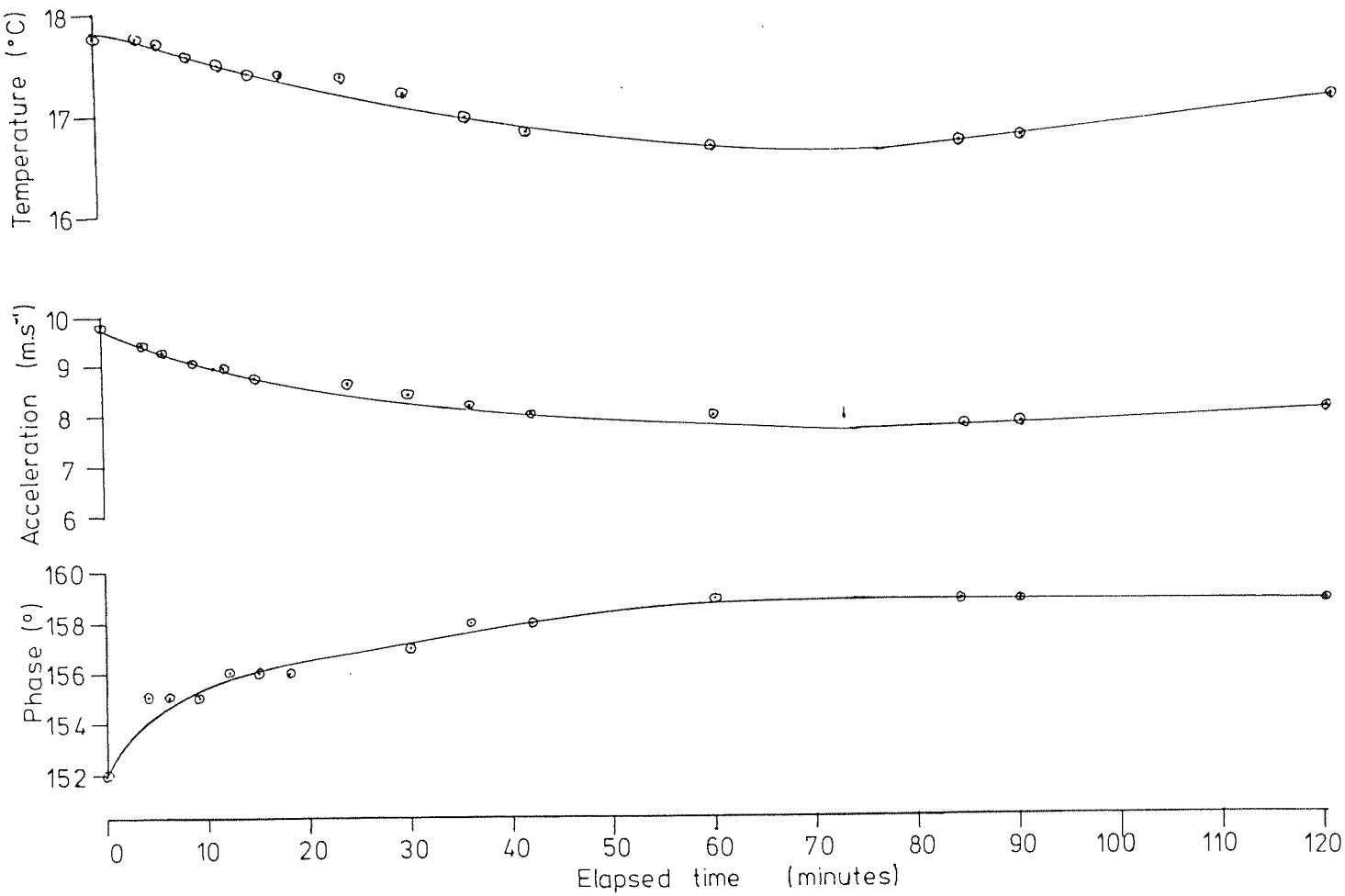

Fig 4-10 Variation of Carrier Response and O-Ring Temperature with Time

which is typical of normal practice.

4.2.2 Final Programme Design

It has already been shown that a number of production parameters may affect the values of the o-ring properties obtained in any tests. The test programme is designed to quantify this. In addition the experimental programme can introduce errors if various factors are not carefully controlled.

The temperature of a rubber compound can have a considerable effect on its properties. Thus the temperature at which the o-ring is tested can have a considerable effect on the measured values of the o-ring stiffness and damping coefficients. With the design of the test rig used it is not possible to maintain a constant temperature. The temperature of the o-ring was monitored throughout the tests by a thermocouple mounted in the o-ring at 90^{o} to the face axis. This position was chosen to have the minimum effect on the measurement of the o-ring properties. The results can then be transformed to a standard temperature using the WLF transform (section 4 - 3).

This method requires that the o-ring temperature is constant throughout the test. Fig 4 - 10 shows the variation of temperature, acceleration and phase with time. This shows that, after a large drop in the level of the acceleration initially, the acceleration remains constant for approximately an hour. The phase angle is also approximately constant over this period. Provided that a settling in period of 30 minutes is allowed, measurements may be made for up to an hour without any appreciable errors occurring.

The amplitude of the sinusoidal deformation will affect the

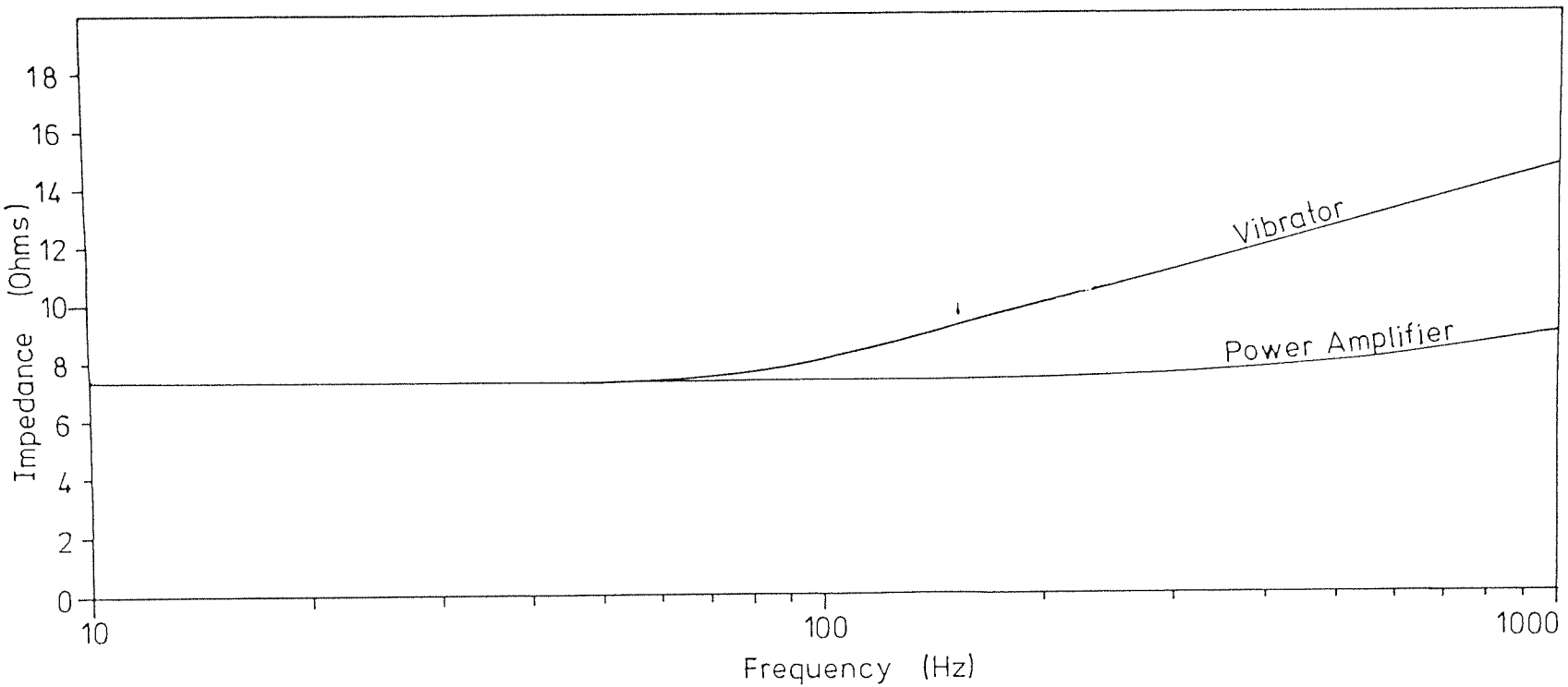

Fig 4-11 Power Amplifier and Vibrator Impedance Diagram

values of the stiffness and damping coefficient. In order to eliminate any errors due to changes in the vibration amplitude, it must be kept constant over the entire frequency range. This was attempted by carrying out the tests at an acceleration level proportional to the square of the frequency.

The actual acceleration levels it was possible to achieve were limited by the test rig. At low frequencies the output impedance of the power amplifier and the input impedance of the vibrator are matched (fig 4 - 11). However at high frequencies, the input impedance of the vibrator increases rapidly whilst the output impedance of the power amplifier remains substantially constant. This causes considerable distortion of the signal generated by the analyser signal generator and limits the upper frequency at which measurements can be made. This in turn limits the lowest frequency at which measurements can be made because the acceleration becomes too small at low frequencies. The useful frequency range is 10 to 1000 Hz (equivalent to 600 - 60,000 rpm). This gives an acceleration range of 0.012 to 120 ms^{-2}, equivalent to a vibration amplitude of 3 μm, or 0.06% of the o-ring cross section diameter.

The final check on the programme design was to ensure that the rig could be assembled the same way each time, without rolling or twisting the o-ring. A perspex carrier was machined to the same dimensions as the steel carrier. The mould flash on an o-ring was marked with white correcting fluid and the o-ring assembled into carrier. The carrier was fitted onto the shaft in the normal way with a very light smear of oil. The assembly procedure was repeated several times, but on no occasion was any twisting or rolling of the o-ring observed.

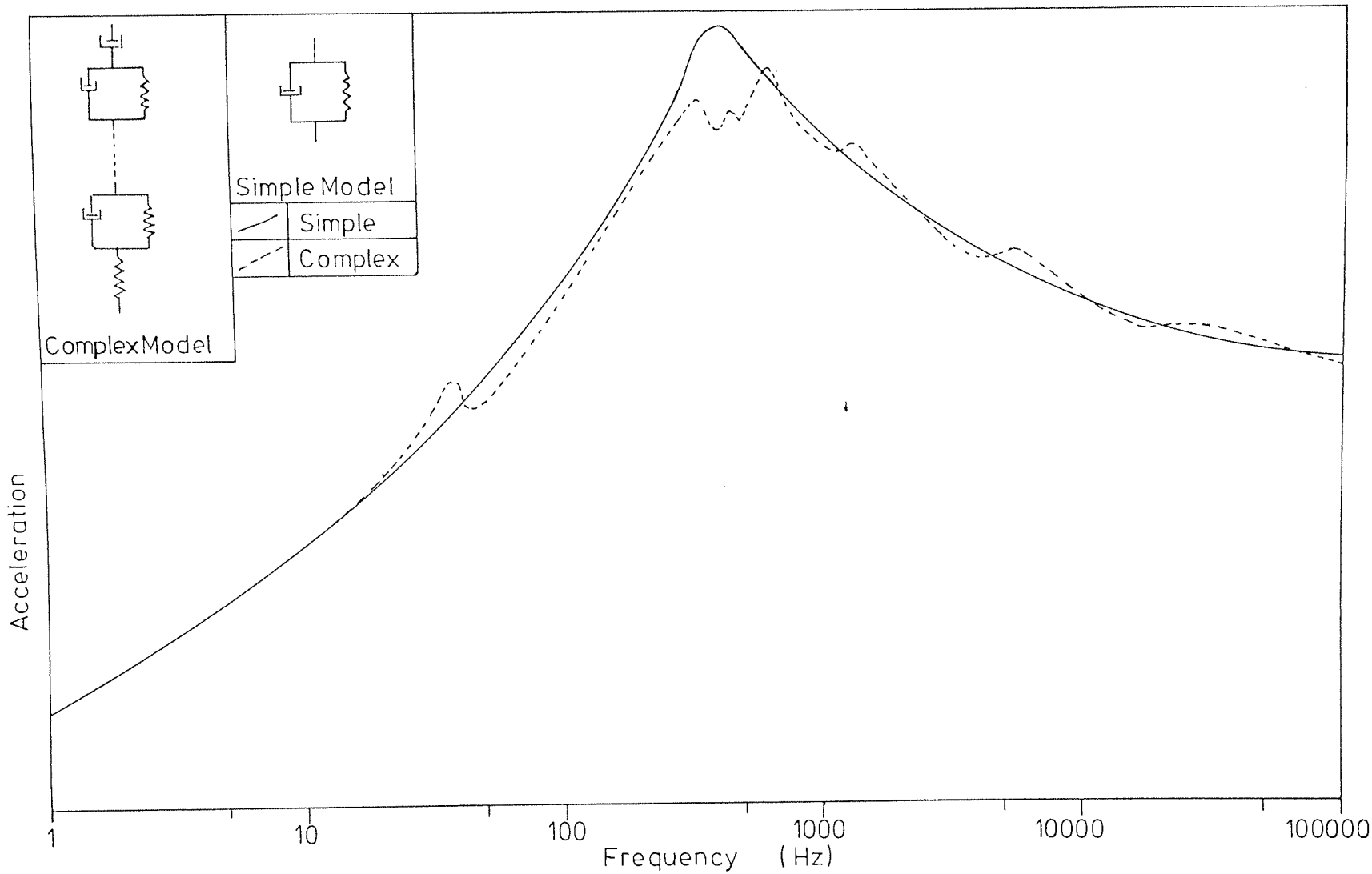

Fig 4-12 Theoretical Response of an O-Ring/Carrier System Simple and Complex Models

The following procedure was adopted:-

(1) Assemble the rig and vibrate for 30 minutes at 300 Hz and 20 N force

(2) For each test frequency, set the required value, set the acceleration level to the required value and measure the force level and phase:-

(a) starting at 10 Hz to 1000 Hz

(b) starting at 1000 Hz to 10 Hz

(c) spot checks throughout the frequency range.

4.3 Analysis Procedure and Estimation of Errors

In this chapter so far the design of the experimental rig and the test programme has been described. This section will consider the analysis of the results and the effect of possible experimental errors.

4.3.1 Viscoelastic Models and Analysis

In chapter 1 the behaviour of a typical elastomer was described. This behaviour is difficult to explain with simple models but more complex models are difficult to analyse. In chapter 3 the analysis of the dynamics of the ring were carried out by assuming that the O-ring behaviour could be described by a simple Kelvin element with constant stiffness and damping. The difference between the response of the two systems is shown in fig (4 - 12), which has been taken from the literature (89). It will be seen that the difference is not very significant. In order to analyse the response it is convenient to model the behaviour using a second order

differential equation with constant coefficients as the solution of such an equation is well known (168). The problem of the variation of the stiffness and damping with frequency may be overcome by carrying out the analysis at each measured frequency rather than using the complete response curve. An analysis of more complex models may be found in the literature (8).

The acceleration of a mass supported on a Kelvin element, as a function of the element properties, excitation force and frequency is given by (168):-

$$\ddot{x} = \frac{-f\omega^2 \sin(\omega t + \phi)}{\sqrt{(s - M\omega^2)^2 + C^2\omega^2}} \qquad 4.3-1$$

where $\tan\phi = \frac{-C\omega}{s - M\omega^2}$

By making the appropriate substitutions, expressions for the stiffness and damping coefficient in terms of the frequency force, acceleration and phase angle between the force and acceleration may be obtained:-

$$S = \omega^2 \left(M - \frac{f\cos\phi}{\ddot{x}}\right) \qquad 4.3-2$$

$$C = \frac{f\omega\sin\phi}{\ddot{x}} \qquad 4.3-3$$

Using these expressions the stiffness and damping coefficient at each frequency may be calculated.

4.3.2 Temperature Correction

In the previous section it was shown that the behaviour of the o-ring varied with its temperature. As it was not possible to maintain the rig at a constant temperature, the temperature of the o-ring during each test was monitored. These temperatures may be used in conjunction with the WLF equation (96) to transform all the results to the same reference temperature. The logarithmic frequency shift from the temperature T at which

measurements are made, to the reference temperature T_o is given by the WLF equation:-

$$\log a_T = - \frac{C_1^o (T - T_o)}{C_2^o + T - T_o} \qquad 4.3-4$$

The measured frequency of the coefficients C_1^o and C_2^o depend on the polymer and the reference temperature. The suppliers of the o-rings had no information on the glass transition temperature of the actual compound, but the polymer is a 39% acrylonitrile butadiene co-polmer. From the literature (144) the glass transition temperatures for the quoted polymers are:-

acrylonitrile 377 K

butadiene 165 K

The glass transition temperature for the compound is found by averaging the values for the individual polymer in proportion with their proportion of the compound.

This gives a glass transition for the nitrile rubber of -25°C. This value is similar to values previously obtained for 70° Hardness nitrile rubbers for other BHRA Fluid Engineering projects. Using this value the coefficients are $C_1^o = 9.29$ and $C_2^o = 96.6$ for a reduced temperature of 20°C. The shift factors are given by:-

$$\log a_T = \frac{-9.29(T - 20)}{(96.6 + T - 20)}$$

4.3.3 Error Analysis

An appreciation of the effect of errors in the experimental data may be obtained from equations 4.3 - 2 and 3. The relative errors are the ratio of the error to the measured value. Thus for the force:-

$$\text{error \%} = \frac{\Delta f}{f} \times 100$$

In the case of the phase angle it is the ratio of the error to the tangent of the measured value. The effect of

Parameter	Error	
Frequency	$\frac{1}{\left(\frac{M\ddot{x}}{f\cos\phi} - 1\right)}$	$\frac{2\Delta\omega}{\omega}$
Mass	$\frac{1}{\left(\frac{M\ddot{x}}{f\cos\phi} - 1\right)}$	$\frac{\Delta m \cdot \ddot{x}}{f\cos\phi}$
Force	$\frac{1}{\left(\frac{M\ddot{x}}{f\cos\phi} - 1\right)}$	$\frac{\Delta f}{f}$
Acceleration	$\frac{1}{\left(\frac{M\ddot{x}}{f\cos\phi} - 1\right)}$	$\frac{\Delta\ddot{x}}{\ddot{x}}$
Phase	$\frac{1}{\left(\frac{M\ddot{x}}{f\cos\phi} - 1\right)}$	$\Delta\phi \tan\phi$

a stiffness

Parameter	Error
Frequency	$\frac{\Delta\omega}{\omega}$
Force	$\frac{\Delta f}{f}$
Acceleration	$\frac{\Delta\ddot{x}}{\ddot{x}}$
Phase	$\frac{\Delta\phi}{\tan\phi}$

b damping

Table 4 - 2 Error Equations

errors on the calculated values of the stiffness (equation 4.3 - 2) is different. The frequency error in the stiffness is twice the error in the frequency. Errors in the remaining measured values have a similar effect on the stiffness as on the damping, but are modified by a magnification factor:-

$$\frac{1}{\left(\frac{M\ddot{x}}{f\cos\phi} - 1\right)}$$

This will be unity at zero frequency where the acceleration is zero, zero at the resonance frequency where the phase is 90^{o} and a value depending on the relative magnitude of the force and acceleration at higher frequencies. Table 4 - 2 gives a full list of the error equations. It is possible to estimate the likely error in the calculated values due to errors in each of the variables.

The Frequency Response Analyser has quoted accuracies of $\pm$ 1% for the frequency scale and the output meters. However a maximum error of $\pm$ 5% at some frequency settings is possible because of the logarithmic nature of the scales. The electronic balance is accurate to about $\pm$ 0.1%. The mass of the o-ring is ignored. If the usual assumption of the effective mass being one third of the actual mass is made this would lead to an error of $\pm$.2% in the mass. The main sources of error are likely to be in setting the acceleration level at low frequencies, and the impedance mis-match at high frequencies. Since the former could be at least $\pm$ 25%, the readings at low frequency must be analysed with caution. Over the middle frequency range, about 25 Hz to 800 Hz, the errors are unlikely to exceed $\pm$ 3%. The maximum error in the calculated value of the stiffness (except below 25 Hz) would thus be $\pm$ 16%, whilst the corresponding error in the damping coefficient would be $\pm$20%. The minimum

likely error (i.e. the accuracy of the apparatus) is $\pm$ 4% for the stiffness and $\pm$ 6% for the damping coefficient.

It is clear from the error equations that phase measurements in particular are frequency dependent and care must be taken at both high and low frequencies. For instance a 1^{o} error in the phase at 179^{o} phase angle gives an error of 5700%! However the form of the phase angle curve is well known (89) and the errors may be reduced by plotting the measured phase angles and smoothing them. Great care must also be taken when setting the acceleration level at low frequencies since the values are very small and even the instrument errors are significant compared with them.

4.3.4 Curve fitting at low frequencies

The results show considerable scatter at low frequencies. However the stiffness values show a clear trend towards a constant value at low frequencies. This is to be expected from equation 4.3 - 2 which reduces to:-

$$S = \frac{f}{\chi}$$

as ω tends to zero

The trend of the damping coefficient curve as χ tends to zero can be obtained from a consideration of equation 4.3-3 :-

$$C = \frac{f \sin \phi}{\omega \chi}$$

Now ϕ is a function of frequency. If the function is a linear one over the low frequency range (0 - 10 Hz) then:-

$$\phi = \phi\ (1 - b\omega)$$

The limiting value of the damping coefficient as the frequency approaches zero is given by:-

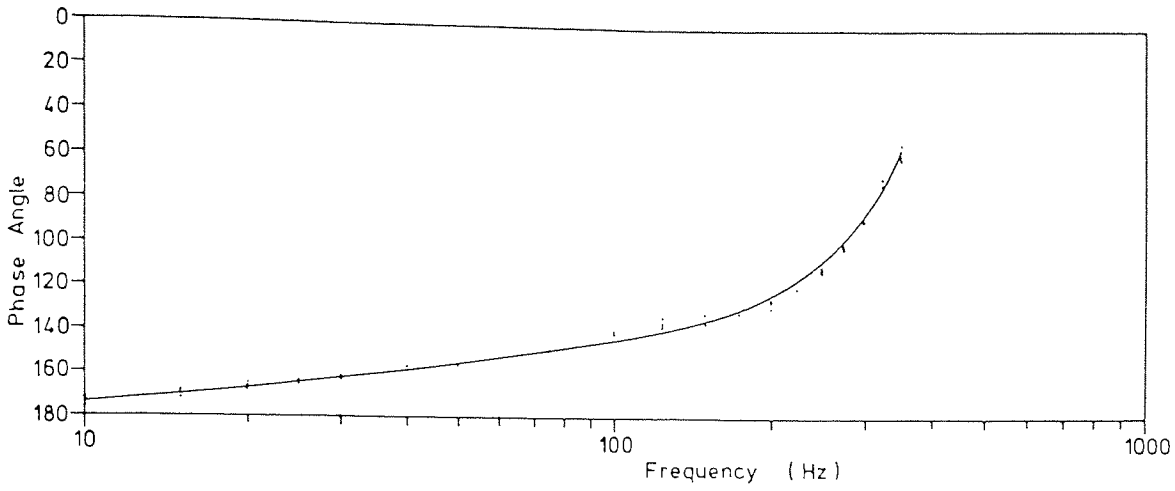

Fig. 4-13 Phase Angles - Five O-Rings from Cavity 11 Mould 5 Batch 1

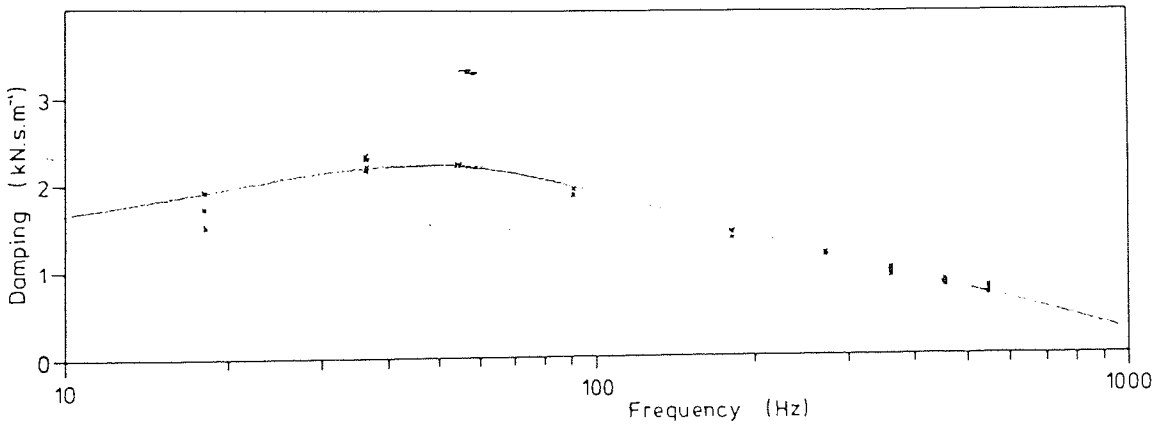

(a) Damping Coefficient

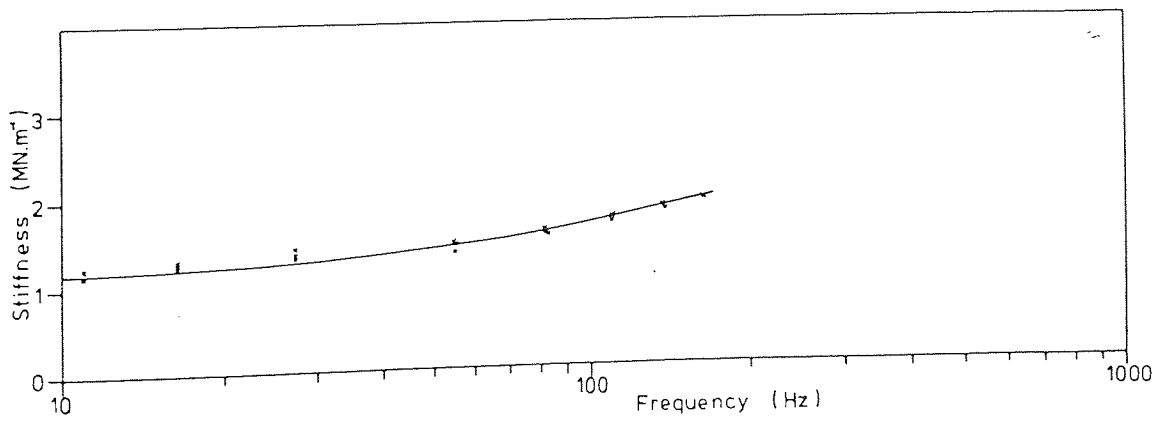

(b) Stiffness

Fig. 4-14 O-Ring properties - Five O-Rings from Cavity 11 Mould 5 Batch 1

$$\lim_{\omega \to 0} tC = b\pi \frac{f}{x}$$

These expressions may be used to fit a curve to the values of the stiffness and damping coefficient at low frequencies.

4.4 Results of the O-Ring Experiments

To assess the trends of the stiffness and damping coefficients at low frequencies, five o-rings were tested at ten times the normal experimental deformation. These rings were from five different charges of cavity eleven of mould number five and were moulded from the first batch of the compound. Fig 4 - 13 is a plot of the phase angles showing the smoothed curve. The values of the stiffness and damping coefficients are plotted on fig 4 - 14. The stiffness shows a clear trend to a constant value of about 1.25×10^6 N.m^{-1} at low frequency. Taking the zero frequency value of stiffness as this value then at 10 Hz, where $\phi = 174^o$ (fig 4 - 13)

$$S = 1.245 \times 10^6 \text{ N.m}^{-1}$$

which is a change of only 0.4% from the zero frequency value.

For the damping coefficient, the phase angle function is required. From fig 4 - 13 this is:-

$$\phi = \phi\ (1 - 0.000442\ \omega)$$

and thus the limiting value of the damping coefficient is:-

$$C = 1.74 \times 10^3 \text{ Nsm}^{-1}$$

At 10 Hz the value of the damping coefficient is:-

$$1.73 \times 10^3 \text{ Nsm}^{-1}$$

These values follow the experimental trends and show that the technique may be used to smooth the experimental results at low frequencies. The analysis is only valid over a small frequency range because the value of $\frac{f}{x}$ will also change. However

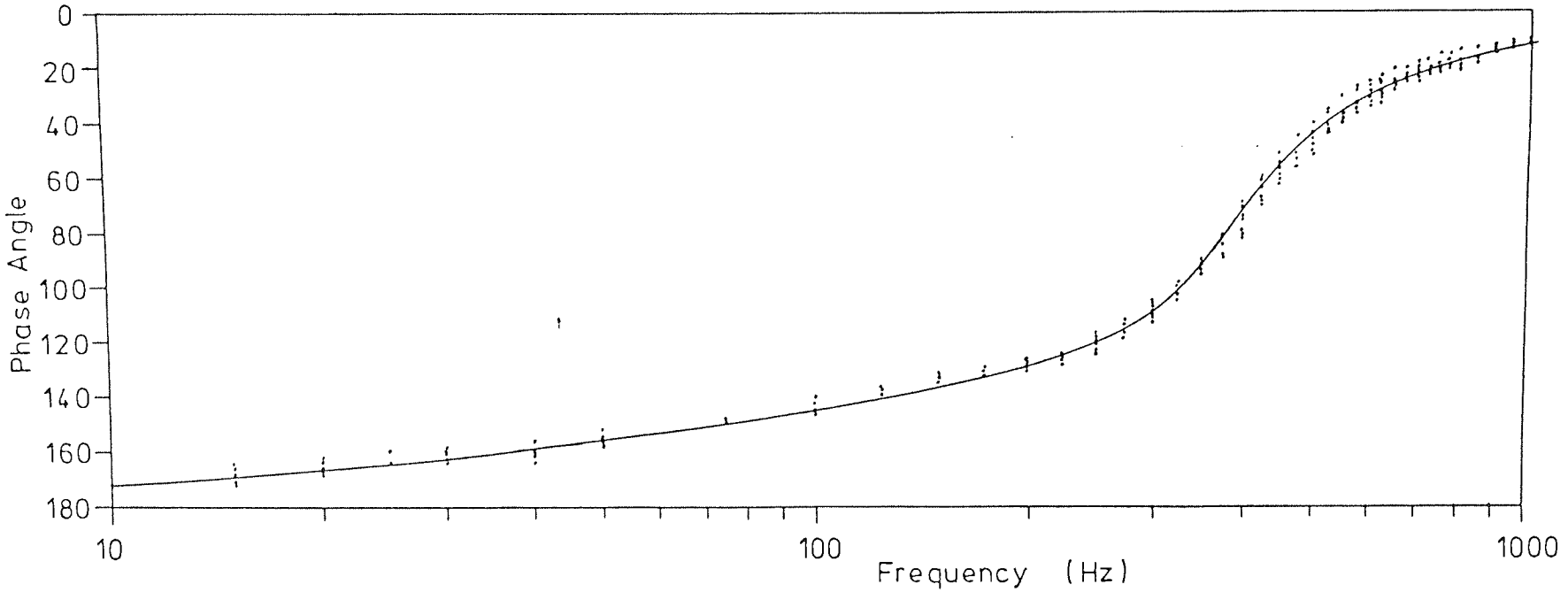

Fig 4-15 Phase Angle Curve - Combined Plot of All 20° C Experimental Runs

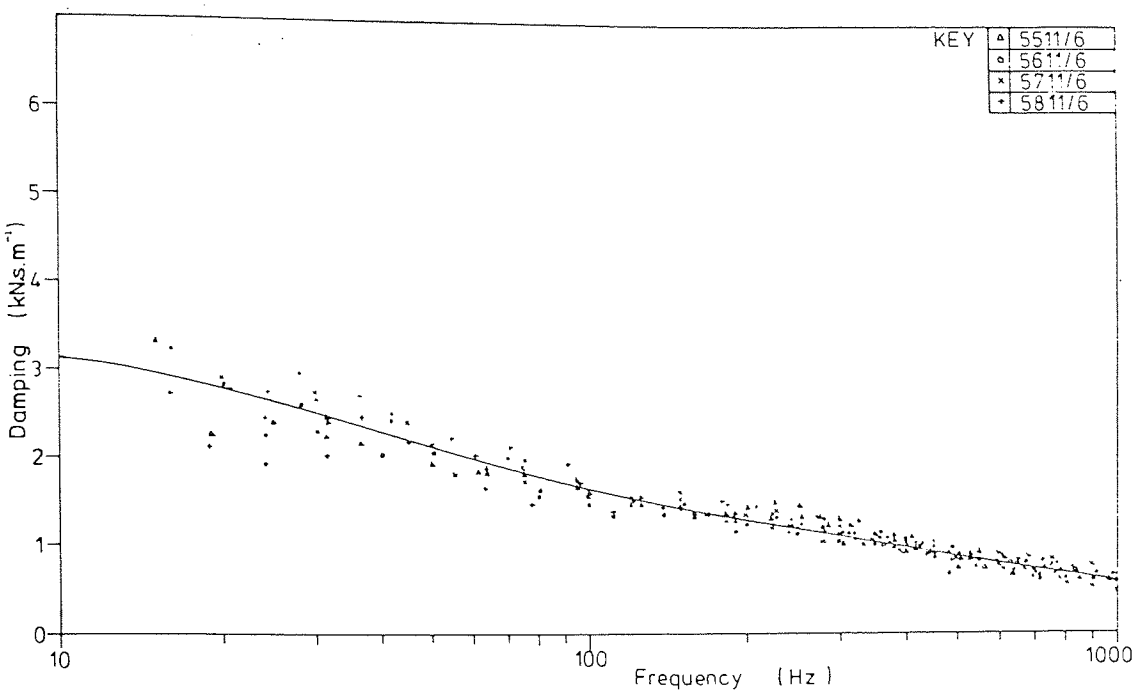

(a) Damping Coefficient

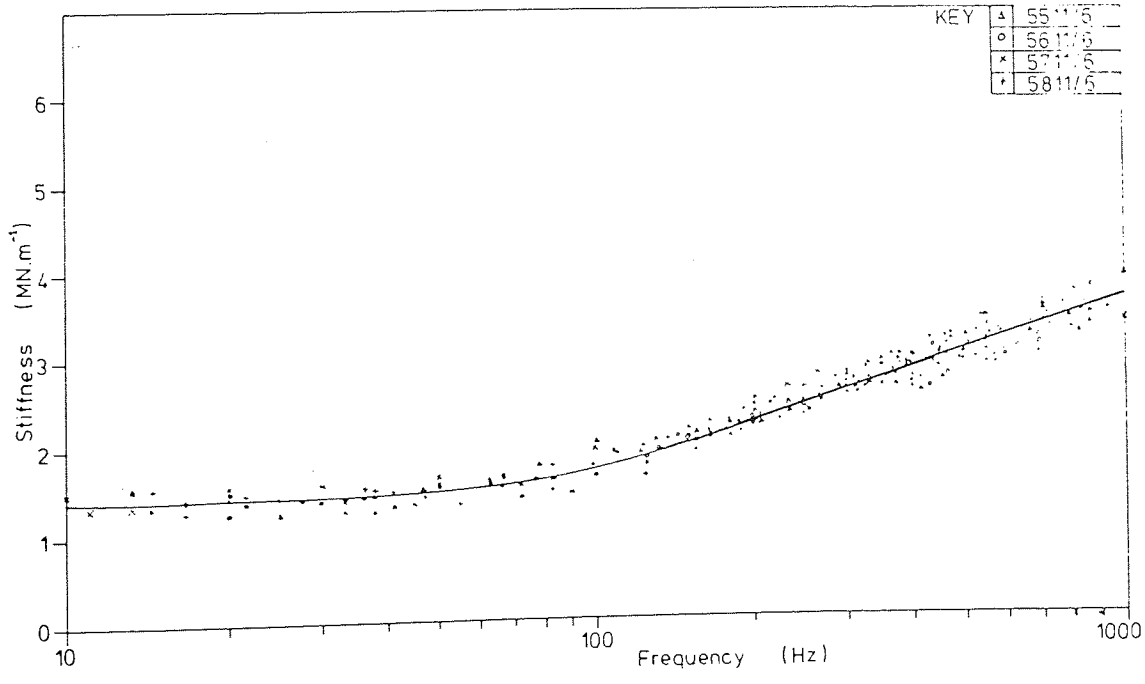

(b) Stiffness

Fig. 4-16 O-Ring Properties - Twenty O-Rings from Cavities 5 to 8 Mould 5 Batch 1

these results show that the method may be used to smooth the experimental results. A similar analysis is applied to the remainder of the results.

To further improve the accuracy of the calculations of stiffness and damping coefficients the phase angles for each run can be smoothed. To facilitate this, all the phase angles for experimental temperatures of $20^{o}C$ have been plotted on fig 4 - 15. A smooth curve has been drawn through the points. This curve is then used as a guide for smoothing the phase angle measurements of all the o-rings.

Once the results have been analysed the stiffnesses are plotted and a best curve drawn through the results. The stiffness at 10 Hz is taken as the static value and used to aid fitting the curve to the damping coefficient plots.

Fig 4 - 16 shows the stiffness and damping coefficients for a total of 20 o-rings moulded in mould number five from batch one of the compound. Five rings each have been tested from cavities five to eight.

From fig 4 - 16b the stiffness at 10 Hz is 1.41×10^{6} $N.m^{-1}$. From the phase angle curve, fig 4 - 10, at 10 Hz the phase angle is given by:-

$$\phi = \pi (1 - 0.000707\, \omega)$$

The value of the damping coefficient at zero frequency:-

$$\lim_{\omega \to 0} tC = 0.000707\, \pi \frac{f}{\chi} = 3.13 \times 10^{3}\ Nsm^{-1}$$

Because of the errors in the measurement of the phase, force and acceleration the exact form of the damping curves at low frequencies is difficult to determine. The curve has been

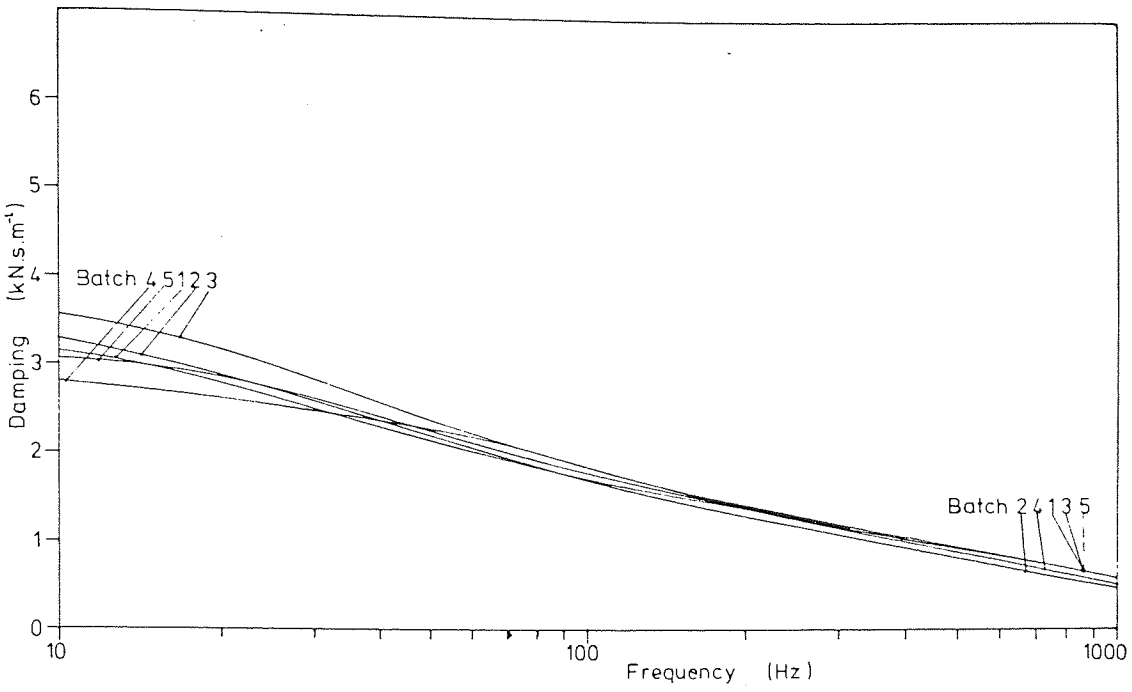

(a) Damping Coefficient

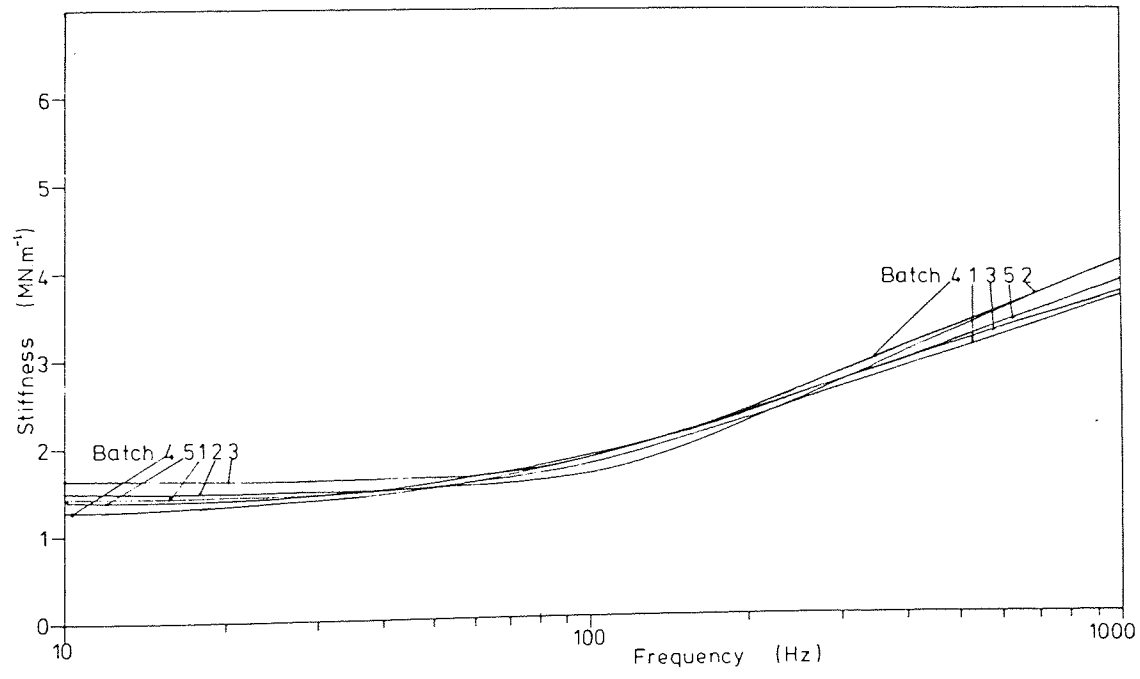

(b) Stiffness

Fig.4-17 O-Ring Properties - Mould 5 Batches 1 to 5

drawn taking into account the calculated value of the damping coefficient at 10 and 0 Hz.

Fig 4 - 17 shows combined curves of stiffness and damping respectively for a series of o-rings from five different batches of the basic polymer compound. Each curve is drawn through the results from five different cavities in mould number five. For batch number one the curves have been taken from figs 4 - 16. The zero frequency values of stiffness and damping coefficient and the calculated value of the damping coefficient at 10 Hz for each of the curves is given in table 4 - 3.

BATCH NUMBER	ZERO FREQUENCY		10 Hz
	STIFFNESS ($N.m^{-1}$)	DAMPING COEFFICIENT ($Ns.m^{-1}$)	DAMPING COEFFICIENT ($Ns.m^{-1}$)
1	1.41×10^6	3.14×10^3	3.12×10^3
2	1.49×10^6	3.30×10^3	3.30×10^3
3	1.61×10^6	3.49×10^3	3.57×10^3
4	1.28×10^6	2.86×10^3	2.83×10^3
5	1.38×10^6	3.08×10^3	3.06×10^3

Table 4 - 3 Stiffness and Damping Coefficients Low Frequency Smoothed Values

Finally a set of five o-rings moulded in a single cavity mould from batch number one of the compound were tested. The results are plotted, together with the best lines for the other batch one o-rings on fig 4 - 18.

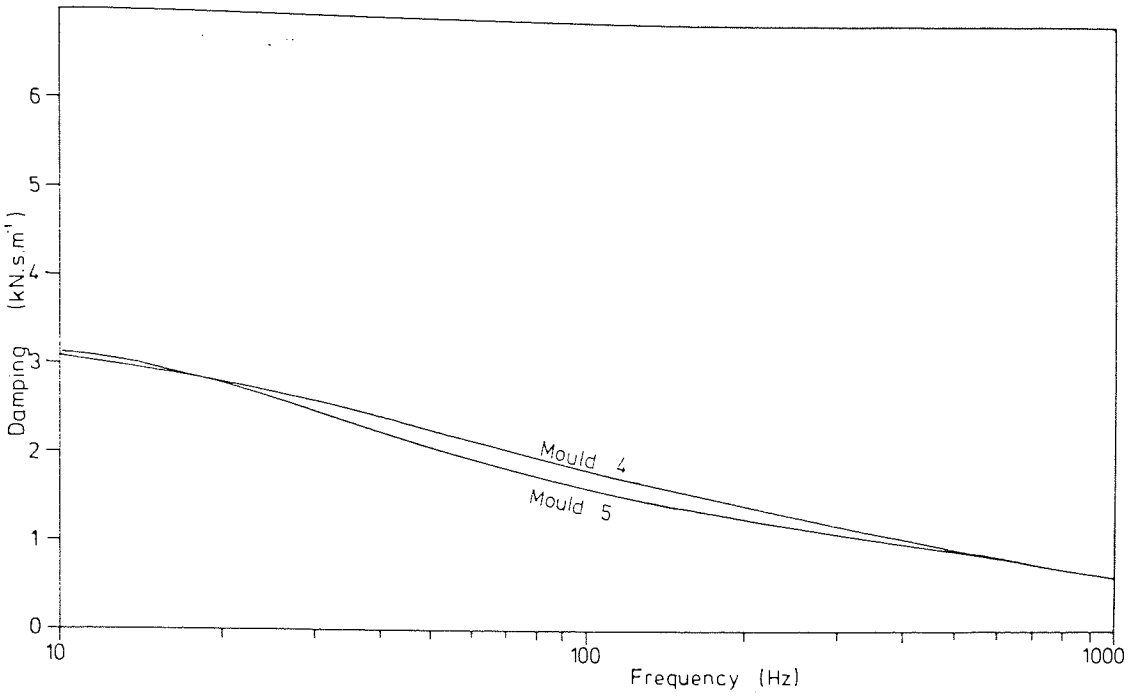

(a) Damping Coefficient

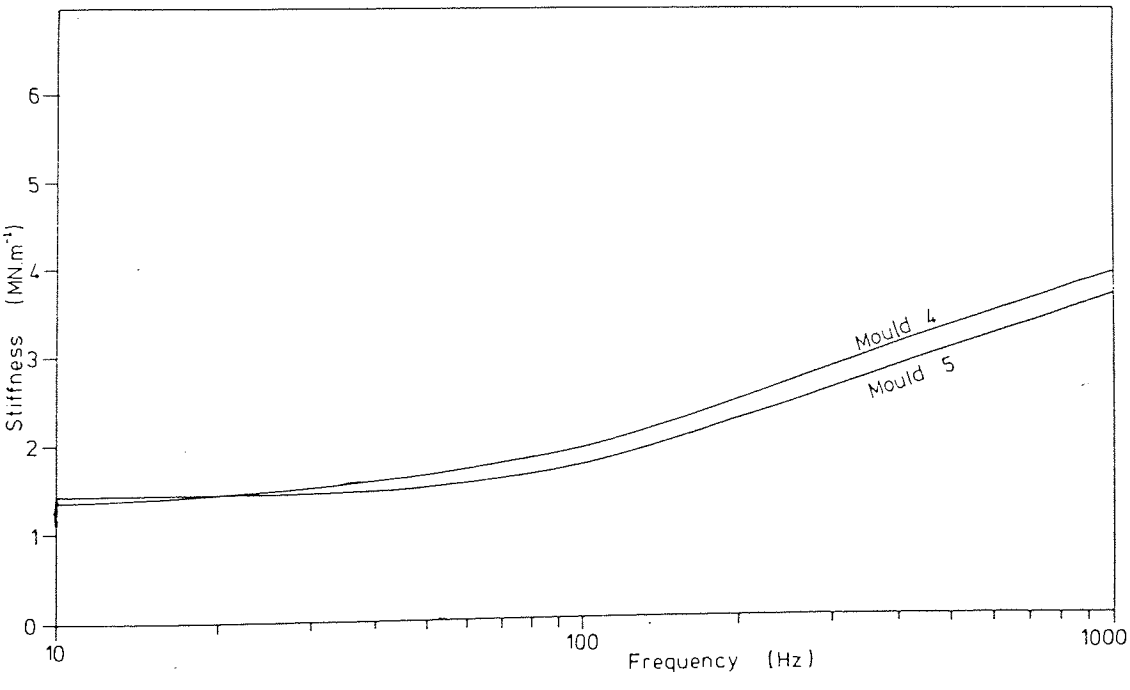

(b) Stiffness

Fig.4-18 O-Ring Properties - Mould 4 and 5 Batch 1

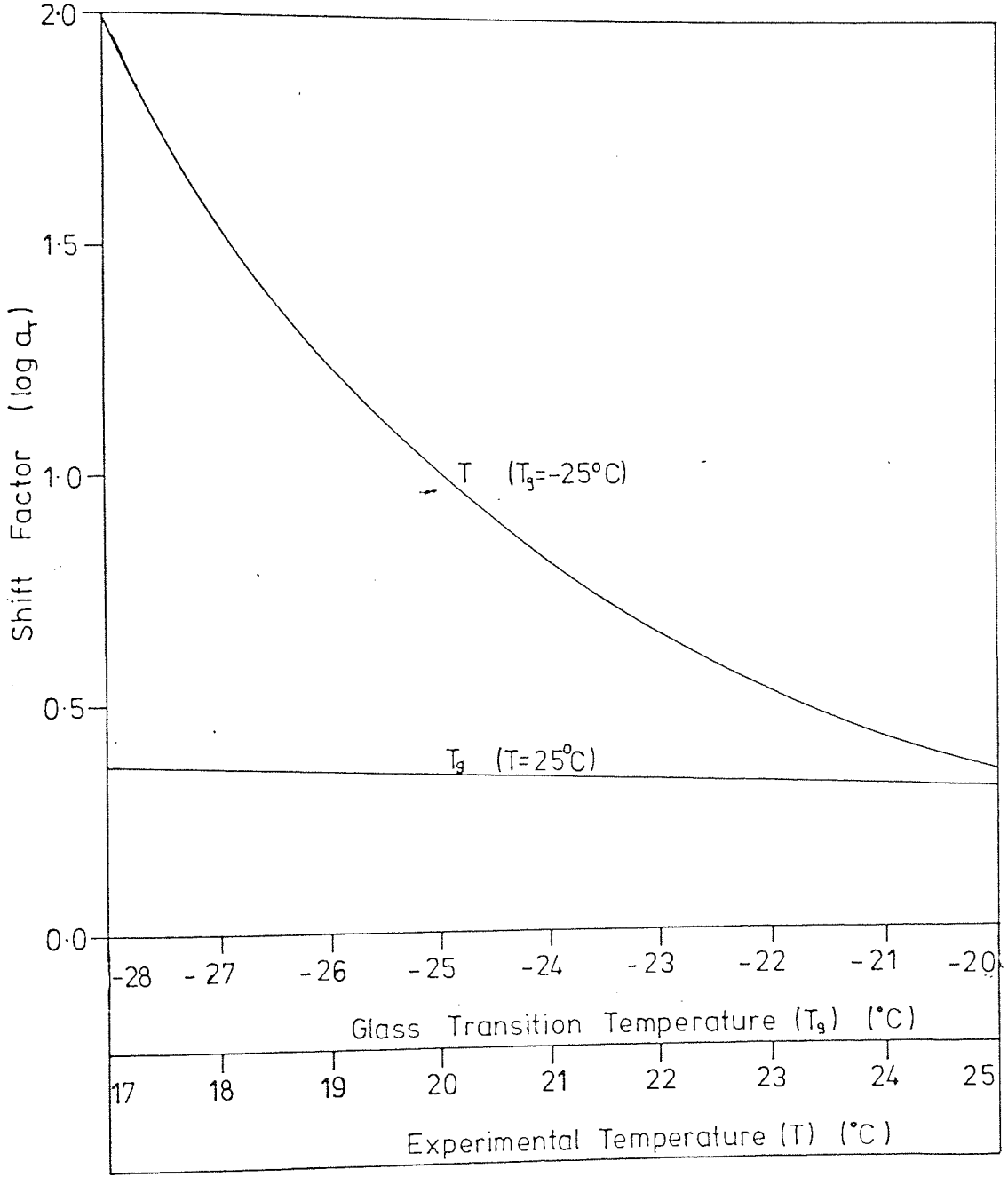

Fig 4-19 Variation of Shift Factor with Experimental (T) and Glass Transition Temperature (T_g) (WLF Transform)

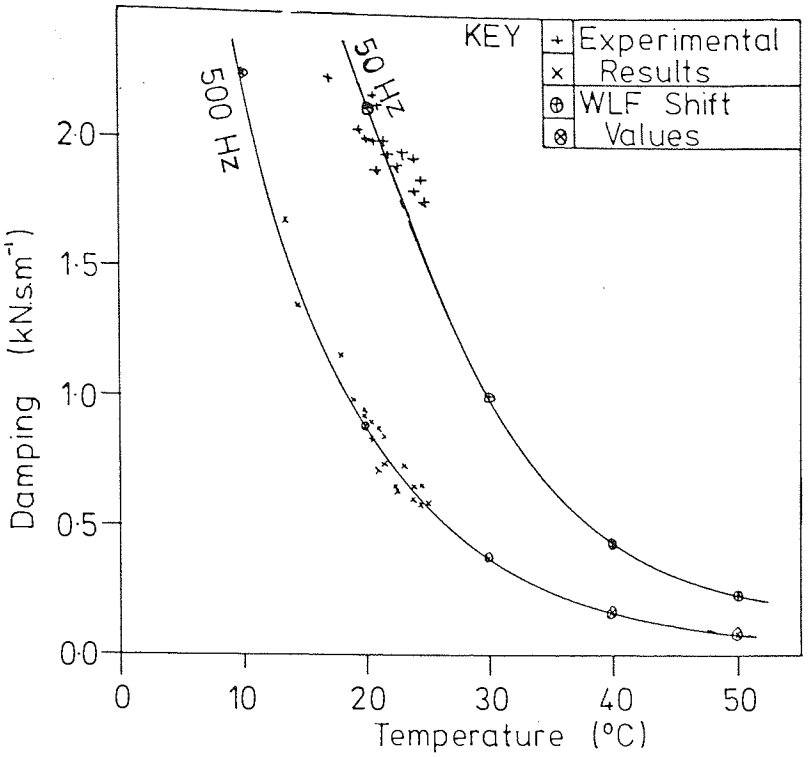

(a) Damping Coefficient

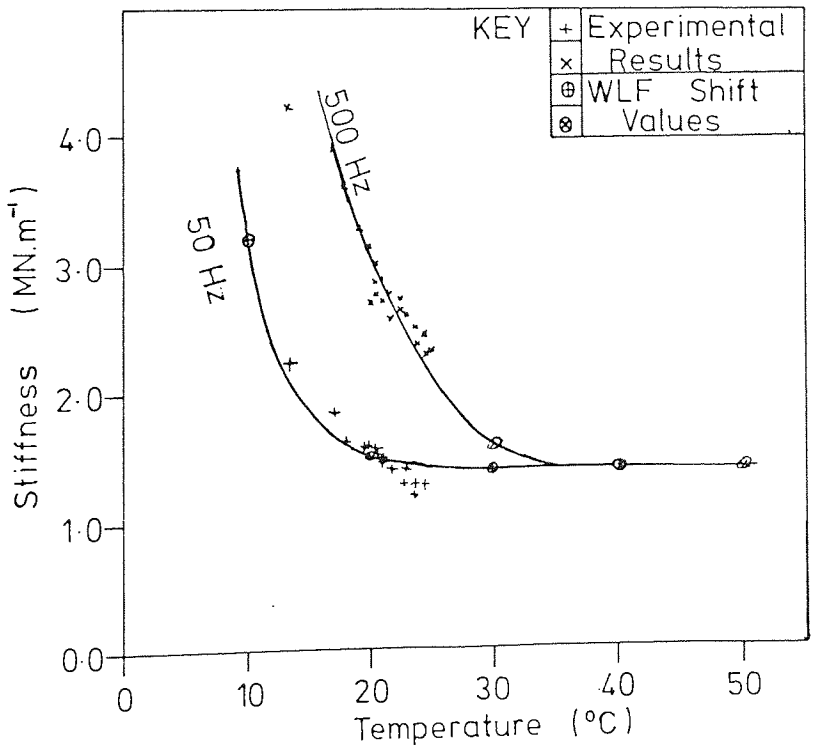

(b) Stiffness

Fig 4-20 The Effect of Temperature on O-Ring Properties

4.5 Discussion

4.5.1 Data Scatter

It is clear from fig 4 - 16 that there is considerable variation in the o-ring properties, even for rings moulded in the same cavity. However, the variations shown on fig 4 - 17 all lie within the variation on fig 4 - 16. It is possible that the reason for the wide variation throughout the frequency range is the lack of control of the o-ring temperature. The o-ring results plotted on fig 4 - 14 show a much smaller variation. All these o-rings were tested at the same temperature ($23^{o}C$) whereas the temperature of the remaining o-rings varied between $17^{o}C$ and $25^{o}C$. In addition the glass transition temperature for the polymer is not accurately known and this combined with the wide temperature variation could lead to the variation of the results.

Fig 4 - 19 is a plot of the WLF equation shift factor against temperature. Two curves are drawn, firstly the shift factor against o-ring temperature and secondly the shift factor against the glass transition temperature. This shows that fairly small errors in the o-ring temperature could lead to large errors in the shift factor. From fig 4 - 19 it can be seen that an error of only $0.5^{o}C$ in the measured experimental temperature would reduce the scatter from $\pm$ 12.5% to $\pm$ 5%.

Fig 4 - 20 shows the possible effect of temperature on the damping and stiffness. The experimental results have been plotted for 50 Hz and 500 Hz. In addition values for different temperatures have been obtained by using the appropriate

WLF shift factors on the curve of fig 4 - 16. It should be borne in mind that both the extrapolations of the experimental data and the transformed values may be considerably in error. However the curves should give a reasonably accurate representation of the likely trends. It is possible that the levelling out of the stiffness predicted by the WLF transform values will not occur in practice, since the transform makes no allowance for chemical changes in the rubber.

In addition to this overall variation in the results, they show the spread suggested by the error analysis carried out in the previous section. In particular, the values of the damping coefficient show the smallest variation between 100 and 300 Hz where the effect of the phase angle errors is the smallest. The maximum error is $\pm$ 12%, which is slightly less than estimated in section 4.3.

The variation in the stiffness also shows a minimum at the mid-frequency range, corresponding to the minimum value of the magnification factor. The maximum spread of the stiffness values is $\pm$ 12.5%, and as with the damping coefficient this is less then predicted.

Both these errors are for the range above 25 Hz. Below this frequency, as predicted, the spread is very much larger. However the smoothing technique applied follows the trends.

4.5.2 Comparison with published data

It is difficult to obtain suitable results from the literature that can be compared with the results presented here. Almost without exception other workers have concerned themselves with obtaining moduli or relaxation spectra, properties

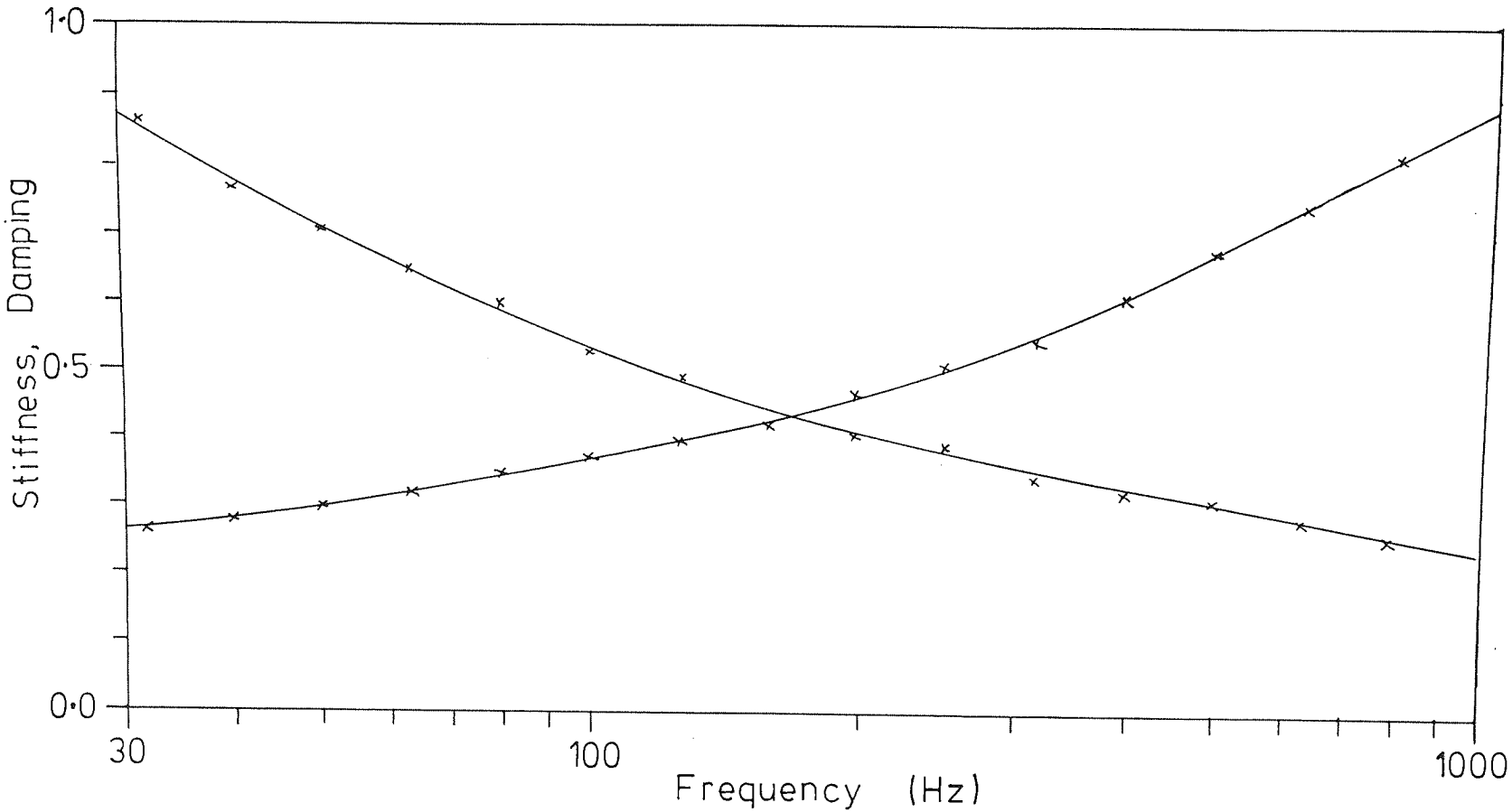

Fig 4-21 Stiffness and Damping Coefficient of Polyvinyl-Acetate from Complex Shear Modulus (arbitrary units)

that are not directly relevant to the behaviour being considered here. It is possible to compare the results qualitatively but it must be appreciated that no great reliance can be placed on the result of the comparison. The values of the real and imaginary parts of the shear modulus for a polyvinyl acetate polymer have been taken from the literature (173). The real part may be compared directly with the stiffness, the modulus and stiffness vary by an area factor. The imaginary part must be further processed before a direct comparison can be made, since the damping coefficient is a viscosity term:-

$$C = \frac{G'' \times f\ (\text{Area})}{\omega}$$

The resultant values have been plotted on fig 4 - 21. These show similar trends to the results obtained here but the distinct change in the form of the stiffness curve is not so apparent. This change, showing the stiffness to have two distinct regions within the frequency range considered, has been noted by other workers (109).

It is possible to compare the present results directly with the only other similar work published so far (159). In this work the basic polymer used was a fluorocarbon rubber (Dupont "Viton") but sufficient information is given to enable an approximate curve to be developed for a 70^{o} hardness nitrile. The paper gives the baseline curve for the fluorocarbon and comparison curves with only one parameter varied. Using these curves fig 4 - 22 has been drawn for a nitrile o-ring. The curves from fig 4 - 16 have been included for comparison purposes. The results have been reduced to $20^{o}C$ using the WLF transform assuming the same glass transition temperature for both nitrile polymers. The stiffness shows good agreement at

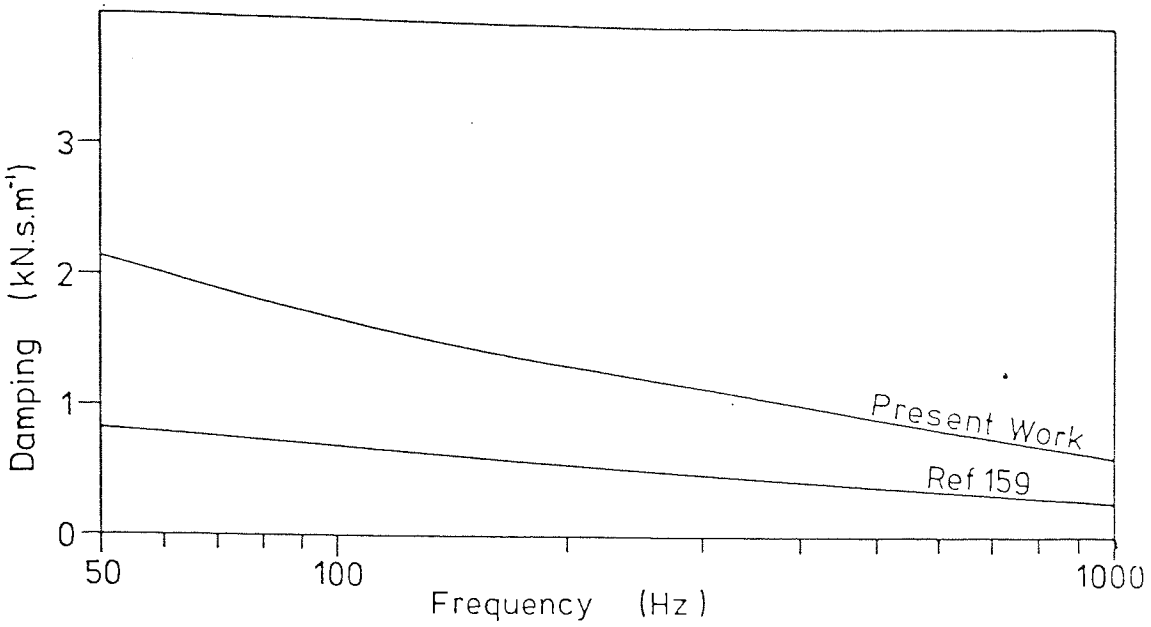

(a) Damping Coefficient

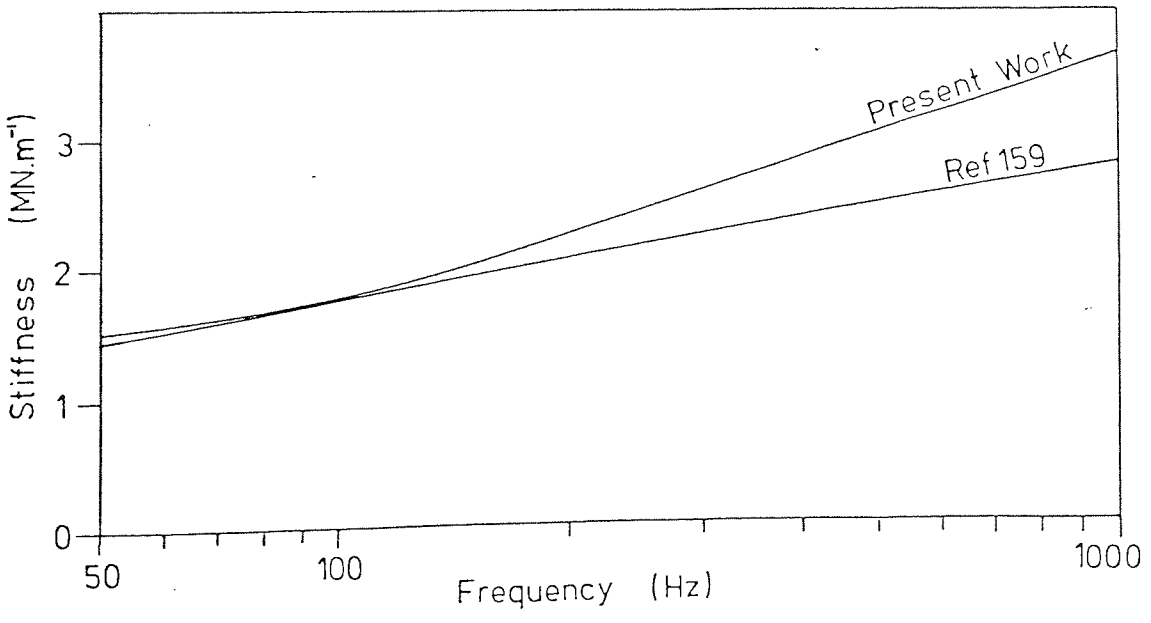

(b) Stiffness

Fig 4-22 Comparison of Experimental Studies

low frequencies, but at high frequencies the agreement is poor. The damping coefficients are very different, the present results being three times those in the reference. No details of the compounding of the o-rings are available and it is impossible to determine the reasons for the difference between the results.

An earlier investigation considered the static behaviour of o-rings in grooves (166). It was concerned with the load required to achieve certain deformations. From the nomograph given in the paper it is possible to predict the load required to deform an o-ring a given distance, knowing the material, cross section diameter and hardness. Knowing the load and deflection the stiffness may be obtained. The deflections used in the present work are outside the range of the nomograph, however an approximate result may be obtained by extrapolation. A load value of 5.1 N is obtained giving a static stiffness of 1.7×10^{6} $N.m^{-1}$.

4.6 Conclusions

It is possible to draw several conclusions from the experimental results. The most important of these is that the stiffness is almost constant from 0 to 60 Hz at 20°C (up to 3600 rpm). This shows that for low frequency vibrations the static value of the stiffness may be used as the dynamic value. This is particularly useful where approximate calculations not involving damping are being made.

Secondly the results show that there is considerable variation in the properties of o-rings even when steps have been taken to reduce the number of possible causes of variation to a minimum. In order to achieve the least possible variation

in the properties of a number of o-rings it appears necessary only to ensure that the rings are all moulded from the same formulation of the compound. The spread of the properties would be no worse than for o-rings moulded from the same batch of compound in the same cavity of a mould.

The operating temperature of an o-ring will have a considerable influence on its performance. Even if the o-ring is below its nominal maximum operating temperature, large variations in the properties can occur as shown by figs 4 - 19 and 4 - 20. However at higher temperatures (over 35°C) the stiffness becomes constant until the temperature becomes sufficiently high to cause thermal degradation of the polymer.

Finally, the results compare well qualitatively with results obtained elsewhere for the moduli of polymers, and they also show good agreement with the results obtained by other workers in related fields.

CHAPTER 5

MECHANICAL SEAL EXPERIMENTS

5.1 Test Rig Design

In this chapter the experiments carried out on a mechanical seal will be described. In the first section the design criteria for the test rig will be discussed, and the final design described. In subsequent sections the design of the experimental program, the analysis procedure and the experimental results will be described.

5.1.1 Design Criteria

The main purpose of these experiments was to quantify the behaviour of the seal ring when it is subject to a shaft vibration. The behaviour is described not only in terms of its motion, both linear and angular, but also in terms of the seal performance, the leakage from the seal and the heat generated at the sliding interface. The rig must therefore be suitable for measuring the motion of the floating ring and for monitoring temperatures and leakage.

A number of parameters were to be investigated (section 5.2) and it was necessary to be able to vary not only the speed, sealed pressure and vibration levels, but also the design of the floating ring.

Two factors must be considered with regard to vibrating the rig. Firstly the method used must be simple, otherwise too

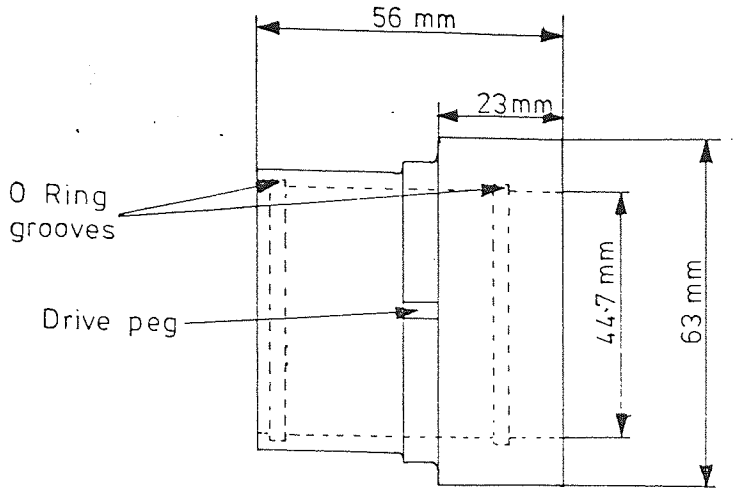

(a) Long Floating Ring

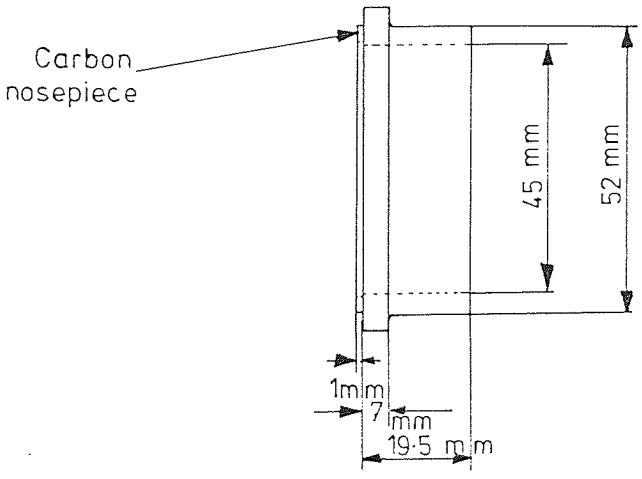

(b) Stator

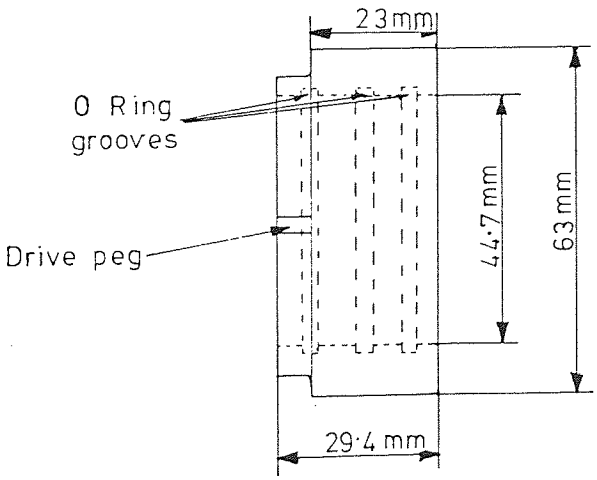

(c) Short Floating Ring

Fig 5-1 Floating Ring and Stator Designs

much time would be needed to develop the technique. Secondly, the vibration frequency range should correspond to that observed in practice. In general the largest amplitudes and forces are associated with the fundamental frequency or close multiples of it (146). Rolling element bearing defects may result in vibration at frequencies 20 or more times the rotational frequency, but at greatly reduced amplitudes and force levels (78).

The sealed pressure and shaft speed should be typical of values to be found in process industries. Most process industry pumps run at 2900 rpm, with some at 1450 rpm and a smaller number at lower speeds. The sealed pressures may range from vacuum to many MPa, but for the unbalanced design typical pressure differentials are from 0.2 - 1 MPa (99). The seal designs should also be typical of commercial practice.

5.1.2 Test Seals

Fig 5 - 1 shows the designs of the floating rings and stator to be used. The floating ring designs were chosen to cover the range of commercial practice. The long tailed design has been the subject of much testing (63) and is designed to perform well at high pressures. The o-ring grooves machined in each ring also cover the range of positions found in commercial seals (see fig 1 - 3). Although neither seal is a commercial design, they are typical of commercial practice and the effect of changing the seal design can be quantified.

The floating rings are machined from a nodular cast iron, Meehanite grade GE. They are driven by a single coil spring, and positive drive is obtained by drive pegs on both the floating ring and the collar.

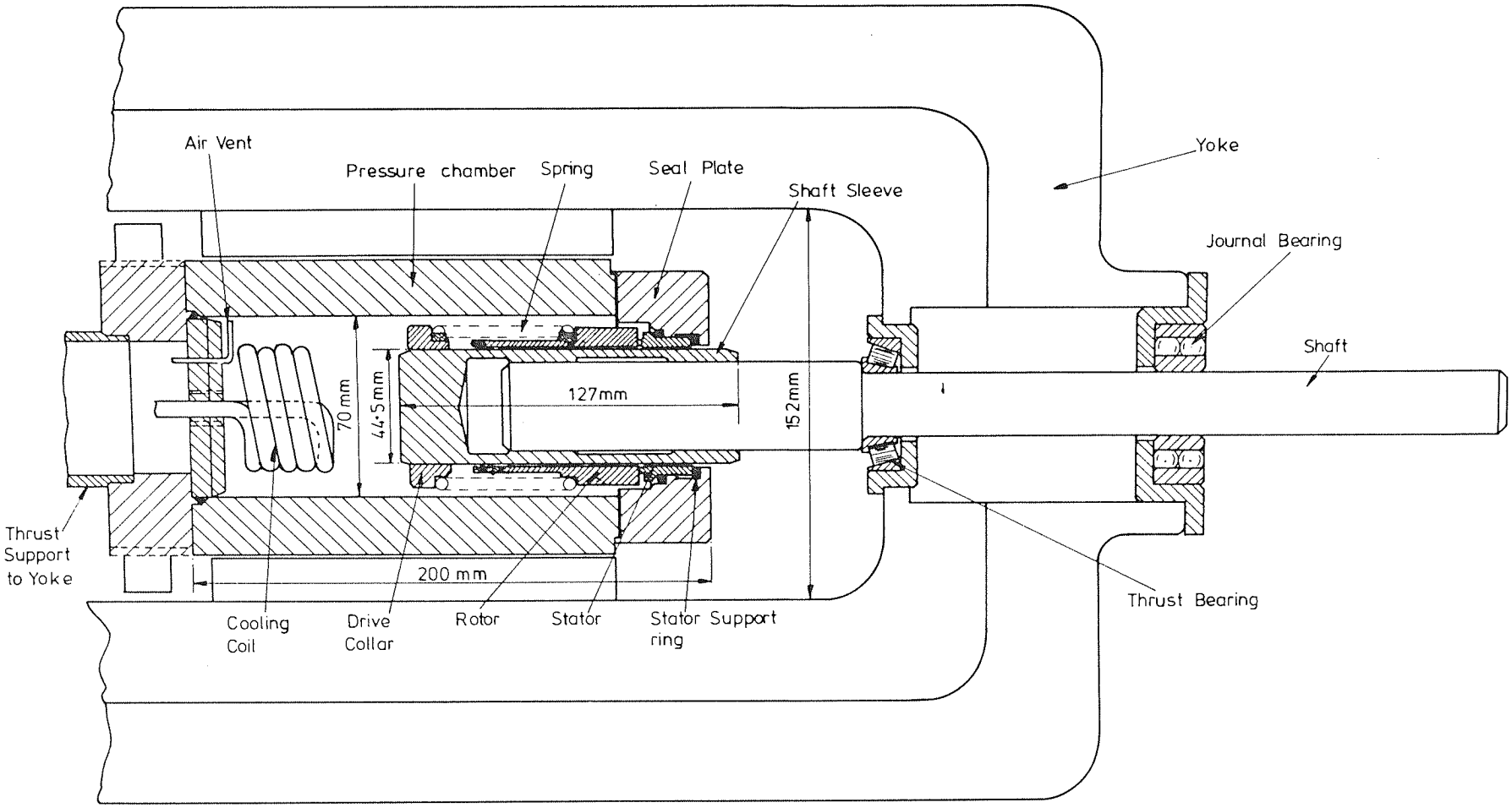

Fig. 5-2 Main Details of Test Rig

The stator is machined from Aluminium Bronze (DTD197) with a carbon ring bonded to it. The carbon ring forms the mating surface for the rotor. Cast iron running against carbon is recommended for hydraulic and lubricating oils by mechanical seal manufacturers. This combination of materials has good dry running properties. The thrust on the stator is taken by the seal plate through a rubber thrust washer. An o-ring provides the secondary seal between the stator and the seal plate.

The o-rings used as a secondary seal between the floating ring and the shaft do not have the same dimensions as those used for the tests described in chapter 4. The mechanical seal o-rings have a smaller section diameter and are for a slightly smaller shaft diameter. The o-rings were obtained from a commercial outlet and were not specially purchased. Their properties were obtained, before and after testing using the techniques described in chapter 4. The results are given in figs 5 - 6 and 5 - 7 and discussed in section 5.5.

5.1.3 Final Rig Design

The test rig is shown in fig 5 - 2, which also gives the main dimensions. This design was chosen as it has been used previously for various work on mechanical seals, and an extensive series of tests on mechanical seal design have been carried out (63). The rig itself required no development for the present research, and the mechanical seal chosen was known to operate successfully at pressures well in excess of those quoted in the design criteria.

The shaft is driven by a variable speed DC motor and is capable of shaft speeds in excess of 3000 rpm. The shaft is

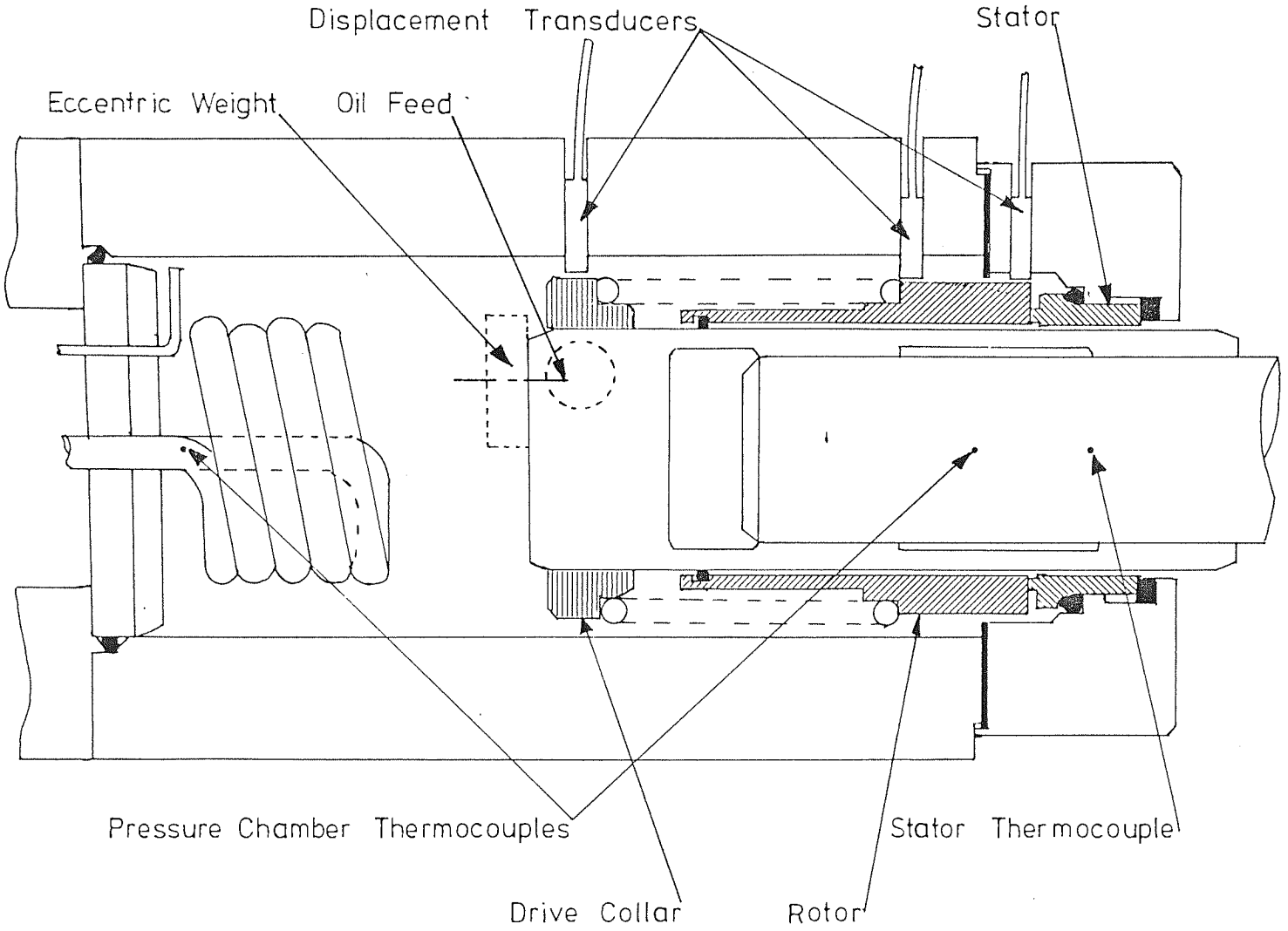

Fig 5-3 Mechanical Seal Rig Transducer Positions

mounted in a journal bearing with a taper roller thrust bearing to take the end thrust on the shaft due to the pressure in the pressure chamber. The end thrust on the pressure chamber is supported by the yoke as shown.

The pressure chamber is filled with a Shell Tellus 27 oil, pressurised by an air operated intensifier. A bleed valve is provided to ensure all the air is expelled on filling the chamber. Whereas in a pump there would be circulation of the liquid surrounding the seal, the oil in the rig chamber is static. The temperature of the oil will therefore rise due to viscous shear in operation. A cooling coil is fitted in the blank end to maintain reasonable temperatures within the pressure chamber and also to enable a measure of the heat flux generated to be made. This cooling is applied at the end away from the seal plate. This is where the cooler liquid would be in a pump. The inlet and outlet temperatures are measured by thermocouples, and in addition the temperature is measured within the pressure chamber and on the stator. The positions of those thermocouples relative to the mechanical seal are shown on fig 5 - 3.

The main limitation of the test rig is the test seal's size. Very small transducers are required to measure the shaft and floating ring displacement, as space is limited and the transducers must be at least twice their diameter apart to prevent problems occurring with interference between the carrier frequencies. However transducers of about 6 mm diameter do not normally have sufficient accuracy for the measurement required. The transducers used are 6.3 mm diameter (0.25 inch), and have a resolution of 0.1 µm and a repeatability of 1 µm. They are a non-contacting inductive type

Item	Manufacturer and Model	Manufacturers Details
Displacement Transducers	Kaman Sciences Model KD-2300-15	Resolution 0.01% Linearity ±0.2% Repeatability 0.1% Temperature Range -32 100°C
Capacitance Transducer - Oscillator	Southern Instruments Type M1828	
- Readout Unit	Southern Instruments Type M1861	Linearity ±0.3% Sensitivity 1%
- Vernier Capacitor	Sullivan Type C858/S	Range 63 to 163 pF
UV Chart Recorder	SE Oscillograph 3006/DL C300 Galvanometers	Resonance frequency 300 Hz
Temperature Measurement - Thermocouples	Fibre Glass Insulated Copper-Constantan (Cu/Cu-Ni)	Range -60°C to 160°C in 24 Ranges Accuracy ±2% FSD

Table 5 - 1 Mechanical Seal Test Rig Instrumentation

with a carrier frequency of approximately 10kHz. To reduce interference between the transducers, all three use the same carrier frequency. This is achieved by utilising the oscillator of the signal conditioning unit of one transducer as a master and operating the other two units as slaves. Three transducers are mounted on the rig in line axially. One monitors the radial motion of the shaft, whilst the other two monitor the radial motion of the floating ring. The relative position of the transducers is shown on fig 5 - 3. To ensure that the transducer mounted in the seal plate is accurately aligned with the other two transducers a locating pin on the pressure chamber aligns with a hole in the seal plate.

To measure the axial motion of the floating ring a capacitance technique was used. The stator acts as one plate of the capacitor and the floating ring as the other. The capacitance is a function of the film thickness. Knowing the area of the interface and the dielectric constant of the oil in the interface the film thickness may be calculated from the capacitance.

The signals from all the transducers were fed to a UV chart recorder. The traces were then analysed to give the radial, axial and angular motions of the floating ring. For the sake of simplicity the vibration frequency has been restricted to the shaft frequency. An eccentric weight could then be used to excite the shaft vibration. The leakage was collected by surrounding the seal plate with an absorbent material. Finally the power absorption was estimated from the heat transfer to the cooling water. A list of the test rig instrumentation is given in table 5 - 1.

The rig design meets all the criteria laid down with the

exception of inducing shaft vibration at frequencies other than the shaft rotation frequency.

5.2 Test Programme

5.2.1 Programme Design Criteria

The test programme is required to provide sufficient information to validate the computer predictions of the seal performance. The computer program (chapter 6) is intended to be used to predict the behaviour of different designs for different conditions, and the experimental programme must be designed to validate the program.

The tests must cover a range of parameters and must be based on conditions occurring in practice. The BHRA Process Industry Seals Survey (99) provides useful information on typical speeds, pressures and vibration levels. This information may be used to ensure the test conditions are practical ones.

If a number of parameters are to be varied it is more cost-effective to vary them one at a time from a standard condition than to scan ranges of all the variables. The test programme was therefore designed to allow each parameter to be varied in turn from a baseline condition.

The information required for comparing with the computer program may be obtained from short or long term tests. Provided that no predictions of seal life, as defined by wearing of the seal faces, is required short term tests allow the results to be obtained in the shortest time.

5.2.2. Test Programme Design

The test programme was designed around a series of short tests. Each test was long enough for the seal to reach a steady operating condition and the required measurements to be made. Only one parameter was varied for each of the tests (except for some of the tests carried out on the short floating ring design). This allows the effect of the various parameters to be quantified.

The mechanical seal floating ring is an unbalanced design. The baseline condition was chosen as a typical application for such a seal. The baseline condition is given in table 5 - 2.

PARAMETER	VALUE
Pressure	0.5 MPa
Shaft Speed	2900 rpm
Film Profile Waviness	1 μm peak to peak 3 waves around the circumference
Rotor Design	Long tailed
O-ring Position	20% of length from interface
Centroid Position	30% of length from interface
O-ring	Nitrile, section 1.78 mm, nominal shaft diameter 44.5 mm
Shaft Vibration	Minimum possible

Table 5 - 2 Baseline Test Conditions

The remaining conditions were chosen to cover the typical operating conditions found by the survey. For the unbalanced design of mechanical seals 1 MPa is the normal maximum recommended sealed pressure. This type of seal is also not

normally used for vacuum work, and a typical minimum sealed pressure is 0.2 MPa. To cover this range four pressures were chosen, the baseline, 0.2, 0.7, and 1.0 MPa. To cover the range of process pump speeds the baseline speed (2900 rpm) and two other speeds, 1450 rpm and 900 rpm were chosen.

Vibration levels in practice are difficult to ascertain, and little is known of the relative vibration of the shaft and housing at the seal. The BHRA Process Industry Seals Survey for instance measured housing vibrations, but not vibration relative to the shaft. The test rig was built stiff to reduce vibration, but no dynamic balancing has been carried out. The vibration was thus due to additional vibration induced by the eccentric weight and any residual shaft run-out or out of balance.

The interface profile may have a considerable effect on the behaviour of the floating ring. Studies of used mechanical seals (118, 139) have shown that many seals wear to a profile consisting of two circumferential waves. It has been shown that the distortions caused by the loading and drive mechanism of many simple mechanical seal designs will result in the floating ring wearing to this profile (120). Tests on unbalanced mechanical seals deliberately lapped to a three wave profile have shown good operation at pressures in excess of those normally accepted for the design (63). It is not clear, however, for how long this profile exists, as it too may wear to two waves. The test programme therefore covers both two and three wave profiles.

The measurements of the floating ring motion were taken when the mechanical seal had reached a steady operating condition. The temperature of the stator was monitored, and when

PARAMETER		BASELINE VALUE	OTHER TEST VALUES			
			1	2	3	4
SHAFT SPEED (rpm)		2900	1450	900		
PRESSURE (MPa)		0.5	0.2	0.7	1.0	
EXCITING VIBRATION	Level	VALUE OCCURRING DURING RUN				
	Frequency	SHAFT FREQUENCY				
FILM WAVINESS	(μm)	1	1			
	(No. of waves)	3	2			
FLOATING RING GEOMETRY	(Centroid)	30%	30%	45%	45%	45%
	(O-ring)	20%	85%	20%	45%	85%
O-RING SECTION		1.78 mm				
O-RING MATERIAL		Nitrile				

Table 5 - 3 Experimental Programme Parameter Values

a steady temperature was reached the floating ring motion, the temperatures of the stator, sealed oil and cooling water, and the cooling water flow rate were measured. In addition to these measurements the shaft and floating ring run-out is measured before bringing the rig up to the test speed, and on stopping the rig.

This test programme fulfils the programme design criteria. The complete test programme is given in table 5 - 3.

5.3 Analysis Technique and Estimation of Errors

5.3.1 Analysis Technique

Three measurements were made during each test run. Firstly the leakage from the seal. Secondly the cooling water flow rate, with the inlet and outlet temperatures and finally the motion of the floating ring. The leakage was collected by blotting paper encircling the seal plate and absorbing the leakage for a measured time (two minutes).

The heat flux dissipated through the cooling coil was obtained from the flow rate and the temperature difference between the inlet and outlet. The thermocouples were not individually calibrated, but the temperature obtained using a Comark Electronic Thermometer Type 1624. Differences occurred in the temperature measured by individual thermocouples when the rig was cold and at a constant temperature. This was not important for the pressure chamber and stator temperature, but introduces an error into the heat flux calculation. The difference between the inlet and outlet temperatures was measured with the rig cold, and the difference applied to the temperature difference measured when the rig is hot.

The motion of the floating ring was measured by three transducers. The axial movement by measuring the total capacitance of the fluid film at the sliding interface of the mechanical seal; and radial and angular motion by two displacement transducers mounted radially 17 mm apart centre to centre.

The capacitance was measured using a variation of a probe developed for measuring film thickness between reciprocating seals and the shaft housing (97). Exact values of the capacitance are obtained by comparing the measured level with the capacitance of a high precision variable capacitor. The system does however have a drawback because it is linear only over the range 0 - 100 pF. In order to limit the capacitance to this range a series capacitor was introduced.

Direct calibration of this transducer is difficult due to the small separations involved and the need to calibrate it on the rig. The film thickness will be calculated from the basic formula for the capacitance of a capacitor (see page 95 for a discussion of possible errors in this approach). The film thickness is given by:-

$$h = \frac{KA}{3.6\pi C}$$

where C is in pF

A is in m^2

h is in m

K is 2.2 for oil

For the mechanical seal $h = \frac{8270}{C}$ μm

The two displacement transducers measure the radial motion of the floating ring. By comparing the outputs from the transducers both the radial and the angular motion can be determined. The radial motion is given by the average of the displacements

measured by the two transducers:-

$$\chi = \frac{D_A + D_B}{2} \text{ mm}$$

The angular motion is the difference between the two displacements divided by their separation:-

$$\psi_\chi = \frac{D_A - D_B}{17} \text{ radians}$$

The measurements of the o-ring properties were analysed using the technique described in chapter 4. They are reduced to a temperature of 20°C as before using the WLF equation. The same factors will be used as the exact formualation of the compound is not known.

5.3.2 Estimation of Errors

The most important requirement of any seal tests is an accurate measurement of the leakage. Great care must be taken to ensure that the measured leakage is an accurate representation of the leakage. Check weighings were therefore made to ensure that the measured values could be corrected for any extraneous fluid absorbed from the test rig in the vicinity of the seal plate. It is still possible for the measurements to be in error due to small changes in the operating conditions occurring, however no significant changes were observed during the test runs. The weighings are accurate to approximately ± 2 mg. This is equivalent to an error in the leakage of approximately ± 0.08 ml/hr.

For the present test program it proved to be impossible to repeat the shaft vibration levels exactly. The repeatability of the results could not therefore be checked directly.

The measurement of the heat flux by monitoring the cooling

water flow is subject to two possible errors. Firstly the accuracy of measuring the flow rate and secondly the accuracy of the temperature measurement. The former may be measured to within a few ml per minute. The accuracy of the temperature measurement is much smaller. The quoted accuracy of the Comark Electronic Thermometer with a Cu/Cu-Ni thermocouple is $\pm$ 0.2^{o}C. At the full flow rate of the cooling water this would result in an error of approximately $\pm$ 20%. By reducing the cooling water flow rate, the accuracy of the flow rate measurement is decreased, but that of the temperature measurement is increased. It is possible to achieve accuracies of $\pm$ 5% and $\pm$ 7% for the flow rate and temperature measurement respectively. The heat flux measured is thus within $\pm$ 12%.

The measurement of the motion of the floating ring has several possible sources of error. Firstly due to the inherent accuracy of the transducers, and the variable capacitor used for the capacitance measurements; these are small, of the order of $\pm$ 1%. Secondly there are errors introduced when interpreting the UV Recorder traces. For instance surface blemishes on the floating ring or the shaft collar may cause the output signals to be distorted and hence difficult to analyse. The thickness of the traces themselves could also lead to inaccuracies in the analysis of $\pm$ 2 or 3%. The transducers used for the measurement of the radial motion were calibrated using feeler gauges. By using a micrometer to measure the feeler gauge thickness it proved to be possible to repeat the measurements within the resolution of the micrometer.

Finally the transducers and their associated signal conditioning may be subject to drift, and the capacitance

measurements affected by stray capacitances. The test results may be corrected for any change in the calibration by calibrating the transducers immediately prior to a test, and then checking the calibration at the end.

The capacitance measurements may be subject to a number of errors. The value used for the dielectric constant (2.2) (97) could be in error due to extensive cavitation, the minimum possible value being that of air (1.0). Low resistance contacts between asperities on the mating faces could result in erroneous readings. The electrical path from the rotor to the signal conditioning unit may be affected by oil from the rig thus introducing stray capacitances again leading to erroneous readings, or a complete breakdown of the circuit. The formula also assumes the plates are parallel, which is not the case for large angular vibrations. The formula for the capacitance in the misaligned case is:-

$$C = \frac{\varepsilon_0}{h_m} \int_{r_i}^{r_0} \int_{0}^{2\pi} \frac{r dr d\theta}{1 + \frac{r_m \psi}{h_m}} \cos\theta$$

which may be integrated and rearranged to give an expression for the mean film thickness:-

$$h_m = \pi\varepsilon_0 \frac{(r_0^2 - r_i^2)}{C\sqrt{1 - \frac{r_m^2 \psi^2}{h_m}}}$$

This may be compared with the expression for the parallel case:-

$$h_m = \frac{\pi\varepsilon_0(r_0^2 - r_i^2)}{C}$$

Thus a misalignment angle giving a change in film thickness of 20% of the mean film thickness ($R\psi = 0.2\ h_m$), would result in an error in the mean film thickness of 2%

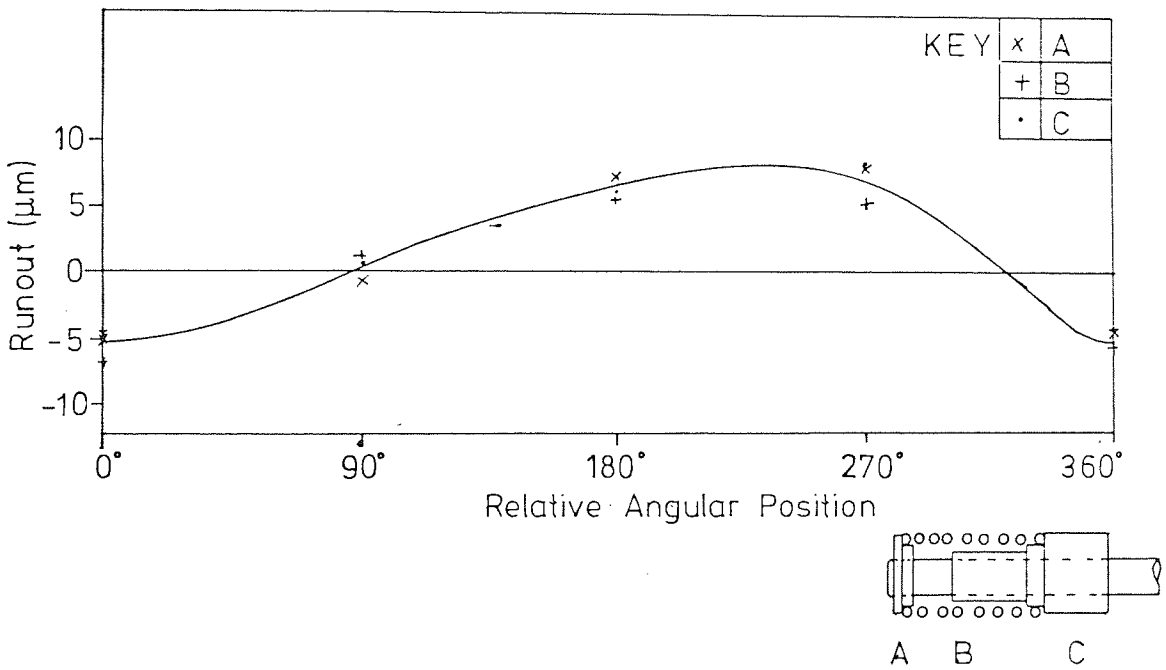

Fig 5-4 Mechanical Seal Rig Shaft Runout

The o-ring measurements are subject to the errors described in chapter 4.

5.4 Results

5.4.1 Initial Rig Tests

Before the rig was assembled the shaft run-out was measured using a finger dial gauge. For this the thrust bearing was loaded manually with a lathe centring tool. Fig 5 - 4 shows the results. The measurements were made at the position of the shaft collar, the tail of the long rotor and the o-ring position near the seal face. No significant difference between the readings was noted. The initial run showed that one of the transducers was drifting. This was replaced by a spare unit. All three transducers then gave consistent readings over a thirty minute period.

It was sometimes difficult to obtain readings from the capacitance probe. Even after an overhaul of the electronics it proved impossible to obtain capacitance readings on some occasions. This problem was not satisfactorily resolved and the recorded axial vibration levels must therefore be treated with caution.

5.4.2 Test Results

The test results are given in tables 5 - 4 to 5 - 7 for the range of test conditions given in table 5 - 3. The results tables give the test conditions, the peak to peak vibration amplitude, the leakage and the power dissipation.

For each test the seal face profiles were carefully lapped. The rotor face was initially lapped flat, then

Fig 5-5 A Typical Floating Ring Profile

deformed to give the required surface profile and again lapped flat. When the distorting force was removed the seal returned to the required surface profile. A typical rotor profile is shown in fig 5 - 5.

For all tests the stator surface was lapped nominally flat. Since all surface profiles were checked by optical interferometry (chapter 1), the surface was flat to better than 0.29 m.

Measurements were taken when the three thermocouples had reached a steady temperature. The measured stator temperatures are given with the tables. The measured vibration levels are spot values taken as the other measurements were made.

Three distinct forms of the capacitance probe signal were observed during the experiments (see figure 5 - 6). The most usual form of the signal was a shaft frequency oscillation about a mean level, and an apparently random small amplitude modulation (fig 5 - 6a). Secondly, for some runs there were random changes in the mean level (fig 5 - 6b). These changes were generally greater than the oscillation amplitude and appeared to have no direct link with other operating changes, such as pressure fluctuations. Finally for some runs there was no measurable variation in the mean capacitance of the probe. The capacitance circuitry was carefully checked but no faults were found. No other satisfactory explanation for the behaviour of the probe could be found, but the possibility of an electronic fault cannot be ruled out.

The o-ring properties are given in fig 5 - 6. Both the stiffness and the damping coefficient show similar trends to the results presented in chapter 4, although the scatter is much greater. The mean values of the stiffness and damping coefficients for frequencies of $48\frac{1}{3}$, $24\frac{1}{6}$ and 15 Hz (2900, 1450 and 900 rpm) are plotted against temperature in fig 6 - 7. This may be compared with fig 4 - 22. The WLF equation has been used to shift the values to the appropriate temperature.

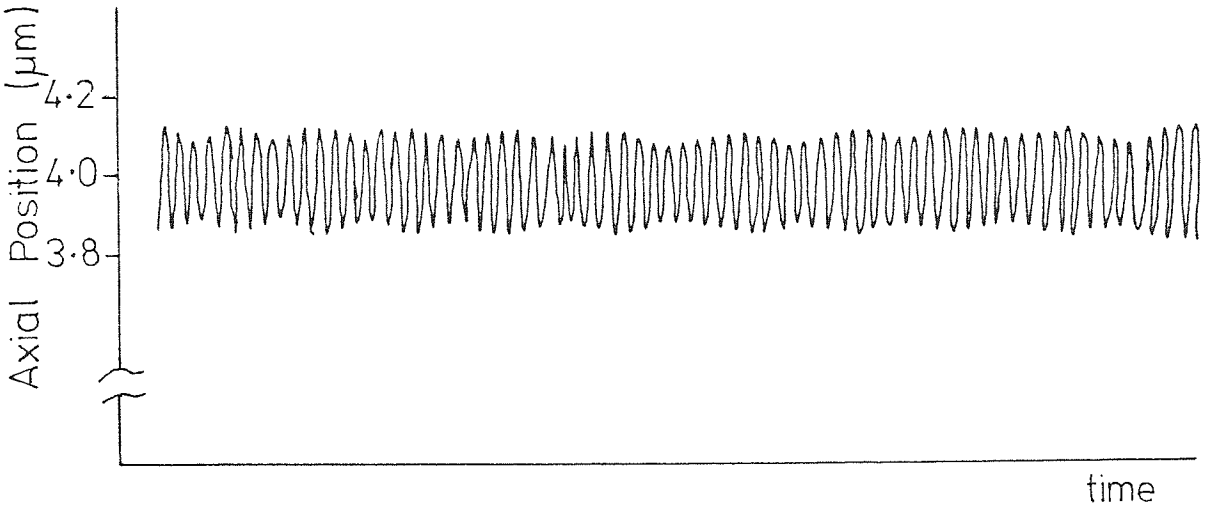

(a) Usual Signal Form

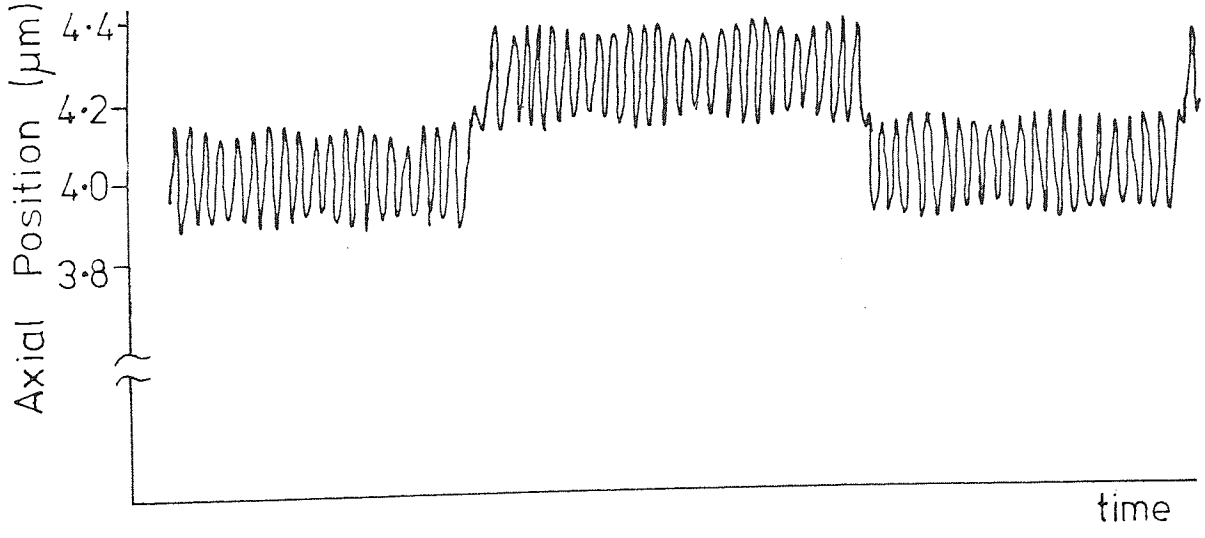

(b) Typical Mean Signal Level Changes

Fig 5-6 Forms of Capacitance Probe Signals

Shaft Vibration (μm)	Floating Ring Vibration (About Centroid)			Mean Film Thickness (μm)	Power Dissipation (W)	Seal Leakage (ml/Hr)	Stator Temperature °C
	Radial (μm)	Axial (μm)	Angular (μRadians)				
21.2	18.4	0.27	1100	3.98	249	0.78	67
85.4	52.3	0.71	2400	3.10	202	12	81
138	126	-	4800	-	180	14.4	90

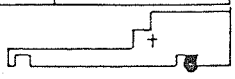

Table 5 - 4 Effect of Shaft Vibration Level on Floating Ring Vibration 2.2 ms^{-1} (2900 rpm) 0.5 MPa Sealed Pressure - out of balance weights applied

Geometry	Shaft Vibration (μm)	Floating ring vibration (About Centroid)			Mean Film Thickness (μm)	Power Dissipation (W)	Seal Leakage (ml/Hr)	Stator Temperature (°C)
		Radial (μm)	Axial (μm)	Angular (μRadians)				
Long (i)	21.2	18.4	0.27	1100	3.98	249	0.73	67
Short(ii)	13.2	40.9	1.2	1100	2.78	202	6.6	62

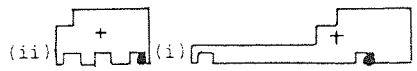

(a) Floating Ring Design with o-ring at 20% (No out-of-balance weight applied)

Geometry	Shaft Vibration (μm)	Floating Ring Vibration (About Centroid)			Mean Film Thickness (μm)	Power Dissipation (W)	Seal Leakage (ml/Hr)	Stator Temperature (°C)
		Radial (μm)	Axial (μm)	Angular (μRadians)				
Long (i)	6.9	25.2	1.79	690	2.53	220	5.7	64
Short(ii	22.3	31.6	0.8	270	1.42	140	9.6	63

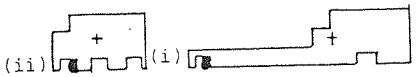

(b) Floating Ring Design with o-ring at 85% (No out-of-balance weight applied)

Geometry	Shaft Vibration (μm)	Floating Ring Vibration (About Centroid)			Mean Film Thickness (μm)	Power Dissipation (W)	Seal Leakage (ml/Hr)	Stator Temperature (°C)
		Radial (μm)	Axial (μm)	Angular (μRadians)				
3 Waves	21.2	18.4	0.27	1100	3.98	249	0.78	67
2 Waves	10.8	13.9	-	340	-	213	13.2	65

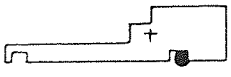

(c) Floating Ring Surface Profile (No out-of-balance weight applied)

Table 5 - 5 Effect of Geometry on Floating Ring Vibration at 4.5 ms^{-1} (2900 rpm) 0.5 MPa Sealed Pressure

O-Ring Position* (%)	Shaft Vibration (µm)	Floating Ring Vibration (About Centroid)			Mean Film Thickness (µm)	Power Dissipation (W)	Seal Leakage (ml/hr)	Stator Temperature (°C)
		Radial (µm)	Axial (µm)	Angular (µRadians)				
+40 (i)	21.2	18.4	0.27	1100	3.38	249	0.78	67
-170(ii)	6.0	35.2	1.73	690	2.53	220	5.7	64

* Relative to centroid position, expressed as a percentage of the distance of the centroid from the sliding interface, positive is towards the interface.

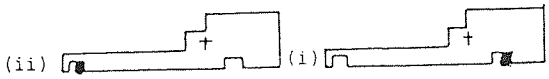

(a) Long Floating Ring (No out-of-balance weights applied)

O-Ring Position* (%)	Shaft Vibration (µm)	Floating Ring Vibration (About Centroid)			Mean Film Thickness (µm)	Power Dissipation (W)	Seal Leakage (ml/hr)	Stator Temperature (°C)
		Radial (µm)	Axial (µm)	Angular (µRadians)				
+55 (i)	13.2	40.3	1.2	1100	2.78	202	7.8	62
0 (ii)	26.3	8.8	0.5	810	2.62	196	6.6	57
-75(iii)	22.3	31.6	0.8	270	1.42	140	9.6	63

* Relative to centroid position, expressed as a percentage of the distance of the centroid from the sliding interface, positive is towards the interface.

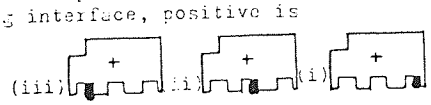

(b) Short Floating Ring (No out-of-balance weights applied)

Table 5 - 6 Effect of o-ring position on Vibration for Short and Long Floating Rings at 2.5 $m.s^{-1}$ (2000 rpm) and 0.5 MPa Sealed Pressure

Pressure (MPa)	Shaft Vibration (μm)	Floating Ring Vibration (About Centroid)			Mean Film Thickness (μm)	Power Dissipation (W)	Seal Leakage (ml/Hr)	Stator Temperature (°C)
		Radial (μm)	Axial (μm)	Angular (μradians)				
0.2	20.3	27.3	0.27	900	3.88	214	0.84	63
0.5	21.2	18.4	0.27	1100	3.08	240	0.78	67
0.7	20.3	32.0	2.55	640	4.71	290	2.04	73
1.0	19.4	32.4	0.35	1000	6.23	357	31.8	85

(a) Pressure (No out-of-balance weights applied)
(2.5 $m.s^{-1}$, 2900 rpm)

Shaft Speed		Shaft Vibration (μm)	Floating Ring Vibration (About Centroid)			Mean Film Thickness (μm)	Power Dissipation (W)	Seal Leakage (ml/Hr)	Stator Temperature (°C)
(ms^{-1})	(rpm)		Radial (μm)	Axial (μm)	Angular (μradians)				
0.78	900	12.5	9.8	0.23	280	5.76	71	0.03	57
1.26	1450	10.8	10.7	0.54	270	5.53	212	0.18	58
2.6	2900	21.2	18.4	0.37	1100	3.08	240	0.78	67

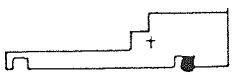

(b) Shaft Speed (No out-of-balance weights applied)
(0.5 MPa)

Table 5 - 7 Effect of Operating Parameters on Vibration Levels - (a) Sealed Pressure (b) Shaft Speed

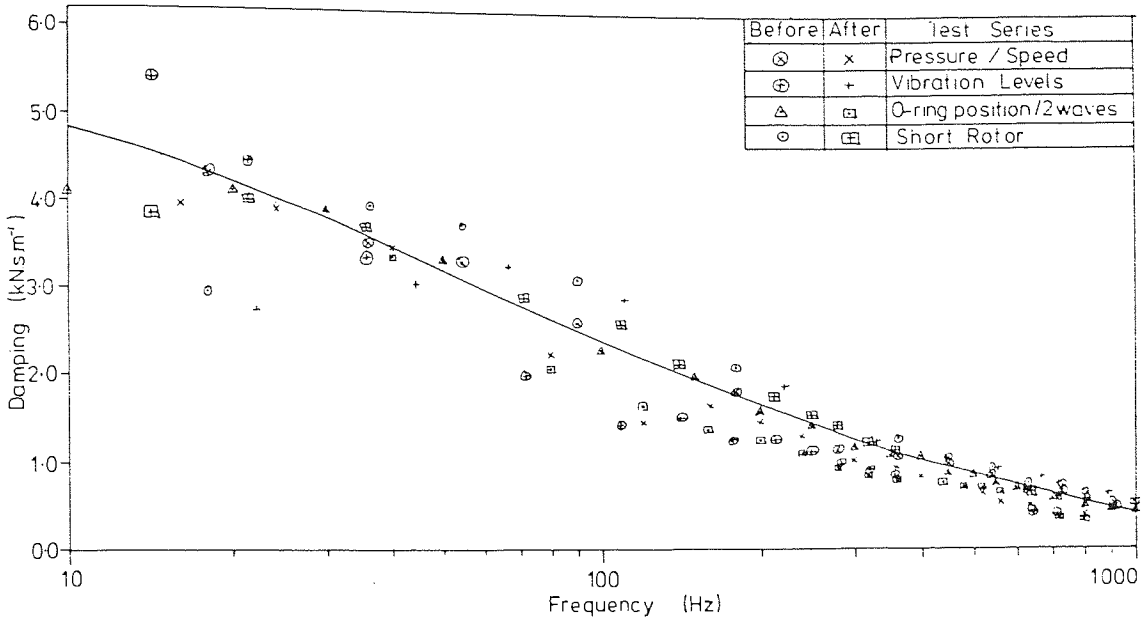

(a) Damping Coefficient

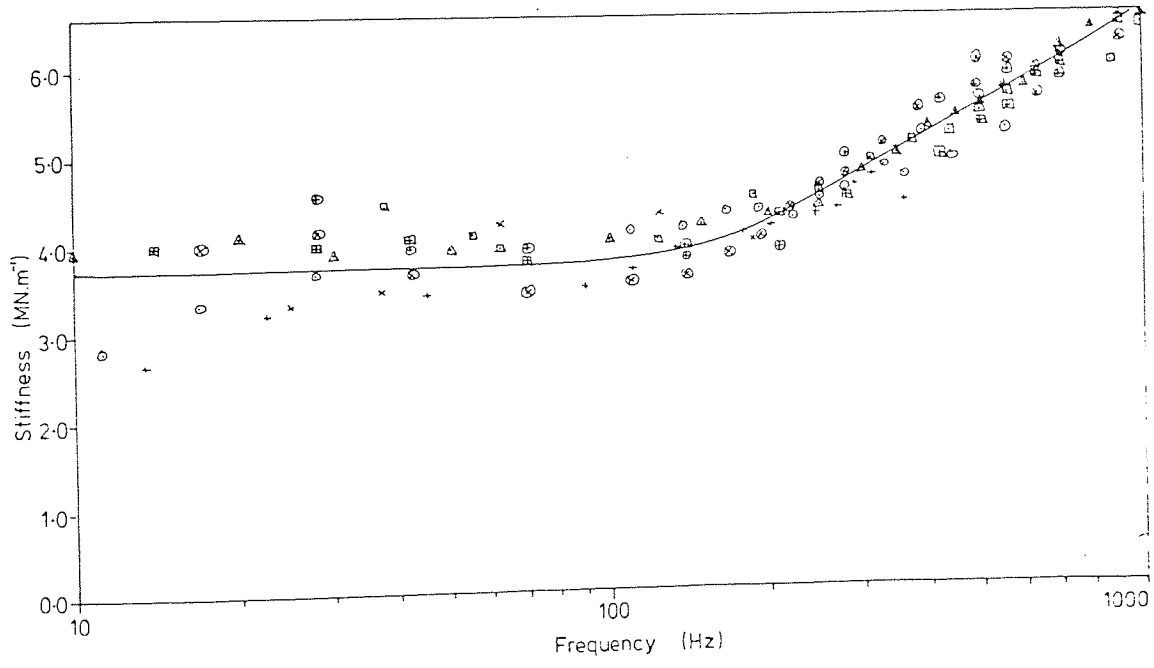

(b) Stiffness

Fig. 5-6 Properties of O-Rings used in Mechanical Seal Experiments

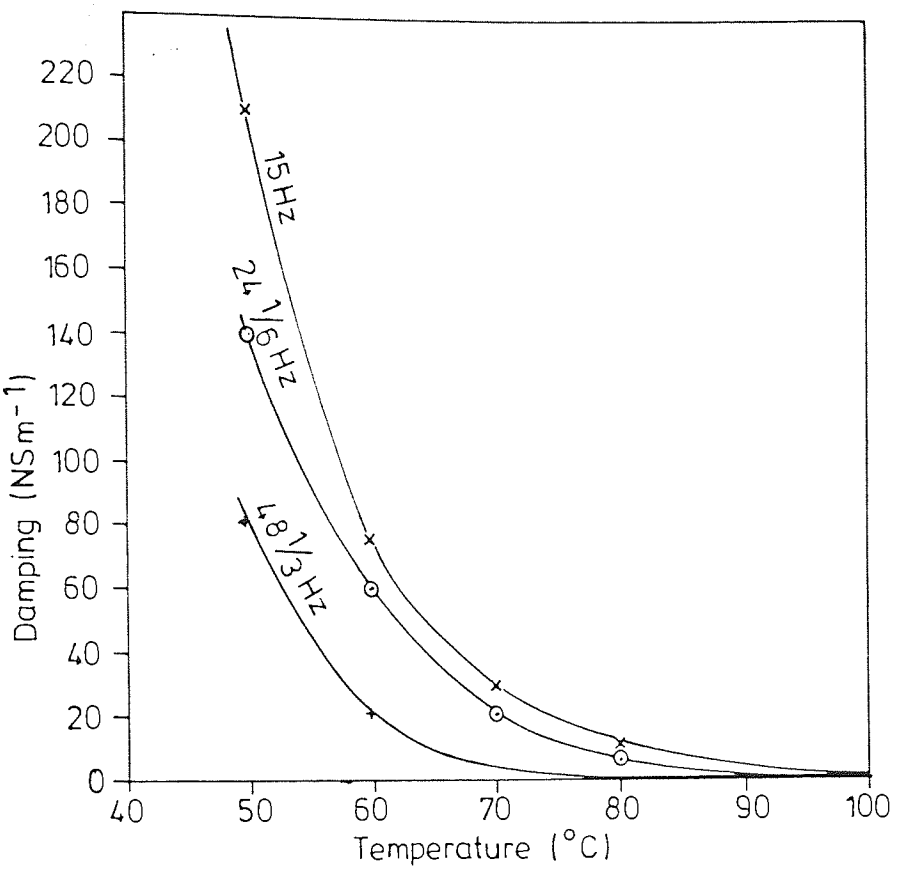

(a) Damping

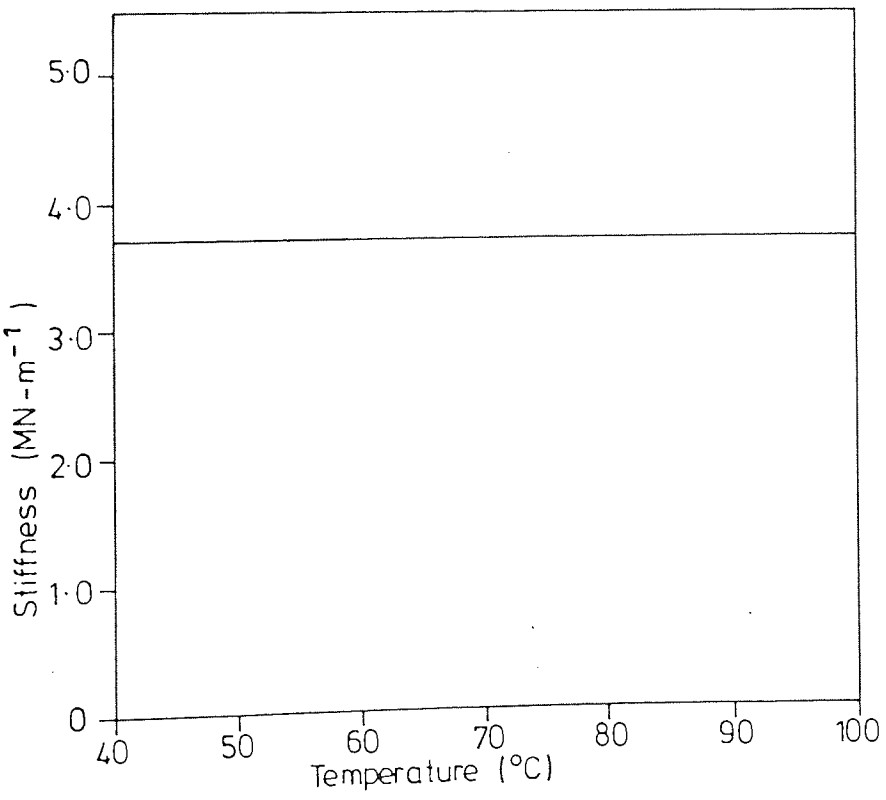

(b) Stiffness

Fig 5-7 Effect of Temperature on Mechanical Seal O-Ring Properties

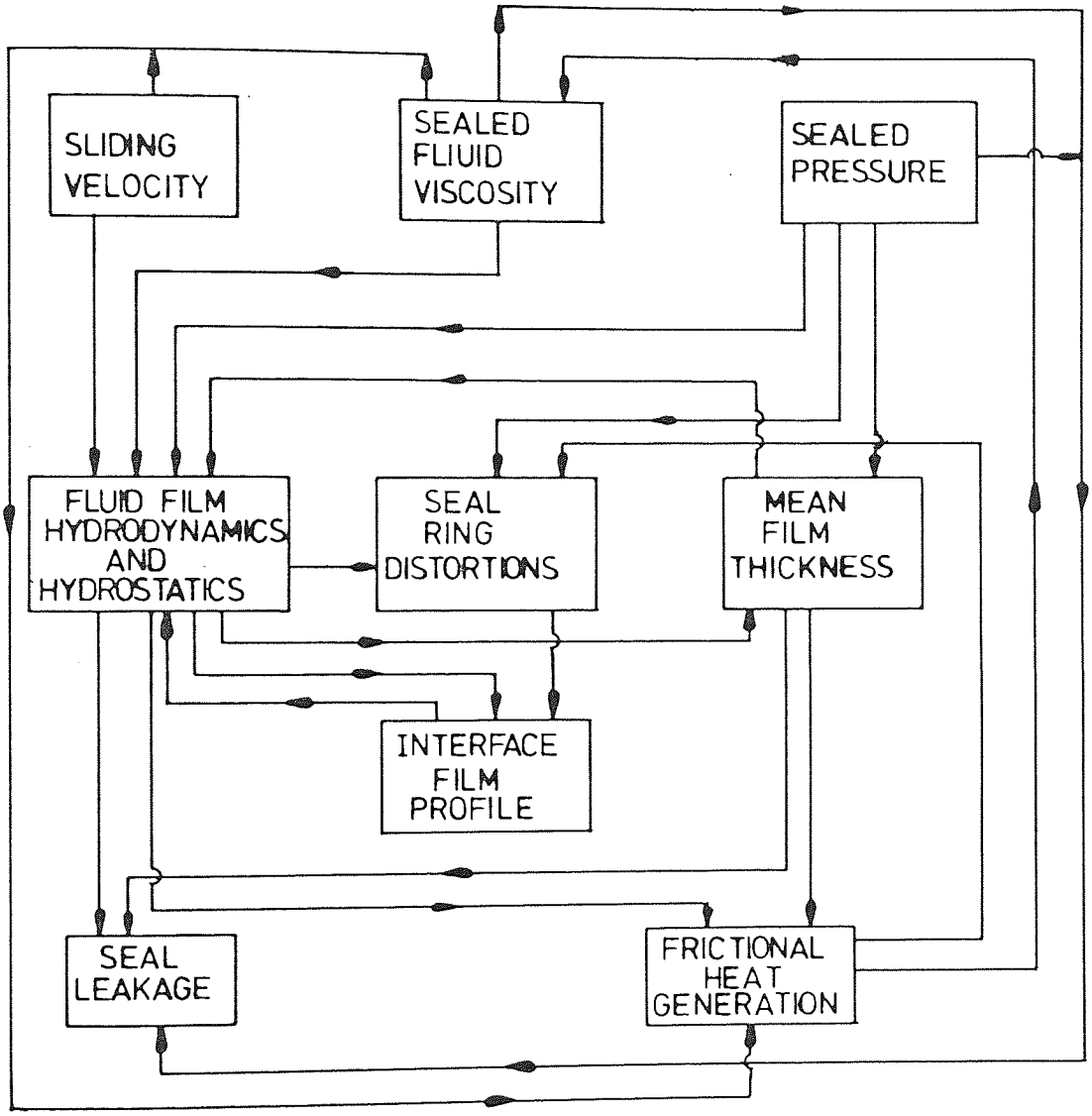

Fig. 5-8 An outline of the Inter-relationships between Factors affecting Mechanical Seal Operating Conditions

5.5 Discussion

Fig 5 - 8 outlines some known inter-relationships between the main mechanical seal operating parameters. The figure clearly shows the complexity of these relationships. For instance, the operating conditions, shaft speed, sealed pressure and sealed fluid, have a direct effect on the leakage from the seal and the heat generated. Increasing either the shaft speed or the sealed pressure will tend to increase both the leakage and the heat generated. However both these factors also have a direct effect on the fluid film hydrodynamics. The sealed pressure also affects the hydrostatics and will have an indirect effect on the hydrodynamics through its effect on the mean film thickness and the distortions of the seal rings. Changes in these parameters will affect the hydrodynamics which in turn results in changes to the distortions and mean film thickness. Thus the effect on the seal performance of a simple change such as an increase in sealed pressure is difficult to predict, without a predictive tool such as a computer program capable of taking into account all the interacting factors.

A multiple linear regression analysis of the experimental and computer results is therefore presented in Appendix G.

5.5.1 Shaft Vibration Levels

It was not possible to obtain a zero shaft vibration level for any of the test runs. Also the only effectively constant shaft vibration occurred in the test series where the rig had not been dismantled between runs (the pressure tests, table

5 - 7a). In this series the floating ring response did not follow the expected trend. The lowest radial, but largest angular , vibration occurred at an intermediate pressure, 0.5 MPa, the baseline condition. The largest radial vibration did occur at the highest pressure (1 MPa), slightly larger than the value at 0.7 MPa. This suggests that, although the rig has been run until the temperatures stabilise, the seal may not have reached a stable operating condition.

For all the tests except the second and third tests of Table 5 - 4, the rig was carefully assembled to ensure runout was a minimum and that there were no unbalanced weights, although the shaft and rig were not dynamically balanced. There is a wide variation in the measured shaft vibration under these conditions and this has an important implication for the practical use of seals. It would appear that dynamic balancing of the shaft may be important if shaft vibration levels, and hence seal vibration, is to be kept to a minimum.

5.5.2 Floating Ring Vibration

A feature of the results is that the measured angular vibration corresponds to axial displacements very much larger than the measured film thickness. Even the smallest angular vibration (61 μRadians) would result in a change of film thickness double the measured film thickness. The largest angular vibration (4600 μRadians) would result in a radial motion of the ends of the floating ring approximately equal to the clearance between the floating ring and the shaft.

As the seal does not leak excessively it must be concluded that the stator followed the angular motion of the floating

ring very closely. This motion would lead to a variation in the compression of the stator secondary seal. For the largest angular vibration this would result in a fluctuating force of $\pm$ 200 N. This is of a similar order of magnitude to the steady axial force on the floating ring due to the sealed pressure and the drive spring.

The axial vibration levels measured are within the range of the film thicknesses measured. The latter are much larger than expected but the leakage rates are not excessive. The thicknesses are however several times larger than those generally reported for mechanical seals (chapter 1). It might be expected that the film thickness would decrease as the sealed pressure, and hence the axial force on the floating ring, increases and also as the speed decreases. This is not the case for the measured values. It has already been explained that there is a complex inter-relationship between the parameters affecting the performance of a mechanical seal. It is thus not possible from these results alone to determine whether the axial measurements are unreliable as suggested in section 5.4.

The radial vibration levels in general follow the shaft vibration. This is consistent with the conclusion in chapter 3 that the radial effects of the fluid film were negligible. The radial motion should thus be the shaft motion modified only by the properties of the o-ring.

For the short rotor the angular amplitude is least when the o-ring is furthest from the interface film (i.e. o-ring at 85%). It might be expected that the minimum amplitude would occur when the o-ring was in line with the centroid. For the long rotor, the amplitude is greatest when the o-ring is furthest from the

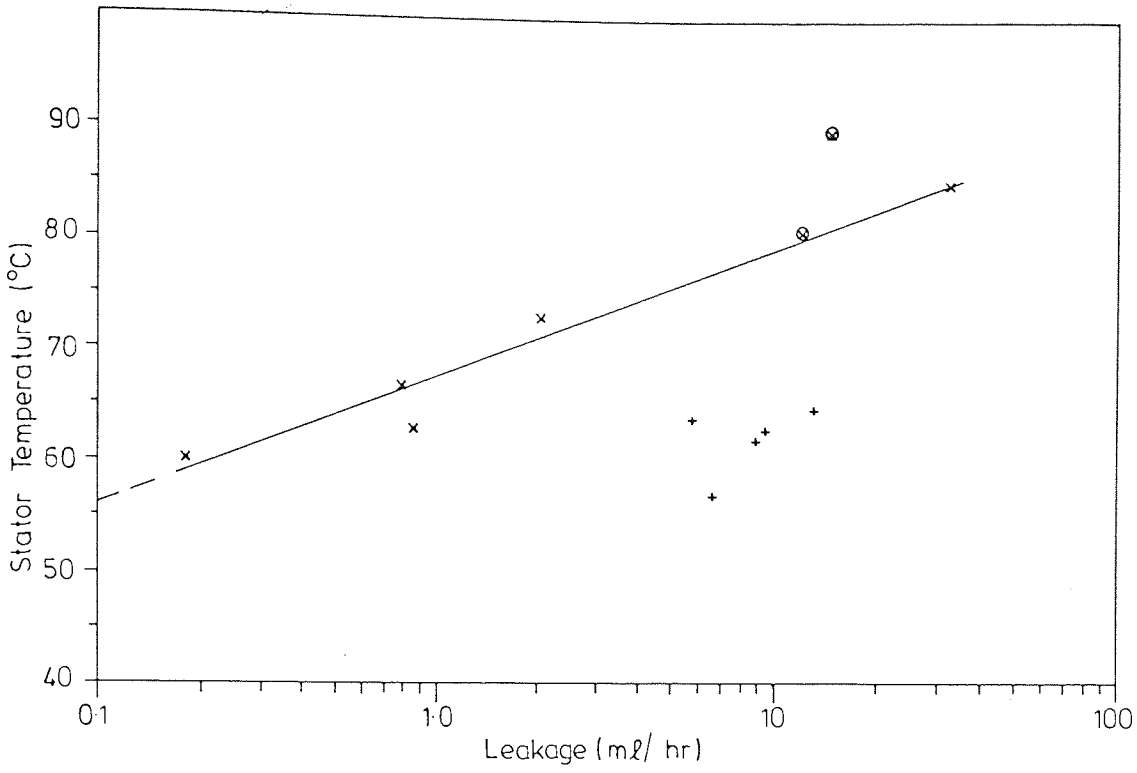

(a) Stator Temperature

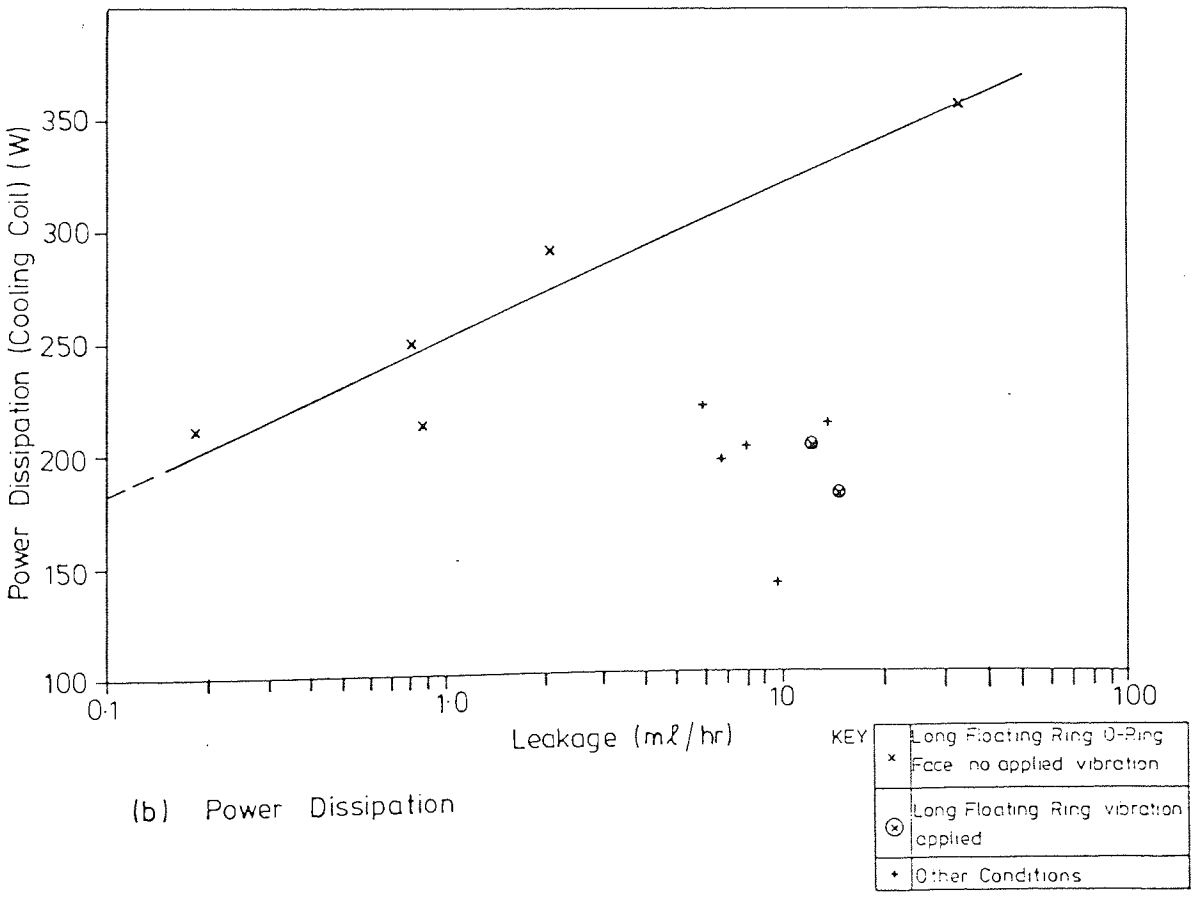

(b) Power Dissipation

Fig 5-9 Experimental Results - Thermal Effects and Leakage

centroid. In addition to the complex relationship between the seal operating parameters it is possible that the liquid between the shaft and the floating ring has an effect on the floating ring's response.

The angular vibration is also least for the two wave surface profile. The three wave pressure field generated by the three wave profile would be expected to be more stable film and hence exhibit lower angular vibration. However changes in the distortions of the seal rings arising from changes in the heat flux generated may change the interface profile and conditions sufficiently to produce a more stable pressure profile.

The angular vibration (when corrected proportionally for the shaft vibration level and actual lever arm length) is largest for the floating ring with the least moment of inertia. However, for the radial and axial modes the largest response corresponds to the smallest inertia only when the o-ring is close to the interface.

5.5.3 Leakage

The leakage increases with the floating ring vibration amplitude, but varies inversely with the power dissipation. This suggests that the mean film thickness increases with the vibration amplitude.

Fig 5 - 9 shows plots of the leakage against stator temperature and power dissipation. A line has been drawn through all the points representing the long floating ring with the o-ring at the interface, except the two points where the floating ring was deliberately vibrated by an out of balance weight. Extrapolating the stator temperature line to ambient

temperature ($17^{o}C$) gives a leakage rate of 0.44×10^{-4} ml/hour. Since this stator temperature would only occur when the seal was stationary, this leakage rate may be taken as the static leakage. The plotted points are for various pressure differentials, however for the baseline condition (sealed pressure 5 bar) this leakage rate implies a mean film thickness of 0.25 μm (assuming parallel faces). This figure may be compared with the initial profile peak amplitude of 0.5 μm ($1\frac{1}{2}$ light bands), which is equivalent to a mean film thickness of 0.5 μm for a zero minimum film thickness.

If the power dissipation line is extrapolated to the same leakage rate, a power of -49 W is obtained. Obviously the cooling water does not transfer heat to the sealed oil and thus this negative value must therefore represent the heat being dissipated by heat transfer from the pressure chamber to the surrounding atmosphere. These observations are probably too simple to account for the complex interactions occurring in practice, but they give a useful indication.

The short floating ring tests do not entirely follow the trends of the long floating ring tests. Thus, whilst the o-ring position giving the lowest vibration levels has the lowest leakage rate, the position with the highest leakage rate does not have the highest vibration levels. In general the short floating ring has the high vibration levels and leakage rates.

The surface profile of the sliding interface has a considerable effect on leakage. Surprisingly, although the vibration levels are lower, the floating ring with the two wave surface profile has a much higher leakage rate. Since the power dissipation is less for this ring, it suggests that the

interface film is thicker.

5.5.4 Stator Temperatures

The stator temperatures appear to be related to both the power dissipation and the floating ring vibration. Thus for the pressure and shaft speed tests, where the vibration levels tend to increase with increasing power dissipation, the stator temperatures also increase. However where the power dissipation falls with increasing vibration, as it does for most of the tests, the stator temperatures do not consistently increase with increasing power dissipation. For the increasing vibration levels at constant speed, pressure and geometry (Table 5 - 4), the stator temperature falls as the vibration levels fall.

The leakage rate is high for these tests, but even a rise of 23°C in the leakage temperature (the stator temperature rise) would require only 0.5 W to be dissipated in the leakage flow. It seems more likely that the vibration, and the means of vibrating the shaft, are causing cavitation within the liquid in the pressure chamber. This could result in a reduction in the heat transfer to the cooling coil, despite a higher heat generation at the sliding interface. Two other observations make this a probable explanation. Firstly, there are other tests with high leakage rates, but without anomalous changes in the power dissipation. Secondly the oil temperatures measured within the pressure chamber showed a higher temperature at the end nearest the cooling coil.

For the tests where the seal geometry or the o-ring position is changed, the stator temperatures follow the changes in the power dissipation. This might be expected, though clearly the temperature of the stator will depend on the way

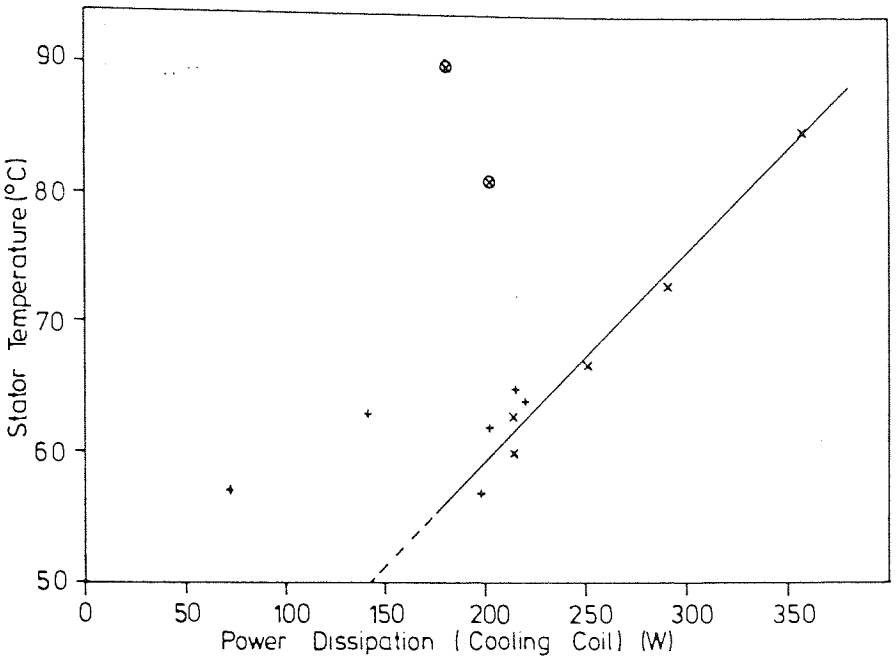

Fig 5-10 Experimental Results - Stator Temperature and Power Dissipation (key fig 5-9)

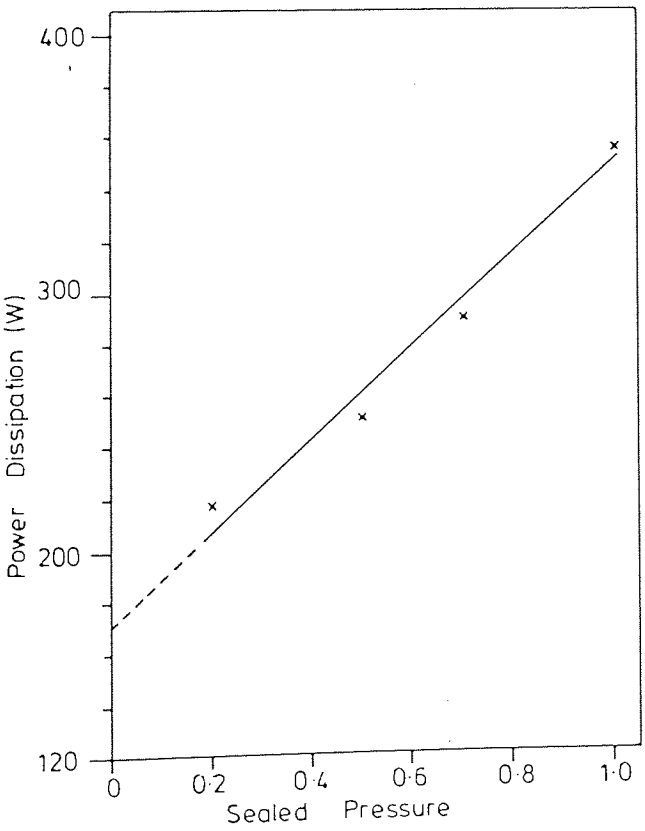

Fig 5-11 Experimental Results - Power Dissipation for pressure varitions only

the heat is transferred from the sliding interface to the surrounding fluid and the housing. The vibration levels may affect this and thus change the measured temperature from the expected value.

5.5.5 Heat Generation

The frictional heat generated in the sliding interface of a mechanical seal is an important feature of its performance. The heat must be conducted away, otherwise the high temperatures generated may result in severe seal distortions, surface cracking due to high local thermal stresses or vaporisation of the sealed fluid in the interface. In these tests the heat generated was not measured directly, but was inferred from the heat transferred to the cooling coil. An examination of fig 5 - 9 has shown that these measured values are too low and approximately 49 W are dissipated externally from the pressure chamber. A plot of stator temperature against power dissipated (fig 5 - 10) shows a similar result, in this case the figure is 60 W. Thus although the relative levels are probably correct, except for the points discussed above, the absolute level is about 50 - 60 W too low.

In general the experiments show that the rate of heat generation is inversely proportional to the vibration level and to the leakage. It is probable that the higher the vibration level the thicker the interface film. Whilst this may result in less risk of damage to the seal rings, the increased leakage could still result in a short useful seal life.

The variation of the heat generated with floating ring vibration is particularly consistent for the series where

sealed pressure and shaft speed are constant. The shaft vibration runs (Table 5 - 4) show a clear trend. However, since there is a variation in the radial, axial and angular vibration it is difficult to determine an exact relationship between the floating ring vibration and the power dissipation. When the shaft speed or sealed pressure is also changed, then the trends are less obvious. Table 5 - 7a shows that the power dissipation increases with pressure irrespective of the shaft vibration. Fig 5 - 11 shows the variation to be almost linear.

The heat generation falls with decreasing speed. This is also the result of the complex inter-relationships between the seal operating parameters. If the power dissipation was entirely due to the frictional heat generated by viscous shear at the sliding interface, then it would be proportional to the shaft speed and inversely proportional to the mean film thickness. The latter is not the case for the majority of the tests. Despite the effects of the other operating parameters this is further evidence that the capacitance measurements were not satisfactory.

5.5.6 O-Ring Properties

The o-ring stiffness and damping coefficients show considerably more scatter than the results presented in chapter 4. However, there is no consistent variation that could be related to changes in the properties that have occurred during the test runs. It is probable that the scatter is a genuine variation in the o-ring properties, as a result of the manufacturing processes. The o-rings used were not specially made, unlike those described in chapter 4, and thus were subject to the normal commercial tolerances on manufacture. No attempt has

been made to carry out a series of tests, similar to those described in chapter four, on commercial o-rings.

Fig 5 - 7 shows the properties for 15, $24\frac{1}{6}$ and $48\frac{1}{3}$ Hz (900, 1450 and 2900 rpm) transformed to the measured stator temperatures using the WLF transform (chapter 4). It can be seen that whilst the stiffness remains constant the damping falls dramatically. The damping values must, however, be treated with caution since they result from an extrapolation of the experimental curve well outside the measured frequency range.

5.6 Conclusions

In general the experiments showed that the vibration levels, except for the axial mode, have a definite relationship with the leakage and power dissipation of the seal. It was suspected that the axial measurements would be in error, and as they do not follow the trends of the other modes they should be disregarded.

The amplitude of the angular vibration is equivalent to a changing film thickness greater than both the measured values and values obtained by other workers. This suggests that the stator follows the motion of the floating ring. The predicted values of the fluid film stiffness in this mode (chapter 3) is much larger than the o-ring stiffness and thus deflection of the resilient stator support is to be expected.

The leakage measurements show that the greater the vibration of the floating ring the greater the leakage. The heat generation falls with increasing vibration and taking these two observations together suggests that the seal operates with a

thicker film when the vibration levels are high. Thus although lower wear rates would be expected, the seal may still have a short life because of an unacceptably high leakage rate. As the tests were merely long enough to take vibration, leakage and power dissipation measurements it was not possible to measure wear rates or other time-dependent effects. Extrapolation of the three plots of stator temperature against leakage and power dissipation, and power dissipation aginst leakage predicts that 50 - 60 W of the heat generated at the sliding interface are dissipated through the pressure chamber walls and not through the heating coil.

The geometry of the floating ring is important. The lowest leakage from the short floating ring seal was higher than from the long rotor. The position of the o-ring is also important. The leakage and vibration levels are less with the o-ring close to the interface, but the effect is less noticeable with the short rotor. Here, the o-ring is necessarily relatively closer to the interface.

The three-wave surface profile gave the best performance, with considerably lower leakage and only marginally higher power dissipation than for two waves. The radial vibration of the three-wave ring is less, though the angular vibration is greater. Thus its performance may be more dependent on the flexibility of the stator mounting.

The small section o-rings used in the mechanical seal tests are much stiffer than the larger rings tested in chapter four. The damping coefficient is also larger at the shaft frequencies considered, but at high frequency falls to similar values. Over the range of temperatures measured for the stator, the

stiffness of the o-rings is constant at 3.7 MN/m^2, but the damping varies from 97 Ns/m at 15 Hz, 57°C to 1 Ns/m at $48\frac{1}{3}$ Hz, 90°C.

The quantitative results presented here have confirmed the qualitative results obtained by the BHRA Process Industry Seals Survey (99), where bearing housing levels were measured. In the present experiments only shaft and floating ring vibrations were measured.

CHAPTER 6

COMPUTER PROGRAMS

In Chapters 2 and 3 the development of Reynolds equation and the equations of motion was described, and their solutions discussed. In this chapter the computer solutions that have been developed will be described. The chapter includes the validation of the programs, and finally the results obtained including a range of values for the fluid film elements and the predicted floating ring responses for the experimental conditions.

6.1 Program Outlines

The computer solutions have been developed separately rather than as one complete mechanical seal design program. However, the programs are written in such a way that they can be combined to give a complete seal performance prediction program without substantial changes to their structure. Unfortunately due to the amount of time spent on the unsuccessful solution technique for the equations of motion it has not proved possible to carry out the combination of the programs and run the resulting program successfully.

The programs have been implemented in Fortran IV on the I.C.L. 1904 s computer at the University of Aston in Birmingham. The two main considerations in the implementation were that

the language used should allow the programs to be, as far as possible, independent of the computer installation, and that the programs should require a minimum time to run. By writing the programs in standard ANSI Fortran IV, and by reducing repeated calculations and nesting of loops and subroutines to a minimum, these aims have largely been achieved. Reducing the running time of the programs by these means does, however, result in the use of more core than would be necessary if the execution time was not so limited.

The Reynolds' Equation solution calculates the fluid film stiffness and damping coefficients as well as solving for the pressure field and the film load capacity. It uses an empirical factor when delineating the cavity region in order to improve on the "Half-Sommerfeld" approximation with a minimum increase in run time (section 6.2.3). The program is described in Section 6.2 and its validation and results in Sections 6.4 and 6.5 respectively.

The Equations of Motion solution has three stages, an equilibrium position for time zero, a special solution for the first time step followed by the general solution. A convergence check is carried out to ensure that the calculated position is physically realistic. This program is described in Section 6.3, and its validation and results in Sections 6.4 and 6.5 respectively. This is the second solution technique to be implemented, the first being described in Appendix B.

(a) Control data

Number of data runs

Run title

*Run time and time interval

Cavity extension factor

Which interface surface profiled

(b) Array dimensions

Interface mesh

Number of degrees of freedom

*Number of input vibration modes

*Number of floating ring cylinders

(c) Interface and sealed fluid details

Outer radius

Width

Profile wave amplitude

Number of waves

Phase angle between $\theta = 0$ and maximum film thickness

Shaft speed

Floating ring position and velocities

Sealed pressure ID and OD

Cavitation pressure

Viscosity

Table 6 - 1 Reynolds' Equation Program Data
entries marked * make the program
compatible with the equations of motion
program

Variable	Coefficient
Force	$\frac{6\,\eta\,\omega\,R_o^4}{h_n^2}$
Stiffness Force - Linear	$\frac{6\,\eta\,\omega\,R_o^4}{h_n^3}$
Stiffness Force - Angular	$\frac{6\,\eta\,\omega\,R_o^5}{h_n^3}$
Stiffness Moment - Linear	$\frac{6\,\eta\,\omega\,R_o^5}{h_n^3}$
Stiffness Moment - Angular	$\frac{6\,\eta\,\omega\,R_o^6}{h_n^3}$
Damping Force - Linear	$\frac{6\,\eta\,R_o^4}{h_n^3}$
Damping Force - Angular	$\frac{6\,\eta\,R_o^5}{h_n^3}$
Damping Moment - Linear	$\frac{6\,\eta\,\omega\,R_o^5}{h_n^3}$
Damping Moment - Angular	$\frac{6\,\eta\,R_o^6}{h_n^3}$

TABLE 6-2 Non-dimensionalising coefficients from equations of motion

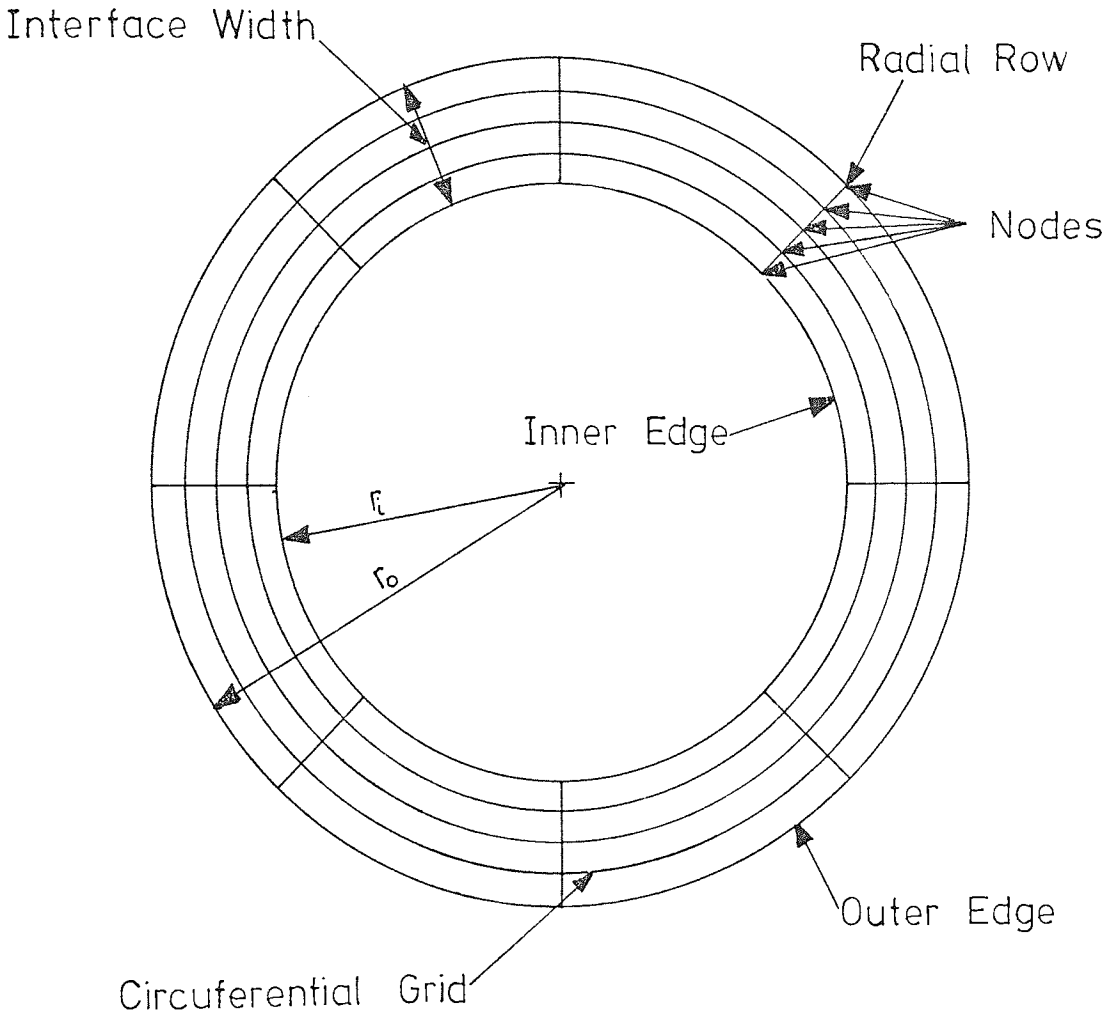

Fig 6-1 Principle of Finite Difference Grid

6.2 Reynolds' Equation Solution

6.2.1 Data

The solution requires only a small amount of data, and this is listed in Table 6-1. From this data the seal interface diameter ratio, the angular velocity and the radial and circumferential mesh spacings are calculated. The program works non-dimensionally and the data is non-dimensionalised using the factors given in Chapter 2. The dimensionalising coefficients for the fluid film elements may be obtained from a consideration of the equations of motion, and are given in Table 6-2.

6.2.2 Pressure Field

The principle of the solution grid is shown in fig. 6 - 1. The pressure and fluid film elements are calculated at each grid node. The nodes at the inner and outer diameters are defined as boundary nodes. The pressures at these nodes are taken as the values of the inside and outside pressure respectively.

The first circumferential node coincides with a maximum film thickness, due to the interface surface profile, at time zero and with the positive X-axis. The numbering scheme is such that there are N nodes and N intervals. Thus nodes N and 1 are separated by one mesh 'interval'.

The boundary nodes for each radial row are used to calculate the constants of integration for that row. The remaining pressures for the row are calculated using these constants. Each row is taken in turn and the pressures calculated. If a pressure less than the cavity pressure is calculated at any

node, no more pressures are calculated for that row and the program proceeds to the next row. Once all the pressures have been calculated the program revises the cavity extent and calculates the load capacity and the fluid film elements.

6.2.3 Cavity Region

In Chapter 1 it was explained that the common assumptions used to delineate the cavity were not correct, and that only a flow conservation technique could be expected to accurately predict the cavity shape. Various models have been suggested to describe the cavity region (83, 88, 100) and these have recently been reviewed with reference to a cylinder - plane geometry. The models may be divided into two broad categories. Firstly that the cavity consists of fluid at a uniform pressure, and the liquid flows around and through it, remaining attached to both the stationary and rotating faces. Secondly that the cavity consists of a gaseous region, and the liquid flow detaches from the stationary face ahead of the cavity and re-attaches within the converging film. It has been shown that the second form does not apply to journal bearings (155). For the mechanical seal, the condition that detachment cavitation shall exist is:-

$$B = 2\alpha$$

where $$B \geqslant \frac{h\,min}{h\,max}$$

and $$\alpha \equiv \frac{\eta U}{S_T}$$

Thus when sealing a liquid with viscosity 3×10^{-3} Nsm^{-2}, surface tension 30×10^{-3} Nm^{-1}, shaft speed 3000 rpm, interface mean diamter 50mm, h_{min} 0.7 µm, h_{max} 1.3 µm this gives:-

$$\alpha \doteq 0.8 \qquad B \geqslant 0.5$$

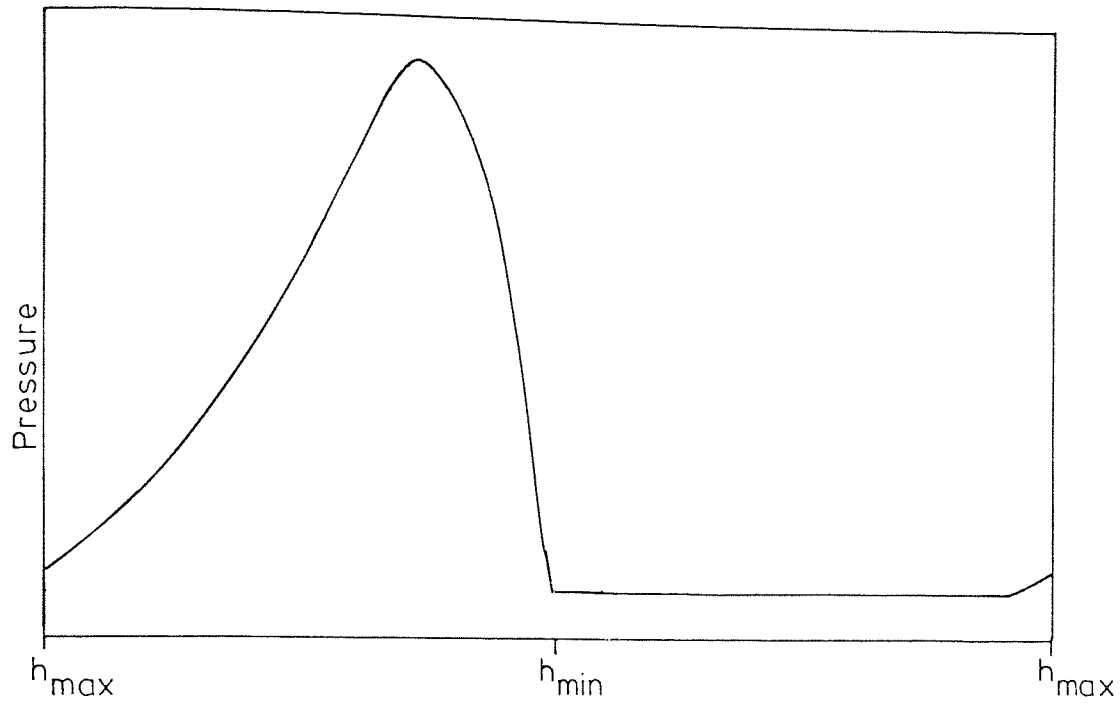

(a) Half Sommerfeld Condition

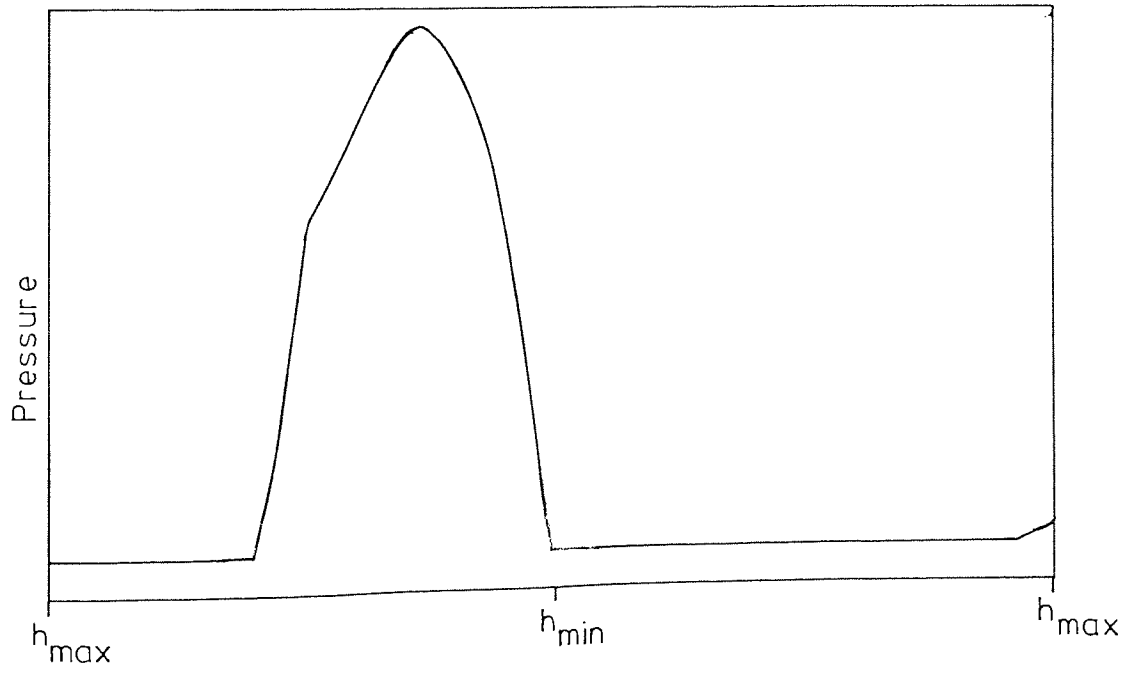

(b) Revised Condition

Revised Present Cavity End Node = Present Cavity End Node + INT ((Next Cavity Start Node - Present Cavity End Node) × Cavity Extension Factor)

Fig 6-2 Determination of Cavity Extent: Circumferential Pressure Profiles

and the condition could be satisfied.

It is therefore difficult to decide upon a satisfactory model. In addition the use of a flow conservation technique, being an iterative process, would violate the requirement for a quick solution.

In order to achieve a quick solution, and in view of the problem defining an accurate model, a purely arbitrary method is used to delineate the cavity. The method is based on the "Half-Sommerfeld" condition (76). The program notes the first and last nodes of each cavity as defined by the "Half-Sommerfeld" condition. Once all the circumferential nodes have been scanned the length of each cavity is extended to give it a more realistic length as has been found by other workers (141). The effect on the circumferential pressure profile is shown in fig 6 - 2. The extension factor is defined in terms of the circumferential grid nodes as follows:-

Revised Present Cavity End Node = Present Cavity End Node
+ INT ((Next Cavity Start Node - Present Cavity End Node) x Cavity Extension Factor)

The values of the "extension factor" have been obtained by comparing the load capacities calculated using this technique with those from a flow conservation solution (see p 120). Within the cavity limits thus calculated, the pressures are set to the cavity pressure and the pressure derivatives to zero.

6.2.4 Fluid Film Elements - Stiffnesses and Damping

The fluid film elements are evaluated from the derivatives of the pressure field at each grid node except the boundaries. The derivatives are calculated using analytical formulae, immediately after the pressures. However, when a pressure less than the cavity

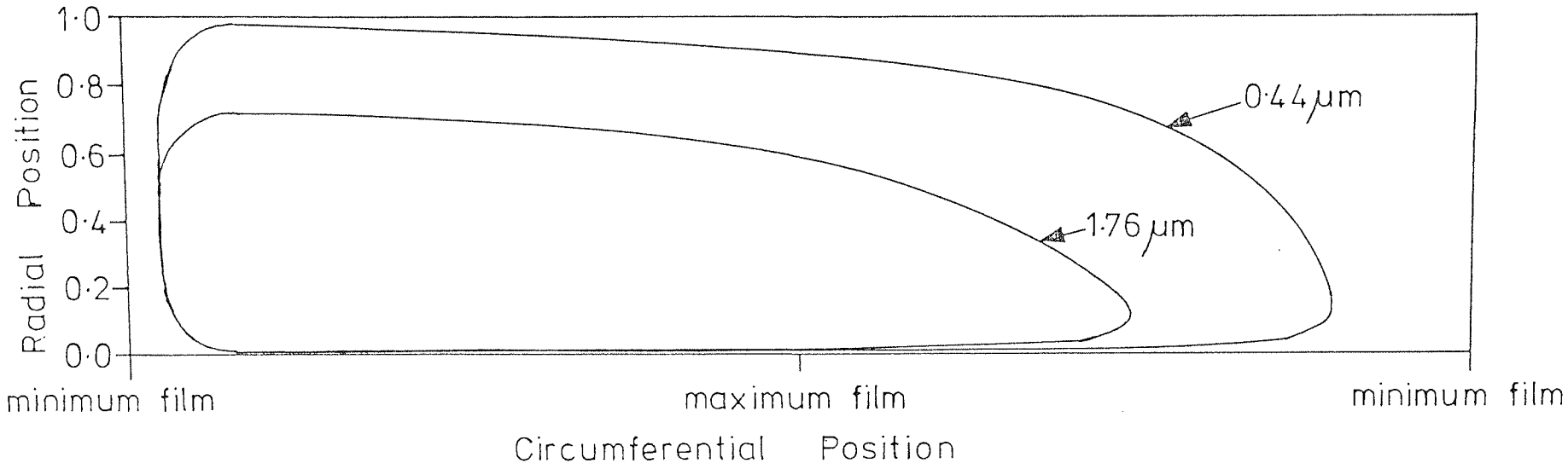

Fig 6-3 Effect of Minimum Film Thickness on Cavity Shape

pressure is obtained for any node on a radial row, no further calculations are carried out for that row. In addition the derivatives are set to zero within the extended cavity, implying that the cavity has no stiffness or damping. This is not strictly true since changes in the film thickness or in the angular misalignment will cause a change in the length of the cavity thus changing the axial load and angular moments generated by the fluid film. However, the solution technique does not permit the calculation of elements within the cavity. The result of this will probably be an over-estimation of the element values. For instance decreasing the film thickness increases the load capacity. This would be partly offset by an increase in the extent of the cavity (fig. 6 - 3) which the method described does not allow. The stiffness calculated would thus be larger than that occuring in practice.

The revised derivatives are integrated to give the force and moment stiffnesses and damping coefficients. The same derivatives are used for both the force and the two moment elements since:-

$$\frac{\partial W}{\partial h_c} = \int_{r_i}^{r_o} \int_{o}^{2\pi} \frac{\partial p}{\partial h_c} \; r \, dr \, d\theta$$

$$\frac{\partial M_t}{\partial h_c} o_x = \int_{r_i}^{r_o} \int_{o}^{2\pi} \frac{\partial p}{\partial h_c} \; r \cos\theta \, r \, dr \, d\theta$$

$$\frac{\partial M_t}{\partial h_c} o_y = \int_{r_i}^{r_o} \int_{o}^{2\pi} \frac{\partial p}{\partial h_c} \; r \sin\theta \; r \, dr \; d\theta$$

To calculate the moment, each derivative is multiplied by the appropriate radius when carrying out the radial integration. The appropriate function of the angle to each circumferential

(a) Array dimensions and control data

Number of degrees of freedom

Number of input vibration modes

Number of cylinders comprising floating ring

Number of timesteps

Title of run

(b) Element values and ring details

O-ring stiffness and damping in shear and compression

spring stiffness

Mass, length, inner and outer radii of floating ring cylinders

O-ring position relative to interface and radius of line of action, and o-ring groove

Length by which spring is compressed on fitting and radius of line of action

Sliding interface width and outer radius

Fluid film element values (in a separate file)

(c) Sealed fluid data

Pressure at inner and outer radius

(d) Input conditions

Shaft vibration amplitudes and frequencies

Initial floating ring displacements and velocities

Table 6 - 3 Equations of Motion Program Input Data

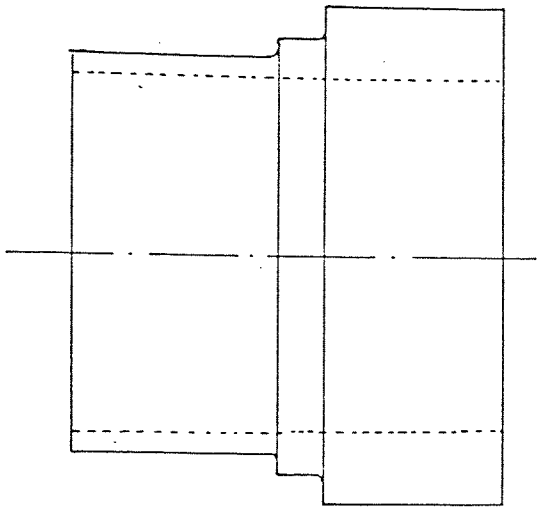

(a)

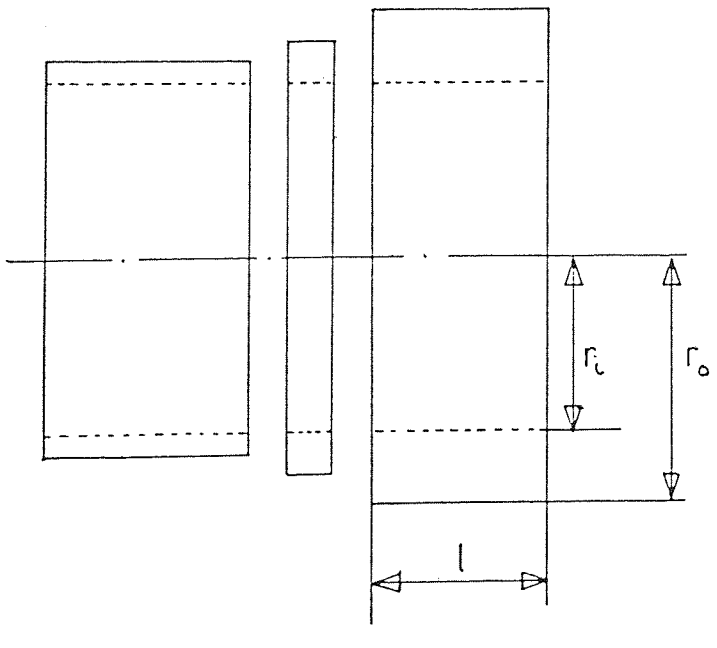

(b)

Fig 6-4 Division of Floating Ring
(a) Floating Ring
(b) Division into parts

node is then applied when carrying out the circumferential integration. Both integrations are carried out using Simpson's First Rule.

6.2.5 Leakage

It is important to be able to predict the leakage from the seal, and this is calculated using the formula given in Chapter 2 for the leakage across a tapered annular gap. Radial flow can only occur outside the cavity and thus only the area of the interface between the revised end of one cavity and the beginning of the next is utilised. The total leakage is the sum of the leakage for each area.

6.3 Equations of Motion Solution

6.3.1 Data

The data required by the program is given in Table 6 - 3. For the purposes of calculating the floating ring mass, inertia and centroid, it is assumed to be divided into a number of cylinders as shown in fig. 6 - 4. Up to ten cylinders may be used without modification of the program. The centroid is obtained by taking moments about the interface, and the inertia by tne usual formula for a thick walled cylinder (124):-

$$I = \frac{M_i}{12} \left(3 r_i^2 + 3 r_o^2 + \ell^2\right)$$

The total inertia of the floating ring is given by:-

$$I_T = \sum_{i=1}^{n} I_i + M_i d_i^2$$

It is also necessary to calculate the constant axial force on the floating ring due to the sealed pressure and the drive

spring. The former is calculated from the pressure difference between the inside and outside of the seal chamber and the annular area bounded by the o-ring groove radius and the sliding interface outer radius. The spring force is calculated from the spring stiffness and the initial compression on fitting.

6.3.2 Equilibrium Position

For the equilibrium position the radial displacements are taken from the data. The remaining positions are obtained by solving for the static equilibrium of the floating ring. The program sets up equations 3.2 - 2 from the data and solves them by Gaussian Elimination. The technique uses pivotal condensation, utilising the term with the largest magnitude. This ensures that the program does not attempt to divide by zero in the reduction process. Should all the elements be zero the matrix is singular and the reduction cannot be completed. The routine will print a warning and return control to the controlling subroutine. The displacements in this case are set to zero.

The axial position calculated is assumed to be the equilibrium position of the floating ring relative to the stator. This value is stored and the axial position set to zero. The initial axial position is then added to the axial displacements at the end of the calculations to give the position relative to the stator.

6.3.3 First timestep

For the first timestep special forms of the difference scheme are used, since the second backward displacement ($[x_o]_{i-2}$) is undefined if $i = 2$. Two possible forms were

described in the final section of chapter 3. Using linear interpolation is quite satisfactory over a large portion of the cycle if the motion is sinusoidal. However near the maxima and minima where the slope changes rapidly the predicted value will be in error. Some form of iterative technique would be needed to predict an accurate value for the backward difference. The error due to using linear interpolation for the backward step is small and the solution will converge rapidly to the analytical values (section 6.4.2). The equations to be solved for this timestep are thus:-

$$\left(\frac{[C]}{\Delta t} + [S]\right)_2 [\chi_o]_2 = [P]_2 + \frac{[C]}{\Delta t}[\chi_o]_1$$

The equations of motion are set up in matrix form using the constant stiffness, damping and forcing function arrays, with the appropriate time dependent elements. The equations are then solved by Gaussian Elimination. As for the equilibrium position the equations cannot be solved if the matrix is singular. To overcome this problem, the matrix assembly technique adds a term:-

$$\frac{[M]}{\Delta t^2}$$

to the diagonal for any row in which the diagonal term is zero. This is necessary since the method can be used to solve for any number of degrees of freedom, and thus some equations could be missing from the matrix. Although the model would be physically correct if, for instance, only the radial OX and angular OY modes existed, the matrix would be considered to be singular by the elimination routine if the above procedure was not adopted. This does not lead to the propagation of incorrect values, and hence the calculation of spurious displacements, since the right hand side will always be zero for the missing modes.

6.3.4 General Form

For the second and subsequent timesteps the general form of the equations may be used. The equations are set up and solved as described above. The calculations proceed until the required number of timesteps have been completed, or the convergence checks, described below, show that the seal has failed.

6.3.5 Convergence Check

The program checks that the results are physically acceptable. No convergence checks are carried out, since all the element values used are independent of the position of the floating ring and the solution is thus not an iterative one.

The first check is to ensure that the radial displacement calculated is not more than the shaft movement plus the clearance, nor less than the shaft movement less the clearance. Thus the position of the floating ring radially is limited by touching the shaft. If the calculated displacement is outside these limits it is reset to the appropriate limiting value.

The limits on the axial position are governed by the need for the seal to have both an adequate minimum film thickness to operate hydrodynamically, and a limited maximum film thickness to keep the leakage to acceptable levels. The axial displacement is checked, and if necessary it will be reset to the appropriate value. For the minimum film thickness it is likely that below 0.15 μm boundary lubrication only will occur and Reynolds' Equation will not apply. Calculations using EHRA

Fluid Engineering's 'FASCAV' program show that at these film thicknesses, if hydrodynamic pressures were generated these would be sufficiently large to cause severe deformation of the seal faces. This value (0.15 μm) will thus be used as the minimum film thickness. It is generally accepted (147) that films of the of 3 μm thick in the interface will result in copious leakage. At such a thickness the seal may be deemed to have failed due to severe leakage. The maximum permitted axial position will therefore be 3 μm.

For the angular rotation of the floating ring it is necessary to ensure that the change in film thickness due to the rotation about either axis does not exceed the film thickness. The maximum change in film thickness is given by:-

$$\Delta h \max = |\psi_x| \sin\theta \max + |\psi_y| \cos\theta \max$$

where θ_{max} is the angular position at which the maximum change occurs and is given by:-

$$\theta \max = 2 \tan^{-1} \left(-\frac{\psi_y}{\psi_x} + \sqrt{\left(\frac{\psi_y}{\psi_x}\right)^2 + 1} \right)$$

This formula gives a value for θ_{max} between 0^o and 90^o. The quadrant in which this value actually lies is immaterial for the purposes of the convergence check. If the change in film thickness exceeds the present calculated film thickness then Ψx and Ψy are both reduced by $\frac{h}{\Delta h}$. This implies that at one point on the circumference the seal faces are touching at the outside edge.

If any of the displacements are set to the limiting values as described above, a parameter is set indicating the mode or modes in which it occurs. Once a converged solution is achieved

```
 COMPARISON WITH FASCAV 1500 RPM PO 3.14 BAR

INPUT  DATA  TABLE  1  -  ARRAY AND OTHER PARAMETERS
-----------------------

NUMBER OF RIGID BODY DEGREES OF FREEDOM        (NM)     5
NUMBER OF INPUT VIBRATION DEGREES OF FREEDOM (NM)     3
MESH FOR REYNOLDS EQUATION CALCULATION     (MP*NP)    15*48


TOTAL TIME CONSIDERED (TIME)                              0.000000        SECS
TIME STEP                (TINT)                           0.100000E 00    SECS
NUMBER OF TIME STEPS                              (NT)    1


INPUT  DATA  TABLE  2  -  SEALED FLUID AND SLIDING INTERFACE PARAMETERS
-----------------------

PRESSURES IN N/SQ.M   VISCOSITY IN N.S/SQ M   LENGTHS INM   ANGLES IN RADIANS


SEALED PRESSURE  ID              (PI)          0.000000E 00
  ..       ..    OD              (PO)          0.314000E 06
CAVITATION PRESSURE             (PCAV)        -0.100000E 04
FLUID VISCOSITY                 (VISC)         0.120000E-02
SHAFT SPEED                     (RPM)          0.150000E 04


FILM PROFILE WAVE AMPLITUDE  (HAMP)            0.440000E-06
 ..     ..  NUMBER OF WAVES     (NW)           3
 ..   ..  GIVEN FILM THICKNESS (HIN)           0.132000E-05
SLIDING INTERFACE WIDTH      (WIDTH)           0.00140
  ..          ..    ID          (RE)           0.01320
CAVITY EXTENSION FACTOR     (CAVFAC)             0.00

ROTOR        : RADIAL  OX     (XO(1))          0.000000E 00
POSITION     : RADIAL  OY     (XO(2))          0.000000E 00
RELATIVE TO  : AXIAL          (XO(3))         -0.132000E-05
SHAFT AXIS   : ANGULAR OX     (XO(4))          0.000000E 00
AND  STATOR  : ANGULAR OY     (XO(5))          0.000000E 00

             : RADIAL OX  (DXODT(1))           0.000000E 00
ROTOR        : RADIAL OY  (DXODT(2))           0.000000E 00
             : AXIAL      (DXODT(3))           0.000000E 00
VELOCITIES   : ANGULAR OX (DXODT(4))           0.000000E 00
             : ANGULAR OY (DXODT(5))           0.000000E 00


DIAMETER RATIO                          (R)    0.99706
CIRCUMFERENTIAL NODE INTERVAL (THINT)          0.13090
RADIAL NODE INTERVAL                   (RINT)  0.00735
SHAFT ANGULAR VELOCITY                (OMEGA) 157.07963

STATOR SURFACE IS PROFILED
```

Table 6-4 Reynolds' Equation Program Data for Comparison with FASCAV

OPERATING CONDITIONS	FASCAV		LUBMEC	
	LOAD (N)	LEAKAGE (ml/Hr)	LOAD (N)	LEAKAGE (ml/Hr)
3 MPa 23000 rpm	186.7	-38.9	189.8	-321
0.942 MPa 23000 rpm	80.3	-5.10	79.9	-8.51
0.314 MPa 23000 rpm	44.2	-1.25	58.8	26.0
0.314 MPa 11000 rpm	29.8	-1.25	30.6	26.1
0.314 MPa 5000 rpm	23.3	-2.30	22.9	27.9
0.314 MPa 1500 rpm	18.2	-5.20	18.4	35.4
0.11 MPa 5000 rpm	11.7	-0.44	13.4	-91.2

Table 6 - 5 Comparison of FASCAV and LUBMEC Results for Load and Leakage for given Operating Conditions

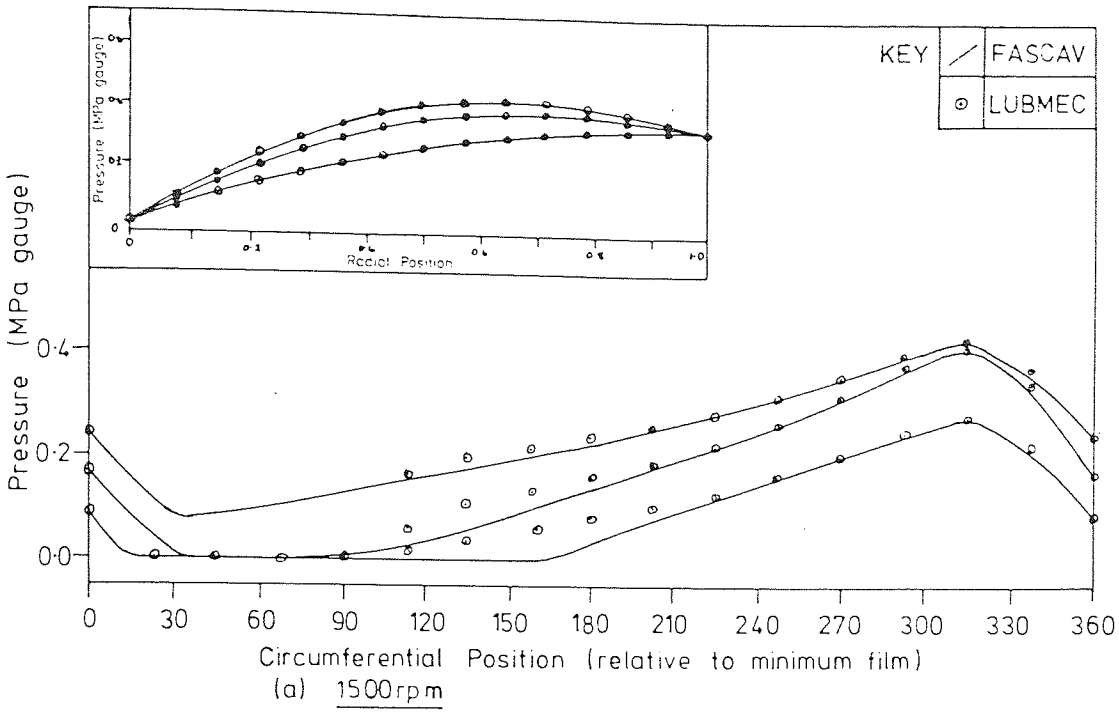

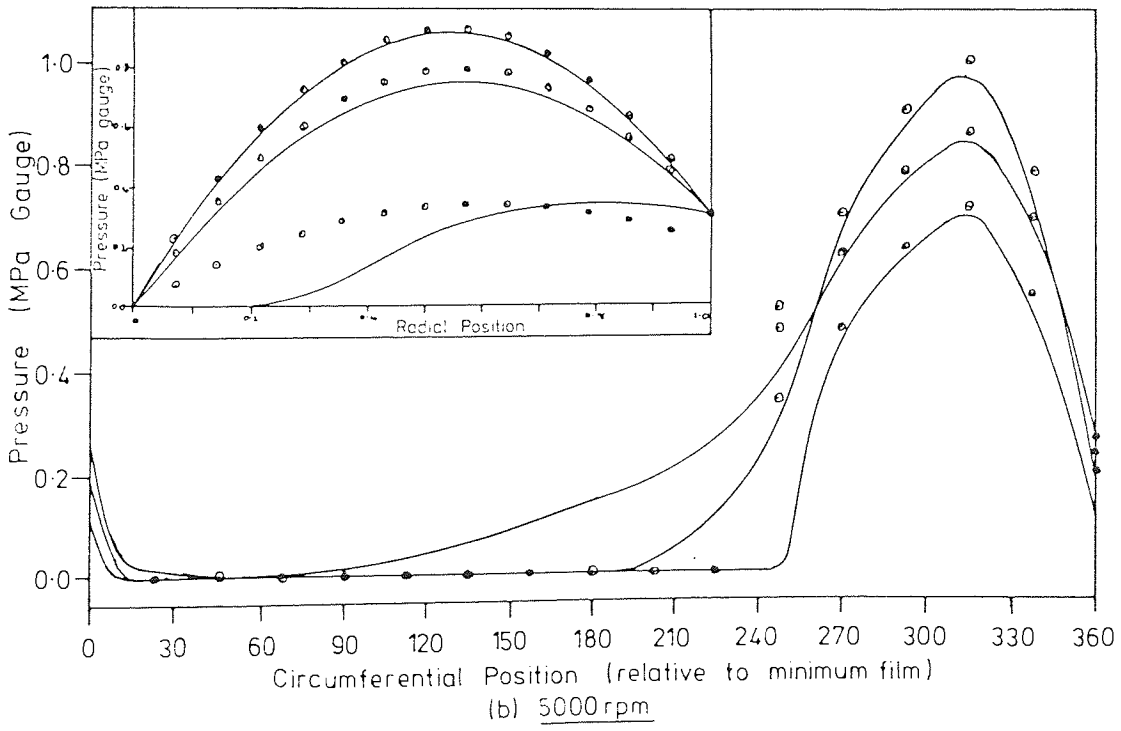

Fig 6-5 Comparison of Pressure Profiles

SPEED rpm / PRESSURE MPa	23000	11000	5000	1500
3	0.0	-	-	-
0.342	0.5	-	-	-
0.314	0.6	0.6	0.4	-0.1
0.11	-	-	0.6	-

Table 6 - 6 Cavity extension factors for Various Speeds and Pressures

for a timestep the indicators are checked. If the same modes are set to the same limiting values for a given number of successive timesteps the seal is deemed to have failed. An error message is printed and the results obtained to this timestep are then printed out.

6.4 Program Validation

6.4.1 Reynolds' Equation Validation

The Reynolds' Equation solution has been tested by comparing the results with a two-dimensional, flow conservation solution known as FASCAV. This program has been developed at BHRA Fluid Engineering for predicting the pressure field and fluid film load capacity for mechanical seals.

Apart from testing the program for errors, the main work has been on validating the cavity treatment. It is difficult to fully test the program logic, and thus comparisons with other results for given data must be carried out. Some of the results from FASCAV have already been published (142) and the data used is given in Table 6 - 4. LUBMEC was run for this data with different extension factors until the load capacity agreed with that calculated by FASCAV, Table 6 - 5, within the limits of the mesh spacing. The extension factors are given in Table 6 - 6 and were used to permit comparison of pressure profiles between FASCAV and LUBMEC.

A comparison of the pressure profiles for 5000 rpm and 1500 rpm is shown on figs 6 - 5(a) and (b) respectively. The inset on each figure shows the radial profiles at various circumferential positions. The agreement is good particularly for 1500 rpm. The differences result from the manner in which the two methods treat the cavitating region of the pressure field. In LUBMEC the cavity extends across

```
 BHRA SEAL TEST RUN CHAPTER 3 DATA

INPUT  DATA  TABLE  1  -  ARRAY AND OTHER PARAMETERS
-----------------------

NUMBER OF RIGID BODY DEGREES OF FREEDOM        (MM)     5
NUMBER OF  INPUT VIBRATION DEGREES OF FREEDOM (NM)     3
MESH FOR REYNOLDS EQUATION CALCULATION     (MP*NP)    1949


TOTAL  TIME CONSIDERED (TIME)                          0.000000        SECS
TIME STEP              (TINT)                          0.100000E 00    SECS
NUMBER OF TIME STEPS                          (NT)     1


INPUT  DATA  TABLE  2  -  SEALED FLUID AND SLIDING INTERFACE PARAMETERS
-----------------------

PRESSURES IN N/SQ.M   VISCOSITY IN N.S/SQ M   LENGTHS INM   ANGLES IN RADIANS


SEALED PRESSURE  ID              (PI)          0.000000E 00
  ..       ..     OD              (PO)          0.700000E 06
CAVITATION PRESSURE             (PCAV)        -0.100000E 04
FLUID VISCOSITY                 (VISC)         0.316000E-02
SHAFT SPEED                      (RPM)         0.300000E 04


FILM PROFILE WAVE AMPLITUDE  (HAMP)            0.300000E-06
  ..     ..  NUMBER OF WAVES     (NW)          1
  ..   ..  GIVEN FILM THICKNESS (HIN)          0.100000E-05
SLIDING INTERFACE WIDTH        (WIDTH)         0.00275
  ..          ..  IN             (RE)         0.02250
CAVITY EXTENSION FACTOR       (CAVFAC)           0.00

ROTOR        : RADIAL  DX     (XO(1))          0.000000E 00
POSITION     : RADIAL  DY     (XO(2))          0.000000E 00
RELATIVE TO  : AXIAL          (XO(3))         -0.150000E-05
SHAFT AXIS   : ANGULAR DX     (XO(4))          0.000000E 00
AND  STATOR  : ANGULAR DY     (XO(5))          0.000000E 00


             : RADIAL DX   (DXODT(1))          0.000000E 00
ROTOR        : RADIAL DY   (DXODT(2))          0.000000E 00
             : AXIAL       (DXODT(3))          0.000000E 00
VELOCITIES   : ANGULAR DX  (DXODT(4))          0.000000E 00
             : ANGULAR DY  (DXODT(5))          0.000000E 00


DIAMETER RATIO                          (R)    0.8[illegible]
CIRCUMFERENTIAL NODE INTERVAL  (THINT)    0.13[illegible]
RADIAL NODE INTERVAL                    (RINT)   0.0[illegible]
SHAFT ANGULAR VELOCITY                  (OMEGA)  314.15927

STATOR SURFACE IS PROFILED
```

Table 6-7 Data for Comparison of Approximate and Computer Values of Fluid Film Elements

ELEMENT	STIFFNESS $N.m^{-1}$		DAMPING $Ns.m^{-1}$	
	CHAPTER 3	LUBMEC	CHAPTER 3	LUBMEC
FORCE DUE AXIAL MOTION	2.8×10^{8}	6.4×10^{8}	4.0×10^{6}	5.4×10^{6}
ANGULAR MOTION	9.4×10^{6}	2.5×10^{6}	1.2×10^{5}	7.1×10^{4}
MOMENT DUE AXIAL MOTION	-5.9×10^{6}	-9.8×10^{6}	-6.8×10^{4}	-9.8×10^{4}
ANGULAR MOTION	-4.9×10^{4}	-9.3×10^{3}	-5.7×10^{2}	-1.2×10^{3}

Table 6 - 8 Comparison of Approximate (from Chapter 2) and Computer Values for Fluid Film Elements

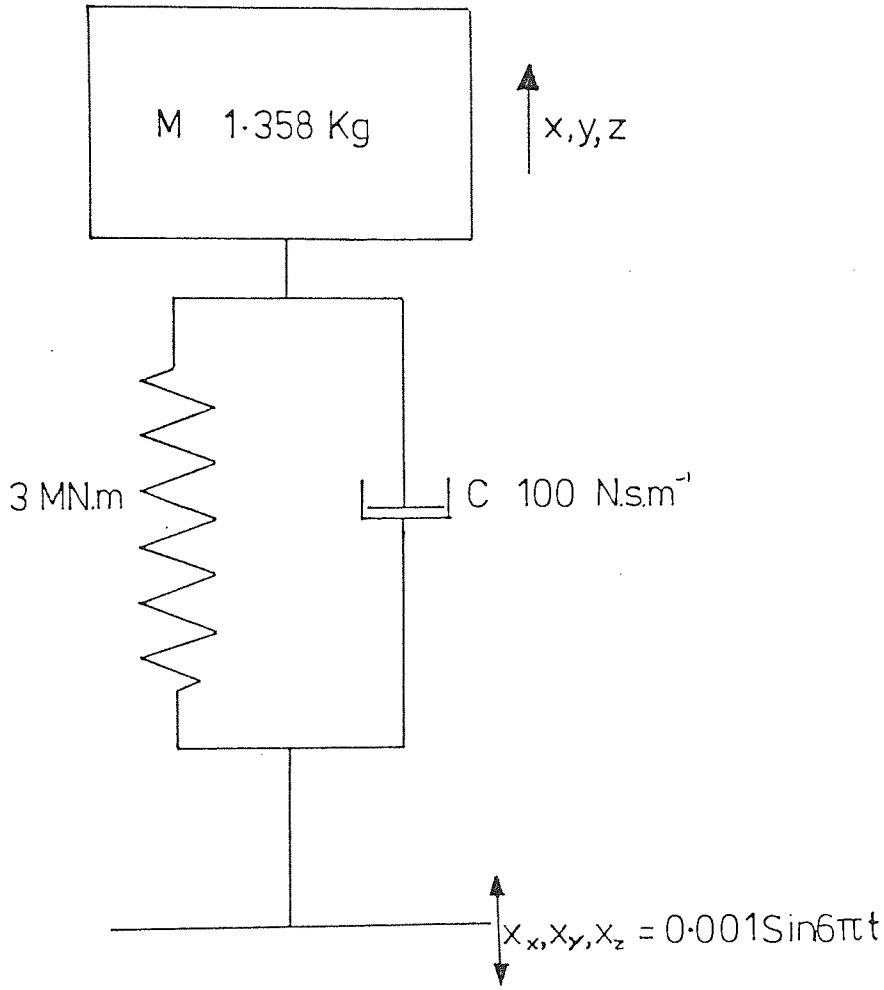

Fig 6-6 Program Test Model Radial and Axial Modes

the entire seal interface width, ending abruptly at the appropriate grid node. In FASCAV the flow conservation results in a tapering cavity as shown in fig 6 - 5. This results in a large difference between the predicted pressure fields at the end of the cavity.

Because of the difference in the cavity shapes, the LUBMEC cavity is shorter for the same load capacity. This results in a greater separation of the end of one cavity and the beginning of the next. It is assumed that all leakage flow must pass between the end of one cavity and the start of the next. Thus LUBMEC will predict a larger leakage than FASCAV because a larger portion of the interface is available for a leakage path.

FASCAV does not calculate the fluid film stiffness and damping coefficients. In order to check the values calculated by LUBMEC, these were compared with the approximate results given in chapter 3. The data for this run is given in Table 6 - 7 and the results are compared in Table 6 - 8.

6.4.2 Equations of Motion

This program has been tested on simple spring-mass-damper model as shown in fig. 6 - 6. Each mode was tested separately, except the angular modes which were tested with the corresponding radial mode.

For the linear modes the displacement of a mass, spring, damper system (fig. 6 - 6) is given by (168):-

$$x = \frac{f \sin(\omega t + \phi)}{\sqrt{(S - M\omega^2)^2 + C^2\omega^2}}$$

$$\text{where } \tan\phi = \frac{-C\omega}{S - M\omega^2} \quad \text{and} \quad f = (CD + S)x$$

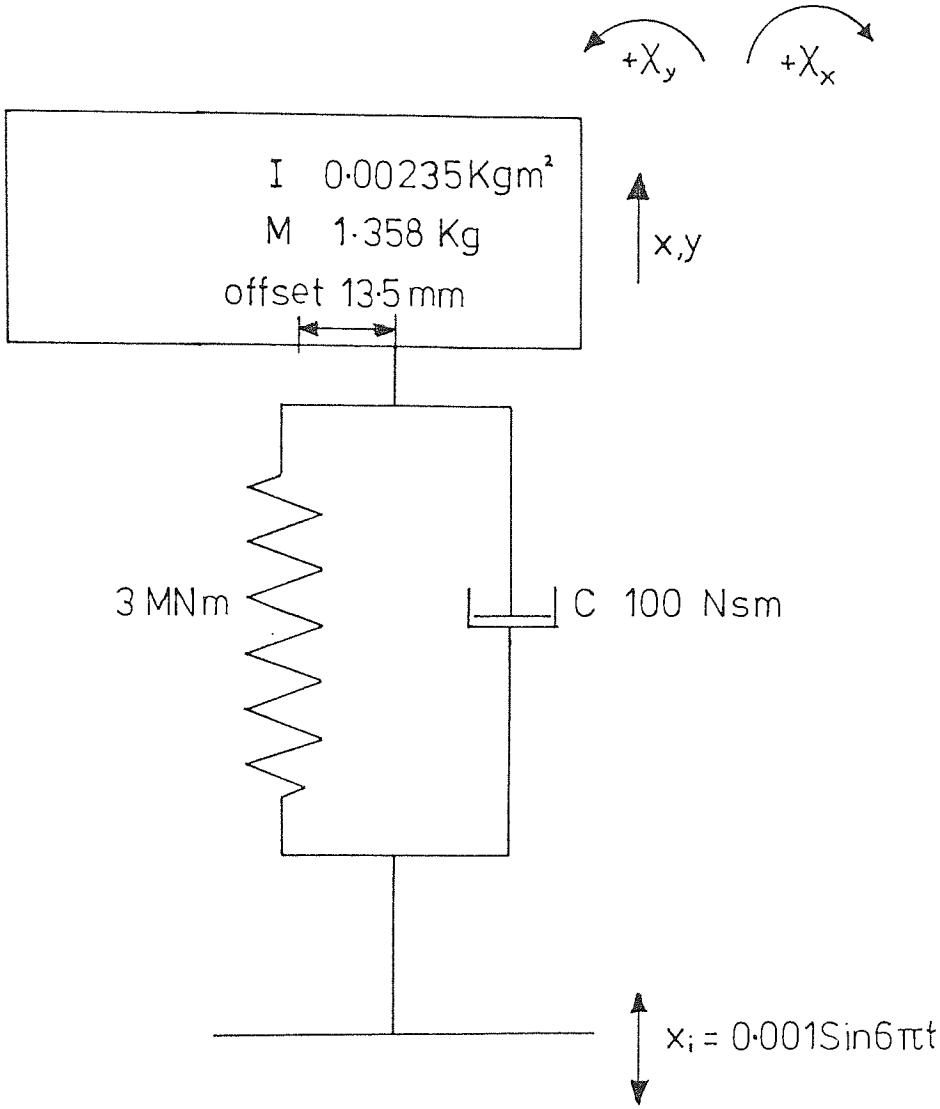

Fig 6-7 Program Test Model - Angular Modes

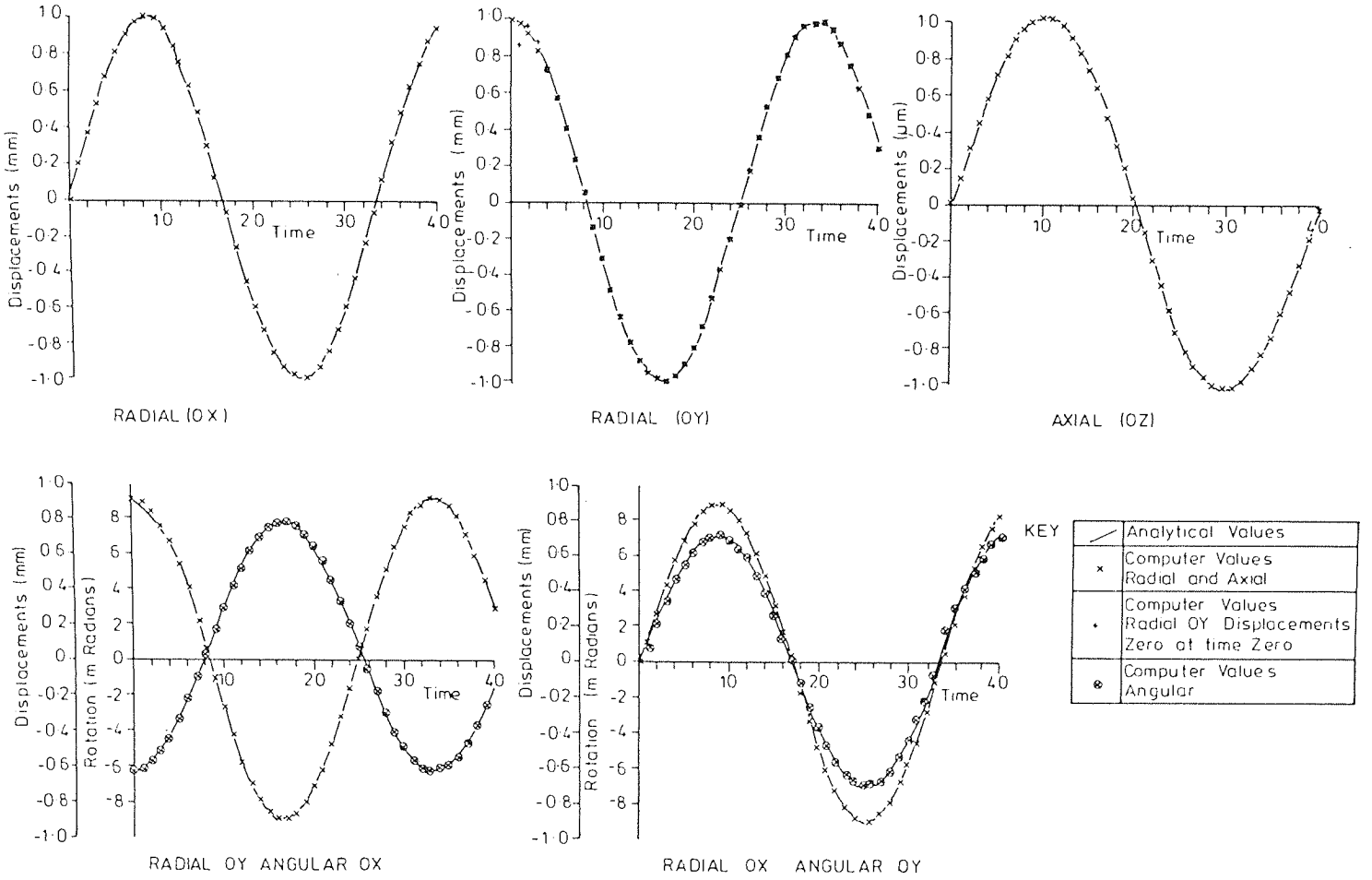

Fig 6-8 Comparison of Analytical and Computer Results

This is, of course, similar to the form used in the analysis in Chapter 4.

For the angular modes the spring-damper element is applied to the mass at some point away from its centroid as shown in fig. 6 - 7. The equations of motion for the radial and angular mode must be solved simultaneously to give the required displacements. The equations are:-

For the radial mode

$$(MD^2 + CD + S)\, x - d\,(CD + S)\, \psi_y = (CD + S)\, x_x$$

For the angular mode

$$-d\,(CD + S)\, x + (ID^2 + CD^2 D + Sd^2)\, \psi_y = -d\,(CD + S)\, x_x$$

These may be combined to give the following expressions for x and ψ_y:-

$$x = \frac{MdC\chi\omega \cos(\omega t + \phi) + MdS\chi \sin(\omega t + \phi)}{\sqrt{((Md^2 + I)S - MI\omega^2)^2 + (Md^2 + I)^2 C^2 \omega^2}}$$

$$\psi_y = \frac{IC\chi\omega \cos(\omega t + \phi) + IS\chi \sin(\omega t + \phi)}{\sqrt{((Md^2 + I)S - MI\omega^2)^2 + (Md^2 + I)^2 C^2 \omega^2}}$$

$$\text{where } \tan\phi = \frac{-(Md^2 + I)\, C}{(Md^2 + I)\, S - MI\omega^2}$$

The analytical and computer results for all five degrees of freedom are given on fig. 6 - 8. It can be seen that there is good agreement between the analytical and computer results. There is a slight variation for the first couple of timesteps. Even for the radial CY results with zero as the initial displacement, the computer results have settled to the analytical ones within six timesteps. These results clearly show that the

```
 EHRA SEAL VISC FOR 57 C

INPUT  DATA  TABLE  1  -  ARRAY AND OTHER PARAMETERS
-----------------------

NUMBER OF RIGID BODY DEGREES OF FREEDOM          (NM)      5
NUMBER OF INPUT VIBRATION DEGREES OF FREEDOM (NN)      3
MESH FOR REYNOLDS EQUATION CALCULATION     (MXMXP)    19X48


TOTAL TIME CONSIDERED (TIME)                              0.000000        SECS
TIME STEP                (TINT)                           0.100000E 00    SECS
NUMBER OF TIME STEPS                              (NT)    1


INPUT  DATA  TABLE  2  -  SEALED FLUID AND SLIDING INTERFACE PARAMETERS
-----------------------

PRESSURES IN N/SQ.M   VISCOSITY IN N.S/SQ M   LENGTHS INM   ANGLES IN RADIANS


SEALED PRESSURE  ID              (PI)          0.000000E 00
  ..       ..    OD              (PO)          0.500000E 06
CAVITATION PRESSURE             (PCAV)        -0.100000E 04
FLUID VISCOSITY                 (VISC)         0.775000E-02
SHAFT SPEED                     (RPM)          0.290000E 04


FILM PROFILE WAVE AMPLITUDE  (HAMP)            0.200000E-06
  ..     ..  NUMBER OF WAVES     (NW)          3
  ..     ..  GIVEN FILM THICKNESS (HIN)        0.130000E-05
SLIDING INTERFACE WIDTH      (WIDTH)           0.06275
  ..       ..      ID            (RE)          0.02600
CAVITY EXTENSION FACTOR     (CAVFAC)             0.70

ROTOR          : RADIAL  OX     (XO(1))        0.000000E 00
POSITION       : RADIAL  OY     (XO(2))        0.000000E 00
RELATIVE TO    : AXIAL          (XO(3))       -0.130000E-05
SHAFT AXIS     : ANGULAR OX     (XO(4))        0.200000E-06
AND  STATOR    : ANGULAR OY     (XO(5))        0.200000E-06
                       \

               : RADIAL OX  (DXODT(1))         0.000000E 00
ROTOR          : RADIAL OY  (DXODT(2))         0.000000E 00
               : AXIAL      (DXODT(3))         0.000000E 00
VELOCITIES     : ANGULAR OX (DXODT(4))         0.000000E 00
               : ANGULAR OY (DXODT(5))         0.000000E 00


DIAMETER RATIO                          (R)     0.99423
CIRCUMFERENTIAL NODE INTERVAL (THINT)   0.10090
RADIAL NODE INTERVAL                    (RINT)  0.00755
SHAFT ANGULAR VELOCITY                  (OMEGA) 303.68729

STATOR SURFACE IS PROFILED
```

Table 6-9 Typical Data for Reynolds' Equation Program

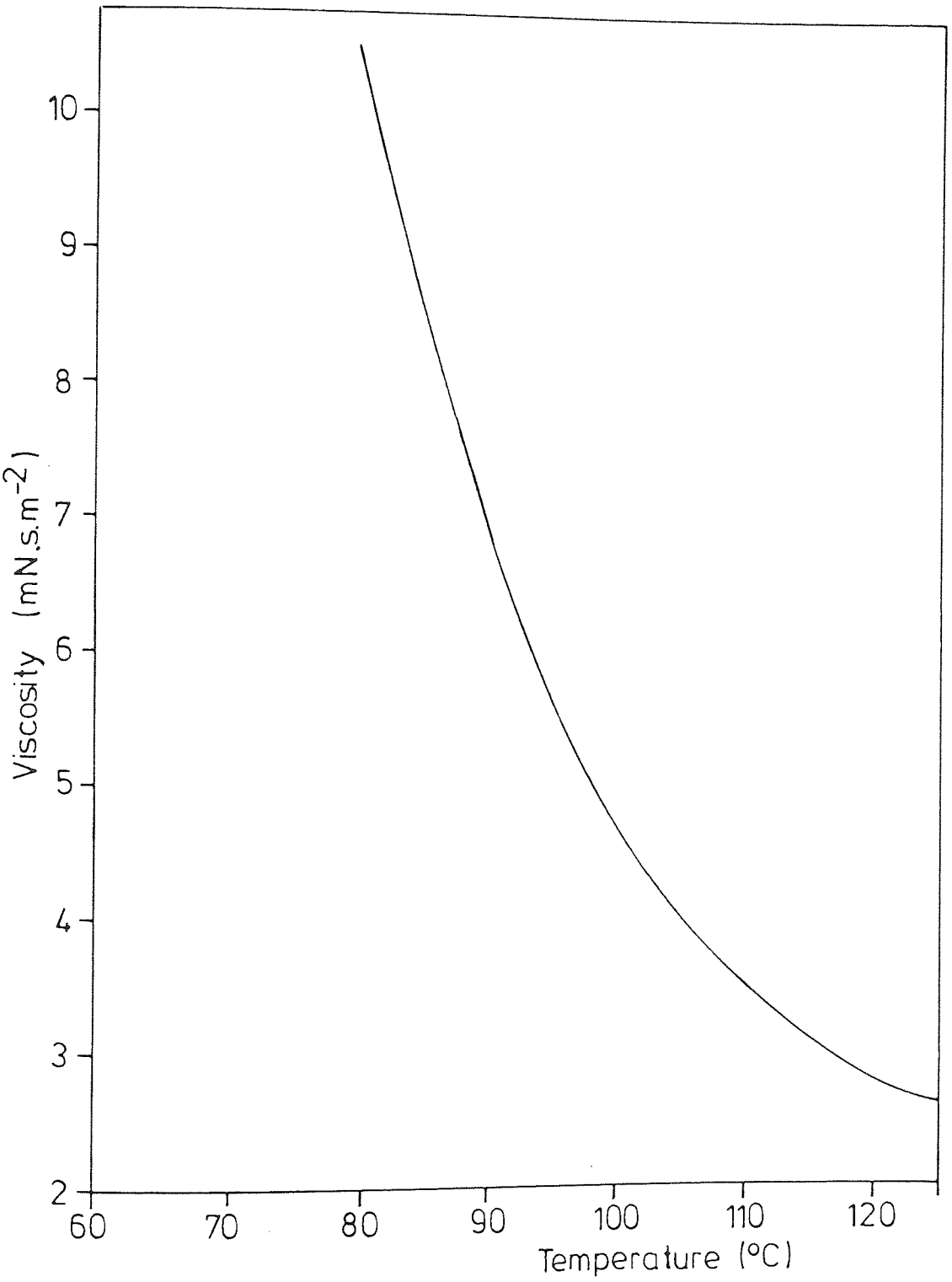

Fig 6-9 Viscosity - Temperature Curve for Shell Tellus 27 Oil

solution technique is stable for the test problems. Further test runs of the program showed that for the radial modes the solution was stable for timesteps equivalent to 18^{o} of arc, compared with the 9^{o} of arc used in obtaining the above results. However, for the mechanical seal axial mode, which is more complex than the simple problem described above, it was found that a timestep equivalent to 5^{o} of arc was necessary to give satisfactory results.

The program was tested on various data for simple models and these runs showed that it was unstable for some combinations. The Gaussian Elimination technique is unstable for very sparse matrices, as can occur when only a few vibration modes exist. An iterative technique such as Gauss-Seidel might overcome this problem, however the matrix making up the left hand side of the equations of motion is not strongly diagonally dominant. The problem may not occur with the less sparse matrix produced for the full problem.

6.5 Results

6.5.1 Reynolds Equation

Once the validation runs had been completed, LUBMEC and FASCAV were run with various values of mean film thickness, and then using a mean film thickness of 1 μm with various values of misalignment. These were used to derive cavity extension factors for the results which are presented below. The extension factors were obtained as described on p 120.

Table 6-9 gives a typical set of data. Fluid properties were provided by the supplier and a viscosity against temperature plot is given in fig 6-9. It has been assumed that the oil temperature in

the interface is 30°C higher than that measured on the stator. Fig 6-10 gives the load capacity, leakage, stiffness and damping coefficients for the range of film thicknesses covered. The actual extension factors used are given in Table 6-10.

MEAN FILM THICKNESS	EXTENSION FACTOR	MEAN FILM THICKNESS	EXTENSION FACTOR
0.4 μm	0.9	1.2 μm	0.7
0.6 μm	0.8	1.4 μm	0.6
0.8 μm	0.75	1.6 μm	0.5
1.0 m	0.7	1.8 μm	0.4

Table 6 - 10 Cavity Extension Factors

Figs 6 - 11 to 6 - 14 give the load capacity, leakage, stiffness and damping coefficients for various values of the two rotations. (Figs 6 - 10 to 6 - 15 are given at the end of this section). The cavity extension factors used are given in Table 6 - 11.

MISALIGNMENT RADIANS	EXTENSION FACTOR			
	x	x	y	y
2	0.7	0.7	0.7	0.7
4	0.7	0.7	0.7	0.7
6	0.6	0.7	0.7	0.7
8	0.6	0.7	0.7	0.7
10	0.6	0.7	0.7	0.7

Table 6 - 11 Extension Factors for Angular Modes

Finally the program was run with viscosities covering the temperature range 80°C to 120°C and the data for the experimental modes. For these a constant cavity extension factor of 0.7 was used. The results are given in fig 6 - 15.

A number of runs had to be carried out to ascertain the correct combination, mean film thickness and cavity extension factor. This was to ensure a satisfactory value for the film load capacity coupled with a mean film thickness close to that calculated by the equations of motion solution. The extension factors and mean film thicknesses are given in Table 6 - 12.

SPEED (rpm)	PRESSURE (MPa)	EXTENSION FACTOR	MEAN FILM THICKNESS (μm)
2900	0.2	0.8	1.3
2900	0.5	0.7	1.0
2900	0.5 (2 waves)	0.7	1.05
2900	0.7	0.6	1.05
2900	1.0	0.5	1.08
1450	0.5	0.6	1.3
900	0.5	0.3	1.25

Table 6 - 12 Extension factors and Mean Film thicknesses for Experimental data

6.5.2 Equations of Motion

The equations of motion program was run with the experimental data. The values of the fluid film elements were taken from the appropriate run of the Reynolds' Equation program. A typical set of data is given in table 6 - 13 and the complete set of runs in table 6 - 14. The amplitudes of the displacements are given in tables 6 - 15 to 6 - 18 (at the end of this section) and may be compared with tables 5 - 4 to 5 - 7.

The o-ring properties have been taken from fig 5 - 6, assuming that the o-ring is at the same temperature as measured on the stator for the experimental run. This may not be the case in practice, but it is the best estimate available. The spring stiffness was measured and found to be 1×10^4 $N.m^{-1}$.

This agrees with the value previously obtained (63) for the rig. The initial compression of the spring was calculated from the rig dimensions.

Three parameters required for the computations, the radii of the lines of action of the spring and o-ring and the distance between the sliding interface and the radial line of action of the o-ring, are difficult to define accurately. Firstly, the spring has a ground end to ensure it seats against the floating ring and is also a push fit on the floating ring. Thus it has an "area of action" rather than a line of action, and a moment may be introduced as a result of friction between the spring and the floating ring. This makes the effective line of action difficult to quantify, and since the wire diameter is only approximately 5% of the coil diameter, the mean coil radius has been taken for the line of action.

Secondly the o-ring's line of action will be affected in a similar manner. The pressure of the sealed fluid will push the o-ring against the sides of the groove resulting in friction and an "area of action". Since the o-ring's cross section diameter is again small compared to its diameter, the mean o-ring radius has been used.

Finally the o-ring will not be central in the groove due to the sealed pressure. It will be forced against the side of the groove closest to the interface. The distance from the interface to the nearest side of the groove, plus half the o-ring cross section diameter will be a good approximation to the position of its radial line of action.

Ideally a range of values for these parameters would be

tested. However the delays resulting from the failure of the first solution technique reduced the amount of computer test runs that could be carried out.

A multiple linear regression analysis on the results has been carried out. Details of this will be found in Appendix G.

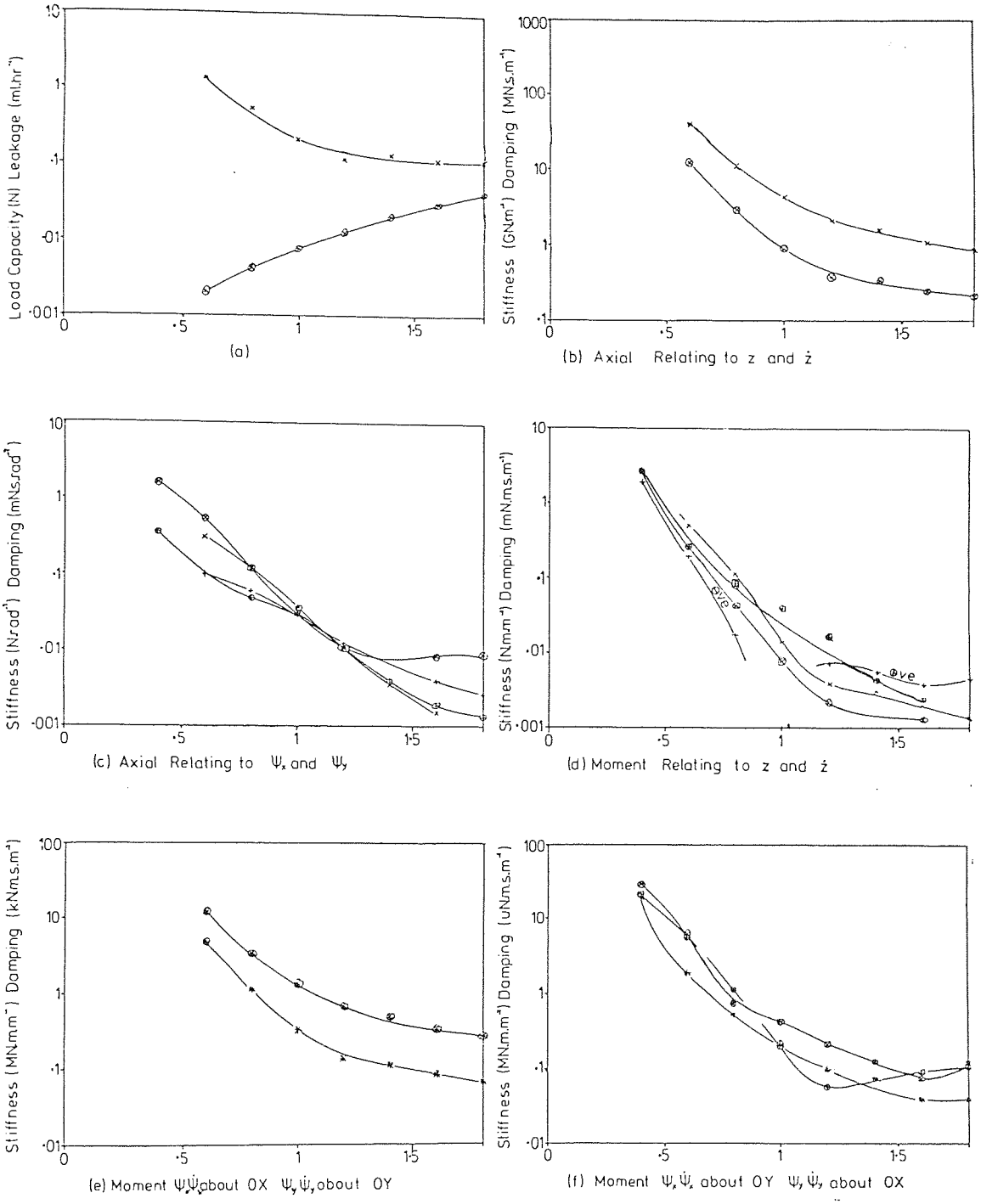

Fig 6-10 Variation of Fluid Film Elements and Leakage with Mean Film Thickness

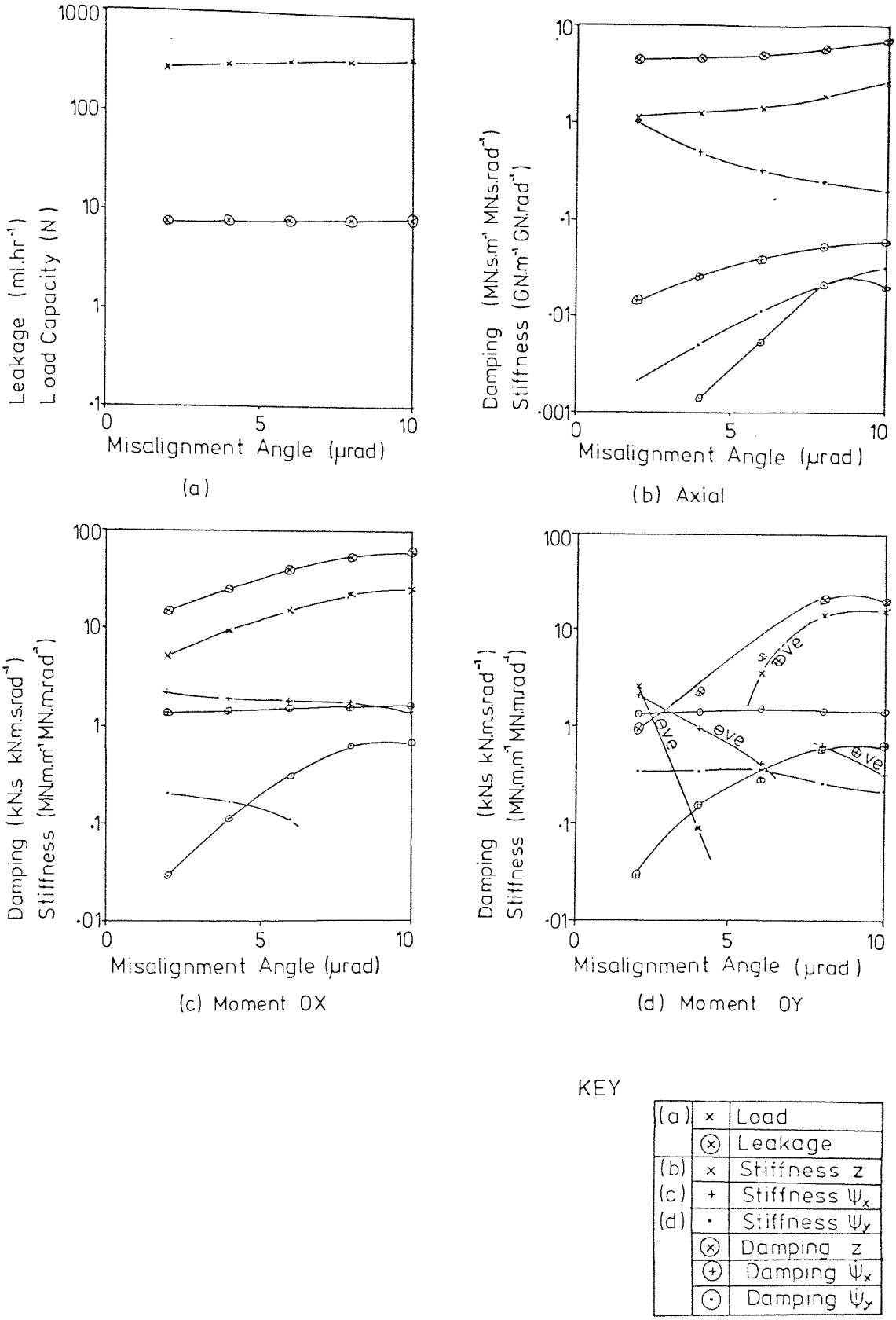

Fig 6-11 Variation of Fluid Film Elements and Leakage with Angular Misalignment about OX (positive)

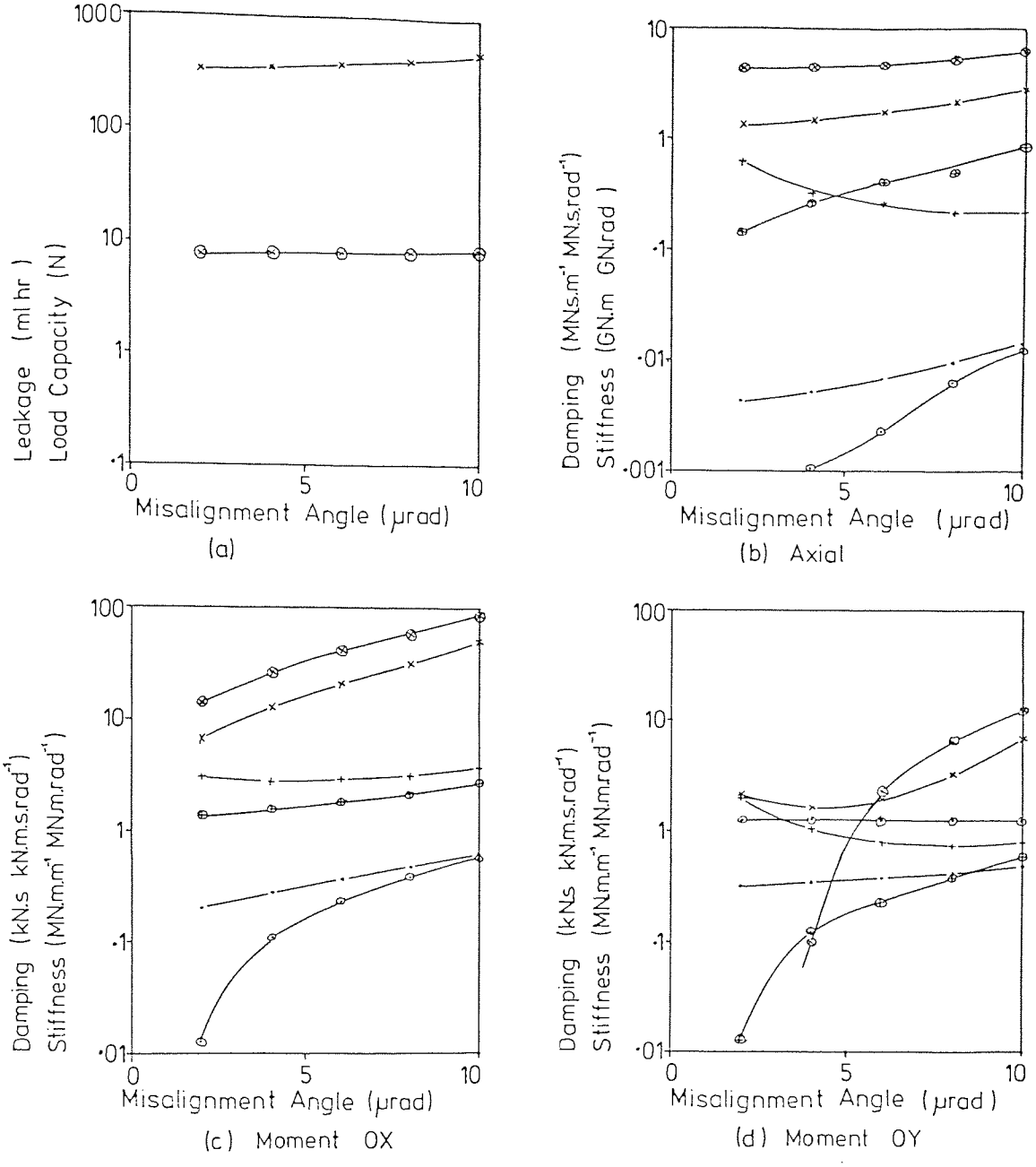

KEY

(a)	×	Load
	⊗	Leakage
(b)	×	Stiffness z
(c)	+	Stiffness Ψ_x
(d)	·	Stiffness Ψ_y
	⊗	Damping z
	⊕	Damping Ψ_x
	⊙	Damping Ψ_y

Fig 6-12 Variation of Fluid Film Elements and Leakage with Angular Misalignment about OX (negative)

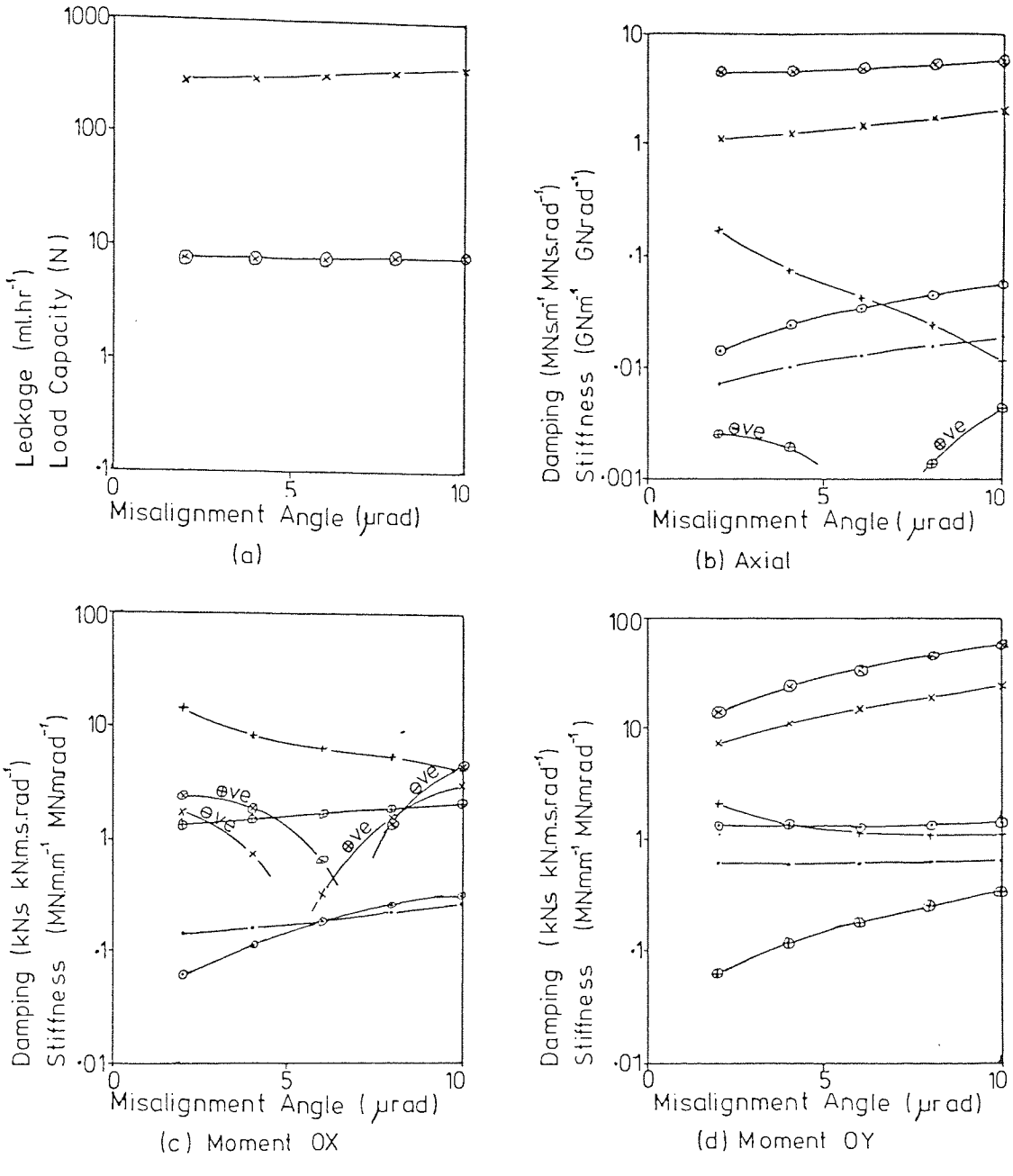

KEY

(a)	×	Load
	⊗	Leakage
(b)	×	Stiffness z
(c)	+	Stiffness Ψ_x
(d)	·	Stiffness Ψ_y
	⊗	Damping z
	⊕	Damping $\dot{\Psi}_x$
	⊙	Damping $\dot{\Psi}_y$

Fig 6-13 Variation of Fluid Film Elements and Leakage with Angular Misalignment about OY (positive)

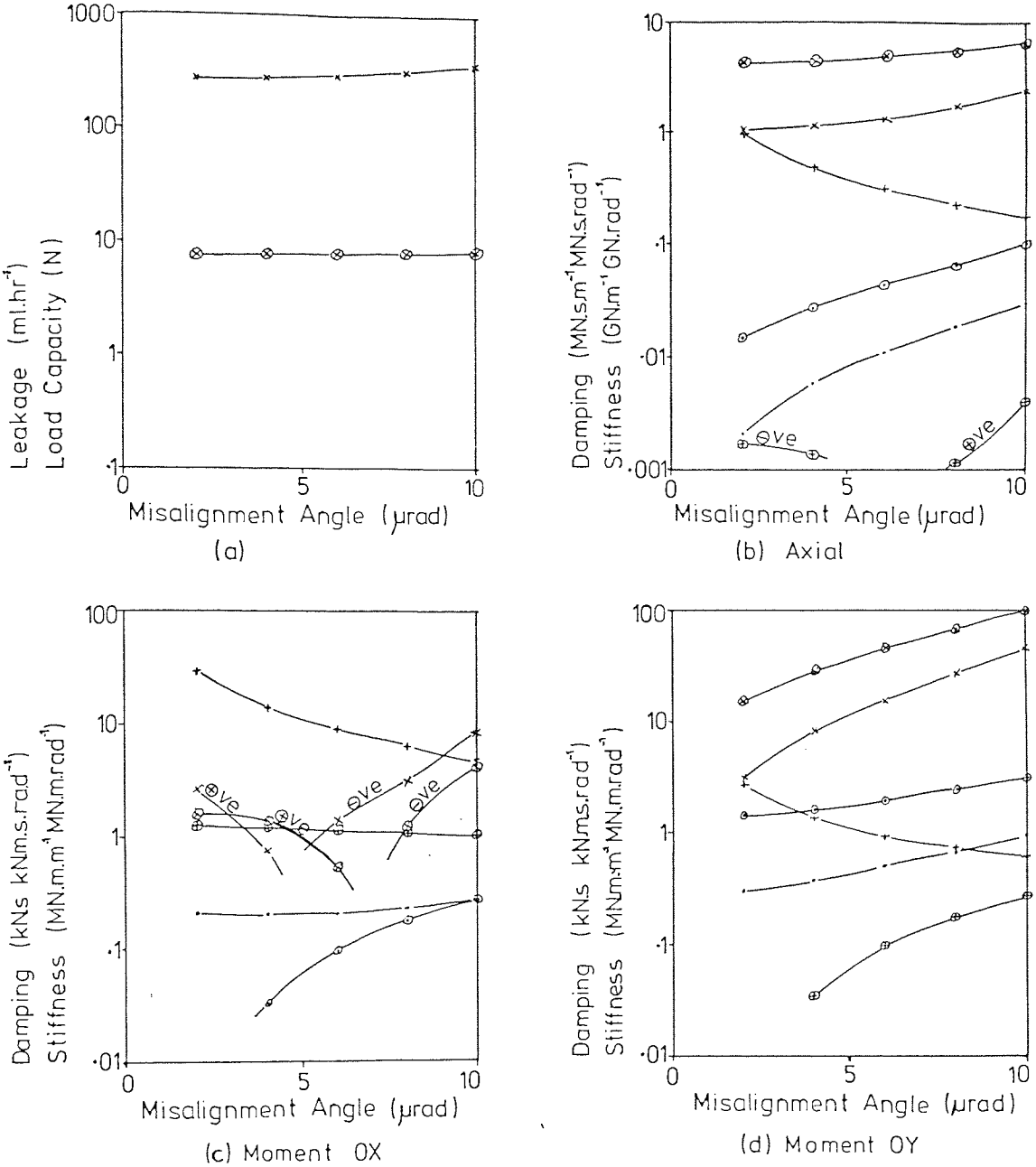

Fig 6-14 Variation of Fluid Film Elements and Leakage with Angular Misalignment about OY (negative)

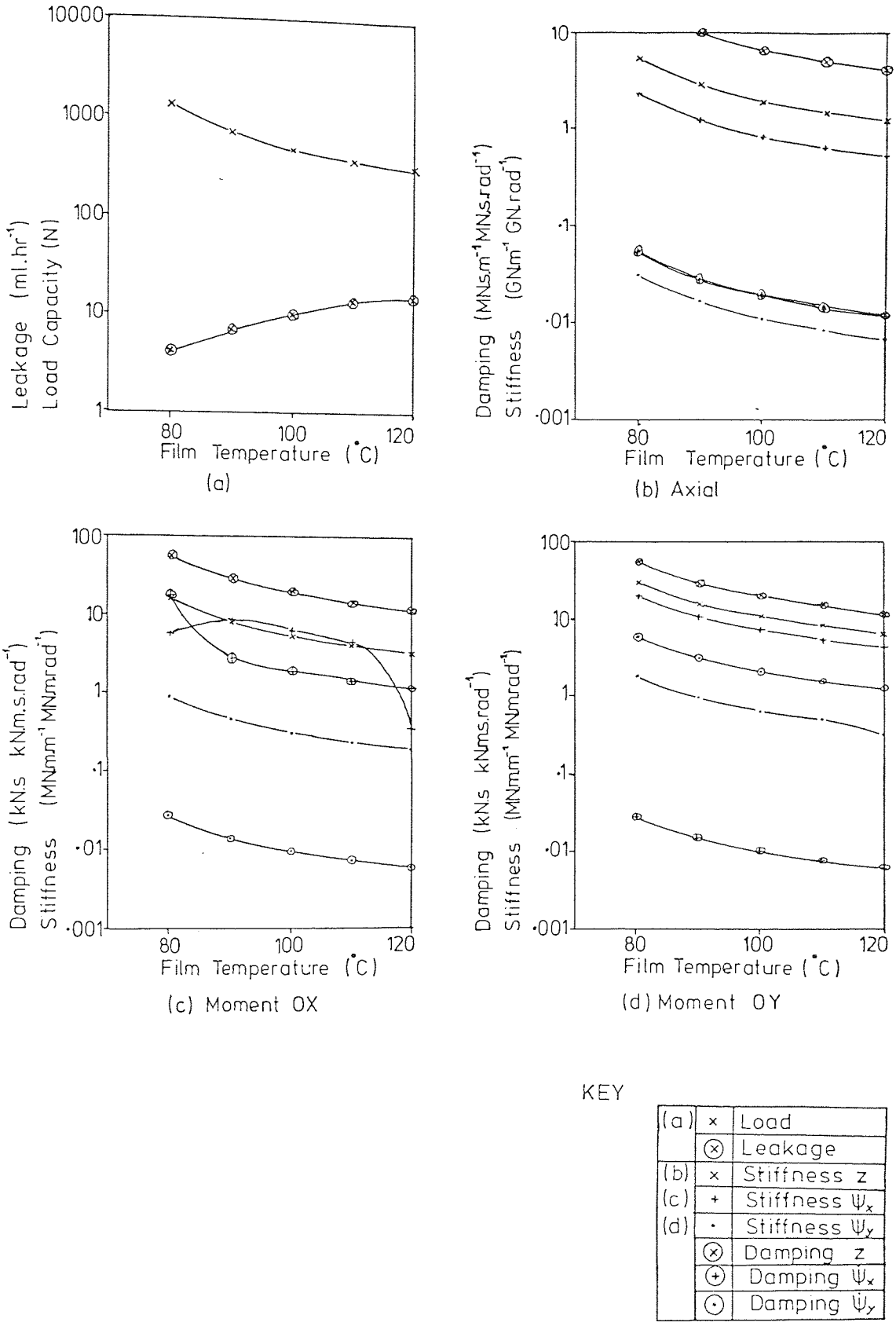

Fig 6-15 Variation of Fluid Film Elements and Leakage with Film Temperature

```
SHROUD SEAL EXPERIMENTAL O-RING TAIL

INPUT DATA TABLE 1 - ARRAY PARAMETERS
-------------------------------------

NUMBER OF RIGID BODY DEGREES OF FREEDOM                    (NM)     6
NUMBER OF INPUT VIBRATION MODES OF FREEDOM                 (NN)     3
MAXIMUM NUMBER OF REYNOLDS ITERATION CALCULATION           (MAXNR)  15*40
NUMBER OF TIME STEPS                                       (NT)     200
NUMBER OF ITERATIONS IN EACH TIMESTEP                      (ITMAX)  1
THE SEAL IS DEEMED TO HAVE FAILED IF ANY
DISPLACEMENT IS SET TO THE SAME LIMITING VALUE IN    3  (NCHECK) SUCCESSIVE TIMESTEPS


INPUT DATA TABLE 2 - ELEMENT VALUES
-----------------------------------

STIFFNESS IN N/M DAMPING IN N.S/M LOAD IN N


O-RING STIFFNESS  COMPRESSION (STIFRC)          0.371000E 07
  ..        ..    SHEAR       (STIFRS)        0.1134000E 07
  ..   DAMPING    COMPRESSION (DAMPRC)        0.110000E 02
  ..        ..    SHEAR       (DAMPRS)        0.336700E 01
SPRING STIFFNESS              (STIFSP)        0.100000E 05


FLUID FILM ELEMENTS

TOTAL LOAD CAPACITY     0.6164888E 03     N

                ELEMENT                          STIFFNESS          DAMPING

AXIAL DUE Z                 (CAP(3/3))      0.2439722E 10     0.852315E 07
  ..   DUE TWIX             (CAP(4/6))      0.1079972E 10     0.246324E 05
  ..   DUE TWIY             (CAP(5/7))      0.1448842E 08     0.253702E 05

ABOUT AXIS OX DUE Z         (CAP(9/11))    -0.6861042E 07    -0.245955E 05
  ..    ..  .. DUE TWIX     (CAP(13/17))   -0.7596116E 07    -0.215014E 04
  ..    ..  .. DUE TWIY     (CAP(15/19))   -0.4141406E 06     0.125413E 02

ABOUT AXIS OY DUE Z         (CAP(8/10))    -0.137166E 08     -0.253790E 05
  ..    ..  .. DUE TWIX     (CAP(12/16))    0.4113224E 07     0.129423E 03
  ..    ..  .. DUE TWIY     (CAP(14/18))   -0.8197147E 06    -0.272270E 04


PRELOAD PRES./SPRING (PFORCE)          0.2045058E 03
TOTAL TIME CONSIDERED (TIME)           0.0700000   SECS
TIME STEP             (TINT)           0.3500030E-03   SECS
CONVERGENCE CRITERION (CHECK)          0.002750

INPUT DATA TABLE 3 - INPUT VIBRATION

AXIS       AMPLITUDE          FREQUENCY        PHASE RELATIVE
             (M)                (HZ)              TO OX
OX      0.670000E-05       0.483333E 02       0.000000E 00
OY      0.670000E-05       0.483333E 02      -0.157080E 01
OZ      0.000000E 00       0.500000E 02       0.000000E 00

INPUT DATA TABLE 4 - FLOATING RING GEOMETRY AND MOMENT OF INERTIA
-----------------------------------------------------------------

LENGHTS IN M  MASS IN KG  INERTIA IN KG*SQ M

THE FLOATING RING CONSISTS OF    3     AXIAL RINGS


 RING                                      INNER       OUTER
NUMBER        MASS          LENGTH         RADIUS      RADIUS

   1       0.24400        0.02300        0.02240     0.03150
   2       0.03140        0.00640        0.02240     0.02770
   3       0.07400        0.02660        0.02240     0.02830


TOTAL MASS OF FLOATING RING (AMASS)          0.350200
MOMENT OF INERTIA - ABOUT OX (OXI)           0.1741661E-03


RADIUS OF LINE OF ACTION OF O-RING      (ROR)      0.02300
DISTANCE BETWEEN O-RING AND INTERFACE   (DORI)     0.00190
PERPENDICULAR DISTANCE O-RING TO C OF G (DOG)     -0.00287
O-RING GROOVE RADIUS                    (RG)       0.02370
RADIUS OF LINE OF ACTION OF SPRING      (RS)       0.02200
INITIAL COMPRESSION  OF SPRING          (SPL)      0.00250
SHAFT/FLOATING RING RADIAL CLEARANCE    (CLEAR)    0.01000

INPUT DATA TABLE 5 - SEALED FLUID AND SLIDING INTERFACE PARAMETERS
------------------------------------------------------------------

PRESSURES IN N/SQ.M   VISCOSITY IN N.S/SQ M    LENGTHS IN M    ANGLES IN RADIANS

SCALED PRESSURE  ID          (PI)        0.000000E 00
  ..        ..   OD          (PO)        0.000000E 00
CAVITATION PRESSURE          (PCAV)     -0.100000E 04


GIVEN FILM THICKNESS         (HIN)       0.100000E-05
SLIDING INTERFACE OD         (PE)        0.07600

ROTOR       : RADIAL  DX     (XO(1))     0.300000E 00
DITTO       : RADIAL  DY     (XO(2))    -0.400000E-05
DITTO       : AXIAL          (XO(3))     0.000000E 00
RELATIVE TO : AXIAL          (XO(4))     0.200000E 00
SHAFT AXIS  : ANGULAR X      (XO(5))     0.000000E 00
AND  STATOR : ANGULAR Y      (XO(6))
```

Table 6-13 Typical Equations of Motion Program Data

Radial Vibration (um)	Rotor	'O' Ring			Stator Temperature (C)	Interface Surface Profile (No.of waves)	Sealed Pressure (MPa)	Shaft Speed (rpm)
		Position from Interface (mm)	Stiffness (M.N.m)	Damping (N.s.m.)				
21.2	long	11.2	3.71	8	67	3	0.5	2900
85.4	long	11.2	3.71	2	81	3	0.5	2900
13.8	long	11.2	3.71	1	90	3	0.5	2900
6.9	long	51.9	3.71	11	64	3	0.5	2900
20.3	long	11.2	3.71	14	63	3	0.2	2900
20.3	long	11.2	3.71	3	73	3	0.7	2900
19.4	long	11.2	3.71	1.5	85	3	1.0	2900
2.5	long	11.2	3.71	68	57	3	0.5	1450
10.8	long	11.2	3.71	75	60	3	0.5	900
10.8	long	11.2	3.71	9	65	2	0.5	2900
13.2	short	5.3	3.71	16	62	3	0.5	2900
26.3	short	13.0	3.71	37	57	3	0.5	2900
22.3	short	23.2	3.71	14	63	3	0.5	2900

Table 6 - 14 Data for Equations of Motion Analysis

Shaft Vibration (μm)	Floating Ring Vibration About Centroid			Mean Film Thickness (μm)	Mean Misalignment Angle (μRadians)	Seal Leakage (ml/Hr)
	Radial (μm)	Axial (μm)	Angular (μRadians)			
21.2	21.4	0.0007	0.023	1.11	1.46	7.75
85.4	81.6	0.004	0.071	0.97	0.98	7.43
138	133	0.008	0.137	0.61	0.73	14.47

Table 6 - 15 Effect of Shaft Vibration Level on Floating Ring Vibration at 2.5 $m.s^{-1}$ (2900 rpm) 0.5 MPa Sealed Pressure (Computed)

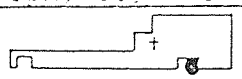

Geometry	Shaft Vibration (μm)	Floating Ring Vibration About Centroid			Mean Film Thickness (μm)	Mean Misalignment Angle (μRadians)	Seal Leakage (ml/Hr)
		Radial (μm)	Axial (μm)	Angular (μRadians)			
Long Short	21.2 13.2	21.4 13.3	0.0007 0.00003	0.023 0.013	1.11 0.94	1.46 0.127	7.75 5.26

(a) Floating Ring Design with o-ring at 20%

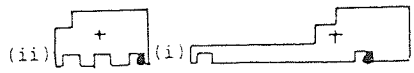

Geometry	Shaft Vibration (μm)	Floating Ring Vibration About Centroid			Mean Film Thickness (μm)	Mean Misalignment Angle (μRadians)	Seal Leakage (ml/Hr)
		Radial (μm)	Axial (μm)	Angular (μRadians)			
Long Short	6.9 22.4	7.0 22.5	0.00001 0.00002	0.028 0.012	1.37 1.20	1.90 0.128	5.26 5.26

(b) Floating Ring Design with o-ring at 85%

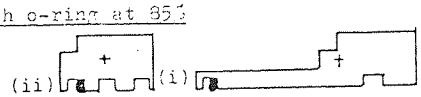

Geometry	Shaft Vibration (μm)	Floating Ring Vibration About Centroid			Mean Film Thickness (μm)	Mean Misalignment Angle (μRadians)	Seal Leakage (ml/Hr)
		Radial (μm)	Axial (μm)	Angular (μRadians)			
3 waves	21.2	21.4	0.0007	0.023	1.11	1.46	7.75
2 waves	10.3	Unstable see section 6 . 6.2					

(c) Surface profile

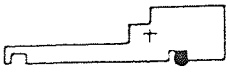

Table 6 - 16 Effect of Geometry on Floating Ring Vibration at 2.5 $m.s^{-1}$ (2900 rpm) 0.5 MPa Sealed Pressure (Computed)

O-Ring Position*	Shaft Vibration (μm)	Floating Ring Vibration About Centroid			Mean Film Thickness (μm)	Mean Misalignment Angle (μRadians)	Seal Leakage (ml/Hr)
		Radial (μm)	Axial (μm)	Angular (μRadians)			
+40 (i)	21.2	21.4	0.0007	0.023	1.11	1.46	7.75
-170 (ii)	6.9	7.0	0.00001	0.028	1.06	1.90	8.26

* Relative to centroid position, expressed as a percentage of the distance of the centroid from the sliding interface, positive is towards the interface.

(a) Long Floating Ring

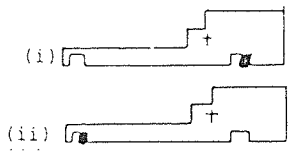

O-Ring Position*	Shaft Vibration (μm)	Floating Ring Vibration About Centroid			Mean Film Thickness (μm)	Mean Misalignment Angle (μRadians)	Seal Leakage (ml/Hr)
		Radial (μm)	Axial (μm)	Angular (μRadians)			
+33 (i)	13.2	13.3	0.00003	0.013	0.94	0.127	8.26
0 (ii)	26.2	26.6	0.00001	0.0004	0.96	0.011	6.4
-73 (iii)	22.4	22.5	0.00002	0.012	1.20	0.123	8.26

* Relative to centroid position, expressed as a percentage of the distance of the centroid from the sliding interface, positive is towards the interface.

(b) Short Floating Ring

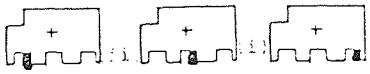

Table 6 - 17 Effect of o-ring position on Vibration for Long and Short Floating Rings at 2.5 x 10^{-7} (2000 rpm) and 0.5 kg Sealed Pressure (computed)

Pressure (MPa)	Shaft Vibration (μm)	Floating Ring Vibration About Centroid			Mean Film Thickness (μm)	Mean Misalignment Angle (μRadians)	Seal Leakage (ml/Hr)
		Radial (μm)	Axial (μm)	Angular (μRadians)			
0.2	20.3	20.6	0.0003	0.030	3.40	0.037	3.13
0.5	21.2	21.4	0.0007	0.023	1.11	1.46	7.75
0.7	20.3	20.5	0.0006	0.033	0.94	0.467	
1.0	19.4	19.6	0.0002	0.009	0.83	0.016	18.58

(a) Sealed Pressure, at 2.5 ms^{-1} (2400 rpm)

Shaft Speed		Shaft Vibration (m)	Floating Ring Vibration About Centroid			Mean Film Thickness (μm)	Mean Misalignment Angle (μRadians)	Seal Leakage (ml/Hr)
(ms^{-1})	(rpm)		Radial (μm)	Axial (μm)	Angular (μRadians)			
0.78	900	2.5	Unstable, see section 6.6.2					
1.25	1450	10.3	10.9	0.00002	0.0009	1.27	0.005	6.56
2.5	2900	21.2	21.4	0.0007	0.023	1.11	1.46	7.75

(b) Shaft speed, at 0.5 MPa Sealed Pressure

Table 6 - 18 Effect of Operating Parameters on Vibration Levels (Computed)

6.6 Discussion

6.6.1 Leakage

The leakage predictions were obtained for the conditions input to the Reynolds' Equation program and thus do not represent the dynamic leakage from the seal. The values may be taken as an instantaneous leakage rate for a given position of the seal.

The leakage values follow the film thickness, sealed pressure and shaft speed changes. As expected the leakage is in general greatest for the thickest film, the highest pressure difference and the highest shaft speed. It should be remembered that the leakage prediction does not take into account the interactions discussed in chapter 5.

6.6.2 Floating Ring Vibration

The problems with program stability mentioned in section 6 - 4 also occurred when solving the mechanical seal problem and it proved to be impossible to obtain a stable solution for 900 rpm and the two wave profile. Lack of time regrettably prevented any checks being carried out to ascertain the reason for the instability.

The results are as expected for a fairly complex spring-mass-damper system. As only the experimentally measured radial shaft vibration was used, the axial vibration is small, and is only the result of the coupling between the axial and angular modes. The angular vibrations are small and the equivalent change in film thickness is well within the calculated mean film thickness. The radial vibration is close to the input vibration with the small angular vibration having little effect on its

magnitude.

The angular vibrations follow the expected trends and are smallest for the cases when the o-ring is closest to the centroid of the floating ring. Thus when the o-ring is at the tail of the rotor (table 6 - 16b) the angular vibration is smallest for the short floating ring where the separation of the o-ring and centroid is 10 mm compared with 32.5 mm for the long floating ring.

Where only the vibration level is changed, table 6 - 15, the mean film thickness decreases with increasing vibration. This is contrary to what would be expected from the calculated leakage rates. However the calculated leakage is also controlled by the cavity length, which is smallest for the highest vibration as a result of the decreased viscosity and hence decreased load capacity. For changes in the operating conditions the film thickness falls with increasing pressure, table 6 - 18a, and with increasing speed, although the change is small for the latter.

The calculations show that the seal floating ring takes up a fixed misalignment. This misalignment is equivalent to change in film thickness that is smaller than the profile wave amplitude. It is, however much larger than the variation in the misalignment angle. Lack of time prevented an investigation of this result. It is possible therefore that if the pressure field was being generated as a result of the surface profile of the rotor, and was thus rotating, the misalignment angle would no longer be fixed. This could result in a very much larger variation in the misalignment angle than was calculated. This could only be investigated by a program combining the two elements that have been developed here, and time prevented this

being carried out (see section 8.4).

6.6.3 Fluid Film Elements - Stiffnesses and Damping

The calculations of the fluid film elements for the various conditions show a wide range of values. Thus for any one element, under certain conditions its value may be negligible compared to the others whilst for a different condition it may be the most significant. This effect shows clearly the importance of predicting the cavity length accurately. Some combinations of cavity length, and position of the pressure field relative to the axes could result in some fluid film elements being zero. Other combinations could result in significant values being calculated.

The load capacity and leakage both increase slightly with increasing misalignment for a constant mean film thickness. For zero misalignment, the load capacity falls by an order of magnitude and the leakage rises by an order of magnitude as the mean film thickness increases from 0.6 μm to 1.8 μm. The effect of the misalignment angle is probably modified by that of the surface profile. The misalignments used are typical of those calculated by the equations of motion solution. The equivalent change in film thickness due to a 1 μRadian misalignment is 0.05 μm peak to peak, an order of magnitude smaller than the surface profile amplitude. It would thus be expected that the effect of the misalignment on the load capacity and leakage would be small. In contrast the change in the mean film thickness results in a change in the minimum film thickness from 0.3 μm to 1.5 μm. This fivefold increase in the minimum film would be expected to have a very significant effect on the load capacity and leakage.

The effect of the interface temperature is also marked. The increase in temperature results in the fluid viscosity decreasing by about 75% as can be seen from fig 6 - 8. These viscosity changes have a direct effect on the load capacity since the viscosity is used in its dimensionalising coefficient. The effect of the changes on the other elements are consistent for the film thickness and temperature changes. With the exception of the moment damping coefficient about OX due to the axial velocity the fluid film stiffness and damping elements have the same changes in their magnitude as the load capacity. The moment damping coefficient about OX due to the axial velocity is negative initially, but changes sign and has a fairly constant value for the thicker films. The reason for this is not clear, however its value is consistent with the other elements for the other changes in the operating conditions which suggests that the program is not in error.

The effect of changing the misalignment is not so clearly defined. The results show similar changes, whichever misalignment is chosen, for the axial stiffnesses and the moment elements about OY. However for the remaining elements this is not the case. There are no consistent changes in the same way as for the changes in mean film thickness and film temperature. This is probably due to the fact that the misalignment changes are not significant compared to the film waviness. These values may be compared with the element values calculated for comparison with the approximate elements calculated in chapter 3. There is a considerable range of element magnitudes, but the signs of the elements relating to axial displacement and velocity are consistent with those in table 6 - 6. The angular elements are not consistent, and again this is probably due to the

interaction of the misalignment and the surface profile, and the fact that the surface has three waves, and not one as in chapter 5. It is interesting to note that for the cases with no misalignment the force stiffness relative to axial motion and the moment stiffness relating to angular motion is significantly larger for the three wave profile, whilst all the remaining elements except the moment damping coefficient relating to angular velocity, are significantly smaller numerically.

When the results for the computer runs with misalignments are compared with table 6 - 8 a different pattern emerges. The stiffnesses are all larger, in some cases by several orders of magnitude, whilst the damping coefficients are of a similar size. This suggests that any improvement in the stability of the three wave profile is due to increased film stiffness only, and that the damping is fairly constant.

6.7 Conclusions

The evaluation of the computer programs described in this chapter has shown that the techniques may be applied to the prediction of the behaviour of a mechanical seal. The computer results obtained have been shown to agree well with approximate predictions of the values.

The dynamic response of the floating ring is typical of a complex spring-mass-damper system. The radial response is close to the input shaft vibration, both in magnitude and phase. The angular response is small and the resultant change in film thickness is well within the predicted mean film thickness. The axial vibration is also small, and results from the coupling

between the angular and axial modes as there is no input shaft vibration in this mode.

The results show a fixed angular misalignment as well as the dynamic displacement. If this was due to the position of the pressure field, then a rotating pressure field could result in the prediction of very much larger angular displacements.

The fluid film elements show a wide range of calculated values. These show the importance of using the correct input conditions for the Reynolds' equation program if accurate values of the elements are to be obtained.

A comparison of the three wave and one wave results show that the three wave profile generates a much stiffer film. The damping coefficients, however, are of similar magnitudes. This suggests that the improved performance of the three wave profile noted experimentally (63) is a result of increased stiffness of the interface fluid film.

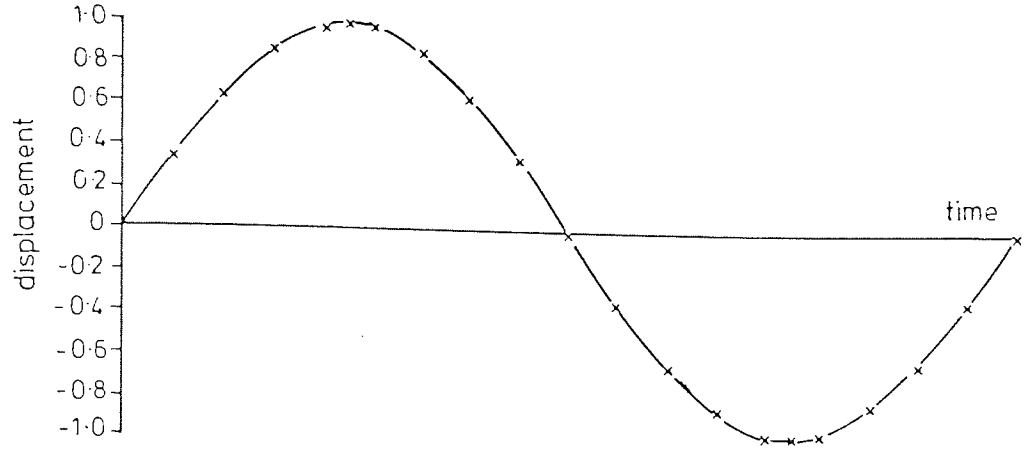

(a) Shaft Vibration

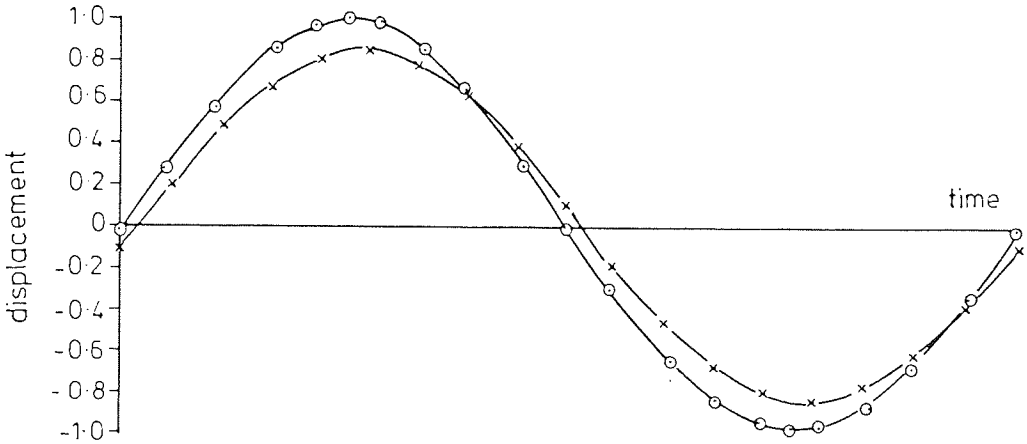

(b) Floating Ring Radial Vibration

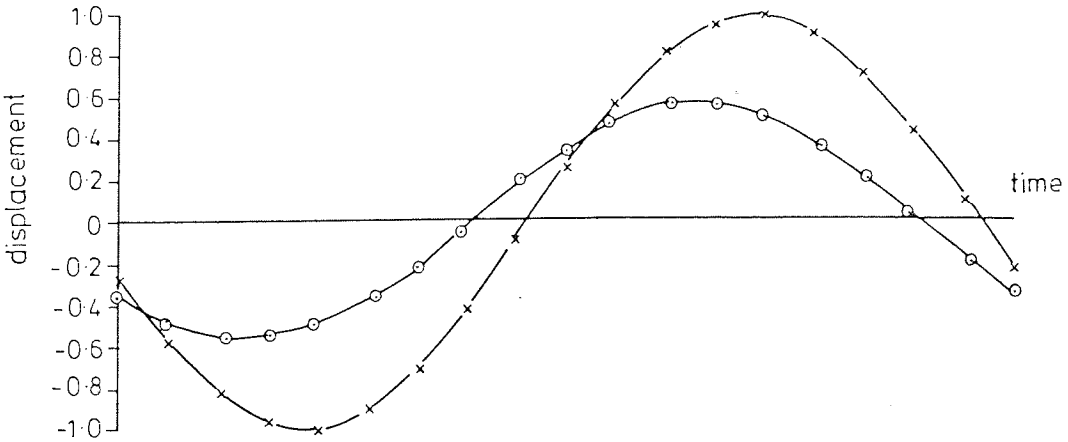

(c) Floating Ring Angular Vibration (For computer predictions constant part removed and values multiplied by 100 before plotting)

KEY | × Experimental | ⊙ Computer

Fig 7-1 Comparison of Experimental and Computer Results - Baseline Condition

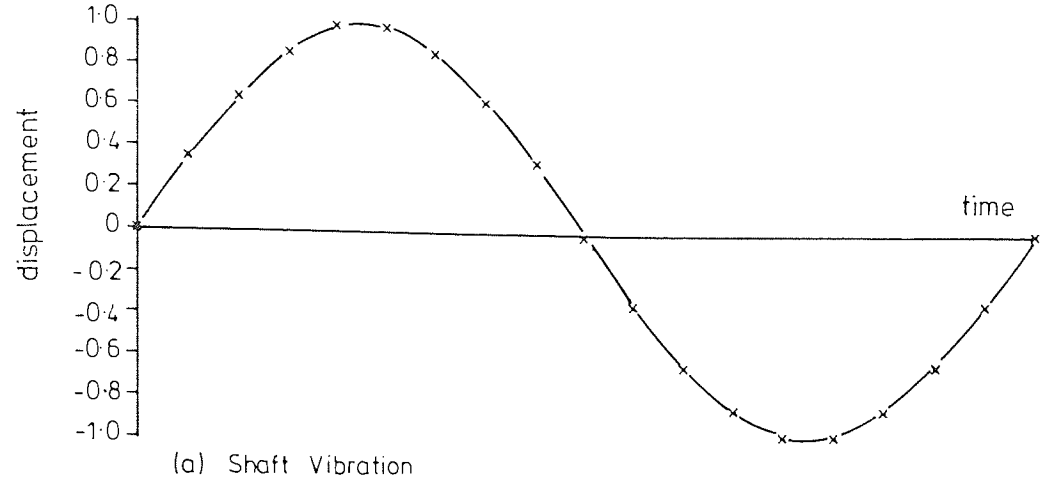

(a) Shaft Vibration

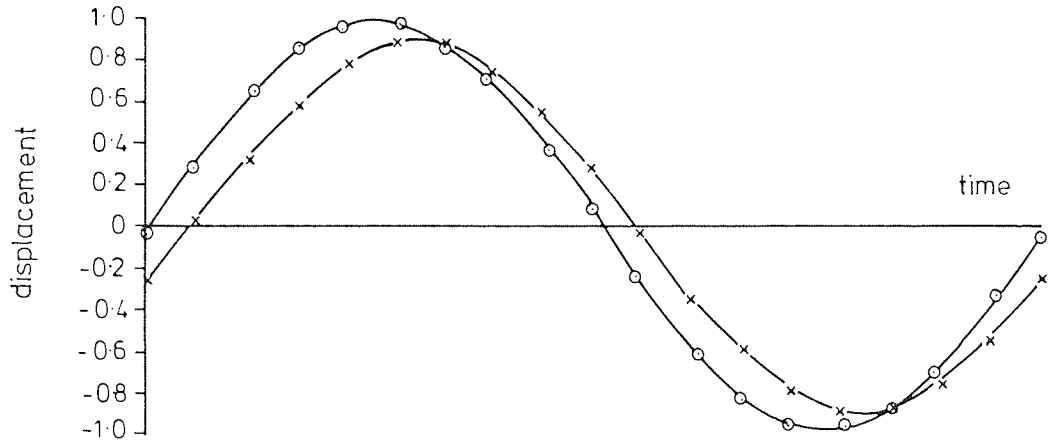

(b) Floating Ring Radial Vibration

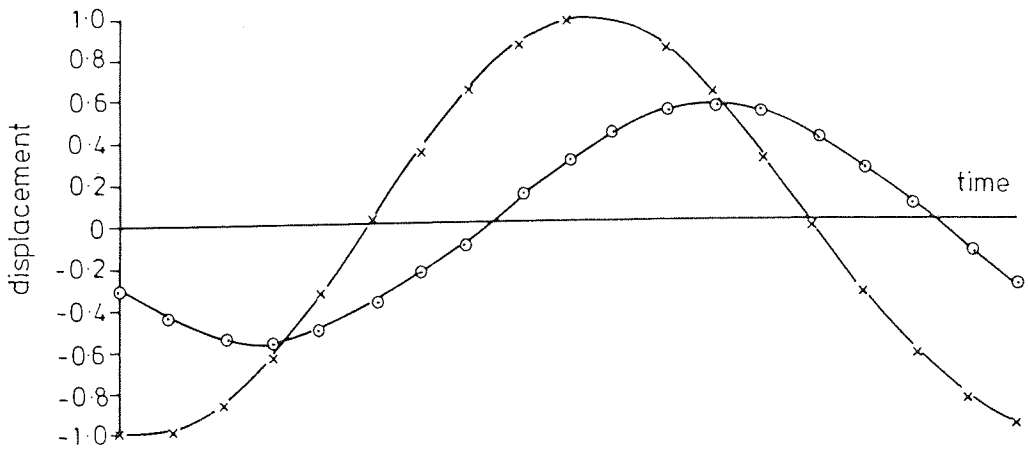

(c) Floating Ring Angular Vibration (Computer values have constant misalignment removed and have be multiplied by 20 before plotting)

KEY | × Experimental | ⊙ Computer

Fig 7-2 Comparison of Experimental and Computer Results-High Vibration Condition

CHAPTER 7

COMPARISON OF THE EXPERIMENTAL AND COMPUTER RESULTS

The experimental and computer results for the mechanical seal have already been discussed in chapters 5 and 6 respectively. In this chapter they will be compared and the computer predictions discussed in the light of the experimental results.

7.1 Vibration

7.1.1. Radial Vibration

Figs 7 - 1 and 7 - 2 give a comparison of the experimental results and computer predictions for the baseline and high vibration conditions respectively. The shaft and floating ring radial vibrations have been normalised using the peak shaft displacement. These two sets of results show particularly good agreement as the experimental radial vibrations are similar in magnitude to the shaft vibration. The computer predictions of the radial vibration all give magnitudes similar to those of the shaft vibration, which is not the case for the experimental results.

A number of factors affect the floating ring vibration, and these must be accurately modelled or given the correct values, if the floating ring vibration is to be predicted. It is possible that some elements that were neglected after carrying out the approximate calculations (chapter 3) may have to be included to improve the accuracy of the predictions.

The fluid around the floating ring may have a considerable effect on the radial damping. Since the ring is not a plain cylinder it is difficult to ascertain whether the damping will be purely radial or will have an angular component as well. Recent computed results for non-rotating concentric cylinders (177) indicate that for the relative diameters and Reynolds' number of the experiments the damping coefficient would be of the order of 10^6 Ns.m.$^{-1}$. This is considerably larger than the damping coefficient of the o-ring secondary seal in compression. The floating ring is, of course, rotating within the housing as well as vibrating and this may modify the value of the damping coefficient. Also the results quoted are for infinite cylinders. Nevertheless, it is probable that the value will be significant for this configuration. The importance of radial damping is supported by the work on bellows seals described in section 1 - 3.

The assumptions made about the o-ring temperature, and hence its properties, may not be correct. The position of the o-ring made it almost impossible to measure its temperature during the experiments. The value used to obtain the properties has been estimated from the stator temperature. The WLF transform will not account for chemical changes that could occur in the rubber as its temperature rises. However, for the high vibration levels good agreement between the computer predictions and experimental results is obtained (fig 7 - 2). Since these results also produced the highest experimental temperatures chemical changes do not seem to be significant. In any case no consistent differences between the o-ring properties before and after the experiments were noted (fig 5 - 6).

The predicted angular vibrations are very much smaller than the measured values. As there is coupling between the radial and angular modes, this may account also partly for the differences between the radial values.

7.1.2 Angular Vibration

The phases of the angular vibration relative to the shaft vibration show good agreement. However the magnitudes are very different. It was noted in chapter 5 that the stator was probably also vibrating and thus following the motion of the floating ring. The computer program assumes that the stator is fixed and thus could not model such a situation. However, by assuming that the total effect is equivalent to the fluid film stiffnesses being in series with the stator secondary seal stiffnesses, an appreciation of the effects may be obtained. The o-ring stiffness in this mode may be taken from the nomograph quoted in chapter 4 (166). This gives a stiffness of 1.76×10^{6} Nm^{-1}. From this and the fluid film element values calculated for the baseline condition the elements given in table 7-1 may be obtained assuming the elements act in series.

ELEMENT		Stiffness
FORCE	due to z	5.29 $MN.m^{-1}$
	due to ψx	0.136 $MN.rad^{-1}$
	due to ψy	0.135 $MN.rad^{-1}$
MOMENT about OX	due to z	-5.86 $MN.m.m^{-1}$
	due to ψx	-2.20 $kN.m.rad^{-1}$
	due to ψy	-0.353 $MN.m.rad^{-1}$
MOMENT about OY	due to z	-11.7 $MN.m.m^{-1}$
	due to ψx	0.781 $N.m.rad^{-1}$
	due to ψy	-21.9 $kN.m.rad^{-1}$

Table 7 - 1 Revised Stiffnesses to take account of Stator Secondary Seal and thrust washer

It was assumed that the damping coefficients remained unchanged and the values were used in the prediction of the angular motion for the baseline condition. The results are compared with the previous predictions and the experimental results in table 7 - 2. The results show that the large angular vibration measured experimentally are almost certainly due to the motion of the stator. The revised elements result in the prediction of much larger angular displacements, although the constant misalignment is of a similar magnitude. The mean film thickness is much larger. However this would be expected as the angular vibration is equivalent to a change in the film thickness of about 1 μm.

MODE	COMPUTER PREDICTIONS		EXPERIMENTAL RESULTS
	INITIAL	REVISED	
Shaft Vibration	21.2 μm	21.2 μm	21.2 μm
Floating Ring Vibration			
- Radial	21.4 μm	21.1 μm	18.4 μm
- Axial	0.0007 μm	0.107 μm	0.27 μm
- Angular	0.023 μrad	49.5 μrad	1100 μrad
Mean Film Thickness	1.11 μm	2.13 μm	3.38 μm
Mean Misalignment Angle	1.46 μrad	1.02 μrad	0.0 μrad

Table 7 - 2 Comparison of Computer Predictions and Experimental Results - Baseline Condition 2.5ms^{-1} (2900 rpm) 0.5 Bar Sealed Pressure

7.1.5 Axial Vibration

The computer predictions of the mean film thickness are in general of the order discussed in chapter 1. However some values approach those measured experimentally, in particular the revised values given in table 7 - 2. When a more advanced

prediction technique is available, the measured values of the mean film thickness and axial vibration will have to be re-assessed.

No excitation of the axial mode was used in the computer predictions, and the computed values are a result of the coupling between the five modes. It is possible that the floating ring was being vibrated axially by the thrust bearing. The cooling coil in the end plate of the rig (fig 5 - 1) did not permit the mounting of a transducer to measure the axial shaft vibration. The rig was, however, assembled with new bearings and thus for the computer predictions it was assumed that any excitation induced by the bearings would be small, and could be neglected.

7.2 Some Discussions of Numerical Stability

7.2.1 The Effect of Floating Ring and Fluid Film Interactions

In chapter 5 the effect of interactions between various factors affecting seal performance was briefly discussed. It was made clear that predicting the effect of changing parameters was difficult. Early in this chapter, other factors have been discussed that could affect the behaviour of the floating ring. However, as the two programs have not been combined, it has not been possible to explore the effect of these interactions using the computer model. This has also meant that the case of the profiled floating ring has not been studied. The computer predictions of the floating ring behaviour are thus not necessarily representative of what happens in practice. In addition the effect of heat generation, both on the interface fluid and on the distortion of the floating ring and stator faces has not

been considered. Indeed, the experimentally measured temperature values have been used to obtain some of the data for the computer runs.

It is possible that the instabilities that occurred when trying to predict the behaviour of the floating ring for 900 rpm and the two wave surface profile are a result of not modelling the interactions between the floating ring vibration and the fluid film. If large floating ring vibrations were predicted this would then result in large changes to the fluid film elements as can be seen from figs 6 - 10 to 6 - 15. The result of these changes could well be the reduction of the instability and thus stable operation would be predicted. Another possible source of incorrect fluid film element values that could lead to instabilities is the combination of cavity extension factors and mean film thicknesses used. Clearly there are a number of combinations that would give acceptable load capacities, but not necessarily suitable values of the fluid film elements.

7.2.2 The Stability of the Solution Technique

In chapter 6 it was noted that instabilities occurred with some combinations of data for very simple models. This suggests that the solution technique is only conditionally stable. A Gauss-Seidel technique for solving the matrix equations was developed, but this too proved to be unstable. Gauss-Seidel techniques for solving matrix equations are iterative and have certain limits on their stability. The technique used requires a strongly diagonally dominant matrix (178). Checks on the equation matrix showed that it did not meet this criterion. Time prevented a thorough investigation of the instability,

however even if this method proves unstable for computer solutions, a number of other methods are available.

7.3 Conclusions

The comparisons between the experimental results and computer predictions have validated the general technique used. There is good correlation between the results, with certain exceptions. (See Appendix G)

The likely sources of the discrepancies have been indicated, though it has not been possible to investigate these thoroughly with the present programs. However, since the method has been shown to be valid, these discrepancies may be removed once certain changes to the programs, mainly as a result of combining them, have been carried out.

CHAPTER 8

CONCLUSIONS FROM THE RESEARCH PROGRAM

8.1 O-Ring Experiments

The o-ring experiments (chapter 4) showed that a wide variation in properties could occur even with o-rings moulded in the same mould from the same batch of a rubber compound. The user of mechanical seals would not be able to guarantee such a close control over the moulding process. The o-rings used for the mechanical seal experiments were obtained from a normal commercial outlet, and these exhibit a much wider scatter of properties (fig 5 - 6) than the other o-rings (fig 4 - 16).

The experiments also showed the importance of temperature when use is being made of measured o-ring properties. The damping of the o-ring in particular falls dramatically with increasing temperature. If the damping were measured at room temperature and then used as the damping coefficient at 100°C, the value could be in error by an order of magnitude. Fortunately the stiffness approaches the zero frequency value as the temperature increases.

The low frequency values of stiffness were found to be almost constant up to 60Hz. However due to problems with making accurate measurements at low frequency the spread of values is large. This necessitated a smoothing technique for the damping coefficient to predict the shape of the curve below about 20Hz.

During the testing of the unsuccessful rig for these

experiments it was noted that above 30Hz the friction between the o-ring and the carrier and shaft decreased almost to zero. This was not noted for the test rig described in chapter 4 as the carrier is held rigid by the vibrator drive. This phenomenum has an important implication for the use of this type of seal. If the friction can be reduced almost to zero under operating conditions, then the seal may fail due to excessive leakage from around the o-ring.

8.2 Mechanical Seal Experiments

These quantified the qualitative results of the BHRA Seals Survey (99) and clearly showed that the seal performance degraded as the vibration levels rose. In the experiments the leakage rose dramatically with increasing vibration as did the stator temperature. The measured power dissipation actually fell with increasing vibration, but it is likely this was due to less heat transfer to the cooling coil, rather than less heat being generated. Although the results suggest the seal operates with a thicker film at the higher vibration levels this would not necessarily mean improved seal life. Thermal effects could cause degradation of the interface components, and the higher leakage rates could rapidly become unacceptably large.

The angular vibration was found to be very much greater than could be accepted by a typical interface film of the order of 1 μm thick. This suggested that the stator was also vibrating. The stator is supported on a rubber thrust washer with an o-ring secondary seal. Their stiffnesses and damping coefficients are likely to be very much smaller than the corresponding values for the fluid film. The measured leakage rates were not excessive, and this further evidence that the

stator was following the floating ring vibration thus maintaining an adequately thin film. A mean film thickness large enough to allow the measured angular vibration would result in copious leakage (147).

The experiments showed that the geometry of the floating ring was important. The long floating ring, which had the smaller radial depth to length ratio gave much less leakage, and only marginally greater stator temperatures. In addition the leakage was least for this ring when the o-ring was closest to the sliding interface. Finally the three wave surface profile exhibited a lower leakage rate than the two wave profile. Again the heat generation and stator temperatures were similar.

8.3 Computer Programs

The predictions of the floating ring vibration proved to be satisfactory for a number of the conditions. In particular the relative phases of the shaft vibration and the radial and angular vibration for the experiments and computer predictions showed good agreement. The angular vibration levels predicted however are very much smaller than those measured experimentally. This confirms the hypothesis that the stator was also vibrating in the experiments. Further predictions using a combination of the fluid film and o-ring stiffnesses to partially model the case of the vibrating stator resulted in much larger angular vibrations being predicted, though still less than the measured values.

The results obtained are typical of the behaviour of a second order spring-mass-damper system with constant coefficients. Nevertheless the computer and experimental results are close in

a number of cases. The technique appears to be sound, though with limitations in its present form.

The Reynolds' Equation solution results show that there is a wide variation in the values of the fluid film elements. This is partly due to the changes in the relative positions of the pressure field and axes resulting from changes in the cavity length. It is possible to calculate near zero values for the elements, if these are symmetrical about an axis. The value of the cavity extension factor must be carefully chosen to ensure that the cavity length being used is a practical one.

The Reynolds' Equation program predicts consistent changes for all the fluid film elements when the film temperature, and hence the fluid viscosity, and the mean film thickness are changed. However, there are no clear trends when the misalignments are changed. This is probably because the misalignments are small compared with the film profile wave amplitude.

8.4 Future Work

During the discussion in chapter 7 of the comparison between the experimental results and the computer predictions various shortcomings of the computer program were highlighted. It is clear that the Reynolds' Equation and Equations of Motion programs need to be combined if the interactions between the floating ring motions and the fluid film are to be accurately modelled. This would also allow the profiled floating ring used in the experiments to be modelled. However there are other problems which also need to be overcome.

Firstly the stability of the solution technique needs further investigation. In the long term it may be beneficial

to utilise a different technique to try to ensure unconditional stability. This would be more satisfactory than the present method which, for some data, may only be stable for a small timestep.

Secondly the mathematical model needs to be improved to cater for the wide range of commercial designs. The obvious first step is to model a floating stator as used in the experiments. This would then enable the performance of the various configurations described in chapter 1 to be predicted.

Thirdly, the experimental results suggest that the effect of temperature, and the fluid around the seal needs to be carefully considered. The modelling of the film profile could be changed to include distortion of the seal faces. If the distortion were known or could be predicted by a thermal model, the effect of this could then be predicted. The fluid around the floating ring was shown in chapter 7 to have a significant damping compared to the o-rings of the experimental rig. It would be relatively easy to include the appropriate element in the radial equations of motion. It may however be difficult to calculate this element accurately. The value used in chapter 7 was for infinite non-rotating cylinders which is not the mechanical seal configuration.

Finally it would be useful to model the effect of speed changes, and the start up condition. It was suggested in chapter 5 that the shaft speed could be modelled in terms of a mean speed and a sinusoidal variation. Such a model could also be extended to the starting condition.

All the above points for development of the computer

program would enable it to be used to predict the seal behaviour more accurately. This would allow the program to be used as a design tool. The program could then be used to ascertain the importance of the various design features found in practice. This, of course would be the main aim of future developments of the program.

Although the mechanical seal experiments were carried out to provide data for validating the computer program, the results also showed various areas needing further investigation. The effect of the fluid around the seal has already been mentioned as an extension to the computer program. In addition to this, it would be useful to attempt to correlate the results for non-rotating and rotating vibrating cylinders by carrying out an investigation of the effect. This would also provide further information for the computer program.

Secondly, it would be useful to carry out further measurements of axial vibrations, utilising a more staisfactory measuring technique. Non-contacting displacement probes could be used to measure the floating ring vibration at a point away from the interface. The present capacitance technique relies on a current path from the floating ring to the shaft via the drive spring which could easily have a varying capacitance. This would be eliminated using inductive probes.

Finally the effect of axial vibration, and radial and axial vibrations at frequencies other than the shaft speed need to be investigated. Rotating stall was mentioned in chapter 1 as a possible source of large radial forces at a frequency of approximately two and a half times shaft frequency. The effect of this and other sources such as worn bearings needs

to be investigated experimentally as well as by computer simulation.

The o-ring experiments have achieved the main aim of demonstrating the variations in o-ring properties occurring in practice for nominally similar rings. However it would be useful to carry out an investigation of o-rings purchased from trade suppliers. Samples could be obtained from various sources and the variation in the properties obtained as described in chapter 4. In addition o-rings moulded from different base polymers could be tested. The technique obviously could also be applied to other rubber seals.

Further rig development would be required before carrying out this work. Some means of maintaining the o-rings, carrier and shaft at a constant temperature is required. The instrumentation needs to be modified to ensure that low frequency values can be measured accurately. This would be aided by the use of a matched power amplifier and vibrator that would allow the use of higher force levies at high frequencies.

APPENDIX A

DETAILED DERIVATION OF APPROXIMATE EQUATIONS

In this appendix the approximate formulae used in Chapter three, but not taken from published sources, are derived. The starting point in each case is Reynolds' Equation in cylindrical polar co-ordinates, assuming that the circumferential pressure gradients are small and may be neglected (the narrow bearing approximation):-

$$\frac{\partial}{\partial r}\left(rh^3\frac{\partial p}{\partial r}\right) = 6\eta r\frac{\partial h}{\partial \theta} + 12\,\eta r\frac{\partial h}{\partial t}$$

A.1 Force Damping Coefficient relating to axial velocity

The damping coefficient relates to the relative axial velocity of the mating faces, $\frac{\partial h}{\partial t}$ (note that $\frac{\partial h}{\partial t} = -V$). Integrating Reynolds' Equation twice, substituting the boundary conditions $P = 0$ at $r = R_i$ and $P = P$ at $r = R_o$, and rearranging gives:-

$$p = \frac{3\eta\omega\frac{\partial h}{\partial \theta} + 6\eta\frac{\partial h}{\partial t}}{2h^3 \ell n R}\left[(r^2 - R_i^2)\ell n R + (R_o^2 - R_i^2)\ell n\frac{r}{R_i}\right] \cdot \frac{p\,\ell n\frac{r}{R_i}}{\ell n R}$$

Now the damping coefficient:-

$$\frac{\partial W}{\partial V} = \int_{R_i}^{R_o}\int_{\frac{\pi}{2}}^{\pi}\frac{\partial p}{\partial V}\,r\,dr\,d\theta$$

The circumferential limits are taken as $\frac{\pi}{2}$ and π since in general the cavity will extend over approximately three quarters of the circumference (142).

Now $$\frac{\partial p}{\partial V} = \frac{-3\eta}{h^3 \ell n R}\left[(r^2 - R_i^2)\ell n R + (R_o^2 - R_i^2)\ell n\frac{r}{R_i}\right]$$

Hence:- $$\frac{\partial W}{\partial V} = \frac{-3\eta}{\ell n R}\int_{R_i}^{R_o}\int_{\frac{\pi}{2}}^{\pi}\left[(r^2 - R_i^2)\ell n R + (R_o^2 - R_i^2)\ell n\frac{r}{R_i}\right]\frac{r\,dr\,d\theta}{h^3}$$

Now h may be expressed in terms of the mean film thickness and wave amplitude:-

$$h = h_m + h_a \cos\theta$$

and thus

$$h^{-3} = (h_m + h_a \cos\theta)^{-3}$$

$$\doteq h_m^{-3} \left(1 - \frac{3 h_a}{h_m} \cos\theta \right)$$

The error resulting from truncating the series in this way can be shown to be of the order of

$$\frac{3h_a^2}{h_m^2} \cos^2\theta$$

By integrating this error expression over the circumferential limits and evaluating it, it can be shown that the error is of the order of 8% of the approximate expression.

Thus

$$\frac{\partial W}{\partial V} = \frac{-3\eta}{h_m^3 \ell n R} \int_{R_i}^{R_o} \left[(r^2 - R_i^2) \ell n R + (R_o^2 - R_i^2) \ell n R \frac{r}{R_i} \right] r\,dr \int_{\frac{\pi}{2}}^{\pi} \left(1 - \frac{3 h_a}{h_m} \cos\theta \right) d\theta$$

$$= \frac{3\eta R_o^4 (1 - R^2)}{h_m^3 \ell n R} \left[(1 + R^2) \ell n R + 1 - R^2 \right] \left(\frac{\pi}{2} + \frac{3 h_a}{h_m} \right)$$

A.2 Force Damping Coefficient relating to Misalignment Velocity

This may be developed in a similar manner to the damping coefficient relating to the axial velocity. In this case:-

$$h = h_o - R_m \psi \cos\theta$$

Thus:-

$$\frac{\partial p}{\partial \psi} = \frac{-3\eta R_m}{\ell n R} \left[(r^2 - R_i^2) \ell n R + (R_o^2 - R_i)^2 \ell n \frac{r}{R_i} \right] \frac{\cos\theta}{h^3}$$

Now

$$\frac{\partial W}{\partial \dot{\psi}} = \int_{R_i}^{R_o} \int_{\frac{\pi}{2}}^{\pi} \frac{\partial p}{\partial \dot{\psi}} r\,dr\,d\theta = \frac{-3\eta R_m}{\ell n R} \int_{R_i}^{R_o} \left[(r^2 - R_i^2) \ell n R + (R_o^2 - R_i^2) \ell n \frac{r}{R_i} \right] r\,dr \int_{\frac{\pi}{2}}^{\pi} \frac{\cos\theta}{h^3} d\theta$$

The radial integral is the same as given in Section A.1, the circumferential integral may be evaluated as follows:-

$$\int_{\frac{\pi}{2}}^{\pi} \frac{\cos\theta}{h^3}\, d\theta = \frac{1}{h_o^3} \int_{\frac{\pi}{2}}^{\pi} \left(\cos\theta + \frac{3 R_m \psi}{h_o} \cos^2\theta\right) d\theta$$

$$= \frac{-1}{h_o^3} \left(1 - \frac{3\pi R_m \psi}{4 h_o}\right)$$

The error resulting from truncating the series in this way can be shown to be of the order of 6%. The damping coefficient is thus given by:-

$$\frac{\partial W}{\partial \dot{\psi}} = \frac{3\eta R_m R_o^4 (1 - R^2)}{h_o^3 \ell n R} \left[(1 + R^2)\ell n R + 1 - R^2\right] \left(1 - \frac{3\pi R_m \psi}{4 h_o}\right)$$

A.3 Moment Stiffness relating to Axial Displacement

In this case:-

$$\frac{\partial m}{\partial h_c} = \int_{R_i}^{R_o} \int_{\frac{\pi}{2}}^{\pi} \frac{\partial p}{\partial h_c} r \cos\theta \, r\, dr\, d\theta$$

Now

$$\frac{\partial p}{\partial h_c} = \frac{-9\eta\omega}{2h^4 \ell n R} \frac{\partial h}{\partial \theta} \left[\left(r^2 - R_i^2\right) \ell n R + \left(R_o^2 - R_i^2\right) \ell n \frac{r}{R_i}\right]$$

$$h = h_c + h_a \cos\theta \qquad \frac{\partial h}{\partial \theta} = -h_a \sin\theta$$

assuming no misalignment of the floating ring.

Hence

$$\frac{\partial M}{\partial h_c} = \frac{9\eta\omega h_a}{2 \ell n R} \int_{R_i}^{R_o} \left[\left(r^2 - R_i^2\right) \ell n R + \left(R_o^2 - R_i^2\right) \ell n \frac{r}{R_i}\right] r^2\, dr \int_{\frac{\pi}{2}}^{\pi} \frac{\sin\theta \cos\theta\, d\theta}{h^4}$$

The integrals taken separately give:-

$$\int_{R_i}^{R_o} \left[\left(r^4 - r^2 R_i^2\right) \ell n R + \left(R_o^2 - R_i^2\right) r^2 \ell n \frac{r}{R_i}\right] dr = -\frac{2}{15} \left(R_o^5 - R_i^5\right) \ell n R - \frac{1}{9} \left(R_o^2 - R_i^2\right)\left(R_o^3 - R_i^3\right)$$

$$\int_{\frac{\pi}{2}}^{\pi} \frac{\sin\theta \cos\theta\ \theta}{h^4} d\theta = \frac{1}{h_c^4} \int_{\frac{\pi}{2}}^{\pi} \left(\sin\theta \cos\theta - \frac{4h_a}{h_c} \sin\theta \cos^2\theta - \frac{6h_a^2}{h_c^2} \sin\theta \cos^3\theta\right) d\theta$$

$$= -\left(\frac{1}{2} + \frac{4h_a}{3h_c} + \frac{3h_a^2}{2h_c^2}\right)$$

The error resulting from this truncation of the series can be shown to be 2%.

The stiffness is thus given by:-

$$\frac{\partial M}{\partial h_c} = \frac{9\,\eta\,\omega\,h_a\,R_o^5}{2\,h_c^4\,\ell n\,R}\left[\frac{2}{15}(1-R^5)\,\ell n\,R + \frac{1}{9}(1-R^2)(1-R^3)\right]\left(\frac{1}{2} + \frac{4h_a}{3h_c} + \frac{3h_a^2}{2h_c^2}\right)$$

A.4 Moment Stiffness relating to Misalignment Angle

In this case:-

$$\frac{\partial M}{\partial \psi} = \int_{R_i}^{R_o}\int_{\frac{\pi}{2}}^{\pi} \frac{\partial p}{\partial \psi}\; r\cos\theta\; r\,dr\,d\theta$$

Now assuming no interface surface profile:-

$$h = h_m - R_m\,\psi\cos\theta$$

$$\text{and}\quad \frac{\partial h}{\partial \theta} = R_m\,\psi\,\sin\theta$$

Thus:-

$$\frac{\partial p}{\partial \psi} = \frac{3\,\eta\,\omega\,R_m\,(h + 3\,R_m\,\psi\cos\theta)\sin\theta}{2\,h^4\,\ell n\,R}\left[(r^2 - R_i^2)\,\ell n\,R + (R_o^2 - R_i^2)\,\ell n\,\frac{r}{R_i}\right]$$

And

$$\frac{\partial M}{\partial \psi} = \frac{3\,\eta\,\omega\,R_m}{2\,\ell n\,R}\int_{R_i}^{R_o}\left[(r^2 - R_i^2)\,\ell n\,R + (R_o^2 - R_i^2)\,\ell n\,\frac{r}{R_i}\right] r^2\,dr \int_{\frac{\pi}{2}}^{\pi}\frac{(h + 3R_m\,\psi\cos\theta)}{h^4}\sin\theta\cos\theta\,d\theta$$

Now the radial integral has been given above, and the circumferential integral is given by:-

$$\int_{\frac{\pi}{2}}^{\pi}\frac{(h + 3\,R_m\,\psi\cos\theta)}{h^4}\sin\theta\,\cos\theta\,d\theta$$

$$= \frac{1}{h_m^4}\int_{\frac{\pi}{2}}^{\pi}(h_m + 2\,R_m\,\psi\cos\theta)\left(1 + \frac{4\,R_m\psi}{h_m}\cos\theta\right)\sin\theta\cos\theta\,d\theta$$

$$= \frac{1}{h_m^3}\left(-\frac{1}{2} + \frac{2\,R_m\,\psi}{h_m} - \frac{2\,R_m^2\,\psi^2}{h_m^2}\right)$$

The error resulting from the truncation of the series can be shown to be of the order of 9%. Thus the stiffness is given by:-

$$\frac{\partial M}{\partial \psi} = \frac{3\eta\omega R_m R_o^5}{2h_m^3 \ell n R}\left[\frac{2}{15}(1-R^5)\ell n R + \frac{1}{9}(1-R^2)(1-R^3)\right]\left(-\frac{1}{2} + \frac{2R_m\psi}{h_m} - \frac{2R_m^2\psi^2}{h_m^2}\right)$$

A.5 Moment Damping Coefficient relating to Axial Velocity

In this case:-

$$\frac{\partial M}{\partial V} = \int_{R_i}^{R_o}\int_{\frac{\pi}{2}}^{\pi} \frac{\partial p}{\partial V} r\cos\theta \, r\, dr\, d\theta$$

$\frac{\partial p}{\partial V}$ was given in A.1 and hence:-

$$\frac{\partial M}{\partial V} = \frac{-3\eta}{\ell n R}\int_{R_i}^{R_o}\left[(r^2 - R_i^2)\ell n R + (R_o^2 - R_i^2)\ell n \frac{r}{R_i}\right] r^2\, dr \int_{\frac{\pi}{2}}^{\pi} \frac{\cos\theta}{h^3}\, d\theta$$

The radial integral has already been evaluated, and the circumferential integral is given by:-

$$\int_{\frac{\pi}{2}}^{\pi} \frac{\cos\theta}{h^3} d\theta \quad \frac{1}{h_m^3}\int_{\frac{\pi}{2}}^{\pi}\left(\cos\theta - \frac{3h_a}{h_m}\cos^2\theta\right) d\theta = -\frac{1}{h_m^3}\left(1 + \frac{3\pi h_a}{4h_m}\right)$$

The error resulting from the truncation of the series can be shown to be of the order of 10%. This gives a damping coefficient:-

$$\frac{\partial M}{\partial V} = \frac{3\eta R_o^5}{h_m^3 \ell n R}\left[\frac{2}{15}(1-R^5)\ell n R + \frac{1}{9}(1-R^2)(1-R^3)\right]\left(1 + \frac{3\pi h_a}{4h_m}\right)$$

A.6 Moment Damping Coefficient relating to Angular Velocity

In this case:-

$$\frac{\partial M}{\partial \dot{\psi}} = \int_{R_i}^{R_o} \int_{\frac{\pi}{2}}^{\pi} \frac{\partial p}{\partial \dot{\psi}} \, r \cos\theta \, r \, dr \, d\theta$$

$\frac{\partial p}{\partial \dot{\psi}}$ is given in A.2 and hence:-

$$\frac{\partial M}{\partial \dot{\psi}} = -\frac{3\eta R_m}{\ell n R} \int_{R_i}^{R_o} \left[(r^2 - R_i^2) \ell n R + (R_o^2 - R_i^2) \ell n \frac{r}{R_i} \right] r^2 \, dr \int_{\frac{\pi}{2}}^{\pi} \frac{\cos^2\theta}{h^3} \, d\theta$$

The radial integral has been evaluated above, and the circumferential integral is given by:-

$$\int_{\frac{\pi}{2}}^{\pi} \frac{\cos^2\theta}{h^3} \, d\theta = \frac{1}{{h_m}^3} \int_{\frac{\pi}{2}}^{\pi} \left(\cos^2\theta + \frac{3 R_m \psi}{h_m} \cos^3\theta \right) d\theta$$

$$= \frac{1}{{h_m}^3} \left(\frac{\pi}{4} - \frac{2 R_m \psi}{h_m} \right)$$

The error resulting from truncating the series may be shown to be of the order of 2%. The damping coefficient is thus given by:-

$$\frac{\partial M}{\partial \dot{\psi}} = \frac{3\eta R_m {R_o}^5}{{h_m}^3 \ell n R} \left[\frac{2}{15} (1 - R^5) \ell n R + \frac{1}{9} (1 - R^2)(1 - R^3) \right] \left(\frac{\pi}{4} - \frac{2 R_m \psi}{h_m} \right)$$

APPENDIX B

THE FIRST SOLUTION TECHNIQUE FOR THE EQUATIONS OF MOTION

B.1 Solution Technique

The first attempt to solve the equations of motion utilised a modified Taylor's Series finite difference scheme (156). The method solves the equations explicitly at each timestep for displacement and velocity. The modified scheme is claimed to result in a truncation error of the order of Δt^6. The normal Taylor's Series expansion for a second order differential equation results in a truncation error of the order of Δt^4.

The displacements are given by:-

$$[x_o]_{i+1} = [A]_i + 2[x_o]_i - [x_o]_{i-1}$$

$$- [M]^{-1}[S]\left(\frac{\Delta t^4}{12}[\ddot{x}_o]_i + \Delta t\,[\dot{x}_o]_i\right) - [M]^{-1}[C]\left(\frac{\Delta t^4}{12}[\ddot{x}_o]_i + \Delta t^2\,[x_o]_i\right)$$

It will be appreciated from this equation that two initial values $[x_o]_1$ and $[x_o]_2$ are required. The starting equation to calculate $[x_o]_2$ is:-

$$[x_o]_2 = [A]_{1,2} + [x_o]_1 + \Delta t\,[\dot{x}_o]_1 - [M]^{-1}[S]\left(\frac{\Delta t^4}{24}[\ddot{x}_o] + \frac{\Delta t^3}{6}[\dot{x}_o]_1 + \frac{\Delta t^2}{2}[x_o]_1\right) - [M]^{-1}[C]\left(\frac{\Delta t^4}{24}[\ddot{x}_o]_1 + \frac{\Delta t^3}{6}[\ddot{x}_o]_1 + \frac{\Delta t^2}{2}[\ddot{x}_o]_1\right)$$

and $[x_o]_1$ is given by the initial conditions. The matrices $[M]$, $[C]$ and $[S]$ are the mass damping and stiffness matrices developed in chapter 3. $[A]$ is developed from $[M]$ and the forcing matrix $[P]$ of equation 3.2 - 6. X $[\dot{x}_o]_{i+1}$, $[\ddot{x}]_i$ and $[\ddot{x}]_i$ are defined as follows:-

$$\Delta t\,[\dot{x}_o]_{i+1} = [A]_{i+1,i} + [x_o]_{i+1} - [x_o]_i - [M]^{-1}[S]\left(\frac{\Delta t^4}{8}[\ddot{x}_o]_i + \frac{\Delta t^3}{3}[\dot{x}_o]_i + \frac{\Delta t^2}{2}[x_o]_i\right) - [M]^{-1}[C]\left(\frac{\Delta t^4}{8}[\ddot{x}_o]_i + \frac{\Delta t^3}{3}[\ddot{x}_o]_i + \frac{\Delta t^2}{2}[\dot{x}_o]_i\right)$$

which has the special form for i = 1:-

$$\Delta t\,[\dot{x}_o]_2 = [A]_{2,1} + [x_o]_2 - [x_o]_1 - [M]^{-1}\,[S]\left(\frac{\Delta t^4}{8}\,[\ddot{x}_o]_1 + \frac{\Delta t^3}{3}\,[\dot{x}_o]_1 + \frac{\Delta t^2}{2}\,[x_o]_1\right) - [M]^{-1}\,[C]\left(\frac{\Delta t^4}{8}\,[\ddot{x}_o]_1 + \frac{\Delta t^3}{3}\,[\ddot{x}_o]_1 + \frac{\Delta t^2}{2}\,[\dot{x}_o]_1\right)$$

$$[\ddot{x}_o]_i \equiv [P]_i - [M]^{-1}\,([S]\,[x_o]_i + [C]\,[\dot{x}_o]_i)$$

$$[\dddot{x}_o]_i \equiv [\dot{P}]_i - [M]^{-1}\,([S]\,[\dot{x}_o]_i + [C]\,[\ddot{x}_o]_i)$$

The matrices $[A]_{i'}$, $[A]_{i+1,i}$ $[A]_{2,1}$ and $[A]_{1,2}$ are developed as follows. Each matrix is defined by an equation of the form:-

$$[A]_i = [M]^{-1} \int_{i-1}^{i+1} [P]_i\, T_i\, dt$$

Where T_i is an auxiliary function:-

for $[A]_{i+1,i}$ $T_i = t - t_{i-1}$ for $t_{i-1} < t < t_i$

and $T_i = t_{i+1} - t$ for $t_i < t < t_{i+1}$

for $[A]_{i+1,i}$

and $[A]_{2,1}$ $T_{i+1,i} = t - t_i$

for $[A]_{1,2}$ $T_{1,2} = t_2 - t$

Each of the required matrices are then developed by carrying out the appropriate integration, either analytically or numerically.

The initial position of the floating ring, that is the position at t_i (=o), must be carefully defined. The initial conditions appropriate to the problem have been described in Section 3.4. For this solution technique, both the radial displacements are set to zero, and it is assumed that all the accelerations are zero. The axial and angular displacements are calculated by assuming static equilibrium as described in chapter 3. The velocities are not zero and are calculated from the shaft velocities:-

$$[\dot{x}_o]_1 = \begin{pmatrix} x_x \omega_x \\ x_y \omega_y \\ x_z \omega_z \\ \frac{x_y \omega_y}{r} \\ \frac{x_x \omega_x}{r} \end{pmatrix}$$

The initial value of $[\ddot{x}_o]_1$ is calculated by the equation given above.

B.2 Computer Solution of the Equations of Motion

The solution technique has three stages. Firstly a static equilibrium solution for the first timestep, secondly a special form of the solution for the second timestep and finally the general form of the solution.

Timestep 1

At this timestep it is assumed that the floating ring is in static equilibrium, and lying concentric with the shaft. The accelerations at this timestep are thus zero. The fluid film elements are then used to set up equation 3.3 - 2 and this is then solved by Gaussian Elimination to give the equilibrium position. If the calculated equilibrium position does not coincide with the input position the calculations are repeated. This continues until adequate convergence has been achieved or a given number of iterations are exceeded. When the calculations are completed, the leakage rate is calculated and this, the fluid film load and the floating ring velocities and displacements are stored. The calculations then proceed to timestep two, the first of the dynamic calculations.

Timestep 2

At this timestep special forms of the solution are used.

The working arrays are set up from the constant arrays in the way described in chapter 6. For this solution technique additional arrays are required.

$$[\dot{P}]\ ;\ [A]_{i}\ ;\ [A]_{i+1,i}\ ;\ [A]_{2,1}\ ;\ [A]_{1,2}\ ;\ [\ddot{x}_o]\ ;\ [\dddot{x}_o]$$

$[\dot{P}]$ is the first differential of $[P]$ with respect to time. $[\ddot{x}_o]$ and $[\dddot{x}_o]$ are calculated using the formulae given above. For timestep two $[A]_{2,1}$ and $[A]_{1,2}$ are required. These are calculated from the same constant arrays as $[P]$ and $[\dot{P}]$. Now:-

$$[A_j]_{2,1} = [M_j]^{-1} \int_{t=0}^{t=\Delta t} [P_{t,j}]\ T_{2,1}\ dt$$

and

$$[A_j]_{1,2} = [M_j]^{-1} \int_{t=0}^{t=\Delta t} [P]\ T_{1,2}\ dt$$

Both these arrays may be evaluated either analytically or numerically. To integrate the expressions analytically is time consuming and extra program core and run time would be needed to evaluate the integrals. Since the expressions for P and T are simple it is easy to evaluate them and integrate the expressions numerically using Simpson's Rules:-

$$[A_j]_{2,1} = [M_j]^{-1} \frac{\Delta t}{6} (y_1 + 4y_2 + y_3)$$

where: $y_1 = ([P_{t,j}]\ T_{2,1})\ t = 0$

$y_2 = ([P_{t,j}]\ T_{2,1})\ t = \Delta t/2$

$y_3 = ([P_{t,j}]\ T_{2,1})\ t = \Delta t$

Similar expressions may be obtained for $[A_j]_{1,2}$.

Having evaluated these expressions the program calculates $[\chi_o]_1$ and $[\dot{x}_o]_1$. The leakage is calculated and it, the load, displacements and velocities stored as before. The calculations then proceed to timestep three where the general form of the solution technique is used.

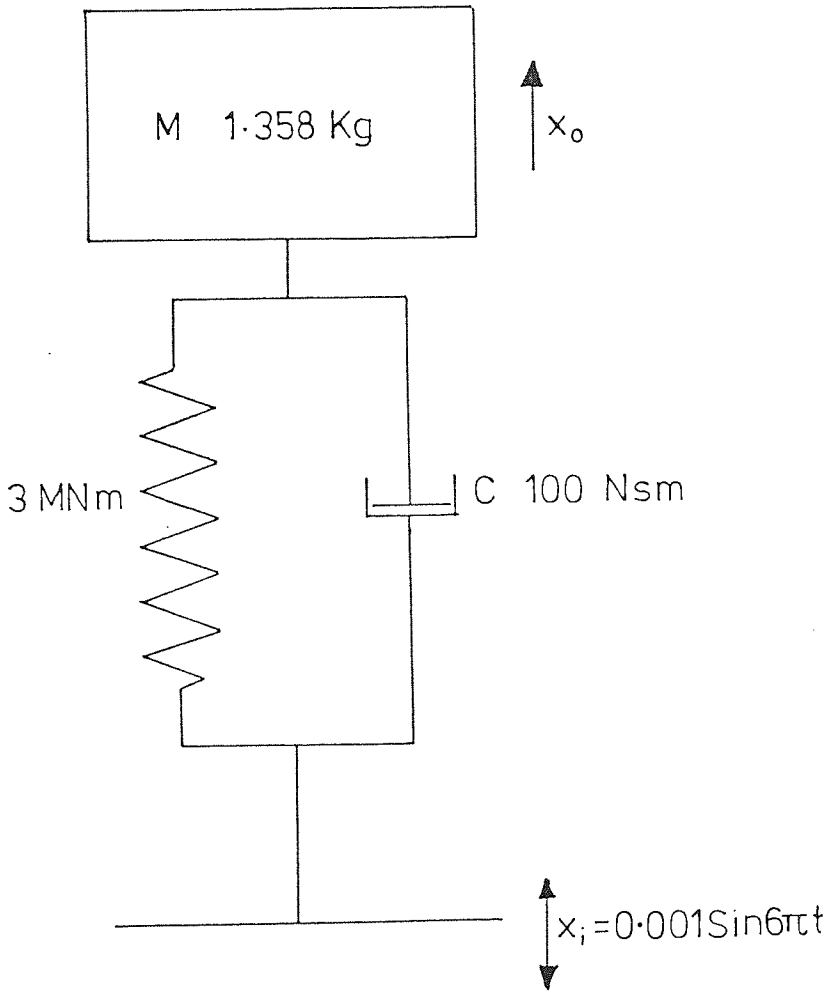

Fig B-1 Simple Model Used for Testing Program

General Solution

For timestep three and the subsequent timesteps it is possible to use the general form of the equations since $[x_o]_{i-1}$ and $[x_o]_{i-2}$ now exist. The technique is similar to that used in timestep two. The general solution equations are used to calculate the displacements and velocities. Arrays $[A]_i$ and $[A]_{i+1,j}$ are required for the solution, and these are set up as follows:-

$$[A_j]_i = [M_j]^{-1} \int_{t=(i-1)\Delta t}^{t=(i+1)\Delta t} [P_{t,j}]\, T_i\, dt$$

$$= [M_j]^{-1} \left(\int_{t=(i-1)\Delta t}^{t=\Delta t} [P_{t,j}]\, (t - t_{i-1})\, dt + \int_{t=i\Delta t}^{t=(i+1)\Delta t} [P_{t,j}]\, (t_{i+1} - t)\, dt \right)$$

$$[A_j]_{i+1,i} = [M_j]^{-1} \int_{t=(i-1)\Delta t}^{t=i\Delta t} [P_{t,j}]\, T_{i+1,i}\, dt$$

$$= [M_j]^{-1} \int_{t=(i-1)\Delta t}^{t=i\Delta t} [P_{t,j}]\, (t - t_i)\, dt$$

These expression may again be evaluated using Simpson's First Rule and an interval of $\frac{\Delta t}{2}$. The leakage is calculated, and it, the load, displacements and velocities stored as before. The calculations then proceed to the next timestep.

The calculations continue until the required number of timesteps have been completed.

B.3 Validation of the Program

The basic program was validated using 'top down' technique. The main subroutines were coded and tested, and then the remaining subroutines added in turn and tested. Once this was completed the program was tested on a one degree of freedom model (fig B - 1). The initial runs showed up various programming

Timestep	Analytical Results	Computer Results				
		Analytical Values	Stiffness Zero	Stiffness Negative	Damping Zero	Damping Negative
0	0	0	0	0	0	0
0.01	0.187×10^{-3}	0.443×10^{-2}	-0.205×10^{-6}	0.101×10^{-4}	-0.103×10^{-1}	-0.101×10^{-3}
0.02	0.368×10^{-3}	0.165×10^{2}	0.973×10^{-4}	-0.745	-0.774	-0.765
0.03	0.536×10^{-3}	0.646×10^{6}	0.179×10^{-3}	-0.315×10^{4}	-0.298×10^{4}	-0.289×10^{4}
0.04	0.685×10^{-3}	0.252×10^{3}	0.278×10^{-3}	-0.133×10^{8}	-0.115×10^{8}	-0.109×10^{8}

Table B - 1 Comparison of Analytical and Computer Results for various computer sizes of Δt

Timestep	Analytical Results	Computer Results Timestep			
		0.01	0.001	0.0005	0.00012
0	0	0	0	0	0
0.002	0.377×10^{-4}		0.205×10^{-4}	0.223×10^{-4}	
0.0024	0.452×10^{-4}				0.230×10^{-4}
0.004	0.753×10^{-4}		0.480×10^{-4}	0.513×10^{-4}	
0.0048	0.904×10^{-4}				0.565×10^{-4}
0.006	0.113×10^{-3}		0.614×10^{-4}	0.694×10^{-4}	0.691×10^{-4}
0.01	0.187×10^{-3}	0.443×10^{-2}	0.104×10^{-3}	0.116×10^{-3}	
0.02	0.368×10^{-3}	0.165×10^{2}	0.222×10^{-3}	0.242×10^{-3}	
0.03	0.536×10^{-3}	0.646×10^{6}	0.315×10^{-3}	0.345×10^{-3}	
0.04	0.685×10^{-3}	0.252×10^{-1}	0.401×10^{-3}	0.442×10^{-3}	

Table B - 2 Comparison of Analytical and Computer Results for various timesteps

errors but once these were eradicated, the program was still found to be diverging. Table B - 1 compares the analytical and computer results and may be compared with fig 6 - 7. Included on this table are all the tests carried out. The next tests were to try physically unreasonable data values, but both negative stiffness and negative damping gave similar results. Reducing the stiffness to zero whilst maintaining the damping at its original value gave more satisfactory results. The initial conclusion drawn from these results was that there were errors in the formulation of quantities involving the stiffness. However careful checks of the theory failed to reveal them. The only remaining possibilty was that the method was unstable for the problem data. This seemed particularly likely since the values of $[\ddot{X}_o]$ and $[\dddot{X}_o]$ increase rapidly, and become the dominant part of the solution after a couple of timesteps. The program was then run with various timestep lengths. Table B - 2 shows the results of these runs. It is clear that the problem is only stable for very small timesteps. The initial timestep used (0.01 sec.) was equivalent to 10.8^{o}, and thus thirty four steps would be required to predict the displacements and velocities for one cycle. However it can be seen from Table B - 2 that even for a timestep of 0.00012 secs, equivalent to over 2800 steps per cycle, the method does not predict the correct displacements. The results suggest that the technique is stable for a band of timesteps, and unstable outside this band. Such a band of stable conditions would be difficult to predict for the complete problem.

It seems likely that the main reasons for the instability is either the inherent problems with the truncated Taylor's Series approach or the result of the technique being a

predictor type using central differencing for the timestep. As the Taylor's Series expansion described in chapter 3 is stable for the problem, it is reasonable to assume that it is the predictive nature of the technique that causes the problems. The displacements and velocities at the present timestep (i + 1) are predicted from the forcing function, displacement, velocity, acceleration and third differential with respect to time at the previous timestep (i) and the displacement at i - 1. The method described in chapters 5 and 6 calculates the displacement in terms of the forcing function at the present timestep and the displacement at the two previous timesteps. The fact that the unsuccessful technique described here is thus purely a predictor method, coupled with the instability of the truncated series probably accounts for the failure. The technique thus requires a very small timestep for stability.

No further investigations have been carried out on this technique. Instead the solution described in chapter 3 was developed and implemented.

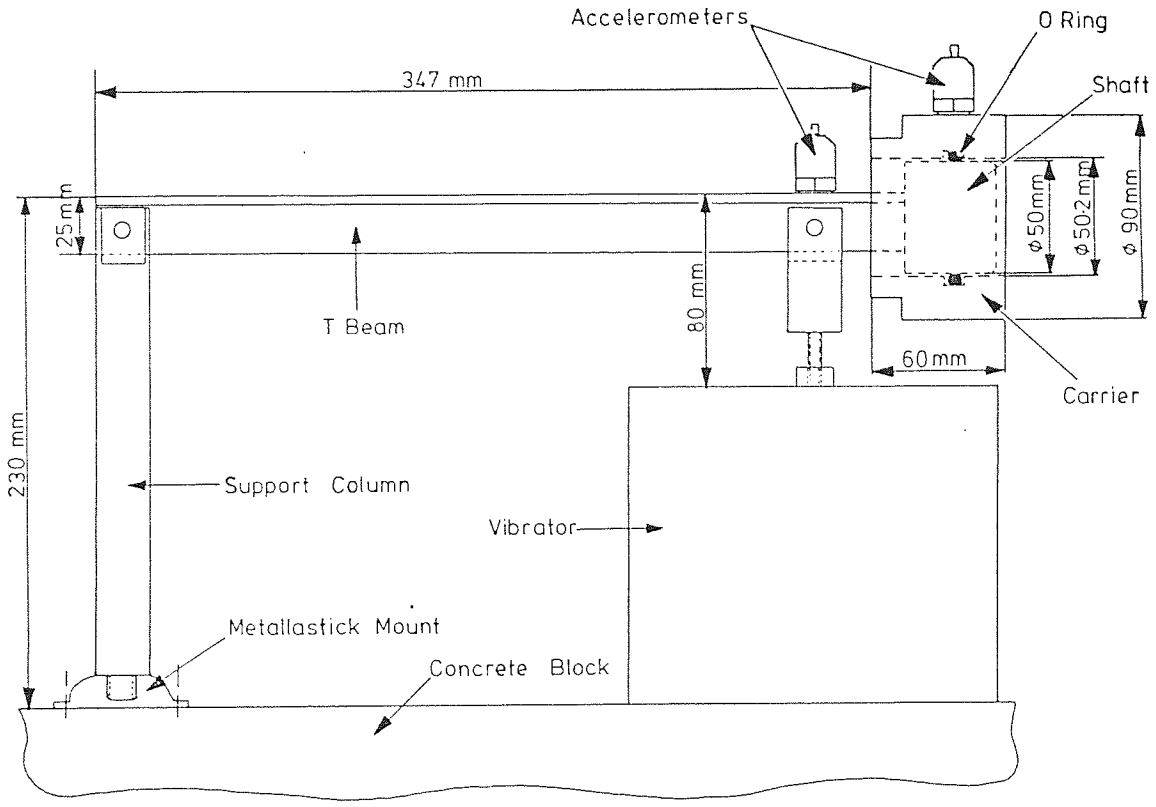

Fig C-1 First O-Ring Test Rig Design

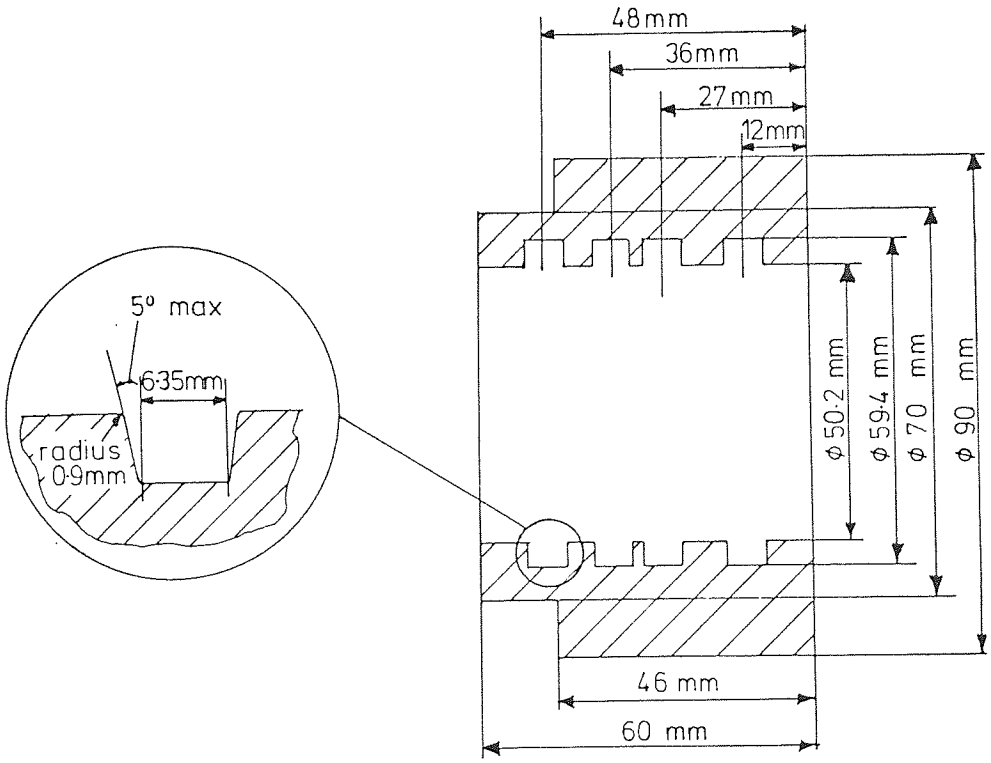

Fig C-2 Typical Carrier Design

APPENDIX C

THE FIRST O-RING TEST RIG

C.1 Test Rig Design

Two test rigs were built in order to carry out the experimental measurements of the stiffness and damping coefficients of o-rings. The first rig proved to be unsatisfactory for this purpose, and hence the second rig, described in chapter four, was built. In this appendix the first rig will be described.

C.1.1 Design Criteria

The test rig was to be used to measure parameters from which the o-ring properties could be calculated. In order to ensure practical results the measurements were to be made in a mechanical seal-like configuration. The rig design thus had to include a shaft that could be vibrated and on which a carrier with an o-ring could be mounted. The input vibration of the shaft and the response of the carrier could then be measured, and from these the properties of the o-ring under test could be calculated.

In addition to being used for the o-ring tests the rig was to be capable of simulating a mechanical seal. For this the o-ring carrier would act as a stationary floating ring, and a rotor and fluid film would be introduced.

C.1.2 Final Rig Design

The design of the test rig is shown in fig C - 1 , and a typical carrier design in fig C - 2 . The weight of the test beam and carrier is partly supported by the pivot and partly by

the vibrator. Since the static load capacity of the vibrator is limited, the shaft and carrier had to be as light as possible. Only a short section of cylindrical shaft was used, the remaining length being T-section aluminium extrusion. The carrier is mounted at the end of the shaft with one face free, in order that the design could simulate a mechanical seal. Each carrier had a number of o-ring grooves as shown and were made from various materials. The input vibration of the shaft was measured by the accelerometer mounted above the vibrator, and the resultant carrier acceleration by an accelerometer mounted on it. A transfer function analyser was used to analyse the signals, and the electronic circuit block diagram is similar to that shown in fig 4 - 9.

C.2 Test Programme

C.2.1 Design Criteria

The test programme was to measure the properties of o-rings over a frequency range covering typical values found in practice. The purpose of the programme was also to discover the effect of various compounding changes on these properties. The test programme has been described in detail in chapter 4 section 2. The main criteria are:-

(a) The test programme must be capable of covering a practical frequency range.

(b) It must be capable of showing the variations in properties between various o-rings.

C.2.2 Final Programme Design

The final programme design was the same as the basic programme design described in chapter 4 section 2. In

this case the frequency range was to be 25 Hz to 2000 Hz at a constant force level. Because the vibrator was partly supporting the mass of the beam and carrier it was not possible to use frequencies lower than 25 Hz without severe distortion of the signal. However, because a constant force was being used, the upper frequency limit was higher than if a constant displacement had been used. In addition to making measurements at the appropriate frequencies, the resonance frequency and acceleration must also be determined for the analysis. Various o-rings were obtained for the test programme to determine the effect on their properties of:-

(a) the cavity in which the ring was moulded

(b) the mould

(c) the compound batch

(d) the compound

(e) the size of the o-ring

(f) the mass and design of the carrier

C.3 Analysis Technique

The results were analysed using simple formulae derived by assuming the o-ring may be modelled by a Kelvin element. The formulae have been derived elsewhere (162), and relate the stiffness and damping coefficient of the o-ring to the acceleration at resonance, the resonance frequency, the carrier mass and the acceleration at the frequency being considered.

$$S = M\omega_r^2(1 - 2\zeta^2)$$

$$C = 2M\omega_r\zeta(1 - 2\zeta^2)^{\frac{1}{2}}$$

$$\zeta = \left[\frac{1}{2}\left(1 \pm \sqrt{1 - \frac{Q^2(1 - 2\Omega^2 + \Omega^4)}{Q^4 - Q^2(2\Omega^2 - 1)}}\right)\right]^{\frac{1}{2}}$$

$$Q = \frac{a_m}{a_r} \quad \text{and} \quad \Omega = \frac{\omega_m}{\omega_r}$$

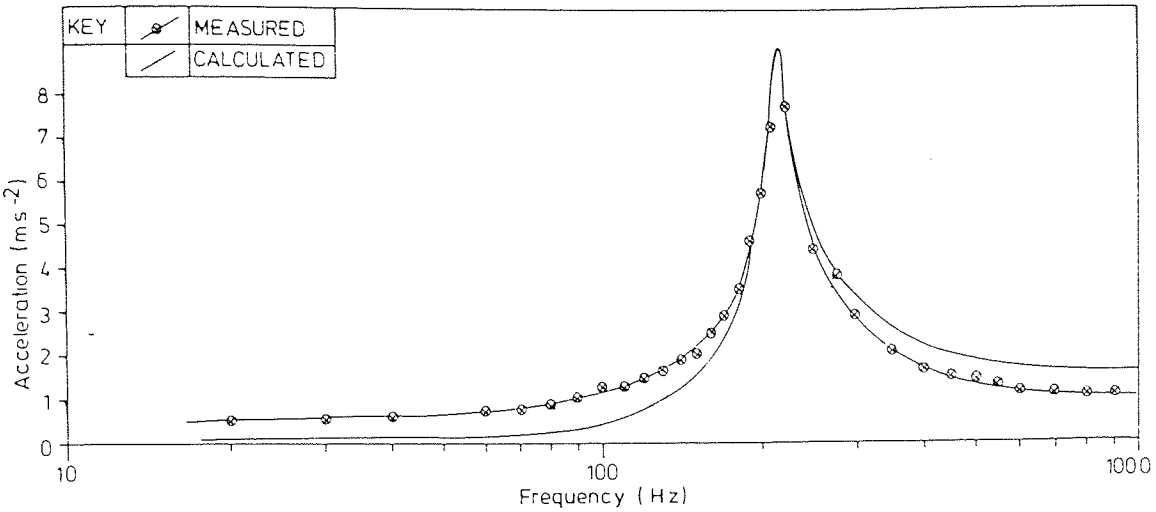

Fig C-3 Measured Carrier Accelerations and Calculated Response using data for 200 Hz

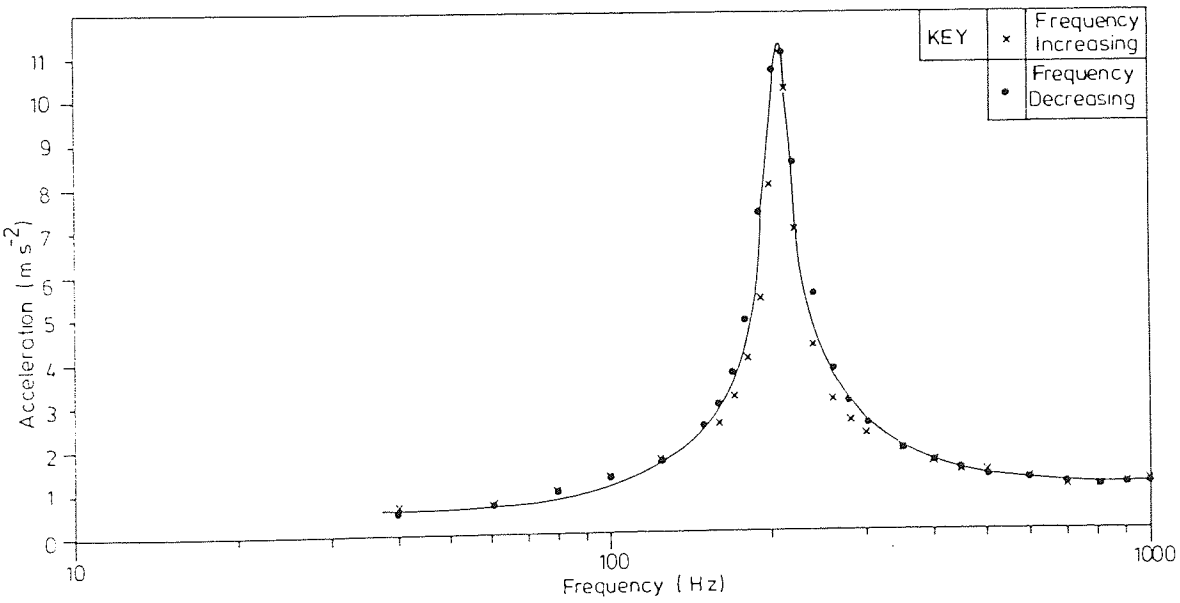

Fig C-4 Measured Carrier Accelerations for Increasing and Decreasing Frequencies

STIFFNESS AND VISCOUS DAMPING COEFFICIENTS:

RUN NO. 2 MATL. NO. 2
CARRIER NO. 2262 CARRIER MASS .635KG
O-RING SECTION 3.530mm

MAX ACCEL. .813 AT FREQ 218.000

FREQ	ACCEL	STIFF	DAMP
20.00	.5425-01	.3799 04	.6494 02
30.00	.5731-01	.7951 04	.8624 02
40.00	.5751-01	.1330 05	.9719 02
60.00	.6800-01	.2108 05	.8982 02
70.00	.8024-01	.2284 05	.8394 02
80.00	.8584-01	.2492 05	.7420 02
90.00	.1059 00	.2542 05	.7131 02
100.00	.1250 00	.2606 05	.6719 02
110.00	.1308 00	.2723 05	.5807 02
120.00	.1466 00	.2780 05	.5267 02
130.00	.1670 00	.2820 05	.4837 02
140.00	.1907 00	.2853 05	.4437 02
150.00	.2011 00	.2903 05	.3744 02
160.00	.2511 00	.2907 05	.3674 02
170.00	.2986 00	.2924 05	.3386 02
180.00	.3582 00	.2941 05	.3071 02
190.00	.4613 00	.2948 05	.2932 02
200.00	.5760 00	.2965 05	.2557 02
210.00	.7243 00	.2983 05	.2078 02
220.00	.7833 00	.3011 05	.8989 01
250.00	.4423 00	.2981 05	.2118 02
275.00	.3810 00	.2960 05	.2664 02
300.00	.2969 00	.2967 05	.2509 02
350.00	.2143 00	.2976 05	.2275 02
400.00	.1691 00	.2984 05	.2040 02
450.00	.1541 00	.2985 05	.2017 02
500.00	.1438 00	.2986 05	.1988 02
550.00	.1312 00	.2989 05	.1885 02
600.00	.1177 00	.2993 05	.1740 02
700.00	.1098 00	.2995 05	.1687 02
800.00	.1102 00	.2993 05	.1735 02
900.00	.1155 00	.2990 05	.1849 02
1850.00	.9528-01	.2997 05	.1597 02
2000.00	.1000 00	.2995 05	.1679 02

Table C-1 Calculated Stiffness and Damping Coefficients

This analysis assumes the measurements are made at a constant force input.

As the analysis technique utilises the entire frequency range, unlike that described in chapter 4 , it requires that the system can be modelled as a second order system throughout the frequency range. There are thus two possible sources of error in the calculated values. Firstly the measured values may be in error, and secondly the mathematical model may be inadequate. It will be seen, however, from the final section of this appendix that the rig was not as stiff as expected, and the mathematical model did not model the behaviour of the rig.

C.4 Experimental Results

Table C - 1 gives a typical set of results from the rig. These values are not constant, and thus one of the assumptions used in the analysis has been violated and the analysis is not applicable. Fig C - 3 is a plot of carrier input acceleration against frequency for a constant input acceleration. Two curves have been plotted, firstly the measured values and secondly a calculated response using the calculated values of the stiffness and damping coefficient at 200 Hz (close to the resonance frequency). It can be seen that whilst the curves are of the same general form, the shapes are quite different.

In order to investigate the reason for this, the vibrator was replaced by an electric motor with an eccentric weight. This would enable the response at higher force levels to be determined. The excitation method proved to be unsatisfactory,

mainly because of the difficulty in measuring the vibration frequency accurately. However one phenomenum was noted that did not occur with the electric vibrator. At a shaft speed of about 1800 rpm (30 Hz) the friction between the o-ring and the carrier and shaft decreased to virtually zero. The loss of friction was sufficient that it was easy to turn the carrier on the shaft by hand, something that was virtually impossible when the carrier was at rest. This behaviour seemed to be related to the force level. It did not occur at the force output level of the vibrator, nor with small out-of-balance weights. The effect was most noticeable with a rotating force vector of at least 150 N.

It is possible that hysteresis effects in the rubber at high force levels prevents the o-ring from tracking the shaft motion. The rubber is unable to return to its undeformed shape resulting in an almost complete loss of interference between the o-ring and the carrier or shaft. It is possible that the effect is accompanied by a rise in the temperature of the o-ring. Unfortunately no temperature measurements were made during these tests. It was not possible to reproduce these effects with the second test rig because of the driving arrangement.

In order to assess whether the results were due to the experimental technique the accelerations were measured on both increasing and decreasing frequency runs. Fig C - 4 shows that there is no significant difference between the results.

The remaining possible sources of the discrepancy between the theory and the results were that the test rig was introducing additional vibration mode and that the theoretical

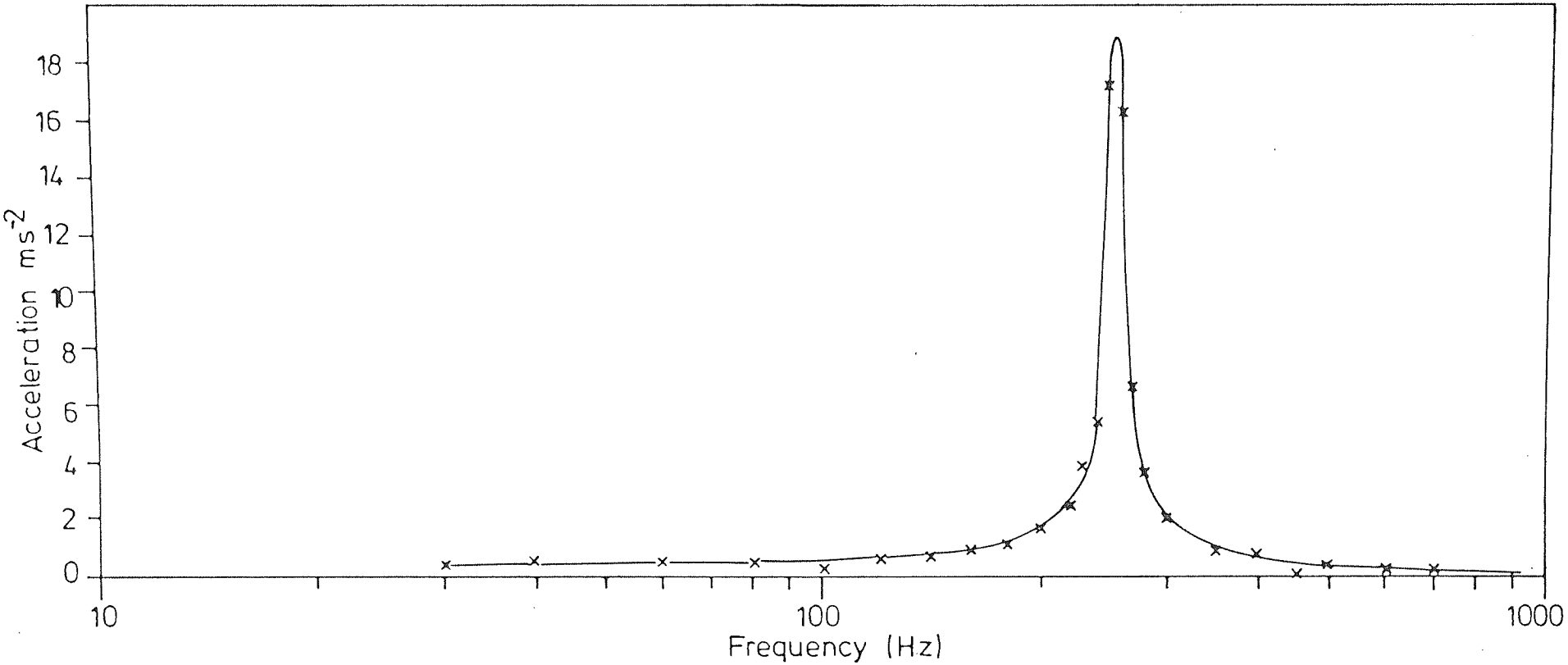

Fig. C-5 Relative Acceleration between Two Points on Test Rig Beam and Shaft

model was incorrect. The behaviour of the test rig was obtained by mounting an accelerometer on the cylindrical portion of the beam. Fig C - 5 shows the response of this accelerometer to a constant input acceleration on the T-beam. Clearly the test rig itself is resonating with a significant resonance amplitude. This showed that the test rig could not be used to measure the o-ring properties without significant errors occurring due to the test rig behaviour.

A new rig design was needed that would be stiff enough to ensure only the o-ring properties were measured. The tests on the first rig also demonstrated the need to measure the input levels at the point of input to the o-ring-carrier system and not some distance away. The rig described in chapter 4 was designed and built embodying these features.

APPENDIX D

REYNOLDS EQUATION COMPUTER PROGRAM FLOW DIAGRAM AND TYPICAL RESULTS

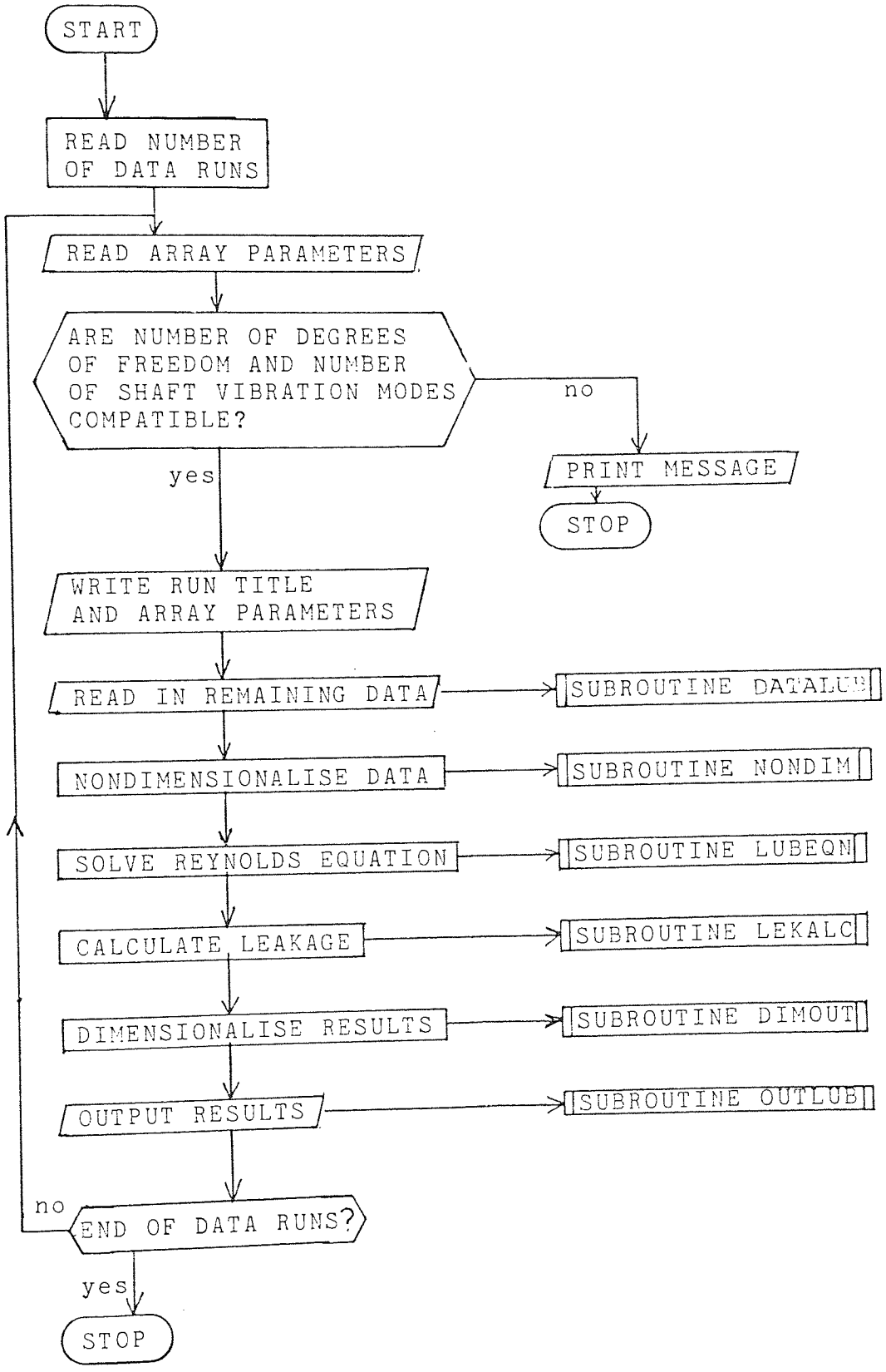

Reynolds Equation Program Main Structure

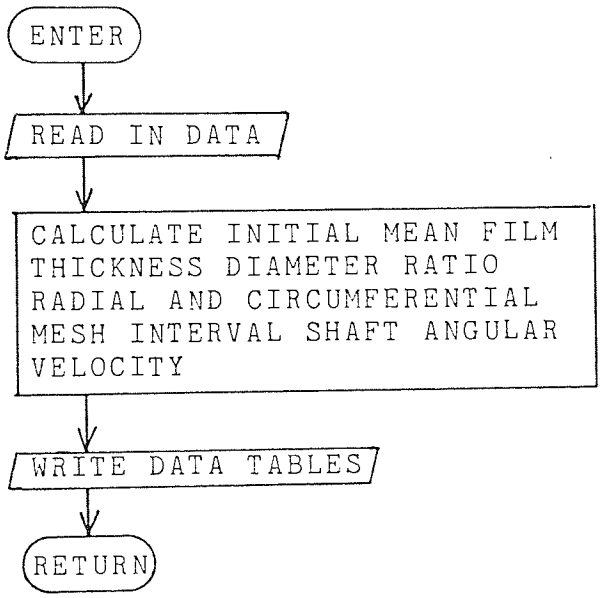

Subroutine Datalub

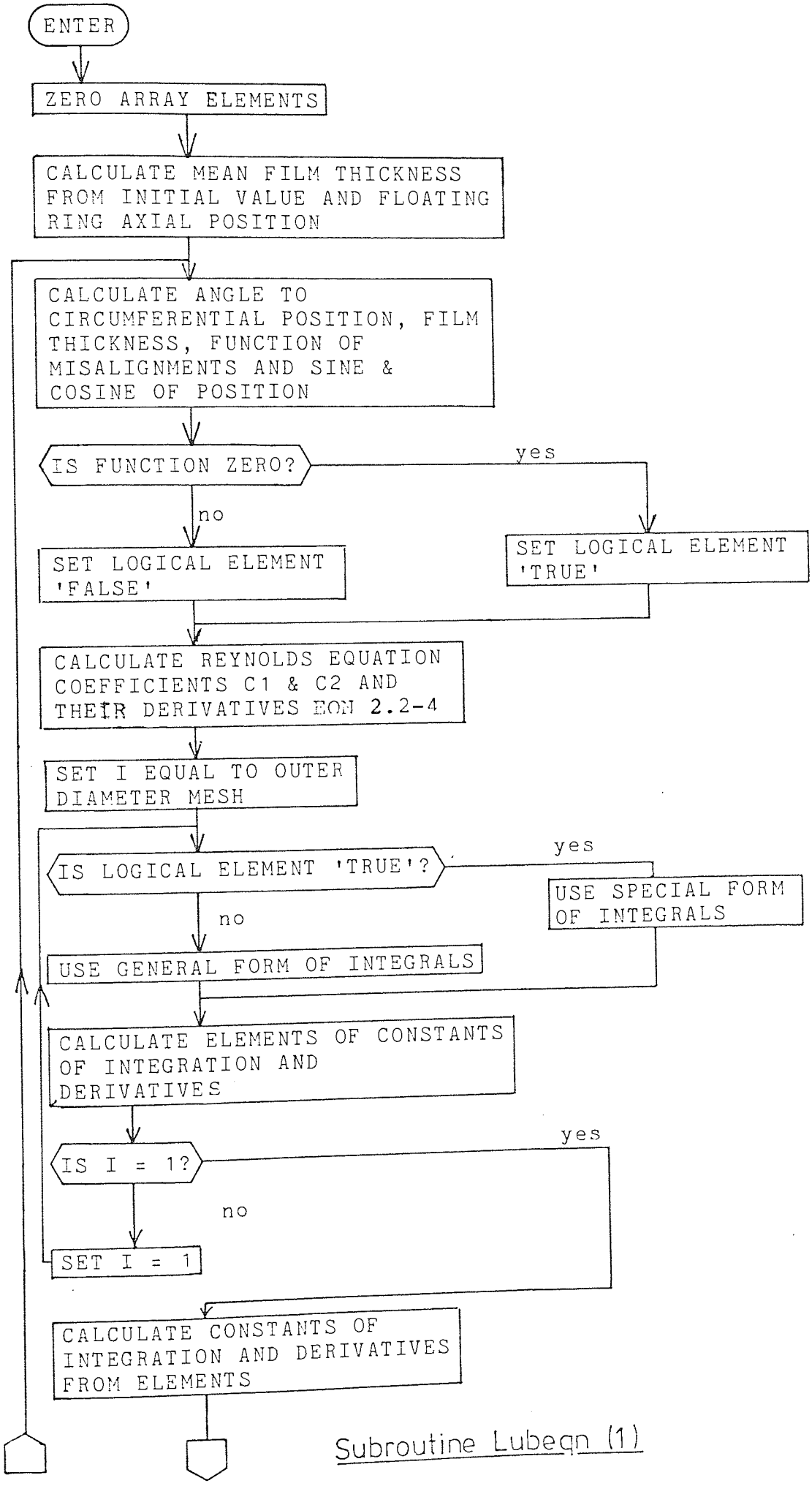

Subroutine Lubeqn (1)

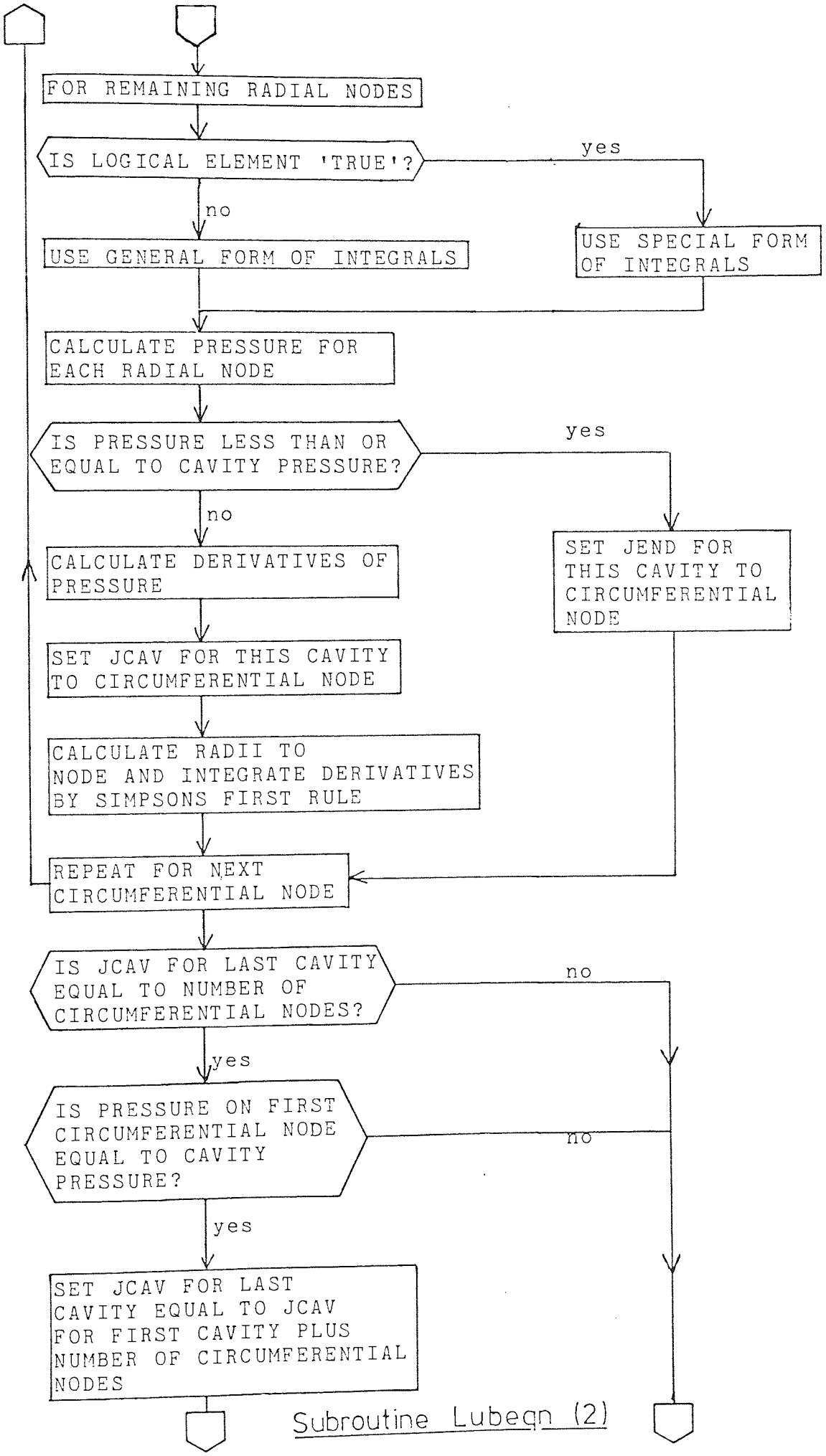

Subroutine Lubeqn (2)

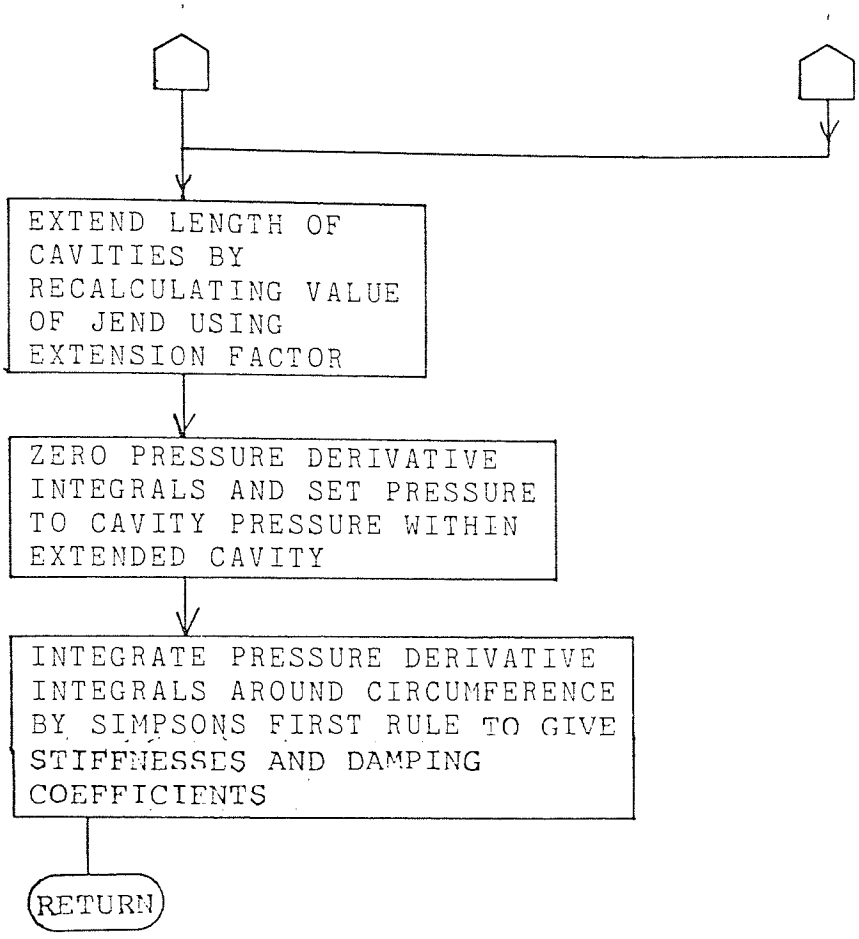

Subroutine Lubeqn (3)

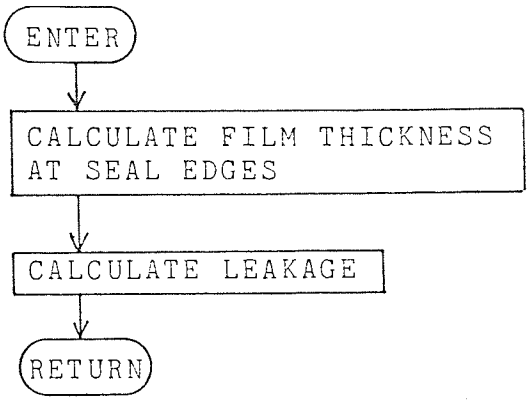

Subroutine Lekalc

```
      LIST
      PROGRAM(FXXX)
      INPUT  1= CRD
      OUTPUT 6= LP1
      OUTPUT 3= LP0
      OUTPUT 5= LP2
      COMPRESS INTEGER AND LOGICAL
      EXTENDED DATA
      TRACE 2
      END
      TRACE 0
      MASTER LUBMEC
C     ******************************
C     *                            *
C     *   THIS PROGRAM CALCULATES  *
C     *                            *
C     *   THE DYNAMIC PERFORMANCE  *
C     *                            *
C     *    OF A MECHANICAL  SEAL   *
C     *                            *
C     ******************************
      DIMENSION PRESS(15,48),FLMTHK(2,48),GL(100),
     1XO(100,5),DXODT(100,5),TITLE(10)
C
C     ARRAYS ARE DYNAMICALLY DIMENSIONED
C
  100 FORMAT(//10X,29(1H*)/10X,1H*,27X,1H*/10X,1H*,6X,
     1 25H PROGRAM EXECUTION HALTED,6X,1H*/10X,1H*,6X,
     2 6H NM  =,I3,6X,6H MM  =,I3,7X,1H*/10X,1H*,2X,
     3 32H THESE VALUES ARE NOT COMPATIBLE,3X,1H*/10X,1H*,7X,
     4 21H IF MM IS LESS THAN 4,9X,1H*/10X,1H*,10X,
     5 17H NM MUST EQUAL MM,10X,1H*/10X,1H*,27X,1H*/10X,29(1H*))
  101 FORMAT(5I3)
  102 FORMAT(10A8)
  103 FORMAT(F10.5,E20.6)
  104 FORMAT(1H1,10A8)
  105 FORMAT(1H1/10X,42H INPUT  DATA  TABLE  1  -  ARRAY AND OTHER,
     111H PARAMETERS/11X,21(1H-))
  106 FORMAT(//
     110X,50H NUMBER OF RIGID BODY DEGREES OF FREEDOM        (MM),2X,I3/
     210X,50H NUMBER OF INPUT VIBRATION DEGREES OF FREEDOM (NM),2X,I3/
     310X,50H MESH FOR REYNOLDS EQUATION CALCULATION     (MP*NP),2X,I3,
     41H*,I2///
     510X,30H TOTAL TIME CONSIDERED (TIME) ,24X,F10.6,6X,5H SECS/
     610X,30H TIME STEP             (TINT) ,16X,E20.6,2X,5H SECS/
     510X,30H NUMBER OF TIME STEPS                        (NT),I5/)
      READ(1,101)NRUNS
      NRUN=0
    1 NRUN=NRUN+1
      IF(NRUN.GT.NRUNS)GO TO 10
      READ(1,101)MP,NP,MM,NM,NI
      READ(1,102)TITLE
      READ(1,103)TIME,TINT
      IF(NM.EQ.MM.OR.MM.GE.4)GO TO 5
       WRITE(6,100)
       GO TO 10
    5 NT=INT(TIME/TINT)+1
      WRITE(6,104)TITLE
      WRITE(6,105)
      WRITE(6,106)MM,NM,MP,NP,TIME,TINT,NT
      CALL CALCOM
     1(MP,NP,NT,PRESS,FLMTHK,XO,DXODT,GL,MM)
```

```
      GO TO 1
   10 CONTINUE
      STOP
      END
      SUBROUTINE CALCONL
     1(MP,NP,NT,PRESS,FLMTHK,XO,DXODT,GL,MM)
C   ****************************************
C   *                                      *
C   *      THIS  SUBROUTINE   CONTROLS     *
C   *                                      *
C   *    THE RUNNING OF THE CALCULATIONS   *
C   *                                      *
C   ****************************************
      DIMENSION PRESS(MP,NP),FLMTHK(2,NP),GL(NT),
     1XO(NT,MM),DXODT(NT,MM)
     2 ,CAP(19),CAPO(19)
  100 FORMAT(4E20.6)
C
C     SET UP THE DATA
C
      CALL DATALUB
     1 (MM,NM,MP,NP,NT,
     3PI,PO,PCAV
     4,VISC,RPM,HAMP,RE,WIDTH,NW,R,RINT,THINT,OMEGA,
     5     HIN,XO,DXODT,IFACOM,CAVFAC)
      ITIMST=1
      IPRT=0
      FILM=0.
      CALL NONDIM
     1  (VISC,OMEGA,GL,MP,NP,NT,NM,PI,PO,PCAV,ITIMST,FILM,TDF,
     2 XO,DXODT,MM,HAMP,HIN,
     3 AMAS,PFORCE,ROH,RS,JOP,SPL,CLEAR,TINT,TIME,SHAFT)
      CALL LUBEQN
     1  (MP,NP,NT,PRESS,CAP,THINT,ITIMST,MM,NW,HAMP,RINT,PI,PO,
     2 PCAV,R,XO(1,3),XO(1,4),XO(1,5),DXODT(1,3),DXODT(1,4),
     3  DXODT(1,5),IFACOM,CAVFAC,TINT,FILM,TDF,OMEGA)
      CALL LEKALC
     1  (MP,NP,R,PI,PO,GL,RINT,THINT,-XO(1,3),XO(1,4)
     2  ,XO(1,5),HAMP,NW,ITIMST,NT,FLMTHK,IFACOM,TINT,
     3  FILM,TDF,OMEGA)
      CALL DIMOUT
     1  (PRESS,CAP,GL,MP,NP,NT,ITIMST,GLO,CAPO,ALOAD,ALO)
      CALL OUTLUB
     1  (PRESS,CAPO,GLO,MP,NP,NT,ITIMST,IPRT)
      WRITE(3,100)CAPO
      RETURN
      END
      SUBROUTINE DATALUB
     1 (MM,NM,MP,NP,NT,
     2PI,PO,PCAV
     4  ,VISC,RPM,HAMP,RE,WIDTH,NW,R,RINT,THINT,OMEGA,
     5     HIN,XO,DXODT,IFACOM,CAVFAC)
      DIMENSION XO(NT,MM),DXODT(NT,MM)
C
C   ************************************************
C   *                                              *
C   *  THIS SUBROUTINE READ IN THE PROBLEM DATA    *
C   *  CALCULATES CONSTANT PARAMETERS AND WRITES   *
C   *   OUT ALL DATA IN TABULAR FORM WITH UNITS    *
C   *                                              *
C   ************************************************
C
  100 FORMAT(4E10.3)
  101 FORMAT(5F10.5)
  116 FORMAT(5I3)
  117 FORMAT(///1X,7CH INPUT  DATA  TABLE  2  -  SEALED FLUID AND SLIDI
```

```
     1NG INTERFACE PARAMETERS,/11X,21(1H-)
     2//10X,75H PRESSURES IN N/SQ.M   VISCOSITY IN N.S/SQ M   LENGTHS IN
     3M   ANGLES IN RADIANS///
     410X,36H SEALED PRESSURE  ID              (PI),E20.6/
     510X,36H   ..      ..     OD              (PO),E20.6/
     610X,36H CAVITATION PRESSURE             (PCAV),E20.6/
     710X,36H FLUID VISCOSITY                 (VISC),E20.6/
     810X,36H SHAFT SPEED                      (RPM),E20.6)
 110 FORMAT(///
     110X,36H FILM PROFILE WAVE AMPLITUDE  (HAMP),E20.6/
     X10X,36H   ..     ..  NUMBER OF WAVES     (NW),6X,I3/
     110X,36H   ..   ..  GIVEN FILM THICKNESS (HIN),E20.6/
     210X,36H SLIDING INTERFACE WIDTH      (WIDTH),5X,F10.5/
     310X,36H    ..        ..     ID           (RE),5X,F10.5/
     510X,36H CAVITY EXTENSION FACTOR     (CAVFAC),7X,F6.2//
     410X,36H ROTOR        : RADIAL  OX     (XO(1)),E20.6/
     510X,36H POSITION     : RADIAL  OY     (XO(2)),E20.6/
     610X,36H RELATIVE TO  : AXIAL          (XO( )),E20.6/
     710X,36H SHAFT AXIS   : ANGULAR OX     (XO(4)),E20.6/
     810X,36H AND  STATOR  : ANGULAR OY     (XO(5)),E20.6/)
 119 FORMAT(/
     910X,36H              : RADIAL OX  (DXODT(1)),E20.6/
     X10X,36H ROTOR        : RADIAL OY  (DXODT(2)),E20.6/
     110X,36H              : AXIAL      (DXODT(3)),E20.6/
     210X,36H VELOCITIES   : ANGULAR OX (DXODT(4)),E20.6/
     310X,36H              : ANGULAR OY (DXODT(5)),E20.6)
 120 FORMAT(///
     110X,38H DIAMETER RATIO                          (R),F10.5/
     210X,36H CIRCUMFERENTIAL NODE INTERVAL (THINT),F10.5/
     310X,35H RADIAL NODE INTERVAL           (RINT),F10.5/
     410X,35H SHAFT ANGULAR VELOCITY        (OMEGA),F10.5)
 121 FORMAT(/10X,26H ROTOR SURFACE IS PROFILED)
 122 FORMAT(/10X,27H STATOR SURFACE IS PROFILED)
      READ(1,100)PI,PO,PCAV,VISC
      READ(1,150)RPM,HAMP
      READ(1,101)RE,WIDTH,CAVFAC
      READ(1,116)NW,IFACOM
      READ(1,100)(XO(1,I),I=1,MM),(DXODT(1,I),I=1,MM)
      HIN=-XO(1,3)
      R=1-WIDTH/RE
      RINT=(1-R)/(MP-1)
      THINT=2.*3.14159265/NP
      OMEGA=2.*3.14159265*RPM/60.
      WRITE(6,117)PI,PO,PCAV,VISC,RPM
      WRITE(6,118)HAMP,NW,HIN,WIDTH,RE,CAVFAC,XO
      WRITE(6,119)DXODT
      WRITE(6,120)R,THINT,RINT,OMEGA
      IF(IFACOM)1,1,2
    1 WRITE(6,122)
      GO TO 3
    2 WRITE(6,121)
    3 CONTINUE
      RETURN
      END
      SUBROUTINE NONDIM
     1  (VISC,OMEGA,RE,MP,NP,NT,MM,PI,PO,PCAV,ITIMST,FILM,TDF,
     2 XO,DXODT,MM,HAMP,HIN,
     3 AMAS,PFORCE,ROR,RS,NOR,SPL,CLEAR,TINT,TIME,SHAFT)
      DIMENSION XO(NT,MM),DXODT(NT,MM)
      COMMON/DIMEN1/FORCND,PRESND,CLND,AMASND,AINND
      COMMON/DIMEN2/SPNDLF,DMNDLF,SPNDRF,DMNDRF,SPNDRM,DMNDRM
C
C  ***********************************************
C  *                                             *
C  *  THIS SUBROUTINE NON-DIMENSIONALISES THE    *
C  *             PROBLEM DATA                    *
```

```
C   *                                                       *
C   *********************************************************
C
      PRESND=6.*VISC*OMEGA*RE*RE/(HIN*HIN)
      FORCND=PRESND*RE*RE
      SFNDLF=FORCND/HIN
      DMNDLF=SFNDLF/OMEGA
      SFNDRF=SFNDLF*RE
      DMNDRF=SFNDRF/OMEGA
      SFNDRM=SFNDRF*RE
      DMNDRM=DMNDRF*RE
      AMASND=DMNDLF/OMEGA
      AINND=AMASND*RE*RE
      QLNN=RE*RE*OMEGA*HIN*(1.0E-06)
C    NON-DIMENSIONALISE THE MASS DISPLACEMENT AND VELOCITY MATRICES
C
      DO 20 I=1,3
       IF(I.GT.MM)GO TO 20
       XO(ITIMST,I)=XO(ITIMST,I)/HIN
       DXODT(ITIMST,I)=DXODT(ITIMST,I)/(OMEGA*HIN)
   20 CONTINUE
      DO 30 I=4,5
       IF(I.GT.MM)GO TO 30
       XO(ITIMST,I)=XO(ITIMST,I)*RE/HIN
       DXODT(ITIMST,I)=DXODT(ITIMST,I)*RE/(OMEGA*HIN)
   30 CONTINUE
C
C    NON-DIMENSIONALISE THE FORCES AND GEOMETRICAL PARAMETERS
C
      PFORCE=PFORCE/FORCND
      PI=PI/PRESND
      PO=PO/PRESND
      PCAV=PCAV/PRESND
      HAMP=HAMP/HIN
      FILM=FILM/HIN
      ROR=ROR/RE
      RS=RS/RE
      DOR=DOR/RE
      SPL=SPL/RE
      CLEAR=CLEAR/HIN
      TINT=TINT*OMEGA
      TIME=TIME*OMEGA
      TDF=HIN*RE
      RETURN
      END
      SUBROUTINE LUBSON
     1  (MP,NP,NT,PRESS,CAP,THINT,ITIMST,MM,NN,HAMP,PINT,PI,PO,
     2 PCAV,R,CLX,CIX,CIY,DCLDT,DCIXDT,DCIYDT,IFACOM,
     3  CAVFAC,TINT,FILM,TDF,OMEGA)
      REAL MDL,MDV,MDCY,MDCY,MDCXT,MDCYT
      COMMON JCAV(48),JENG(43)
      COMMON/PH/PHASE
      LOGICAL LOG1
      DIMENSION  PRESS(MP,NP),CAP(19),DPDL(16),
     1 MDL(48),MDV(48),MDCY(48),MDCY(48),MDCXT(48),MDCYT(48),
     2 DPDCX(16),DPDCY(16),DPDCXT(16),DPDCYT(16),DPDV(16),M(48)
     3  ,MDL(48),MDV(48),MDCX(48),MDCY(48),MDCXT(48),MDCYT(48)
C                                                       *
C   *********************************************************
C   *                                                     *
C   *  THIS SUBROUTINE SOLVES REYNOLDS EQUATION           *
C   *  AND CALCULATES THE LOAD CAPACITY STIFFNESS         *
C   *  AND DAMPING COEFFICIENT OF THE FILM                *
C   *                                                     *
C   *  THE METHOD ASSUMES ALL PARAMETERS ARE              *
C   *              NON-DIMENSIONAL                        *
```

```
C   *                                                    *
C   ******************************************************
C
C
C    ZERO ALL ARRAYS AND SET UP INITIAL VALUES
C
       IJ=1
        DO 1 I=1,10
         JEND(I)=0
     1   JCAV(I)=0
       CL=FILY-CLX
       DO 24 J=1,NP
       PRESS(1,J)=PI
        PRESS(NP,J)=PO
        DO 2 I=1,MP
         DPDL(I)=0.0
         DPDV(I)=0.0
         DPDCX(I)=0.
         DPDCY(I)=0.
         DPDCXT(I)=0.
     2   DPDCYT(I)=0.
       W(J)=0.
       WDL(J)=0.
       WDV(J)=0.
       WDCX(J)=0.
       WDCY(J)=0.
       WDCXT(J)=0.
       WDCYT(J)=0.
       MDL(J)=0.
       MDV(J)=0.
       MDCX(J)=0.
       MDCY(J)=0.
       MDCXT(J)=0.
       MDCYT(J)=0.
C
C    CALCULATE LOCAL ANGLE AND FILM THICKNESSES
C
       THETA=(J-1)*THINT+PHASE
        LOG1=.FALSE.
        CLCOS=CL+HAMP*COS(ONE*THETA-IFACOM*(ITIMST-1)*TINT
      1   *OMEGA*TDF)
        CT=COS(THETA)
        ST=SIN(THETA)
        CI=CIX*ST-CIY*CT
        IF(ABS(CI)-1.0E-08)4,4,3
     3   CI2=CI*CI
        CI3=CI2*CI
        GO TO 5
     4   LOG1=.TRUE.
     5   CLCOS2=CLCOS**2
         CLCOS3=CLCOS**3
C
C    CALCULATE CONSTANTS AND THEIR DERIVATIVES
C
        C1=-HAMP*(ONE-2*IFACOM)*SIN(ONE*THETA-IFACOM*(ITIMST-1)
      1   *TINT*OMEGA*TDF)-2.*DCLDT
        C2=-(CIX*CT+CIY*ST+2.*(CIXDT*ST-DCIYDT*CT))
        DC1DV=-2.
        DC2DCX=-CT
        DC2DCY=-ST
        DC2CXT=-2.*ST
        DC2CYT=2.*CT
C
C    CALCULATE THE INTEGRALS AT THE EDGES AND HENCE CALCULATE
C    THE CONSTANTS OF INTEGRATION
C
```

```
      AKIN=0.
      AKID=0.
       AKDLN1=0.
       AKDLN2=0.
       AKDV1=0.
       AKCXN1=0.
       AKCXN2=0.
       AKCYN1=0.
       AKCYN2=0.
       AKCXT1=0.
       AKCYT1=0.
      I=NP
    6 IF(LOG1)GO TO 9
      CALL INTGEN
     1 (R,I,RINT,AINT1,AINT2,AINT3,DI1DL,DI2DL,DI3DL,
     2  DI1DCX,DI2DCX,DI3DCX,DI1DCY,DI2DCY,DI3DCY,CLCOS,CLCOS2,CLCOS3,
     3  CT,ST,CI,CI2,CI3)
      GO TO 10
    9  CALL INTSPC
     1 (R,I,RINT,AINT1,AINT2,AINT3,DI1DL,DI2DL,DI3DL,CT,ST,
     2  DI1DCX,DI2DCX,DI3DCX,DI1DCY,DI2DCY,DI3DCY,CLCOS,CLCOS2,CLCOS3)
   10 AKIN=-AKIN+C1*AINT1/2.+C2*AINT2/3.
      AKID=-AKID-AINT3
      AKDLN1=-AKDLN1+0.5*C1*DI1DL+C2*DI2DL/2.
      AKDLN2=-AKDLN2-DI3DL
      AKDV1=-AKDV1+0.5*AINT1*DC1DV
      AKCXN1=-AKCXN1+0.5*C1*DI1DCX+C2*DI2DCX/3.+AINT2*DC2DCX/3.
      AKCXN2=-AKCXN2-DI3DCX
      AKCYN1=-AKCYN1+0.5*C1*DI1DCY+C2*DI2DCY/3.+AINT2*DC2DCY/3.
      AKCYN2=-AKCYN2-DI3DCY
      AKCXT1=-AKCXT1+AINT2*DC2CXT/3.
      AKCYT1=-AKCYT1+AINT2*DC2CYT/3.
      IF(I.EQ.1)GO TO 11
      I=1
      GO TO 6
C
C    CALCULATE THE CONSTANTS OF INTEGRATION
C    AND THEIR DERIVATIVES
C
   11 AK1=(AKIN-PI+PC)/AKID
      AK2=PI-0.5*C1*AINT1-C2*AINT2/3.-AK1*AINT3
      DK1DL=AKDLN1/AKID-AKIN*AKDLN2/(AKID**2)
      DK2DL=-0.5*C1*DI1DL-C2*DI2DL/3.-AK1*DI3DL-AINT3*DK1DL
      DK1DV=AKDV1/AKID
      DK2DV=-.5*AINT1*DC1DV-AINT3*DK1DV
      DK1DCX=AKCXN1/AKID-AKIN*AKCXN2/(AKID**2)
      DK2DCX=-.5*C1*DI1DCX-(AINT2*DC2DCX+C2*DI2DCX)/3.
     1 -AK1*DI3DCX-AINT3*DK1DCX
      DK1DCY=AKCYN1/AKID-AKIN*AKCYN2/(AKID**2)
      DK2DCY=-.5*C1*DI1DCY-(AINT2*DC2DCY+C2*DI2DCY)/3.
     1 -AK1*DI3DCY-AINT3*DK1DCY
      DK1CXT=AKCXT1/AKID
      DK2CXT=-AINT2*DC2CXT/3.-AINT3*DK1CXT
      DK1CYT=AKCYT1/AKID
      DK2CYT=-AINT2*DC2CYT/3.-AINT3*DK1CYT
C
C    CALCULATE THE INTEGRALS AND THEIR DERIVATIVES
C    AT THE INTERNAL POINTS
C
      DO 15 I=2,NP-1
       IF(LOG1)GO TO 14
       CALL INTGEN
     1 (R,I,RINT,AINT1,AINT2,AINT3,DI1DL,DI2DL,DI3DL,
     2  DI1DCX,DI2DCX,DI3DCX,DI1DCY,DI2DCY,DI3DCY,CLCOS,CLCOS2,CLCOS3,
     3  CT,ST,CI,CI2,CI3)
       GO TO 15
```

```
   14      CALL INTSPC
     1 (R,I,RINT,AINT1,AINT2,AINT3,DI1DL,DI2DL,DI3DL,CT,ST,
     2  DI1DCX,DI2DCX,DI3DCX,DI1DCY,DI2DCY,DI3DCY,CLCOS,CLCOS2,CLCOS3)
C
C    CALCULATE THE PRESSURE AT THE INTERNAL NODES
C
   15      PRESS(I,J)=.5*C1*AINT1+C2*AINT2/3.+AK1*AINT3+AK2
C
C    APPLY HALF SOMMERFELD CAVITATION CONDITIONS HERE
C
C
C    IF CAVITY PRESSURE CALCULATED JUMPT TO
C    END OF J LOOP
C
        IF(PRESS(I,J).LE.PCAV)GO TO 31
C
C    CALCULATE THE DERIVATIVES OF THE PRESSURE NOTE THAT
C    THE DERIVATIVES ARE ZERO AT THE EDGES AND WITHIN
C    THE CAVITY
C
        DPDL(I)=0.5*C1*DI1DL+C2*DI2DL/3.+AK1*DI3DL+AINT3*DK1DL+DK2DL
        DPDV(I)=AINT1*DC1DV/2.+AINT3*DK1DV+DK2DV
        DPDCX(I)=.5*C1*DI1DCX+(AINT2*DC2DCX+C2*DI2DCX)/3.
     1  +AK1*DI3DCX+AINT3*DK1DCX+DK2DCX
        DPDCY(I)=.5*C1*DI1DCY+(AINT2*DC2DCY+C2*DI2DCY)/3.
     1  +AK1*DI3DCY+AINT3*DK1DCY+DK2DCY
        DPDCXT(I)=AINT2*DC2CXT/3.+AINT3*DK1CXT+DK2CXT
        DPDCYT(I)=AINT2*DC2CYT/3.+AINT3*DK1CYT+DK2CYT
   18   CONTINUE
C
C    STORE NODE OF BEGINING  OF CAVITY
C
        IF(JEND(IJ).NE.0)IJ=IJ+1
        JCAV(IJ)=J
C
C    INTEGRATE THE PRESSURE AND ITS DERIVATIVES USING
C    SIMPSONS RULES FIRST INTEGRATE ALONG EACH CIRCUMFERENTIAL
C    LINE AND STORE THE INTEGRAL
C
   25   MP1=MP-1
        DO 30 I=2,MP1,2
         I1=I+1
         R1=R+(I-1)*RINT
         R2=R+I*RINT
         R12=R1*R1
         R22=R2*R2
         W(J)=W(J)+PRESS(I,J)*4.*R1+PRESS(I1,J)*2.*R2
         WDL(J)=WDL(J)+DPDL(I)*4.*R1+DPDL(I1)*2.*R2
         WDV(J)=WDV(J)+DPDV(I)*4.*R1+DPDV(I1)*2.*R2
         WDCX(J)=WDCX(J)+DPDCX(I)*4.*R1+DPDCX(I1)*2.*R2
         WDCY(J)=WDCY(J)+DPDCY(I)*4.*R1+DPDCY(I1)*2.*R2
         WDCXT(J)=WDCXT(J)+DPDCXT(I)*4.*R1+DPDCXT(I1)*2.*R2
         WDCYT(J)=WDCYT(J)+DPDCYT(I)*4.*R1+DPDCYT(I1)*2.*R2
         MDL(J)=MDL(J)+DPDL(I)*R12*4.+DPDL(I1)*R22*2.
         MDV(J)=MDV(J)+DPDV(I)*R12*4.+DPDV(I1)*R22*2.
         MDCX(J)=MDCX(J)+DPDCX(I)*R12*4.+DPDCX(I1)*R22*2.
         MDCY(J)=MDCY(J)+DPDCY(I)*R12*4.+DPDCY(I1)*R22*2.
         MDCXT(J)=MDCXT(J)+DPDCXT(I)*R12*4.+DPDCXT(I1)*R22*2.
   30    MDCYT(J)=MDCYT(J)+DPDCYT(I)*R12*4.+DPDCYT(I1)*R22*2.
        W(J)=(W(J)+PRESS(1,J)-PRESS(MP,J))*RINT/3.
        WDL(J)=WDL(J)*RINT/3.
        WDV(J)=WDV(J)*RINT/3.
        WDCX(J)=WDCX(J)*RINT/3.
        WDCY(J)=WDCY(J)*RINT/3.
        WDCXT(J)=WDCXT(J)*RINT/3.
        WDCYT(J)=WDCYT(J)*RINT/3.
```

```
      MDL(J)=MDL(J)*RINT/3.
      MDV(J)=MDV(J)*RINT/3.
      MDCX(J)=MDCX(J)*RINT/3.
      MDCY(J)=MDCY(J)*RINT/3.
      MDCXT(J)=MDCXT(J)*RINT/3.
      MDCYT(J)=MDCYT(J)*RINT/3.
C
C   JUMP IF NOT CAVITY REGION
C
      GO TO 34
C
C   STORE END NODE OF CAVITY
C
   31 JEND(IJ)=J
      I=MP
   34 CONTINUE
C
C   INTEGRATE THE RADIAL INTEGRALS TO OBTAIN THE TOTAL
C   LOAD CAPACITY AND THE STIFFNESS AND DAMPING COEFFICIENTS
C
C
C   FIRST REPROCESS THE HALF SOMMERFELD CAVITY
C   BOUNDARIES TO GIVE A MORE REALISTIC CAVITY
C
      IF(JCAV(IJ)-NP)39,35,39
   35 DO 37 IIM=1,MP
       IF(PRESS(IIM,1)-PCAV)37,37,36
   36  JCAV(IJ)=JCAV(I)+NP
       GO TO 39
   37 CONTINUE
      IF(JEND(IJ).EQ.0)JEND(IJ)=JEND(1)+NP
   39 CONTINUE
      IF(JEND(IJ)-NP)44,41,44
   41 DO 43 IIM=1,MP
       IF(PRESS(IIM,1)-PCAV)43,42,43
   42  JEND(IJ)=JEND(I)+NP
   43 CONTINUE
   44 CONTINUE
      DO 50 I=1,10
       IF(JEND(I))51,51,45
   45  IF(JCAV(I+1))51,46,47
   46  JC=1
       JV=1
       IF(JCAV(1).EQ.0)JV=2
       JCAV(I+1)=JCAV(JV)+NP
   47  JEND(I)=JEND(I)+INT((JCAV(I+1)-JEND(I))*CAVFAC)
       IF(JEND(I).GT.NP)JEND(I)=JEND(I)-NP
       IF(JC.EQ.1)JCAV(I+1)=0
        JC=0
   50 CONTINUE
   51 CONTINUE
C
C   REPROCESS THE PRESSURE AND ITS DERIVATIVES FOR THE NEW CAVITY
C
      DO 71 I=1,10
       IF(JEND(I).EQ.0)GO TO 72
       IF(JCAV(I).NE.0.OR.JCAV(I+1).NE.0)GO TO 64
       JEND(I)=NP
       GO TO 69
   64  IF(JCAV(I).EQ.0)GO TO 71
       IF(JEND(I)-JCAV(I)+1)69,71,70
   65  IF(JCAV(I).EQ.NP)GO TO 69
       JP1=JCAV(I)+1
       JP2=NP
   66  DO 68 JJ=JP1,JP2
        DO 67 II=2,MP-1
```

```
      PRESS(II,JJ)=PCAV
      W(JJ)=(MP-1)*PCAV*RINT*(R+1)/2.
      WDL(JJ)=0.
      WDV(JJ)=0.
      WDCX(JJ)=0.
      WDCY(JJ)=0.
      WDCXT(JJ)=0.
      WDCYT(JJ)=0.
      MDL(JJ)=0.
      MDV(JJ)=0.
      MDCX(JJ)=0.
      MDCY(JJ)=0.
      MDCXT(JJ)=0.
      MDCYT(JJ)=0.
   66 IF(JP2.EQ.JEND(I))GO TO 71
   69 JP1=1
      JP2=JEND(I)
      GO TO 66
   70 JP1=JCAV(I)+1
      JP2=JEND(I)
      GO TO 66
   71 CONTINUE
   72 CONTINUE
C     WRITE(9,100)W,WDL,WDV,WDCX,WDCY,WDCXT,WDCYT,
C    1              MDL,MDV,MDCX,MDCY,MDCYT,MDCYT
  100 FORMAT(5X,5E30.8)
      DO 82 I=1,19
   82  CAP(I)=0.
      DO 83 J=2,NP,2
       J1=J+1
       IF(J1.GT.NP)J1=J1-NP
       ST1=SIN((J-1)*THINT)
       ST2=SIN(J*THINT)
       CT1=COS((J-1)*THINT)
       CT2=COS(J*THINT)
C
C    CARRY OUT CIRCUMFERENTIAL INTEGRATION
C
       NP1=NP/4+1
       NP2=NP/2+1
       NP3=3*NP/4+1
       SIGN=1
       SIGN1=1
       SIGN3=1
       SIGN31=1
       IF(J.GT.NP1.AND.J.LT.NP2.OR.J.GT.NP3)SIGN=-1
       IF(J1.GT.NP1.AND.J1.LT.NP2.OR.J1.GT.NP3)SIGN1=-1
       IF(J.GT.NP2)SIGN3=-1
       IF(J1.GT.NP2)SIGN31=-1
       CAP(1)=CAP(1)+W(J)*4.+W(J1)*2.
       CAP(2)=CAP(2)-WDL(J)*4.-WDL(J1)*2.
       CAP(3)=CAP(3)+WDV(J)*4.+WDV(J1)*2.
       CAP(4)=CAP(4)+WDCX(J)*4.+WDCX(J1)*2.
       CAP(5)=CAP(5)+WDCY(J)*4.+WDCY(J1)*2.
       CAP(6)=CAP(6)+WDCXT(J)*4.+WDCXT(J1)*2.
       CAP(7)=CAP(7)+WDCYT(J)*4.+WDCYT(J1)*2.
       CAP(8)=CAP(8)-MDL(J)*CT1*4.-MDL(J1)*CT2*2.
       CAP(9)=CAP(9)+MDL(J)*ST1*4.+MDL(J1)*ST2*2.
       CAP(10)=CAP(10)+MDV(J)*CT1*4.+MDV(J1)*CT2*2.
       CAP(11)=CAP(11)-MDV(J)*ST1*4.-MDV(J1)*ST2*2.
       CAP(12)=CAP(12)+MDCX(J)*CT1*4.+MDCX(J1)*CT2*2.
       CAP(13)=CAP(13)-MDCX(J)*ST1*4.-MDCX(J1)*ST2*2.
       CAP(14)=CAP(14)+MDCY(J)*CT1*4.+MDCY(J1)*CT2*2.
       CAP(15)=CAP(15)-MDCY(J)*ST1*4.-MDCY(J1)*ST2*2.
       CAP(16)=CAP(16)+MDCXT(J)*CT1*4.+MDCXT(J1)*CT2*2.
       CAP(17)=CAP(17)-MDCXT(J)*ST1*4.-MDCXT(J1)*ST2*2.
```

```
      CAP(18)=CAP(18)+MDCYT(J)*CT1*4.+MDCYT(J1)*CT2*2.
      CAP(19)=CAP(19)-MDCYT(J)*ST1*4.-MDCYT(J1)*ST2*2.
   83 CONTINUE
      DO 85 I=1,19
   85   CAP(I)=CAP(I)*THINT/3.
      WRITE(3,191)(JCAV(I),JEND(I),I=1,10)
  191 FORMAT(2I10)
      RETURN
      END
      SUBROUTINE INTGEN
     1 (R,I,RINT,AINT1,AINT2,AINT3,DI1DL,DI2DL,DI3DL,
     2  DI1DCX,DI2DCX,DI3DCX,DI1DCY,DI2DCY,DI3DCY,CLCOS,CLCOST,CLCOS3,
     3  CT,ST,CI,CI2,CI3)
C
C  ***************************************************
C  *                                                 *
C  *     THIS SUBROUTINE CALCULATES THE INTEGRALS    *
C  *     AND THEIR DERIVATIVES FOR THE GENERAL CASE  *
C  *                                                 *
C  ***************************************************
C
C
C    CALCULATE LOCAL RADIUS AND FILM THICKNESS
C
      RAD=R+(I-1)*RINT
      H=CLCOS-RAD*CI
      H2=H*H
      H3=H2*H
C
C    CALCULATE INTEGRALS AND DERIVATIVES
C
      AINT1=(-1./H+CLCOS/(2.*H2))/CI2
      DI1DL=(2./(2.*H2)-CLCOS/H3)/CI2
```

```
      DI1DCY=CT*((RAD/H2-RAD*CLCOS/H3)/CI2+AINT1*3./CI)
      AINT3=-(ALOG(ABS(H))+2.*CLCOS/H-CLCOS2/(H2*2.))/CI3
      DI2DL=-(3./H-3.*CLCOS/H2+CLCOS2/H3)/CI3
      DI2DCX=ST*((RAD/H-3.*RAD*CLCOS/H2+RAD*CLCOS2/H3)/CI3
     1 -3.*AINT2/CI)
      DI2DCY=-CT*((RAD/H-3.*RAD*CLCOS/H2+RAD*CLCOS2/H3)/CI3
     1  -3.*AINT2/CI)
      AINT3=-(ALOG(ABS(H/RAD))-2.*RAD*CI/H-(RAD**2)*CI2/(2.*H2))
     1  /CLCOS3
      DI3DL=-AINT3*3./CLCOS+(1./H+3.*RAD*CI/H2
     1  +(RAD**2)*CI2/H3)/CLCOS3
      DI3DCX=RAD*ST*(3./H+3.*RAD*CI/H2+(RAD**2)*CI2/H3)
     1  /CLCOS5
      DI3DCY=-RAD*CT*(3./H+3.*RAD*CI/H2
     1 +(RAD**2)*CI2/H3)/CLCOS3
      RETURN
      END
      SUBROUTINE INTSPC
     1 (R,I,RINT,AINT1,AINT2,AINT3,DI1DL,DI2DL,DI3DL,CT,ST,
     2  DI1DCX,DI2DCX,DI3DCX,DI1DCY,DI2DCY,DI3DCY,CLCOS,CLCOS2,CLCOS3)
C
C  ***************************************************
C  *                                                 *
C  *     THIS SUBROUTINE CALCULATES THE  INTEGRALS   *
C  *     AND THEIR DERIVATIVES FOR THE SPECIAL CASE  *
C  *               WHERE H=CL+COS(ANG) ONLY          *
C  *                                                 *
C  ***************************************************
C
C
C    CALCULATE LOCAL RADIUS
C
       RAD=R+(I-1)*RINT
C
C    CALCULATE INTEGRALS AND REMAINING DERIVATIVES
C
       AINT1=(RAD**2)/(CLCOS3*2.)
       DI1DL=-3.*AINT1/CLCOS
       DI1DCX=-DI1DL*ST*RAD
       DI1DCY=DI1DL*CT*RAD
       AINT2=(RAD**3)/(CLCOS3*3.)
       DI2DL=-3.*AINT2/CLCOS
       DI2DCX=-DI2DL*ST*RAD
       DI2DCY=DI2DL*CT*RAD
       AINT3=ALOG(RAD)/CLCOS3
       DI3DL=-3.*AINT3/CLCOS
       DI3DCX=-DI3DL*ST*RAD
       DI3DCY=DI3DL*CT*RAD
       RETURN
       END
       SUBROUTINE LEKALC
      1  (NP,NP2,PI,PO,GL,RINT,THINT,CLX,CIX,CIY,HAMP,NW,
      2ITINST,NT,FLMTHK,IFACON,TINT,FILM,TDF,OMEGA)
       COMMON JCAV(40),JENP(40)
       DIMENSION FLMTHK(2,NP),GL(NT)
C
C  ***************************************************
C  *                                                 *
C  *  THIS SUBROUTINE CALCULATES THE SEAL LEAKAGE    *
C  *   BASED ON THE FLOW THROUGH A CONVERGING OR     *
C  *   DIVERGING SLOT WITH TAPERED CROSS SECTION     *
C
```

```
C    *                                                    *
C    *     THE CALCULATIONS  ARE  CARRIED OUT FOR         *
C    *     THE PORTION OT THE CIRCUMFERENCE LYING         *
C    *              BETWEEN  THE  CAVITIES                *
C    *                                                    *
C    ******************************************************
C
C
C    CALCULATE THE FILM THICKNES  AT THE SEAL EDGES
C
       CL=FILM-CLX
       DO 1 J=1,NP
       THETA=(J-1)*THINT
       FLMTHK(1,J)=CL+HAMP*COS(NW*THETA+IFACOM*(ITIMST-1)
      1  *TINT*OMEGA*TDF)+R*CIY*COS(THETA)-R*CIX*SIN(THETA)
     1 FLMTHK(2,J)=CL+HAMP*COS(NW*THETA+IFACOM*(ITIMST-1)
      1  *TINT*OMEGA*TDF)+CIY*COS(THETA)-CIX*SIN(THETA)
       QOU=0.
C
C    CALCULATE THE LEAKAGE ACROSS THE SEAL BETWEEN EACH CAVITY
C
       DO 6 I=1,48
        IF(JEND(I).EQ.0)GO TO 7
        JEND1=JEND(I)
        JCAV1=JCAV(I)+1
       IF(JEND1-JCAV1)5,6,2
     2 JQ2=JEND1
       JQ3=NP
     3 DO 4 J=JQ2,JQ3
       JQ1=J+1
       IF(J.EQ.NP)JQ1=1
       HH=(FLMTHK(1,J)+FLMTHK(1,JQ1))/(FLMTHK(2,J)+FLMTHK(2,JQ1))
       AA=(FLMTHK(1,J)+FLMTHK(1,JQ1)-R*(FLMTHK(2,J)+FLMTHK(2,JQ1)))
      1/((1.-R)*2.)
       B=(HH-1.)*(1.-R/HH)/(1.-R)
       CC=B*(2.+B*(1.+R/HH)/(2.*(1.-R/HH)))
       FAC1=CC+ALOG(HH/R)
       QOU=QOU+(PI-PO)*(AA**2)/FAC1
     4 CONTINUE
       IF(JQ3.EQ.JCAV1)GO TO 6
       JQ2=1
       JQ3=JCAV1
       GO TO 3
     5 JQ2=JEND1
       JQ3=JCAV1
       GO TO 3
     6 CONTINUE
     7 CONTINUE
       QL(ITIMST)=QOU*THINT
       RETURN
       END
       SUBROUTINE DIMOUT
      1 (PRESS,CAP,QL,MP,NP,NT,ITIMST,QLO,CAPO,ALOAD,ALO)
       DIMENSION PRESS(MP,NP),CAP(19),QL(NT),
      1 CAPO(19)
C    ******************************************************
C    *                                                    *
C    *       THIS SUBROUTINE DIMENSIONALISES THE          *
C    *    RESULTS FOR THE REYNOLDS EQUATION SOLUTION      *
C    *                                                    *
C    ******************************************************
C
       COMMON/DIMEN1/FORCND,PRESND,QLND,AMASND,AINND
       COMMON/DIMEN2/SFMDLF,DMNDLF,SFNDRF,DMNDRF,SFNDRM,DMNDRM
C
C    DIMENSIONALISE THE PRESSURES
```

```
C
      DO 8 J=1,NP
       DO 9 I=1,MP
        PRESS(I,J)=PRESS(I,J)*PRESND
    8 CONTINUE
C
C     WRITE THE LOAD AND LEAKAGE FOR THIS TIMESTEP TO
C     WORKING VARIABLES AND DIMENSIONALISE
C
      QLO=QL(ITIMST)*QLND
C
C     WRITE THE FILM ELEMENTS TO A WORKING ARRAY
C     AND DIMENSIONALISE
C
      CAPO(1)=CAP(1)*FORCND
      CAPO(2)=CAP(2)*SFNDLF
      CAPO(3)=CAP(3)*DMNDLF
      CAPO(4)=CAP(4)*SFNDRF
      CAPO(5)=CAP(5)*SFNDRF
      CAPO(6)=CAP(6)*DMNDRF
      CAPO(7)=CAP(7)*DMNDRF
      CAPO(8)=CAP(8)*SFNDRF
      CAPO(9)=CAP(9)*SFNDRF
      CAPO(10)=CAP(10)*DMNDRF
      CAPO(11)=CAP(11)*DMNDRF
      CAPO(12)=CAP(12)*SFNDRM
      CAPO(13)=CAP(13)*SFNDRM
      CAPO(14)=CAP(14)*SFNDRM
      CAPO(15)=CAP(15)*SFNDRM
      CAPO(16)=CAP(16)*DMNDRM
      CAPO(17)=CAP(17)*DMNDRM
      CAPO(18)=CAP(18)*DMNDRM
      CAPO(19)=CAP(19)*DMNDRM
      RETURN
      END
      SUBROUTINE OUTLUB
     1 (PRESS,CAPO,QLO,MP,NP,NT,ITIMST,IPRT)
C
C     ***********************************************
C     *                                             *
C     *      THIS SUBROUTINE OUTPUTS THE PRESSURE   *
C     *    FIELD AND FLUID FILM STIFFNESS DAMPING   *
C     *             COEFFICIENT AND LEAKAGE         *
C     *                                             *
C     ***********************************************
C
      LOGICAL LOG
      DIMENSION CAPO(19),PRESS(MP,NP),IVAL(16)
  101 FORMAT(///10X,14H OUTPUT  TABLE,I4,20H    REYNOLDS EQUATION,
     1 20H RESULTS AT TIMESTEP,I5/11X,17(1H-)///)
  107 FORMAT(///10X,20H FLUID FILM ELEMENTS//
     1 10X,20H TOTAL LOAD CAPACITY,F17.6,5X,2H N///
     2 24X,8H ELEMENT,16X,16H STIFFNESS (N/M),12H    DAMPING (NS/M)//
     3 10X,7H AXIAL DUE Z                    (CAP(2/3)),2E17.6/
     4 10X,7H   --    DUE CHIX               (CAP(4/6)),2E17.6/
     5 10X,7H   --    DUE CHIY               (CAP(5/7)),2E17.6//
     6 10X,3H ABOUT AXIS OX DUE Z            (CAP(8/11)),2E17.6/
     7 10X,7H   --     --  -- DUE CHIX       (CAP(10/17)),2E17.6/
     8 10X,7H   --     --  -- DUE CHIY       (CAP(15/19)),2E17.6//
     9 10X,3H ABOUT AXIS OY DUE Z            (CAP(9/13)),2E17.6/
     X 10X,7H   --     --  -- DUE CHIX       (CAP(12/16)),2E17.6/
     1 10X,7H   --     --  -- DUE CHIY       (CAP(14/18)),2E17.6//)
  103 FORMAT(/11X,2E20.6,11X,E20.6,9X,E20.4)
  104 FORMAT(///10X,15(I3,4X)///)
  105 FORMAT(///10X,25H LEAKAGE RATE AT TIMESTEP,I5,5H   IS,E20.9,
     1 5H  ML/MIN//)
```

```
 110 FORMAT(5(/),31X,25H PRESSURE FIELD (KN/SQ.M)/
    132X,24(1H-)///50X,9H I VALUES)
 111 FORMAT(I5,2X,-3P15F7.0)
 112 FORMAT(2H J,I3,2X,-3P15F7.0)
 114 FORMAT(2H V,I3,2X,-3P15F7.0)
 115 FORMAT(2H A,I3,2X,-3P15F7.0)
 116 FORMAT(2H L,I3,2X,-3P15F7.0)
 117 FORMAT(2H U,I3,2X,-3P15F7.0)
 118 FORMAT(2H E,I3,2X,-3P15F7.0)
 119 FORMAT(2H S,I3,2X,-3P15F7.0)
     IPRT=IPRT+1
     WRITE(6,101)IPRT,ITIMST
     WRITE(6,107)CAPO(1),CAPO(3),CAPO(7),CAPO(4),CAPO(6),CAPO(5),
    1 CAPO(7),CAPO(9),CAPO(11),CAPO(13),CAPO(17),CAPO(15),CAPO(19),
    2  CAPO(8),CAPO(10),CAPO(12),CAPO(16),CAPO(14),CAPO(18)
       WRITE(6,105)ITIMST,QLO
     I1=1
     I2=NP
     JV1=(NP/2)-3
     JV2=(NP/2)+4
     WRITE(6,110)
     DO 22 I=I1,I2
  22  IVAL(I)=I
     WRITE(6,104)(IVAL(I),I=I1,I2)
     DO 15 J=1,NP
     IF(J.LT.JV1.OR.J.GT.JV2)GO TO 15
     JV=J-JV1+1
     GO TO(7,15,8,9,10,11,12,14),JV
   7 WRITE(6,112)J,(PRESS(I,J),I=I1,I2)
     GO TO 15
   8 WRITE(6,114)J,(PRESS(I,J),I=I1,I2)
     GO TO 15
   9 WRITE(6,115)J,(PRESS(I,J),I=I1,I2)
     GO TO 15
  10 WRITE(6,116)J,(PRESS(I,J),I=I1,I2)
     GO TO 15
  11 WRITE(6,117)J,(PRESS(I,J),I=I1,I2)
     GO TO 15
  12 WRITE(6,118)J,(PRESS(I,J),I=I1,I2)
     GO TO 15
  14 WRITE(6,119)J,(PRESS(I,J),I=I1,I2)
     GO TO 15
  15 WRITE(6,111)J,(PRESS(I,J),I=I1,I2)
  15 CONTINUE
     RETURN
     END
    FINISH
```

BHRA SEAL VISC FOR 37 C

OUTPUT TABLE 1 REYNOLDS EQUATION RESULTS AT TIMESTEP 1

FLUID FILM ELEMENTS

TOTAL LOAD CAPACITY 0.198654E 03 N

ELEMENT		STIFFNESS (N/M)	DAMPING (NS/M)
AXIAL DUE Z	(CAP(2/3))	0.561414E 09	0.379169E 07
.. DUE CHIX	(CAP(4/6))	0.376584E 10	-0.125744E 05
.. DUE CHIY	(CAP(5/7))	-0.111465E 08	-0.139930E 05
ABOUT AXIS OX DUE Z	(CAP(9/11))	-0.193576E 06	-0.708456E 03
.. .. .. DUE CHIX	(CAP(13/17))	-0.334574E 08	-0.918637E 03
.. .. .. DUE CHIY	(CAP(15/19))	-0.107777E 05	0.302251E 03
ABOUT AXIS OY DUE Z	(CAP(8/10))	-0.925312E 05	-0.639350E 03
.. .. .. DUE CHIX	(CAP(12/16))	0.429591E 08	-0.165835E 03
.. .. .. DUE CHIY	(CAP(14/18))	-0.310437E 06	-0.137469E 04

LEAKAGE RATE AT TIMESTEP 1 IS 0.640633666E 01 ML/MIN

PRESSURE FIELD (KN/SQ.M)

I VALUES

J	1	2	3	4	5	6	7	8	9	10	11	12	13	14	15
1	0.	-1.	-1.	-1.	-1.	-1.	-1.	-1.	-1.	-1.	-1.	-1.	-1.	-1.	500.
2	0.	-1.	-1.	-1.	-1.	-1.	-1.	-1.	-1.	-1.	-1.	-1.	-1.	-1.	500.
3	0.	-1.	-1.	-1.	-1.	-1.	-1.	-1.	-1.	-1.	-1.	-1.	-1.	-1.	500.
4	0.	-1.	-1.	-1.	-1.	-1.	-1.	-1.	-1.	-1.	-1.	-1.	-1.	-1.	500.
5	0.	-1.	-1.	-1.	-1.	-1.	-1.	-1.	-1.	-1.	-1.	-1.	-1.	-1.	500.
6	0.	-1.	-1.	-1.	-1.	-1.	-1.	-1.	-1.	-1.	-1.	-1.	-1.	-1.	500.
7	0.	1837.	3368.	4654.	5639.	6346.	6775.	6930.	6812.	6424.	5768.	4845.	3653.	2209.	500.
8	0.	1379.	1379.	3448.	4482.	4827.	4137.	4137.	4482.	4482.	3792.	3103.	2413.	2413.	500.
9	0.	172.	259.	215.	302.	302.	302.	388.	302.	431.	345.	345.	474.	474.	500.
10	0.	-1.	-1.	-1.	-1.	-1.	-1.	-1.	-1.	-1.	-1.	-1.	-1.	-1.	500.
11	0.	-1.	-1.	-1.	-1.	-1.	-1.	-1.	-1.	-1.	-1.	-1.	-1.	-1.	500.
12	0.	-1.	-1.	-1.	-1.	-1.	-1.	-1.	-1.	-1.	-1.	-1.	-1.	-1.	500.
13	0.	-1.	-1.	-1.	-1.	-1.	-1.	-1.	-1.	-1.	-1.	-1.	-1.	-1.	500.
14	0.	-1.	-1.	-1.	-1.	-1.	-1.	-1.	-1.	-1.	-1.	-1.	-1.	-1.	500.
15	0.	-1.	-1.	-1.	-1.	-1.	-1.	-1.	-1.	-1.	-1.	-1.	-1.	-1.	500.
16	0.	-1.	-1.	-1.	-1.	-1.	-1.	-1.	-1.	-1.	-1.	-1.	-1.	-1.	500.
17	0.	-1.	-1.	-1.	-1.	-1.	-1.	-1.	-1.	-1.	-1.	-1.	-1.	-1.	500.
18	0.	-1.	-1.	-1.	-1.	-1.	-1.	-1.	-1.	-1.	-1.	-1.	-1.	-1.	500.
19	0.	-1.	-1.	-1.	-1.	-1.	-1.	-1.	-1.	-1.	-1.	-1.	-1.	-1.	500.
20	0.	-1.	-1.	-1.	-1.	-1.	-1.	-1.	-1.	-1.	-1.	-1.	-1.	-1.	500.
21	0.	-1.	-1.	-1.	-1.	-1.	-1.	-1.	-1.	-1.	-1.	-1.	-1.	-1.	500.

	22	0.	-1.	-1.	-1.	-1.	-1.	-1.	-1.	-1.	-1.	-1.	-1.	-1.	-1.	500.
V	23	0.	1838.	3388.	4655.	5641.	6347.	6777.	6932.	6814.	6427.	5771.	4847.	3660.	2210.	500.
A	24	0.	1203.	2218.	3049.	3697.	4159.	4460.	4573.	4508.	4271.	3859.	3273.	2520.	1595.	500.
L	25	0.	16.	33.	63.	92.	124.	152.	189.	226.	265.	307.	356.	404.	450.	500.
U	26	0.	-1.	-1.	-1.	-1.	-1.	-1.	-1.	-1.	-1.	-1.	-1.	-1.	-1.	500.
E	27	0.	-1.	-1.	-1.	-1.	-1.	-1.	-1.	-1.	-1.	-1.	-1.	-1.	-1.	500.
S	28	0.	-1.	-1.	-1.	-1.	-1.	-1.	-1.	-1.	-1.	-1.	-1.	-1.	-1.	500.
	29	0.	-1.	-1.	-1.	-1.	-1.	-1.	-1.	-1.	-1.	-1.	-1.	-1.	-1.	500.
	30	0.	-1.	-1.	-1.	-1.	-1.	-1.	-1.	-1.	-1.	-1.	-1.	-1.	-1.	500.
	31	0.	-1.	-1.	-1.	-1.	-1.	-1.	-1.	-1.	-1.	-1.	-1.	-1.	-1.	500.
	32	0.	-1.	-1.	-1.	-1.	-1.	-1.	-1.	-1.	-1.	-1.	-1.	-1.	-1.	500.
	33	0.	-1.	-1.	-1.	-1.	-1.	-1.	-1.	-1.	-1.	-1.	-1.	-1.	-1.	500.
	34	0.	-1.	-1.	-1.	-1.	-1.	-1.	-1.	-1.	-1.	-1.	-1.	-1.	-1.	500.
	35	0.	-1.	-1.	-1.	-1.	-1.	-1.	-1.	-1.	-1.	-1.	-1.	-1.	-1.	500.
	36	0.	-1.	-1.	-1.	-1.	-1.	-1.	-1.	-1.	-1.	-1.	-1.	-1.	-1.	500.
	37	0.	-1.	-1.	-1.	-1.	-1.	-1.	-1.	-1.	-1.	-1.	-1.	-1.	-1.	500.
	38	0.	-1.	-1.	-1.	-1.	-1.	-1.	-1.	-1.	-1.	-1.	-1.	-1.	-1.	500.
	39	0.	1782.	3282.	4510.	5465.	6149.	6565.	6713.	6600.	6225.	5593.	4700.	3554.	2152.	500.
	40	0.	1167.	2154.	2962.	3594.	4050.	4332.	4442.	4381.	4150.	3751.	3185.	2453.	1558.	500.
	41	0.	31.	63.	95.	130.	163.	198.	234.	270.	306.	344.	382.	421.	460.	500.
	42	0.	-1.	-1.	-1.	-1.	-1.	-1.	-1.	-1.	-1.	-1.	-1.	-1.	-1.	500.
	43	0.	-1.	-1.	-1.	-1.	-1.	-1.	-1.	-1.	-1.	-1.	-1.	-1.	-1.	500.
	44	0.	-1.	-1.	-1.	-1.	-1.	-1.	-1.	-1.	-1.	-1.	-1.	-1.	-1.	500.
	45	0.	-1.	-1.	-1.	-1.	-1.	-1.	-1.	-1.	-1.	-1.	-1.	-1.	-1.	500.
	46	0.	-1.	-1.	-1.	-1.	-1.	-1.	-1.	-1.	-1.	-1.	-1.	-1.	-1.	500.
	47	0.	-1.	-1.	-1.	-1.	-1.	-1.	-1.	-1.	-1.	-1.	-1.	-1.	-1.	500.
	48	0.	-1.	-1.	-1.	-1.	-1.	-1.	-1.	-1.	-1.	-1.	-1.	-1.	-1.	500.

APPENDIX E

EQUATIONS OF MOTION COMPUTER PROGRAM FLOW DIAGRAM AND TYPICAL RESULTS

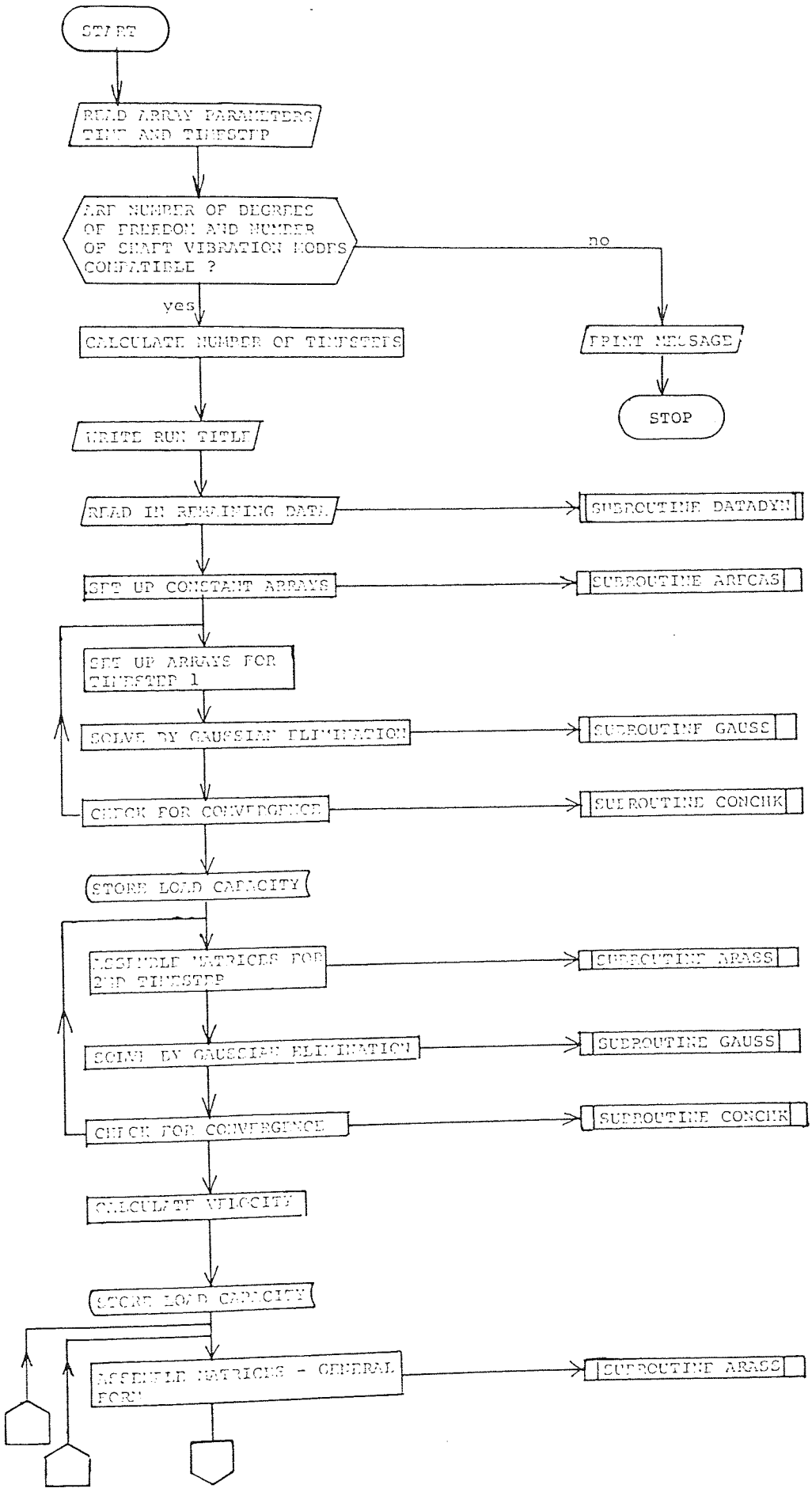

Equations of Motion Program Main Structure (1)

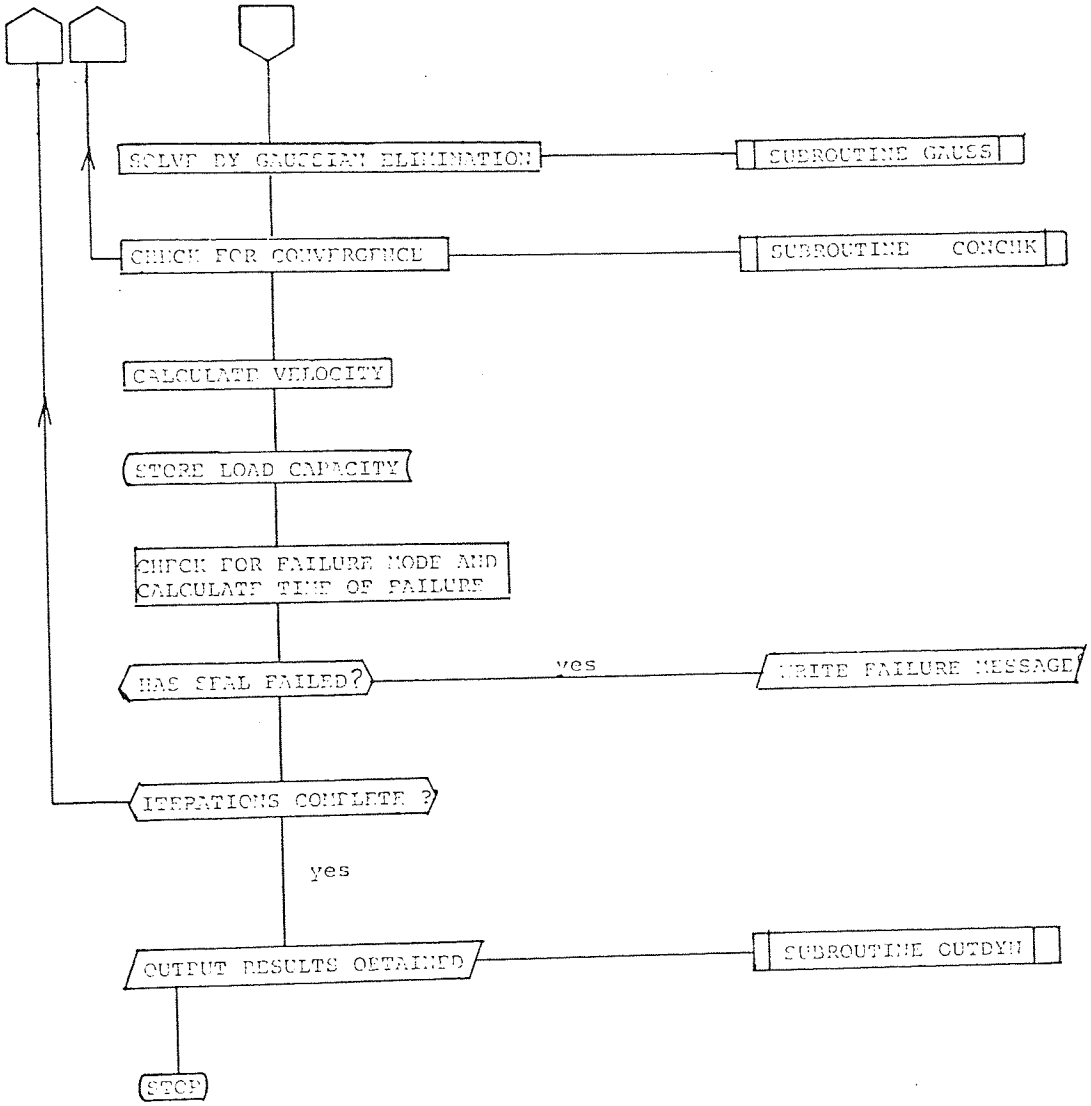

Equations of Motion Program Main Structure (2)

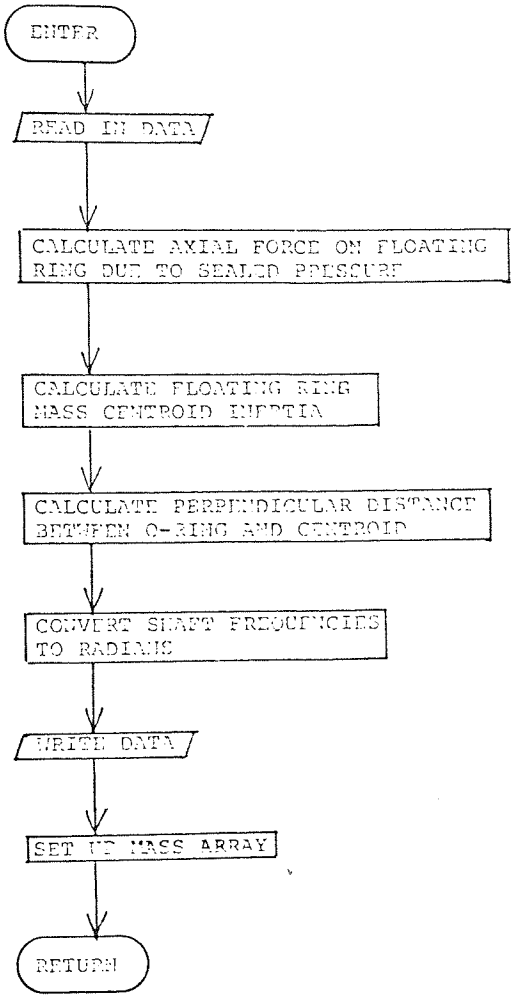

Subroutine Datadyn

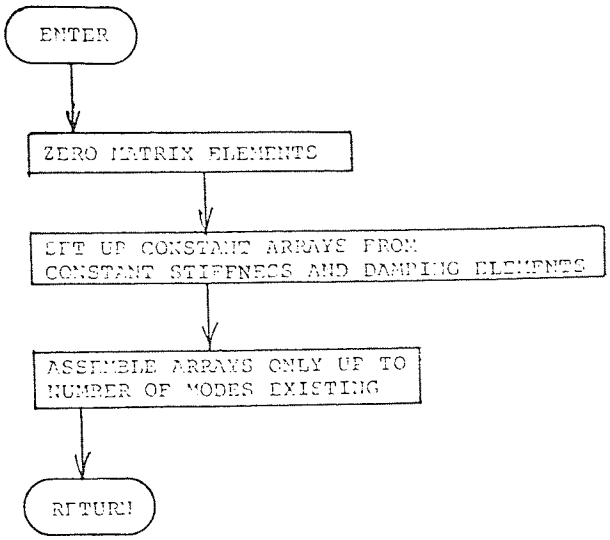

Subroutine Arfcas

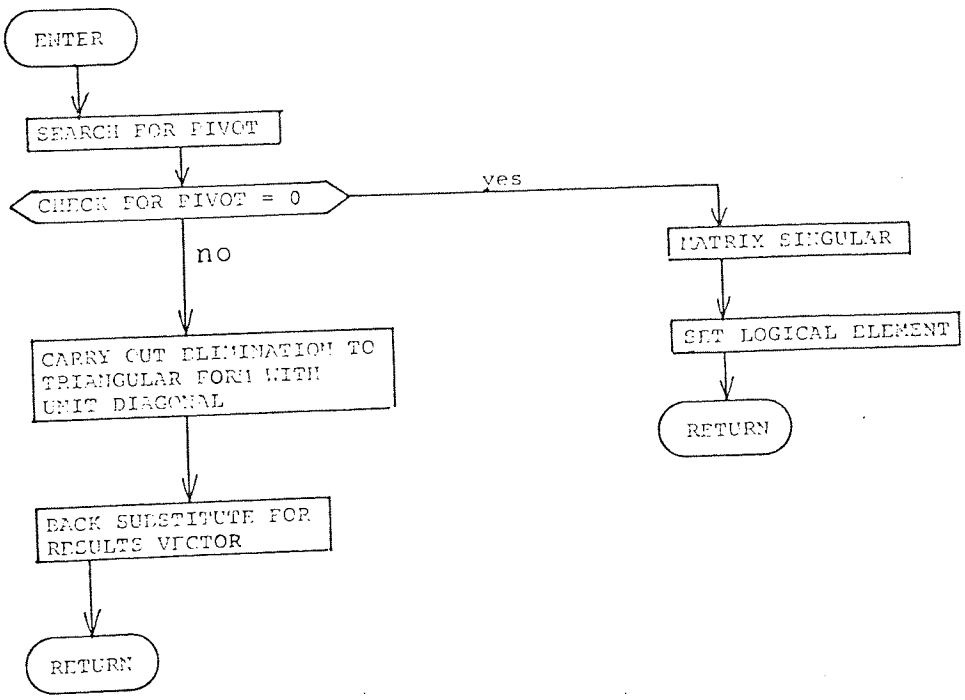

Subroutine Gauss

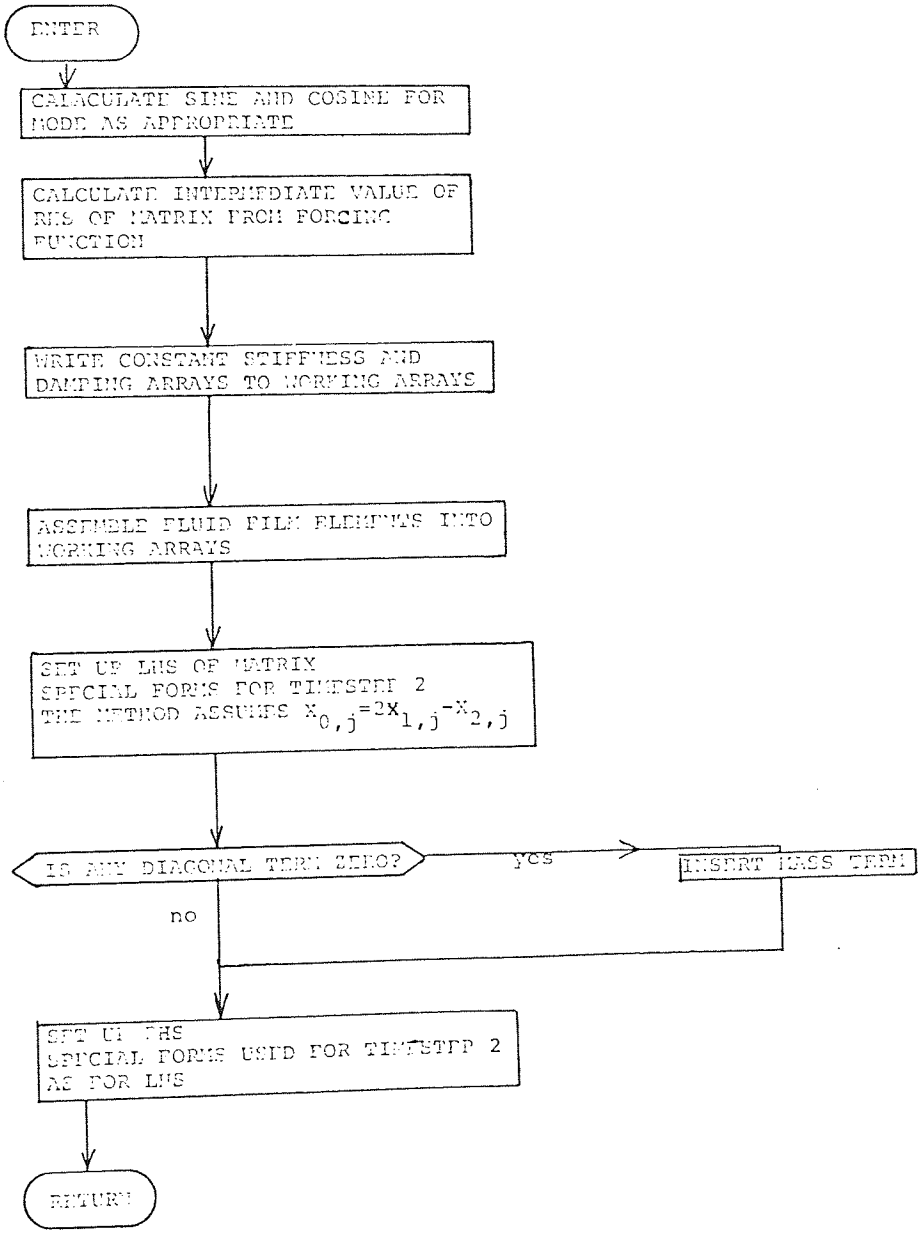

Subroutine Arass

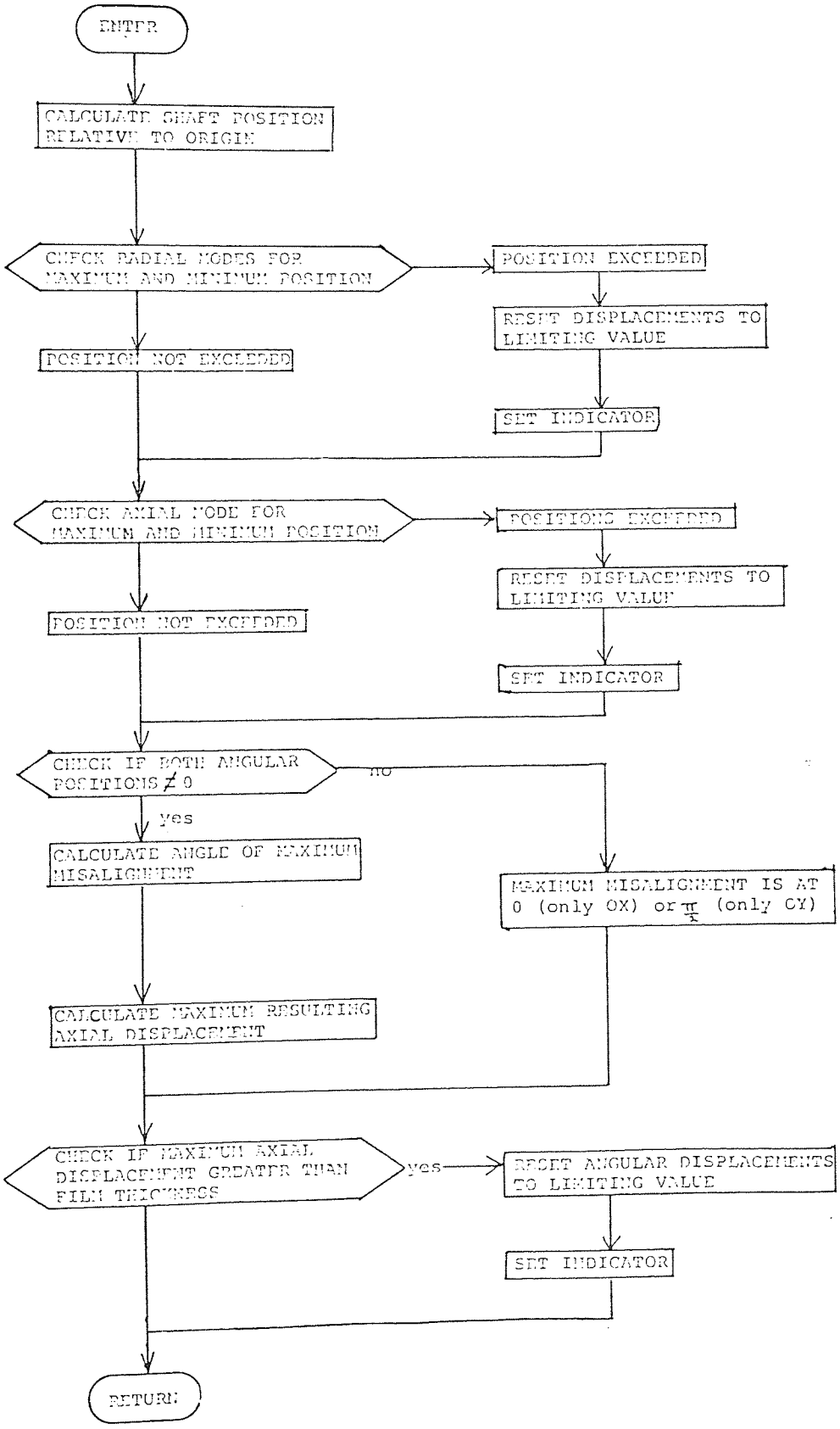

Subroutine Conchk

```
      LIST
      PROGRAM(FXXX)
      INPUT  1 = CR0
      INPUT  3 = CR2
      INPUT  5 = CR1
      OUTPUT 2 = LP0
      OUTPUT 6 = LP1
      OUTPUT 7 = LP7
      OUTPUT 8 = LP6
      COMPRESS INTEGER AND LOGICAL
      EXTENDED DATA
      COMPACT PROGRAM
      TRACE 2
      END
      TRACE 0
      MASTER DYMEC
C     ******************************
C     *                            *
C     *  THIS PROGRAM CALCULATES   *
C     *                            *
C     *  THE DYNAMIC PERFORMANCE   *
C     *                            *
C     *   OF A MECHANICAL  SEAL    *
C     *                            *
C     ******************************
C
      DIMENSION PRESS(15,40),FLMTHK(2,48),GL(500),
     1XO(500,5),DXODT(500,5),ALOAD(500),TITLE(10),AMAS(5),
     2 STIFF(5,5),DAMP(5,5),RHS(5),ALHS(5,5),XOX(5),SHAFT(3,3),
     3AP(5,4),PEA(5),S(5,5),C(5,5)
     4,RRO(10),RRI(10),AMA(10),EL(10)
C
C     ARRAYS ARE DYNAMICALLY DIMENSIONED
C
  100 FORMAT(//10X,39(1H*)/10X,1H*,37X,1H*/10X,1H*,6X,
     1 25H PROGRAM EXECUTION HALTED,6X,1H*/10X,1H*,6X,
     2 6H NM  =,I3,6X,6H MM  =,I3,7X,1H*/10X,1H*,2X,
     3 32H THESE VALUES ARE NOT COMPATIBLE,3X,1H*/10X,1H*,7X,
     4 31H IF MM IS LESS THAN 4,9X,1H*/10X,1H*,10X,
     5 17H NM MUST EQUAL MM,10X,1H*/10X,1H*,27X,1H*/10X,39(1H*))
  101 FORMAT(5I5)
  102 FORMAT(10A8)
  103 FORMAT(F10.5,E20.6)
      READ(5,101)MP,NP,MM,NM,NI
      READ(5,102)TITLE
      READ(5,103)TIME,TINT
      IF(NM.EQ.MM.OR.MM.GE.4)GO TO 5
       WRITE(6,100)NM,MM
       GO TO 10
    5 NT=INT(TIME/TINT)+1
      WRITE(6,102)TITLE
      CALL CALCOND2
     1(MP,NP,NT,PRESS,FLMTHK,XO,DXODT,ALOAD,SHAFT
     1,AMAS,STIFF,DAMP,RHS,ALHS,XOX,MM,NM,TIME,TINT,
     2AP,PEA,S,C,RRO,RRI,AMA,EL,NI,GL)
   10 CONTINUE
      STOP
      END
      SUBROUTINE CALCOND2
     1(MP,NP,NT,PRESS,FLMTHK,XO,DXODT,ALOAD,SHAFT
     1,AMAS,STIFF,DAMP,RHS,ALHS,XOX,MM,NM,TIME,TINT,
     2AP,PEA,S,C,RRO,RRI,AMA,EL,NI,GL)
```

```
C   ****************************************
C   *                                      *
C   *      THIS  SUBROUTINE   CONTROLS     *
C   *                                      *
C   *    THE RUNNING OF THE CALCULATIONS   *
C   *                                      *
C   ****************************************
      LOGICAL LOG2,LOCCHK
      DIMENSION PRESS(MP,NP),FILMTHK(2,NP),CL(NT),DXODT(NT,MM),
     1XO(NT,MM),AMAS(MM),STIFF(MM,MM),DAMP(MM,MM),
     1AP(MM,4),PEA(MM),S(MM,MM),C(MM,MM),SHAFT(NM,2),XOX(MM),
     2ALOAD(NT),CAP(19),PHS(MM),ALHS(MM,MM),NC(7),N(7),
     3 RRO(NI),RRI(NI),AMA(NI),EL(NI),X1(3),A(3,3),B(3)
  105 FORMAT(///27H NOT CONVERGED AT TIMESTEP ,I5)
  106 FORMAT(///10X,34H MATRIX NOT INVERTIBLE AT TIMESTEP,I5,5X,
     1 32H XO SET TO LAST TIMESTEPS VALUES/)
  110 FORMAT(///10X,54(1H*)/,10X,1H*,52X,1H*/
     110X,20H*  SEAL FAILED AFTER,F10.6,24H  SECONDS (ITERATION   */
     210X,1H*,3X,6HNUMBER,I5,32H  ) DUE TO TOUCHING SHAFT (AXIS OX)   */
     310X,1H*,52X,1H*/10X,54(1H*)///)
  112 FORMAT(///10X,54(1H*)/,10X,1H*,52X,1H*/
     110X,20H*  SEAL FAILED AFTER,F10.6,24H  SECONDS (ITERATION   */
     210X,1H*,3X,6HNUMBER,I5,32H  ) DUE TO TOUCHING SHAFT (AXIS OY)   */
     310X,1H*,52X,1H*/10X,54(1H*)///)
  114 FORMAT(///10X,54(1H*)/,10X,1H*,52X,1H*/
     110X,20H*  SEAL FAILED AFTER,F10.6,24H  SECONDS (ITERATION   */
     210X,1H*,3X,6HNUMBER,I5,32H  ) DUE TO TOUCHING STATOR (AXIAL)    */
     310X,1H*,52X,1H*/10X,54(1H*)///)
  116 FORMAT(///10X,54(1H*)/,10X,1H*,52X,1H*/
     110X,20H*  SEAL FAILED AFTER,F10.6,24H  SECONDS (ITERATION   */
     210X,1H*,4X,6HNUMBER,I5,32H  )  DUE  TO  EXCESSIVE  LEAKAGE,5X,1H*/
     310X,1H*,52X,1H*/10X,54(1H*)///)
  118 FORMAT(///10X,54(1H*)/,10X,1H*,52X,1H*/
     110X,20H*  SEAL FAILED AFTER,F10.6,24H  SECONDS (ITERATION   */
     210X,1H*,3X,6HNUMBER,I5,32H  ) DUE TO TOUCHING STATOR (ROCKING)  */
     310X,1H*,52X,1H*/10X,54(1H*)///)

C
C     SET UP THE DATA
C
      CALL DATADYN
     1 (MM,NM,MP,NP,NT,SHAFT,STIFRC,STIFRS,STIFSP,DAMPRC,
     2DAMPRS,ROR,RS,DOR,AMAS,TINT,PFORCE,TIME,CAP,SPL,EL,
     3PI,PO,PCAV,RRO,RRI,AMA,NI,CLEAR,ITMAX,CHECK,HIN,XO,NCHECK)
      CALL AREAS
     1  (STIFRC,DAMPRC,STIFRS,DAMPRS,SHAFT,AMAS,TINT,
     2DOR,CAP,PFORCE,STIFF,DAMP,MM,AP,ROR,NM,STIFSP,RS)

C
C     CALCULATE INITIAL POSITION ITERATION 1 TIME ZERO
C
      ANDF=1
      ITIMST=1
      ITINIT=1
      FILM=HIN
    2 CONTINUE

C
C     SOLVE FOR EQUILIBRIUM POSITION AT TIMESTEP 1
C
      A(1,1)=STIFRS+STIFSP+CAP(2)
      A(1,2)=CAP(5)
      A(1,3)=CAP(4)
      A(2,1)=CAP(7)
      A(2,2)=STIFRS*(ROR**2)/2.+STIFSP*(RS**2)/2.+
     1       STIFRC*(DOR**2)+CAP(12)
      A(2,3)=CAP(14)
      A(3,1)=CAP(6)
      A(3,2)=CAP(13)
```

```
      A(3,3)=STIFRS*(ROR**2)/2.+STIFSP*(RS**2)/2.
     1       +STIFRC*(DOR**2)+CAP(15)
      B(1)=PFORCE-CAP(1)
      B(2)=STIFRC*DOR*XO(1,2)
      B(3)=STIFRC*DOR*XO(1,1)
      NG=3
      CALL GAUSS
     1  (NG,A,B,X1,LOG2)
      IF(.NOT.LOG2)GO TO 21
      WRITE(2,100)ITIMST
      GO TO 21
   20 FILM=FILM-X1(1)
      IF(MM.LT.4)GO TO 21
      XO(1,4)=X1(2)
      IF(MM.LT.5)GO TO 21
      XO(1,5)=X1(3)
   21 CONTINUE
      NCHK=-1
      CALL CONCHK
     1 (XO,CAP,HIN,HAMP,ITINIT,ITIMST,LOGCHK,MM,CLEAR,NCHK,NT,CHECK
     1 ,SHAFT,TINT,NM,NC)
      IF(LOGCHK)GO TO 22
      ITINIT=ITINIT+1
      IF(ITINIT.LE.ITMAX)GO TO 2
      WRITE(2,106)ITIMST
   22 ALOAD(1)=CAP(1)
C
C     CALCULATE THE STARTING VALUES ITERATION 2 TIME STEP 1
C
      ITIMST=2
      ITST=1
C
C     ASSEMBLE MATRIX COEFFICIENTS
C
   23  CALL ARASS
     1  (AMAS,STIFF,DAMP,PFORCE,RHS,ALHS,XO,NT,ANDF,
     2CAP,MM,ITIMST,TINT,SHAFT,AP,PEA,NM,S,C)
C
C     SOLVE THE EQUATIONS OF MOTION
C
      CALL GAUSS
     1  (S,ALHS,RHS,XOX,LOG3)
      IF(.NOT.LOG3)GO TO 30
      WRITE(2,105)ITIMST
      DO 29 I=1,MM
   29  XO(ITIMST,I)=XO(ITIMST-1,I)
      GO TO 33
   30 DO 31 I=1,MM
   31  XO(ITIMST,I)=XOX(I)
   33 NCHK=-1
      CALL CONCHK
     1 (XO,CAP,HIN,HAMP,ITINIT,ITIMST,LOGCHK,MM,CLEAR,NCHK,NT,CHECK
     1 ,SHAFT,TINT,NM,NC)
      IF(LOGCHK)GO TO 35
      DO 34 I=1,MM
   34  DXODT(2,I)=(XO(2,I)-XO(1,I))/TINT
      ITST=ITST+1
      IF(ITST.LE.ITMAX)GO TO 23
      WRITE(2,106)ITIMST
   35 ALOAD(2)=CAP(1)
C
C     CALCULATE THE LOAD AND POSITION FOR EACH TIME STEP
C
   36 ITIMST=ITIMST+1
C
      ITIM=1
```

```
C
C     ASSEMBLE MATRIX COEFFICIENTS
C
   37 CALL ARASS
     1   (AMAS,STIFF,DAMP,PFORCE,RHS,ALHS,XO,NT,ANDF,
     2CAP,MM,ITIMST,TINT,SHAFT,AP,PEA,NM,S,C)
C
C     SOLVE EQUATIONS OF MOTION
C
      CALL GAUSS
     1   (S,ALHS,RHS,XOX,LOGZ)
      IF(.NOT.LOGZ)GO TO 43
      WRITE(2,108)ITIMST
      DO 47 I=1,MM
   47  XO(ITIMST,I)=XO(ITIMST-1,I)
      GO TO 46
   43 DO 44 I=1,MM
   44   XO(ITIMST,I)=XOX(I)
   46 NCHK=-1
      CALL CONCHK
     1 (XO,CAP,HIN,DAMP,ITINIT,ITIMST,LOGCHK,MM,CLEAR,NCHK,NT,CHECK
     1 ,SHAFT,TINT,NM,NC)
      IF(LOGCHK)GO TO 59
      DO 50 I=1,MM
   50   DXODT(ITIMST,I)=(XO(ITIMST-2,I)-4.*XO(ITIMST-1,I)
     1                 +3.*XO(ITIMST,I))/(2.*TINT)
      ITIM=ITIM+1
      IF(ITIM.LE.ITMAX)GO TO 37
      WRITE(2,106)ITIMST
   59   ALOAD(ITIMST)=CAP(1)
C
C    CHECK FOR SEAL FAILURE DUE TO FLOATING RING
C    EXCEEDING OPERATING LIMITS
C
        DO 64 I=1,7
        N(I)=N(I)+NC(I)
   64 CONTINUE
      NFAIL=1
C
C    SET UP MODE OF FAILURE NFAIL=1 SUCCESSFUL OPERATION
C
        DO 69 I=1,7
        IF(N(I)-NCHECK)69,67,67
   67   NFAIL=I+1
        GO TO 70
   69 CONTINUE
   70 STPTIM=(ITIMST-1)*TINT
      GO TO(72,76,78,80,82,84,86),NFAIL
C
C    CHECK FOR MAXIMUM NUMBER OF ITERATIONS
C
   72 IF(ITIMST.GE.NT)GO TO 90
        ITIM=1
        GO TO 36
C
C    WRITE OUT FAILURE MODE
C
   76 WRITE(6,110)STPTIM,ITIMST
        GO TO 90
   80 WRITE(6,112)STPTIM,ITIMST
        GO TO 90
   82 WRITE(6,114)STPTIM,ITIMST
        GO TO 90
   84 WRITE(6,116)STPTIM,ITIMST
        GO TO 90
   86 WRITE(6,118)STPTIM,ITIMST
```

```
   90 CONTINUE
C
C     OUTPUT RESULTS
C
       DO 95 I=1,ITIMST
        XO(I,3)=XO(I,3)-FILM
   95 CONTINUE
       CALL OUTDYN
      1(ALOAD,NT,XO,DXODT,MM,GL,ITIMST,TIME,IPAT)
       RETURN
       END
       SUBROUTINE DATADYN
      1 (MM,NM,MP,NP,NT,SHAFT,STIFRC,STIFRS,STIFSP,DAMPRC,
      2DAMPRS,ROR,RS,DOR,AMAS,TINT,PFORCE,TIME,CAP,SPL,EL,
      3PI,PO,PCAV,RRO,RRI,AMA,NI,CLEAR,ITMAX,CHECK,HIN,XO,NCHECK)
C   ************************************************
C   *                                              *
C   *    THIS SUBROUTINE READS IN THE PROBLEM DATA *
C   *                                              *
C   ************************************************
       DIMENSION SHAFT(NM,3),CAP(19),RRO(NI),RRI(NI),AMA(NI),EL(NI)
      1 ,AMAS(MM),SHAFTI(3,3),XO(NT,MM)
  200 FORMAT(/24H ENTERED SUBROUTINE DATA)
  100 FORMAT(4E20.6)
  101 FORMAT(8F10.5)
  102 FORMAT(9I2)
  103 FORMAT(1H1/10X,43H INPUT  DATA  TABLE  1  -  ARRAY PARAMETERS/
     111X,21(1H-))
  104 FORMAT(//
     110X,50H NUMBER OF RIGID BODY DEGREES OF FREEDOM       (MM),2X,I3/
     210X,50H NUMBER OF INPUT VIBRATION DEGREES OF FREEDOM (NM),2X,I3/
     310X,50H MESH FOR REYNOLDS EQUATION CALCULATION     (MP*NP),2X,I3,
     41H*,I2/
     510X,50H NUMBER OF TIME STEPS                          (NT),I5/
     610X,50H NUMBER OF ITERATIONS IN EACH TIMESTEP      (ITMAX),2X,I3/
     X10X,50H THE SEAL IS DEEMED TO HAVE FAILED IF ANY         /
     110X,50H DISPLACEMENT IS SET TO THE SAME LIMITING VALUE IN,I5,
     231H  (NCHECK) SUCCESSIVE TIMESTEPS//)
  105 FORMAT(///10X,41H INPUT  DATA  TABLE  2  -  ELEMENT VALUES/
     111X,21(1H-)//10X,34H STIFFNESS IN N/M DAMPING IN N-S/M,
     110H LOAD IN N/)
  106 FORMAT(//10X,39H O-RING STIFFNESS  COMPRESSION (STIFRC),2X,E20.6/
     1          10X,39H    --      --   SHEAR       (STIFRS),2X,E20.6/
     2          10X,39H    --   DAMPING COMPRESSION (DAMPRC),2X,E20.6/
     3          10X,39H    --      --   SHEAR       (DAMPRS),2X,E20.6/
     4          10X,39H SPRING STIFFNESS            (STIFSP),2X,E20.6/)
  107 FORMAT(///10X,20H FLUID FILM ELEMENTS//
     110X,20H TOTAL LOAD CAPACITY,E17.6,5X,2H N///
     224X,8H ELEMENT,21X,16H STIFFNESS       ,17H   DAMPING        //
     310X,36H AXIAL DUE Z                    (CAP(3/3)),2E17.6/
     410X,36H   --    DUE CHIX               (CAP(4/6)),2E17.6/
     510X,36H   --    DUE CHIY               (CAP(5/7)),2E17.6//
     610X,36H ABOUT AXIS OX DUE Z           (CAP(8/11)),2E17.6/
     710X,36H   --     --  -- DUE CHIX      (CAP(12/17)),2E17.6/
     810X,36H   --     --  -- DUE CHIY      (CAP(18/19)),2E17.6//
     910X,36H ABOUT AXIS OY DUE Z           (CAP(9/10)),2E17.6/
     X10X,36H   --     --  -- DUE CHIX      (CAP(13/16)),2E17.6/
     110X,36H   --     --  -- DUE CHIY      (CAP(14/15)),2E17.6/)
  109 FORMAT(///10X,42H INPUT  DATA  TABLE  3  -  INPUT VIBRATION/
     111X,21(1H-)
     3//10X,15H SHAFT VIBRATION//
     410X,5H AXIS,6X,10H AMPLITUDE,8X,10H FREQUENCY,6X,
     5 15H PHASE ANGLE/33X,4H (M),16X,5H (HZ),12X,6H TO OX/
     610X,2H OX,3E19.6/10X,2H OY,3E19.6/10X,5H OZ,3E19.6/)
  110 FORMAT(//10X,
     1    45H RADIUS OF LINE OF ACTION OF O-RING       (ROR),2X,F10.5/
```

```
     51OX,45H DISTANCE BETWEEN O-RING AND INTERFACE  (DORI),2X,F10.5/ .
     41OX,46H PERPENDICULAR DISTANCE O-RING TO C OF G (DOR),2X,F10.5/
     51OX,46H O-RING GROOVE RADIUS                    (RG),2X,F10.5/
     61OX,46H RADIUS OF LINE OF ACTION OF SPRING      (RS),2X,F10.5/
     71OX,46H INITIAL COMPRESSION  OF SPRING         (SPL),2X,F10.5/
     81OX,46H SHAFT/FLOATING RING RADIAL CLEARANCE (CLEAR),2X,F10.5//)
  111 FORMAT(/
     51OX,30H PRELOAD PRES./SPRING (PFORCE),2X,E20.6/
     51OX,26H TOTAL TIME CONSIDERED (TIME) ,8X,F10.6,2X,5H SECS/
     61OX,30H TIME STEP             (TINT) ,2X,E20.6,2X,5H SECS/
     71OX,30H CONVERGENCE CRITERION (CHECK),8X,F10.6//)
  112 FORMAT(///10X,71H INPUT  DATA  TABLE  4  -  FLOATING RING GEOMETRY
     1 AND MOMENT OF INERTIA/11X,21(1H-)//
     21OX,45H LENGHTS IN M  MASS IN KG  INERTIA IN KG*SQ M//
     31OX,30H THE FLOATING RING CONSISTS OF,I5,4X,
     412H AXIAL RINGS/)
  113 FORMAT(//12X,5H RING,31X,6H INNER,6X,6H OUTER/11X,7H NUMBER,
     16X,5H MASS,7X,7H LENGTH,5X,7H RADIUS,5X,7H RADIUS/)
  114 FORMAT(15X,I3,4X,F10.5,3X,F10.5,2X,F10.5,2X,F10.5)
  115 FORMAT(///
     11OX,36H TOTAL MASS OF FLOATING RING (AMASS),3X,F10.6/
     21OX,36H MOMENT OF INERTIA - ABOUT OX (OXI) ,2X,E20.6//)
  117 FORMAT(///10X,74H INPUT  DATA  TABLE  5  -  SEALED FLUID AND SLIDI
     1NG INTERFACE PARAMETERS,/11X,21(1H-)
     2//10X,61H PRESSURES IN N/SQ.M   VISCOSITY IN N.S/SQ M    LENGTHS I
     3N M    ANGLES IN RADIANS///
     41OX,36H SEALED PRESSURE  ID              (PI),E20.6/
     51OX,36H    ..        ..  OD              (PO),E20.6/
     61OX,36H CAVITATION PRESSURE            (PCAV),E20.6//)
  118 FORMAT(///
     11OX,36H GIVEN FILM THICKNESS            (HIN),E20.6/
     51OX,36H SLIDING INTERFACE OD             (RE),5X,F10.5//
     41OX,36H ROTOR       : RADIAL  OX     (XO(1)),E20.6/
     51OX,36H POSITION    : RADIAL  OY     (XO(2)),E20.6/
     61OX,36H RELATIVE TO : AXIAL          (XO(3)),E20.6/
     71OX,36H SHAFT AXIS  : ANGULAR OX     (XO(4)),E20.6/
     81OX,36H AND  STATOR : ANGULAR OY     (XO(5)),E20.6//)
C      WRITE(2,200)
       READ(5,100)((SHAFTI(I,J),J=1,3),I=1,NM),STIFRC,STIFRS,
      1STIFSP,DAMPRC,DAMPRS,HIN
       READ(5,101)ROR,DORI,SPL,RE,RS,RC,CLEAR,CHECK
       READ(5,100)PI,PO,PCAV
       READ(5,101)(AMA(I),ORI(I),RRO(I),EL(I),I=1,NI)
       READ(5,100)(XO(1,I),I=1,MM)
       READ(5,102)ITMAX,NCHECK
       READ(5,102)CAP
       PFORCE=3.141592654*(RE+RC)*(RE-RS)*PO
      1+STIFSP*SPL
C
C     CALCULATE MOMENTS OF INERTIA OF RING
C     MADE UP OF AXIAL RINGS
C
       AMO=0.
       AMASS=0.
        OXI=0.
       DO 3 I=1,NI
        FAC=0.
        IF(I.EQ.1)GO TO 2
        DO 1 J=1,I-1
     1   FAC=FAC+EL(J)
     2  FAC=FAC+EL(I)/2.
        AMO=AMO+AMA(I)*FAC
     3  AMASS=AMASS+AMA(I)
       GLR=AMO/AMASS
       DO 5 I=1,NI
        GLL=0.
```

```
      IF(I.EQ.1)GO TO 5
       DO 4 J=1,I-1
    4   GLL=GLL+EL(J)
    5  GLL=GLL+EL(I)/2.
    6  OXI=OXI+AMA(I)*(3.*(RRI(I)**2)+3.*(RRO(I)**2)+(EL(I)**2))/12.
     1 +AMA(I)*((GLG-GLL)**2)
C
C    CALCULATE PERPENDICULAR DISTANCE BETWEEN O-RING AND CENTROID
C
      DOR=GLG-DORI
C
C    CONVERT SHAFT VIBRATION FREQUENCY TO RADIANS PER SEC
C
      DO 20 I=1,NM
       SHAFT(I,1)=SHAFTI(I,1)
       SHAFT(I,2)=SHAFTI(I,2)*6.283185307179
   20  SHAFT(I,3)=SHAFTI(I,3)*3.141592654/180
      WRITE(6,103)
      WRITE(6,104)MM,NM,MP,NP,NT,ITMAX,NCHECK
      WRITE(6,105)
      WRITE(6,106)STIFRC,STIFRS,DAMPRC,DAMPRS,STIFSP
      WRITE(6,107)CAP(1),CAP(2),CAP(3),CAP(4),CAP(6),CAP(5),CAP(7),
     1 CAP(9),CAP(11),CAP(13),CAP(17),CAP(15),CAP(19),CAP(8),CAP(10),
     2  CAP(12),CAP(16),CAP(14),CAP(18)
      WRITE(6,111)PFORCE,TIME,TINT,CHECK
      WRITE(6,109)(SHAFT(I,1),SHAFTI(I,2),SHAFT(I,3),I=1,NM)
      WRITE(6,112)NI
      WRITE(6,113)
      WRITE(6,114)(I,AMA(I),EL(I),RRI(I),RRO(I),I=1,NI)
      WRITE(6,115)AMASS,OXI
      WRITE(6,116)ROR,DORI,DOR,RC,RS,SPL,CLEAR
      WRITE(6,117)PI,PO,PCAV
      WRITE(6,118)HIN,RE,(XO(1,I),I=1,MM)
      DO 35 I=1,3
       IF(I.GT.MM)GO TO 40
       AMAS(I)=AMASS
   35 CONTINUE
      DO 39 I=4,5
      IF(I.GT.MM)GO TO 40
       AMAS(I)=OXI
   39 CONTINUE
   40 CONTINUE
      RETURN
      END
      SUBROUTINE ARRCAS
     1  (STIFRC,DAMPRC,STIFRS,DAMPRS,SHAFT,AMAS,TINT,
     2DOR,CAP,PFORCE,STIFF,DAMP,MM,AP,ROR,NM,STIFSP,RS)
C
C    ***************************************************
C    *                                                 *
C    *    THIS SUBROUTINE SETS UP THE ARRAYS           *
C    *    STIFF AND DAMP AND THE FACTORS OF ARRAY      *
C    *     PEA THAT ARE INDEPENDANT OF TIME            *
C    *                                                 *
C    ***************************************************
C
      DIMENSION AMAS(MM),CAP(19),SHAFT(NM,3),STIFF(MM,MM),
     1DAMP(MM,MM),AP(MM,4)
C
C    FIRST ZERO ALL THE ARRAY ELEMENTS
C
      DO 1 J=1,MM
      DO 1 I=1,MM
      STIFF(I,J)=0.0
    1 DAMP(I,J)=0.0
C
```

```
C    SET UP THE CONSTANT VALUES OF THE ELEMENTS
C
       STIFF(1,1)=STIFRC
       DAMP(1,1)=DAMPRC
       AP(1,1)=DAMPRC*SHAFT(1,1)*SHAFT(1,2)
       AP(1,2)=STIFRC*SHAFT(1,1)
       IF(MM.LT.2)GO TO 50
       DAMP(2,2)=DAMPRC
       STIFF(2,2)=STIFRC
       AP(2,1)=DAMPRC*SHAFT(2,1)*SHAFT(2,2)
       AP(2,2)=STIFRC*SHAFT(2,1)
       IF(MM.LT.3)GO TO 50
       DAMP(3,3)=DAMPRS
       STIFF(3,3)=STIFRS+STIFSP
       AP(3,1)=DAMPRS*SHAFT(3,1)*SHAFT(3,2)
       AP(3,2)=(STIFRS+STIFSP)*SHAFT(3,1)
       IF(MM.LT.4)GO TO 50
       DAMP(4,4)=DAMPRC*(DOR**2)+DAMPRS*(ROR**2)/2.
       STIFF(4,4)=STIFRC*(DOR**2)+STIFRS*(ROR**2)/2.+STIFSP*(RS**2)/2.
       AP(4,1)=-DAMPRC*DOR*SHAFT(2,1)*SHAFT(2,2)
       AP(4,2)=-STIFRC*DOR*SHAFT(2,1)
       DAMP(2,4)=-DAMPRC*DOR
       DAMP(4,2)=DAMP(2,4)
       STIFF(2,4)=-STIFRC*DOR
       STIFF(4,2)=STIFF(2,4)
       IF(MM.LT.5)GO TO 50
       DAMP(5,5)=DAMP(4,4)
       STIFF(5,5)=STIFF(4,4)
       AP(5,1)=DAMPRC*DOR*SHAFT(1,1)*SHAFT(1,2)
       AP(5,2)=STIFRC*DOR*SHAFT(1,1)
       DAMP(1,5)=-DAMP(2,4)
       DAMP(5,1)=-DAMP(2,4)
       STIFF(1,5)=-STIFF(2,4)
       STIFF(5,1)=-STIFF(4,2)
    50 CONTINUE
C   TEMPORARY WRITE OUT
       RETURN
       END
       SUBROUTINE GAUSS
      1 (N,A,B,X,LOG2)
       LOGICAL LOG2
       DIMENSION A(N,N),B(N),X(N)
       INTEGER P,Q
C
C    ****************************************
C    *                                      *
C    *     THIS SUBROUTINE  SOLVES THE      *
C    *          EQUATIONS OF MOTION         *
C    *                                      *
C    ****************************************
C
       LOG2=.FALSE.
       DO 24 J=1,N-1
        P=J
        DO 4 K=J+1,N
         IF(ABS(A(K,J)).GT.ABS(A(P,J)))P=K
    4   CONTINUE
        IF(ABS(A(P,J)).GE.1.0E-10)GO TO 8
    6    LOG2=.TRUE.
         GO TO 13
    8   CONTINUE
        IF(P-J)17,17,10
   10   Z=B(J)
        B(J)=B(P)
        B(P)=Z
        DO 15 K=J,N
```

```
      Z=A(J,Q)
      A(J,Q)=A(P,Q)
   16 A(P,Q)=Z
   17 CONTINUE
      DO 23 K=J+1,N
      Z=A(K,J)/A(J,J)
      B(K)=B(K)-B(J)*Z
      DO 22 Q=J,N
   22 A(K,Q)=A(K,Q)-A(J,Q)*Z
   23 CONTINUE
   24 CONTINUE
      DO 32 KK=1,N
      K=N-KK+1
      X(K)=B(K)
      IF(K-N)29,31,31
   29 DO 30 J=K+1,N
   30 X(K)=X(K)-A(K,J)*X(J)
   31 X(K)=X(K)/A(K,K)
   32 CONTINUE
   33 CONTINUE
      RETURN
      END
      SUBROUTINE CONCHK
     1  (X,CA,HI,HA,IT1,IT2,L,M,CR,N1,N2,CK,SH,TI,N3,NC)
      LOGICAL L
      DIMENSION X(N2,M),XOLD(9),CA(19),SH(N3,3),CAOLD(19)
     1  ,NC(7)
C
C    ***********************************************
C    *                                             *
C    *  THIS SUBROUTINE CHECKS THE DISPLACEMENTS   *
C    *        AND FILM ELEMENTS FOR CONVERGENCE    *
C    *                                             *
C    ***********************************************
C
      IF(N1)1,32,33
C
C    CALCULATE THE SHAFT POSITION
C
    1 SHFTM1=SH(1,1)*SIN(SH(1,2)*(IT2-1)*TI+SH(1,3))
      IF(NM.LT.2)GO TO 2
      SHFTM2=SH(2,1)*SIN(SH(2,2)*(IT2-1)*TI+SH(2,3))
C
C   CHECK MAXIMUM POSITION OX
C
    2 RADCHK=SHFTM1+CR
      IF(X(IT2,1)-RADCHK)4,3,3
    3 X(IT2,1)=RADCHK
      NC(2)=0
      NC(1)=1
      GO TO 6
    4 NC(1)=0
C
C    CHECK MINIMUM POSITION OX
C
      RADCHK=SHFTM1-CR
      IF(X(IT2,1)-RADCHK)5,5,6
    5 X(IT2,1)=RADCHK
      NC(2)=1
    6 IF(M.LT.2)GO TO 32
C
C    CHECK MAXIMUM POSITION OY
C
      RADCHK=SHFTM2+CR
      IF(X(IT2,2)-RADCHK)7,7,7
    7 X(IT2,2)=RADCHK
```

```
      NC(4)=0
      NC(7)=1
      GO TO 10
    9 NC(3)=0
C
C     CHECK MINIMUM POSITION OY
C
      RADCHK=SHFTM2-CR
      IF(X(IT2,2)-RADCHK)9,9,10
    9 X(IT2,2)=RADCHK
      NC(4)=1
   10 IF(M.LT.3)GO TO 52
      AXCHK=-(0.15E-04)/RI-HA
      AXCHK2=20.*AXCHK

C
C     CHECK AXIAL POSITION
C
      IF(M-4)52,14,17
   14 IF(ABS(X(IT2,4)).LT.1.0E-08)GO TO 25
      IF(ABS(X(IT2,4)).LT.ABS(X(IT2,3)))GO TO 25
      X(IT2,4)=X(IT2,3)
      NC(7)=1
      GO TO 26
      IF(X(IT2,3).GT.AXCHK2)GO TO 12
      X(IT2,3)=AXCHK2
      NC(5)=1
      NC(6)=0
      GO TO 17
   12 IF(X(IT2,3).LT.AXCHK)GO TO 17
      X(IT2,3)=AXCHK
      NC(5)=0
      NC(6)=1

C
C     CHECK ANGULAR POSITION
C
   17 ITHANG=1
      IF(ABS(X(IT2,4)).LT.1.0E-08)ITHANG=ITHANG+1
      IF(ABS(X(IT2,5)).LT.1.0E-06)ITHANG=ITHANG+2
      GO TO (22,21,22,25),ITHANG
   23 THANG=2.*ATAN(-X(IT2,5)/X(IT2,4)+SQRT((X(IT2,5)/X(IT2,4))
     1         **2+1.))
      GO TO 24
   21 THANG=0.
      GO TO 24
   22 THANG=3.1415926/2.
   24 DELTAH=ABS(X(IT2,4))*SIN(THANG)+ABS(X(IT2,5))*COS(THANG)
      IF(ABS(DELTAH).LT.1.0E-09)GO TO 25
      IF(DELTAH.LE.ABS(X(IT2,3)))GO TO 25
      X(IT2,4)=X(IT2,4)*ABS(X(IT2,3))/DELTAH
      X(IT2,5)=X(IT2,5)*ABS(X(IT2,3))/DELTAH
      NC(7)=1
      GO TO 26
   25 NC(7)=0

C
C     CHECK FOR CONVERGENCE - DISPLACEMENTS
C
   26 L=.TRUE.
      DO 31 I=1,MX
      IF(IT1.EQ.1)GO TO 30
      IF(ABS(XOLD(I)).LT.1.0E-09)GO TO 30
      DCHK=ABS(X(IT2,I)-XOLD(I))/XOLD(I)
      IF(DCHK.GT.CK)L=.FALSE.
   30 XOLD(I)=X(IT2,I)
   31 CONTINUE
      GO TO 52
```

```
C
C    CHECK FOR CONVERGENCE - VELOCITIES
C
   33 L=.TRUE.
      DO 36 I=1,19
       IF(IT1.EQ.1)GO TO 36
       IF(ABS(CAOLD(I)).LT.1.0E-03)GO TO 36
       DCHK=ABS(CA(I)-CAOLD(I))/CAOLD(I)
       IF(DCHK.GT.CK)L=.FALSE.
   36  CAOLD(I)=CA(I)
   52 CONTINUE
      RETURN
      END
      SUBROUTINE ARASS
     1  (AMAS,STIFF,DAMP,PFORCE,RHS,ALHS,XO,NT,ANDF,
     2CAP,MM,ITIMST,TINT,SHAFT,AP,PEA,NM,S,C)
      DIMENSION AMAS(NM),STIFF(MM,MM),DAMP(MM,MM),
     1    PHS(MM),ALHS(MM,MM), CAP(19),XO(NT,MM),
     2 SHAFT(NM,3),AP(MM,4),PEA(MM),S(MM,MM),C(MM,MM)
C
C   ***********************************************
C   *                                             *
C   *    THIS SUBROUTINE ASSEMBLES THE MATRICES   *
C   *              FOR EACH TIMESTEP              *
C   *                                             *
C   ***********************************************
C
      DO 25 I=1,MM
      TEA=(ITIMST-1)*TINT
    1 GO TO(2,3,2,3,4),I
C
C                 THE GENERAL FORMULA FOR COS AND SIN
C
    2 CS=COS(SHAFT(I,2)*TEA*ANDF+SHAFT(I,2))
      SN=SIN(SHAFT(I,2)*TEA*ANDF+SHAFT(I,3))
      GO TO 5
C
C                SPECIAL FORM FOR I=4
C
    3 CS=COS(SHAFT(2,2)*TEA*ANDF+SHAFT(2,2))
      SN=SIN(SHAFT(2,2)*TEA*ANDF+SHAFT(2,3))
      GO TO 5
C
C                  SPECIAL FORM FOR I=5
C
    4 CS=COS(SHAFT(1,2)*TEA*ANDF+SHAFT(1,3))
      SN=SIN(SHAFT(1,2)*TEA*ANDF+SHAFT(1,3))
C
C    SET UP PEA(I)
C
    5 PEA(I)=(AP(I,1)*CS+AP(I,2)*SN)
      IF(I.EQ.2)PEA(I)=PEA(I)+PFORCE-CAP(1)
   25 CONTINUE
C
C                 SET UP WORKING ARRAYS S (STIFFNESS) AND
C                 C (DAMPING)
      DO 40 J=1,MM
      DO 30 I=1,MM
       S(I,J)=STIFF(I,J)
   30 C(I,J)=DAMP(I,J)
      IF(MM.LT.3)GO TO 35
      C(2,2)=C(2,2)+CAP(2)
      S(2,3)=S(2,3)+CAP(2)
      IF(MM.LT.4)GO TO 35
      C(2,4)=CAP(5)
      C(4,2)=CAP(11)
```

```
      C(4,4)=C(4,4)+CAP(17)
      S(3,4)=CAP(4)
      S(4,3)=CAP(9)
      S(4,4)=S(4,4)+CAP(11)
      IF(MM.LT.5)GO TO 35
      C(4,5)=CAP(19)
      C(5,3)=CAP(10)
      C(5,4)=CAP(16)
      C(5,5)=C(5,5)+CAP(18)
      S(3,5)=CAP(5)
      S(4,5)=CAP(15)
      S(5,3)=CAP(8)
      S(5,4)=CAP(12)
      S(5,5)=S(5,5)+CAP(14)
C
C    SET UP THE EQUATION ARRAYS
C
C
C    THIS FORMULATION ASSUMES XO(0,I)=2*XO(1,I)-XO(2,I)
C
   35 N=ITIMST
C
C    FIRST THE LEFT HAND SIDE SPECIALS FORMS ARE USED FOR ITIMST=2
C
      DO 45 I=1,MM
       DO 45 J=1,MM
        IF(N-2)40,40,41
   40   ALHS(I,J)=C(I,J)/TINT+S(I,J)
        IF(I.EQ.J.AND.ABS(ALHS(I,J)).LE.1.0E-10)
     1  ALHS(I,J)=AMAS(I)/(TINT**2)
        GO TO 45
   41   ALHS(I,J)=3.*C(I,J)/(2.*TINT)+S(I,J)
        IF(I.EQ.J)ALHS(I,J)=ALHS(I,J)+AMAS(I)/(TINT**2)
   45 CONTINUE
C
C    SECOND THE RIGHT HAND SIDE SPECIAL FORMS USED FOR ITIMST=2
C
      DO 54 I=1,MM
       RHS(I)=0.
       DO 50 J=1,MM
        IF(N-2)46,46,47
   46   RHS(I)=RHS(I)+C(I,J)*XO(1,J)/TINT
        GO TO 50
   47   RHS(I)=RHS(I)+2.*C(I,J)*XO(N-1,J)/TINT
     1  -C(I,J)*XO(N-2,J)/(TINT*2.)
   50  CONTINUE
       IF(N-2)52,52,53
   52  RHS(I)=RHS(I)+PEA(I)
       GO TO 54
   53  RHS(I)=RHS(I)+PEA(I)+2.*AMAS(I)*XO(N-1,I)/(TINT**2)
     1  -AMAS(I)*XO(N-2,I)/(TINT**2)
   54 CONTINUE
      RETURN
      END
      SUBROUTINE OUTDYN
     1 (ALOAD,NT,XO,DXODT,MM,EL,ITIMST,TIME,IPRT)
C
C   ***************************************************
C   *                                                 *
C   *    THIS SUBROUTINE OUTPUTS THE CALCULATED       *
C   *    LOAD AND FLOATING RING POSITION  IN          *
C   *                TABULAR FORM                     *
C   *                                                 *
C   ***************************************************
C
      DIMENSION ALOAD(NT),XO(NT,MM),DXODT(NT,MM),EL(NT)
```

```
  110 FORMAT(///10X,14H OUTPUT  TABLE,I4,22H -  FLOATING RING DISP,
     113HLACEMENTS (M)/11X,17(1H-)///
     210X,9H TIMESTEP,4X,10H RADIAL OX,7X,10H RADIAL OY,9X,
     36H AXIAL,8X,11H ANGULAR OX,6X,11H ANGULAR OY/)
  111 FORMAT(//10X,14H OUTPUT  TABLE,I4,22H -  FLOATING RING VELO,
     112HCITIES (M/S)/11X,17(1H-)///
     210X,9H TIMESTEP,4X,10H RADIAL OX,7X,10H RADIAL OY,9X,
     36H AXIAL,8X,11H ANGULAR OX,6X,11H ANGULAR OY/)
  112 FORMAT(//10X,14H OUTPUT  TABLE,I4,25H -  INTERFACE LOAD (KG),
     127H  AND SEAL LEAKAGE (ML/MIN)/11X,17(1H-)///
     210X,9H TIMESTEP,6X,5H LOAD,11X,8H LEAKAGE/)
  113 FORMAT(13X,I3,6X,E12.5,5X,E12.5,5X,E12.5,5X,E12.5
     1 ,5X,E12.5)
  114 FORMAT(13X,I3,6X,E12.5,5X,E12.5)
  115 FORMAT(4E20.9)
  116 FORMAT(E10.3,I5)
C
C    SET LOOP LIMITS TO THE PRESENT TIMESTEP
C    SET THE TABLE NUMBER TO ALLOW FOR THE TABLES
C    OF REYNOLDS EQUATION RESULTS
C
       NNT=ITIMST
       IPRT=IPRT+1
       WRITE(6,110)IPRT
C
C    WRITE OUT DISPLACEMENTS
C
       WRITE(6,113)(I,(XO(I,J),J=1,MM),I=1,NNT)
       IPRT=IPRT+1
       WRITE(6,111)IPRT
C
C    WRITE VELOCITIES
C
       WRITE(6,113)(I,(DXODT(I,J),J=1,MM),I=1,NNT)
       IPRT=IPRT+1
       WRITE(6,112)IPRT
C
C    WRITE LOAD AND LEAKAGE
C
       WRITE(6,114)(I,ALOAD(I),QL(I),I=1,NNT)
C
C    WRITE RESULTS TIME AND NUMBER OF TIMESTE
C    COMPLETED TO 4 SEPARATE FILE FOR PLOTTING
C
       WRITE(7,115)(XO(I,1),I=1,NNT),(DXODT(I,1),I=1,NNT)
       WRITE(7,115)(XO(I,2),I=1,NNT),(DXODT(I,2),I=1,NNT)
       WRITE(7,115)(XO(I,3),I=1,NNT),(DXODT(I,3),I=1,NNT)
       WRITE(7,115)(XO(I,4),I=1,NNT),(DXODT(I,4),I=1,NNT)
       WRITE(7,115)(XO(I,5),I=1,NNT),(DXODT(I,5),I=1,NNT)
       WRITE(7,116)TIME,NNT
       RETURN
       END
       FINISH
```

BHRA SEAL EXPERIMENTAL O-RING TAIL

OUTPUT TABLE 1 - FLOATING RING DISPLACEMENTS (m)

TIMESTEP	RADIAL DX	RADIAL DY	AXIAL	ANGULAR DX	ANGULAR DY
1	0.00000E 00	-0.69000E-05	-0.13512E-05	-0.35439E-07	-0.71146E-06
2	0.70815E-06	-0.68411E-05	-0.13350E-05	0.11985E-07	-0.74057E-06
3	0.14248E-05	-0.67782E-05	-0.13212E-05	-0.10042E-09	-0.75958E-06
4	0.21391E-05	-0.66145E-05	-0.13071E-05	0.96898E-08	-0.78464E-06
5	0.28534E-05	-0.63176E-05	-0.12938E-05	0.49313E-08	-0.80845E-06
6	0.34957E-05	-0.60149E-05	-0.12812E-05	0.84240E-08	-0.83515E-06
7	0.41136E-05	-0.55998E-05	-0.12693E-05	0.70575E-08	-0.86196E-06
8	0.46821E-05	-0.51339E-05	-0.12581E-05	0.83724E-08	-0.88999E-06
9	0.51969E-05	-0.45940E-05	-0.12474E-05	0.81272E-08	-0.91825E-06
10	0.56532E-05	-0.40148E-05	-0.12373E-05	0.87279E-08	-0.94703E-06
11	0.60461E-05	-0.33967E-05	-0.12278E-05	0.98014E-08	-0.97593E-06
12	0.63709E-05	-0.27273E-05	-0.12187E-05	0.91213E-08	-0.10050E-05
13	0.66234E-05	-0.20329E-05	-0.12102E-05	0.92512E-08	-0.10340E-05
14	0.68006E-05	-0.13148E-05	-0.12021E-05	0.94449E-08	-0.10628E-05
15	0.69005E-05	-0.58200E-06	-0.11945E-05	0.95654E-08	-0.10914E-05
16	0.69221E-05	0.15723E-06	-0.11872E-05	0.96958E-08	-0.11196E-05
17	0.68651E-05	0.89455E-06	-0.11804E-05	0.97928E-08	-0.11474E-05
18	0.67304E-05	0.16217E-05	-0.11739E-05	0.98836E-08	-0.11746E-05
19	0.65192E-05	0.23006E-05	-0.11678E-05	0.99553E-08	-0.12013E-05
20	0.62341E-05	0.30132E-05	-0.11620E-05	0.10018E-07	-0.12274E-05
21	0.58781E-05	0.36618E-05	-0.11565E-05	0.10068E-07	-0.12528E-05
22	0.54554E-05	0.42691E-05	-0.11514E-05	0.10111E-07	-0.12776E-05
23	0.49707E-05	0.48281E-05	-0.11465E-05	0.10146E-07	-0.13016E-05
24	0.44294E-05	0.53327E-05	-0.11418E-05	0.10176E-07	-0.13248E-05
25	0.38376E-05	0.57771E-05	-0.11375E-05	0.10200E-07	-0.13473E-05
26	0.32021E-05	0.61563E-05	-0.11333E-05	0.10220E-07	-0.13691E-05
27	0.25299E-05	0.64663E-05	-0.11294E-05	0.10239E-07	-0.13900E-05
28	0.18287E-05	0.67027E-05	-0.11257E-05	0.10254E-07	-0[illegible]+-05
29	0.11064E-05	0.68637E-05	-0.11222E-05	0.10269E-07	-0.14296E-05
30	0.37106E-06	0.69473E-05	-0.11189E-05	0.10283E-07	-0.14482E-05
31	-0.36896E-06	0.69524E-05	-0.11158E-05	0.10297E-07	-0.14661E-05
32	-0.11033E-05	0.68791E-05	-0.11128E-05	0.10311E-07	-0.14832E-05
33	-0.18297E-05	0.67281E-05	-0.11100E-05	0.10326E-07	-0.14997E-05
34	-0.25340E-05	0.65012E-05	-0.11074E-05	0.10342E-07	-0.15154E-05
35	-0.32102E-05	0.62009E-05	-0.11049E-05	0.10360E-07	-0.15305E-05
36	-0.38509E-05	0.58306E-05	-0.11025E-05	0.10378E-07	-0.15449E-05
37	-0.44484E-05	0.53945E-05	-0.11003E-05	0.10396E-07	-0.15587E-05
38	-0.49963E-05	0.48975E-05	-0.10982E-05	0.10419E-07	-0.15720E-05
39	-0.54888E-05	0.43452E-05	-0.10961E-05	0.10442E-07	-0.15846E-05
40	-0.59192E-05	0.37439E-05	-0.10943E-05	0.10465E-07	-0.15968E-05
41	-0.62837E-05	0.31003E-05	-0.10925E-05	0.10489E-07	-0.16084E-05
42	-0.65778E-05	0.24217E-05	-0.10908E-05	0.10514E-07	-0.16196E-05
43	-0.67983E-05	0.17158E-05	-0.10892E-05	0.10539E-07	-0.16303E-05
44	-0.69426E-05	0.99047E-06	-0.10877E-05	0.10564E-07	-0.16407E-05
45	-0.70092E-05	0.25399E-06	-0.10862E-05	0.10589E-07	-0.16506E-05
46	-0.69984E-05	-0.48036E-06	-0.10849E-05	0.10613E-07	-0.16602E-05
47	-0.69069E-05	-0.12192E-05	-0.10836E-05	0.10636E-07	-0.16695E-05
48	-0.67392E-05	-0.19394E-05	-0.10824E-05	0.10657E-07	-0.16785E-05
49	-0.64960E-05	-0.26376E-05	-0.10812E-05	0.10677E-07	-0.16873E-05
50	-0.61802E-05	-0.33061E-05	-0.10801E-05	0.10695E-07	-0.16957E-05
51	-0.57955E-05	-0.39372E-05	-0.10791E-05	0.10710E-07	-0.17039E-05
52	-0.53454E-05	-0.45239E-05	-0.10781E-05	0.10722E-07	-0.17120E-05
53	-0.48350E-05	-0.50596E-05	-0.10772E-05	0.10732E-07	-0.17198E-05
54	-0.42724E-05	-0.55426E-05	-0.10763E-05	0.10738E-07	-0.17275E-05

55	-0.[illegible]E-05	-0.59542E-05	-0.10755E-05	0.10741E-07	-0.17356E-05
56	-0.30096E-05	-0.63031E-05	-0.10747E-05	0.10739E-07	-0.17423E-05
57	-0.23245E-05	-0.65908E-05	-0.10740E-05	0.10734E-07	-0.17495E-05
58	-0.16138E-05	-0.67842E-05	-0.10733E-05	0.10725E-07	-0.17566E-05
59	-0.98554E-06	-0.69111E-05	-0.10726E-05	0.10719E-07	-0.17635E-05
60	-0.14792E-06	-0.69599E-05	-0.10720E-05	0.10695E-07	-0.17703E-05
61	0.59072E-06	-0.69303E-05	-0.10714E-05	0.10674E-07	-0.17769E-05
62	0.13220E-05	-0.68224E-05	-0.10709E-05	0.10648E-07	-0.17834E-05
63	0.20637E-05	-0.66374E-05	-0.10704E-05	0.10619E-07	-0.17898E-05
64	0.27299E-05	-0.63776E-05	-0.10699E-05	0.10587E-07	-0.17960E-05
65	0.33905E-05	-0.60458E-05	-0.10694E-05	0.10551E-07	-0.18021E-05
66	0.40123E-05	-0.56458E-05	-0.10690E-05	0.10511E-07	-0.18080E-05
67	0.45890E-05	-0.51820E-05	-0.10685E-05	0.10469E-07	-0.18137E-05
68	0.51113E-05	-0.46598E-05	-0.10681E-05	0.10424E-07	-0.18193E-05
69	0.55763E-05	-0.40850E-05	-0.10678E-05	0.10377E-07	-0.18247E-05
70	0.59777E-05	-0.34640E-05	-0.10674E-05	0.10328E-07	-0.18299E-05
71	0.63109E-05	-0.28040E-05	-0.10671E-05	0.10277E-07	-0.18348E-05
72	0.65722E-05	-0.21123E-05	-0.10668E-05	0.10226E-07	-0.18396E-05
73	0.67587E-05	-0.13968E-05	-0.10665E-05	0.10174E-07	-0.18442E-05
74	0.68683E-05	-0.66553E-06	-0.10662E-05	0.10122E-07	-0.18485E-05
75	0.68996E-05	0.73253E-07	-0.10660E-05	0.10071E-07	-0.18526E-05
76	0.68524E-05	0.81121E-06	-0.10657E-05	0.10020E-07	-0.18564E-05
77	0.67272E-05	0.15400E-05	-0.10655E-05	0.99702E-08	-0.18600E-05
78	0.65253E-05	0.22514E-05	-0.10653E-05	0.99226E-08	-0.18633E-05
79	0.62492E-05	0.29374E-05	-0.10651E-05	0.98771E-08	-0.18664E-05
80	0.59018E-05	0.35902E-05	-0.10649E-05	0.98341E-08	-0.18692E-05
81	0.54872E-05	0.42025E-05	-0.10647E-05	0.97942E-08	-0.18717E-05
82	0.50099E-05	0.47674E-05	-0.10645E-05	0.97575E-08	-0.18740E-05
83	0.44754E-05	0.52785E-05	-0.10644E-05	0.97245E-08	-0.18760E-05
84	0.38897E-05	0.57299E-05	-0.10642E-05	0.96954E-08	-0.18777E-05
85	0.32594E-05	0.61167E-05	-0.10641E-05	0.96705E-08	-0.18792E-05
86	0.25917E-05	0.64345E-05	-0.10640E-05	0.96500E-08	-0.18804E-05
87	0.18940E-05	0.66795E-05	-0.10639E-05	0.96339E-08	-0.18814E-05
88	0.11743E-05	0.68475E-05	-0.10637E-05	0.96225E-08	-0.18822E-05
89	0.43960E-06	0.69341E-05	-0.10636E-05	0.96159E-08	-0.18829E-05
90	0.29371E-06	0.69353E-05	-0.10635E-05	0.96137E-08	-0.18831E-05
91	-0.10039E-05	0.68491E-05	-0.10634E-05	0.96163E-08	-0.18833E-05
92	-0.17410E-05	0.67491E-05	-0.10633E-05	0.96236E-08	-0.18833E-05
93	-0.24474E-05	0.65307E-05	-0.10632E-05	0.96348E-08	-0.18831E-05
94	-0.31467E-05	0.62306E-05	-0.10631E-05	0.96505E-08	-0.18828E-05
95	-0.37912E-05	0.58760E-05	-0.10631E-05	0.96701E-08	-0.18824E-05
96	-0.43[illegible]E-05	0.54673E-05	-0.10630E-05	0.96935E-08	-0.18819E-05
97	-0.49[illegible]E-05	0.49567E-05	-0.10629E-05	0.97202E-08	-0.18813E-05
98	-0.54453E-05	0.44104E-05	-0.10628E-05	0.97499E-08	-0.18807E-05
99	-0.58828E-05	0.38143E-05	-0.10628E-05	0.97822E-08	-0.18800E-05
100	-0.62546E-05	0.31752E-05	-0.10627E-05	0.98169E-08	-0.18793E-05
101	-0.65[illegible]E-05	0.25002E-05	-0.10627E-05	0.98531E-08	-0.18786E-05
102	-0.67851E-05	0.17969E-05	-0.10626E-05	0.98908E-08	-0.18779E-05
103	-0.69379E-05	0.10734E-05	-0.10625E-05	0.99293E-08	-0.18772E-05
104	-0.70127E-05	0.33779E-06	-0.10625E-05	0.99682E-08	-0.18766E-05
105	-0.70094E-05	-0.40166E-06	-0.10624E-05	0.10007E-07	-0.18761E-05
106	-0.69277E-05	-0.11366E-05	-0.10624E-05	0.10045E-07	-0.18756E-05
107	-0.67684E-05	-0.19507E-05	-0.10623E-05	0.10083E-07	-0.18753E-05
108	-0.65334E-05	-0.25590E-05	-0.10623E-05	0.10118E-07	-0.18750E-05
109	-0.62254E-05	-0.33620E-05	-0.10623E-05	0.10152E-07	-0.18749E-05
110	-0.58477E-05	-0.38679E-05	-0.10623E-05	0.10184E-07	-0.18749E-05
111	-0.54049E-05	-0.44592E-05	-0.10622E-05	0.10212E-07	-0.18750E-05
112	-0.49015E-05	-0.50013E-05	-0.10621E-05	0.10238E-07	-0.18752E-05
113	-0.43446E-05	-0.54969E-05	-0.10621E-05	0.10261E-07	-0.18757E-05
114	-0.37374E-05	-0.59103E-05	-0.10620E-05	0.10279E-07	-0.18763E-05
115	-0.30897E-05	-0.62670E-05	-0.10620E-05	0.10294E-07	-0.18770E-05
116	-0.24078E-05	-0.65530E-05	-0.10620E-05	0.10305E-07	-0.18779E-05
117	-0.16994E-05	-0.67649E-05	-0.10619E-05	0.10311E-07	-0.18789E-05
118	-0.97204E-06	-0.69006E-05	-0.10619E-05	0.10314E-07	-0.18799E-05

119	-0.23535E-06	-0.69583E-05	-0.10619E-05	0.10311E-07	-0.18812E-05
120	0.50376E-06	-0.69376E-05	-0.10619E-05	0.10305E-07	-0.18825E-05
121	0.12565E-05	-0.68805E-05	-0.10618E-05	0.10294E-07	-0.18840E-05
122	0.19544E-05	-0.67622E-05	-0.10618E-05	0.10279E-07	-0.18855E-05
123	0.26756E-05	-0.64167E-05	-0.10618E-05	0.10260E-07	-0.18871E-05
124	0.33138E-05	-0.58669E-05	-0.10618E-05	0.10237E-07	-0.18888E-05
125	0.39413E-05	-0.50974E-05	-0.10617E-05	0.10210E-07	-0.18905E-05
126	0.45232E-05	-0.52376E-05	-0.10617E-05	0.10180E-07	-0.18922E-05
127	0.50534E-05	-0.47217E-05	-0.10617E-05	0.10147E-07	-0.18939E-05
128	0.55734E-05	-0.41526E-05	-0.10617E-05	0.10112E-07	-0.18957E-05
129	0.59178E-05	-0.35565E-05	-0.10617E-05	0.10074E-07	-0.18974E-05
130	0.62746E-05	-0.28805E-05	-0.10617E-05	0.10033E-07	-0.18991E-05
131	0.65443E-05	-0.21921E-05	-0.10617E-05	0.99936E-08	-0.19007E-05
132	0.67299E-05	-0.14788E-05	-0.10617E-05	0.99517E-08	-0.19022E-05
133	0.68580E-05	-0.74874E-06	-0.10617E-05	0.99094E-08	-0.19037E-05
134	0.68993E-05	-0.10509E-07	-0.10616E-05	0.98670E-08	-0.19051E-05
135	0.68400E-05	0.72708E-06	-0.10616E-05	0.98251E-08	-0.19063E-05
136	0.67437E-05	0.14581E-05	-0.10616E-05	0.97841E-08	-0.19074E-05
137	0.65505E-05	0.21719E-05	-0.10616E-05	0.97445E-08	-0.19084E-05
138	0.62837E-05	0.28612E-05	-0.10616E-05	0.97068E-08	-0.19092E-05
139	0.59433E-05	0.35182E-05	-0.10616E-05	0.96712E-08	-0.19099E-05
140	0.55361E-05	0.41354E-05	-0.10616E-05	0.96383E-08	-0.19104E-05
141	0.50659E-05	0.47060E-05	-0.10616E-05	0.96084E-08	-0.19107E-05
142	0.45375E-05	0.52234E-05	-0.10616E-05	0.95818E-08	-0.19109E-05
143	0.39574E-05	0.56819E-05	-0.10617E-05	0.95588E-08	-0.19109E-05
144	0.33317E-05	0.60763E-05	-0.10617E-05	0.95398E-08	-0.19107E-05
145	0.26681E-05	0.64021E-05	-0.10617E-05	0.95248E-08	-0.19104E-05
146	0.19734E-05	0.66556E-05	-0.10617E-05	0.95140E-08	-0.19099E-05
147	0.12558E-05	0.68340E-05	-0.10617E-05	0.95076E-08	-0.19093E-05
148	0.52338E-06	0.69352E-05	-0.10617E-05	0.95057E-08	-0.19085E-05
149	-0.21569E-06	0.69582E-05	-0.10617E-05	0.95082E-08	-0.19076E-05
150	-0.95301E-06	0.69026E-05	-0.10617E-05	0.95151E-08	-0.19065E-05
151	-0.16803E-05	0.67691E-05	-0.10617E-05	0.95264E-08	-0.19053E-05
152	-0.23893E-05	0.65592E-05	-0.10617E-05	0.95413E-08	-0.19041E-05
153	-0.30720E-05	0.62753E-05	-0.10617E-05	0.95613E-08	-0.19027E-05
154	-0.37207E-05	0.59205E-05	-0.10617E-05	0.95847E-08	-0.19013E-05
155	-0.43282E-05	0.54989E-05	-0.10617E-05	0.96115E-08	-0.18999E-05
156	-0.48875E-05	0.50152E-05	-0.10617E-05	0.96416E-08	-0.18984E-05
157	-0.53923E-05	0.44750E-05	-0.10617E-05	0.96745E-08	-0.18968E-05
158	-0.58369E-05	0.38842E-05	-0.10617E-05	0.97100E-08	-0.18953E-05
159	-0.62164E-05	0.32495E-05	-0.10617E-05	0.97476E-08	-0.18938E-05
160	-0.65264E-05	0.25782E-05	-0.10617E-05	0.97869E-08	-0.18924E-05
161	-0.67634E-05	0.18773E-05	-0.10617E-05	0.98274E-08	-0.18910E-05
162	-0.69248E-05	0.11562E-05	-0.10617E-05	0.98687E-08	-0.18896E-05
163	-0.70087E-05	0.42151E-06	-0.10617E-05	0.99104E-08	-0.18884E-05
164	-0.70142E-05	-0.31792E-06	-0.10617E-05	0.99516E-08	-0.18872E-05
165	-0.69413E-05	-0.10538E-05	-0.10617E-05	0.99927E-08	-0.18862E-05
166	-0.67907E-05	-0.17772E-05	-0.10616E-05	0.10032E-07	-0.18853E-05
167	-0.65641E-05	-0.24816E-05	-0.10616E-05	0.10071E-07	-0.18845E-05
168	-0.62641E-05	-0.31575E-05	-0.10616E-05	0.10107E-07	-0.18839E-05
169	-0.58942E-05	-0.37978E-05	-0.10616E-05	0.10141E-07	-0.18834E-05
170	-0.54583E-05	-0.43952E-05	-0.10616E-05	0.10172E-07	-0.18831E-05
171	-0.49616E-05	-0.49430E-05	-0.10616E-05	0.10200E-07	-0.18829E-05
172	-0.44096E-05	-0.54350E-05	-0.10616E-05	0.10224E-07	-0.18829E-05
173	-0.38085E-05	-0.58656E-05	-0.10616E-05	0.10245E-07	-0.18831E-05
174	-0.31651E-05	-0.62301E-05	-0.10616E-05	0.10262E-07	-0.18834E-05
175	-0.24867E-05	-0.65212E-05	-0.10616E-05	0.10275E-07	-0.18839E-05
176	-0.17809E-05	-0.67447E-05	-0.10615E-05	0.10283E-07	-0.18846E-05
177	-0.10557E-05	-0.68991E-05	-0.10615E-05	0.10287E-07	-0.18853E-05
178	-0.31933E-06	-0.69557E-05	-0.10615E-05	0.10287E-07	-0.18863E-05
179	0.42000E-06	-0.69439E-05	-0.10615E-05	0.10282E-07	-0.18873E-05
180	0.11539E-05	-0.68536E-05	-0.10615E-05	0.10272E-07	-0.18885E-05
181	0.18740E-05	-0.66860E-05	-0.10615E-05	0.10259E-07	-0.18898E-05
182	0.25724E-05	-0.64429E-05	-0.10615E-05	0.10242E-07	-0.18911E-05
183	0.32316E-05	-0.61372E-05	-0.10615E-05	0.10220E-07	-0.18926E-05
184	0.38723E-05	-0.57423E-05	-0.10615E-05	0.10195E-07	-0.18941E-05
185	0.44852E-05	-0.52923E-05	-0.10615E-05	0.10166E-07	-0.18956E-05

186	0.49951E-05	-0.47830E-05	-0.10615E-05	0.10135E-07	-0.18971E-05
187	0.54739E-05	-0.42195E-05	-0.10615E-05	0.10100E-07	-0.18997E-05
188	0.58902E-05	-0.36085E-05	-0.10615E-05	0.10064E-07	-0.19002E-05
189	0.62393E-05	-0.29567E-05	-0.10615E-05	0.10025E-07	-0.19018E-05
190	0.65174E-05	-0.22715E-05	-0.10615E-05	0.99849E-08	-0.19032E-05
191	0.67211E-05	-0.15607E-05	-0.10615E-05	0.99438E-08	-0.19047E-05
192	0.68484E-05	-0.83225E-06	-0.10615E-05	0.99021E-08	-0.19060E-05
193	0.68976E-05	-0.94436E-07	-0.10615E-05	0.98603E-08	-0.19072E-05
194	0.68683E-05	0.64444E-06	-0.10615E-05	0.98190E-08	-0.19084E-05
195	0.67607E-05	0.13760E-05	-0.10615E-05	0.97784E-08	-0.19094E-05
196	0.65762E-05	0.20921E-05	-0.10615E-05	0.97392E-08	-0.19102E-05
197	0.63167E-05	0.27845E-05	-0.10615E-05	0.97016E-08	-0.19110E-05
198	0.59852E-05	0.34456E-05	-0.10615E-05	0.96663E-08	-0.19116E-05
199	0.55852E-05	0.40677E-05	-0.10615E-05	0.96335E-08	-0.19120E-05
200	0.51220E-05	0.46439E-05	-0.10615E-05	0.96037E-08	-0.19123E-05

APPENDIX G

REGRESSION ANALYSIS

G.1 INTRODUCTION

The experiments described in Chapter 5 were originally conceived as a means of obtaining data for validating the computer program (Chapter 6). A parameter perturbation technique was therefore used, and this results in a large spread of the values for leakage and vibration for some values of the variables (eg sealed pressure of 0.5 MPa and a shaft speed of 2900 rpm). The results therefore, are not entirely suited to statistical analysis. However, analysing the results qualitatively proved difficult (p98), and a regression analysis has therefore been carried out to identify possible trends.

Statistical analysis routines are available as computer software packages. The NAG Library routines for correlation and linear regression, implemented on the ICL 1904S computer at the University of Aston in Birmingham have been used to analyse the results of the experiments and computer predictions. A short program has been written to call up the routines and print the results, and the methods used and the variables selected will be described in section G.2. The results obtained are given in section G.3, these are discussed and conclusions are drawn in section G.4.

G.2 ANALYSIS TECHNIQUE

The correlation analysis has been carried out using the NAG routine G02BAF. This routine calculates Pearson product-moment correlation coefficients for variables whose values may be represented on an ordinal scale. These coefficients represent the strength of the association between the variables. The mathematical relationship between the variables, in terms of an equation, has been obtained by means of a multiple linear regression technique using either the NAG routine G02CGF (linear regression with a constant term) or routines G02BDF and G02CHF (linear regression with no constant term). Full details of the routines and the underlying statistics may be found in the NAG Library Manual (179).

Two forms of the equation relating the variables may be obtained:-

(1) $y = a_0 + a_1x_1 + a_2x_2 + \ldots a_nx_n$

(2) $y = a_0.x_1^{a_1}.x_2^{a_2} \quad \ldots x_n^{a_n}$

where y is the dependent variable.

$x_1 - x_n$ are the independent variables

$a_0 - a_n$ are the regression coefficients.

Equation (1) is obtained using the data without modification, and equation (2) is obtained by taking natural logarithms of all the data before carrying out the regression.

The routines used provide data to enable the user to predict the significance of the calculated regression coefficients and also to assess the overall significance of the regression. The analysis

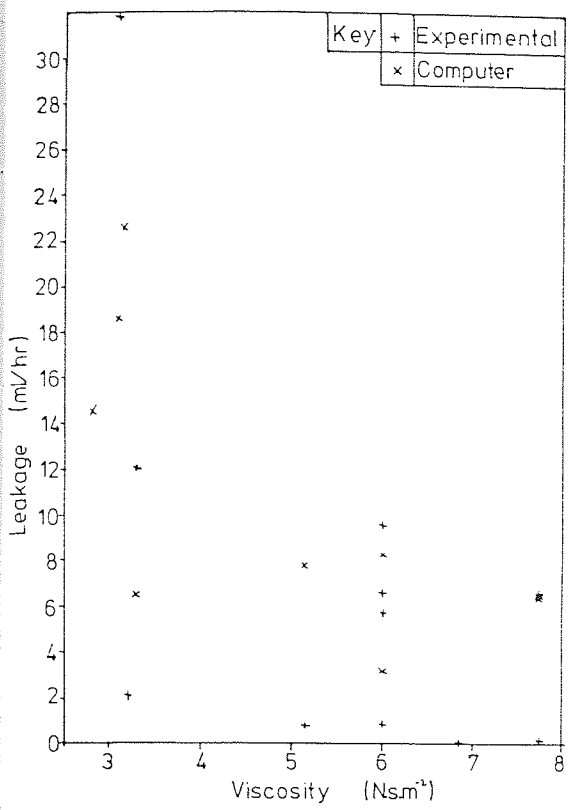

Fig G-1 Scattergraph Leakage and Interface Fluid Viscosity

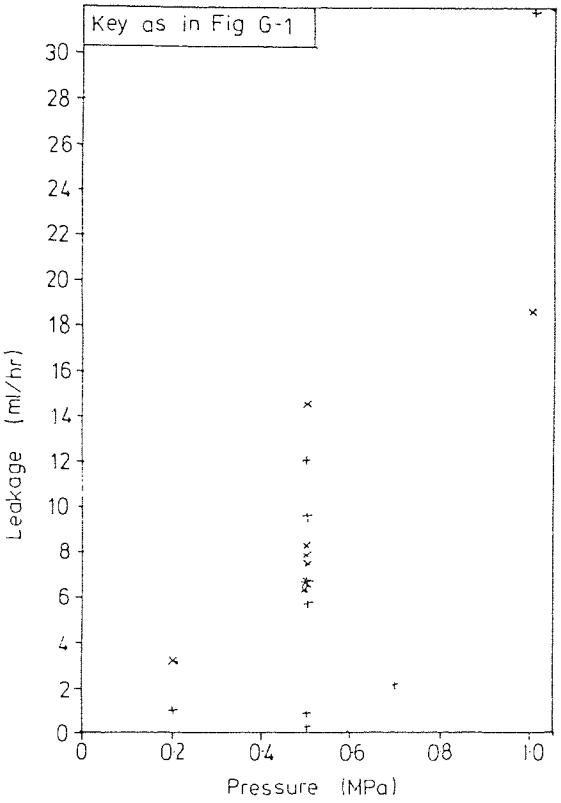

Fig G-2 Scattergraph Leakage and Seal Pressure

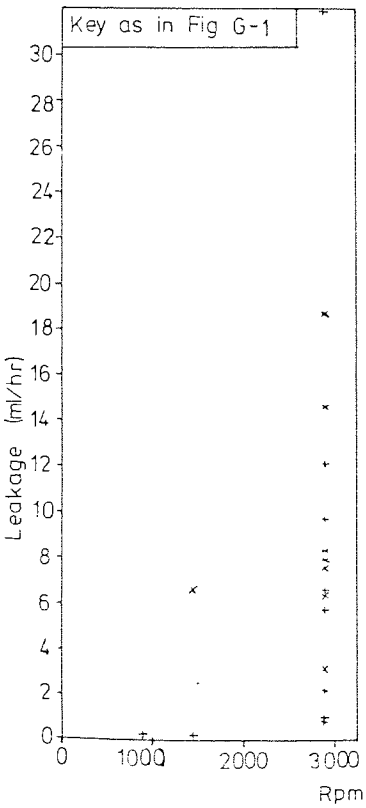

g G-3 Scattergraph Leakage and Shaft Speed

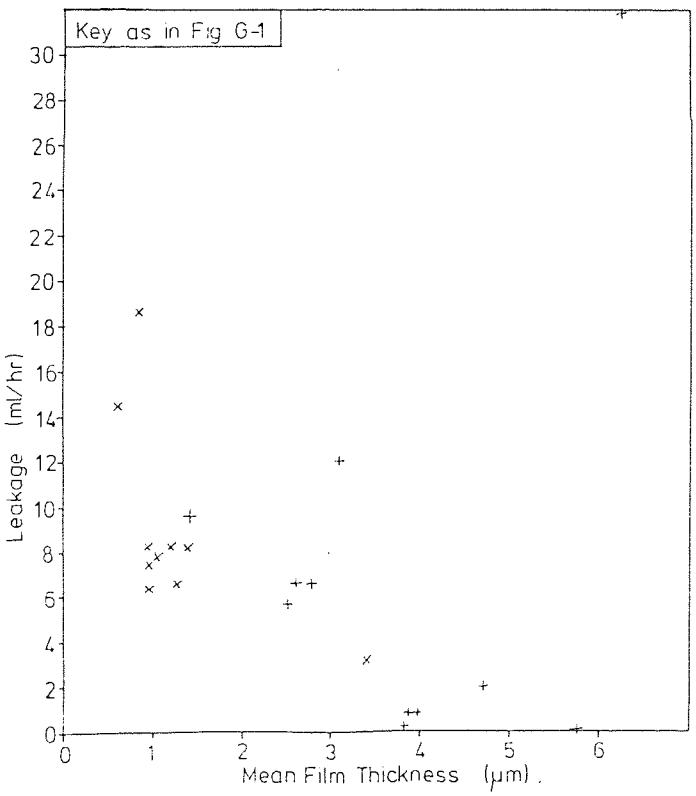

Fig G-4 Scattergraph Leakage and Mean Film Thickness

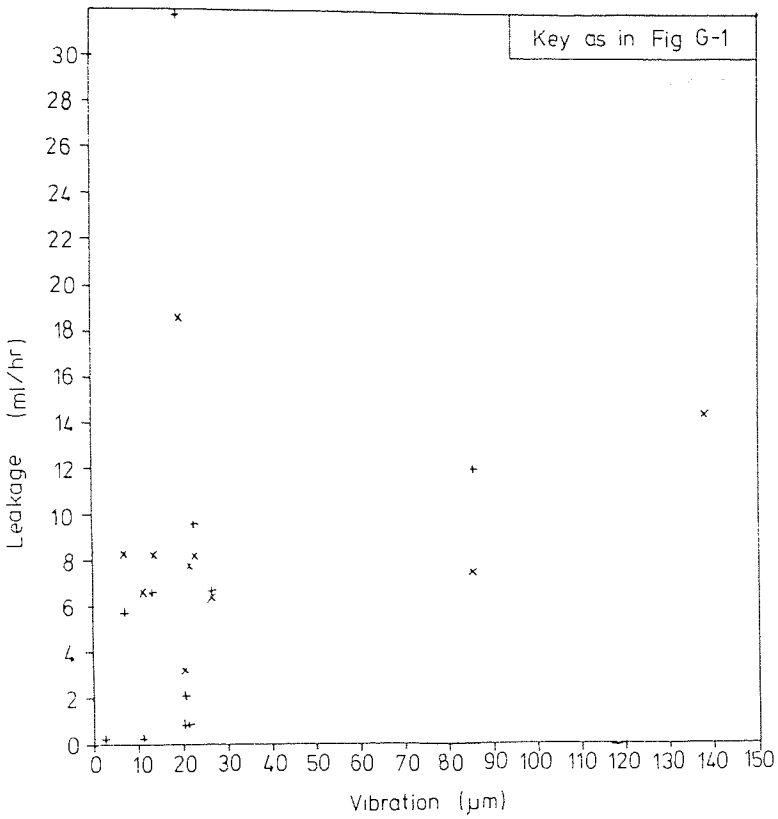

Fig G-5 Scattergraph Leakage and Shaft Vibration

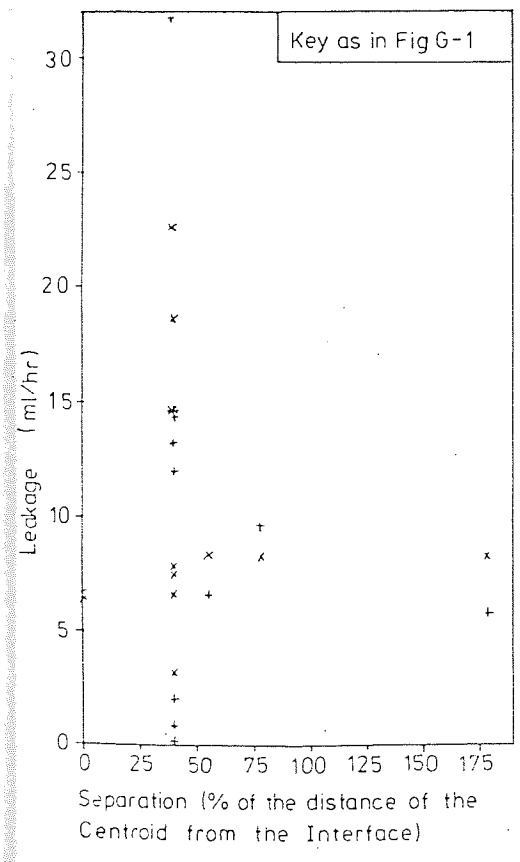

Fig G-6 Scattergraph Leakage and Separation of O-Ring and Centroid

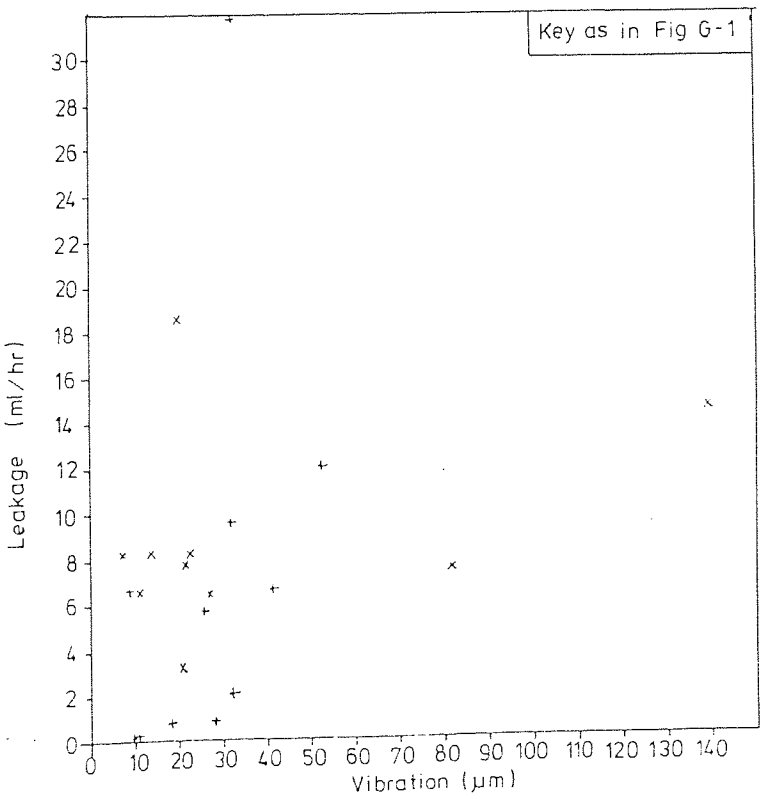

Fig G-7 Scattergraph Leakage and Radial Floating Ring Vibration

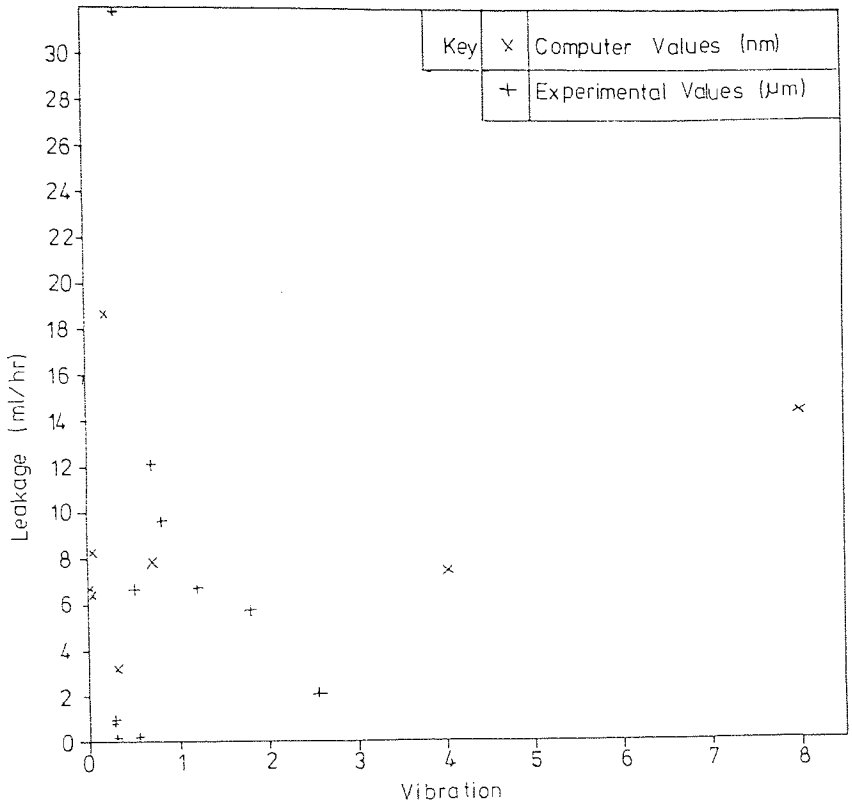

Fig G-8 Scattergraph Leakage and Axial Vibration

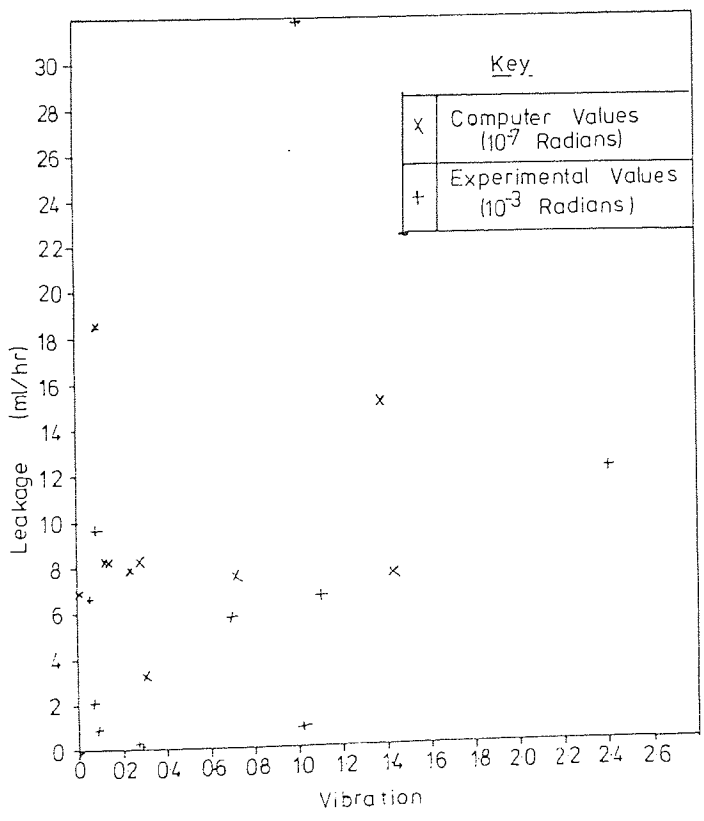

Fig G-9 Scattergraph Leakage and Angular Vibration

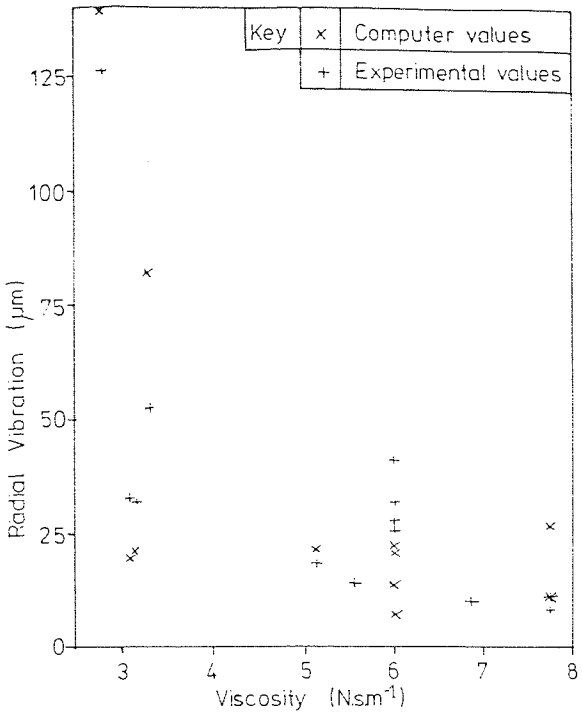

Fig G-10 Scattergraph Radial Vibration and Interface Fluid Viscosity

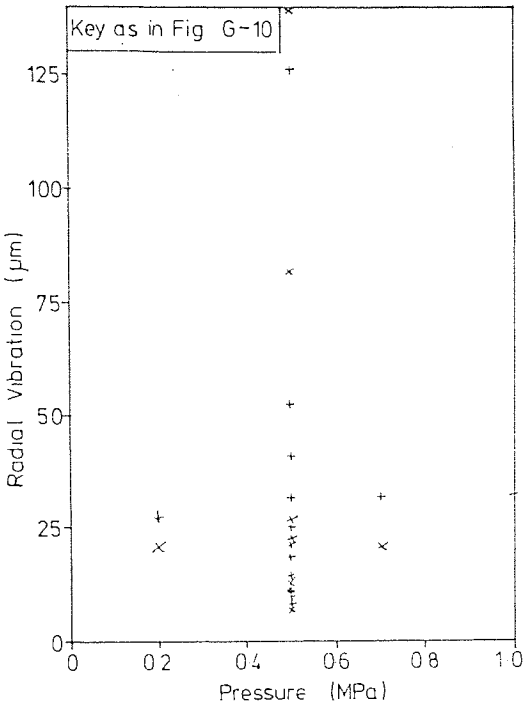

Fig G-11 Scattergraph Radial Vibration and Sealed Pressure

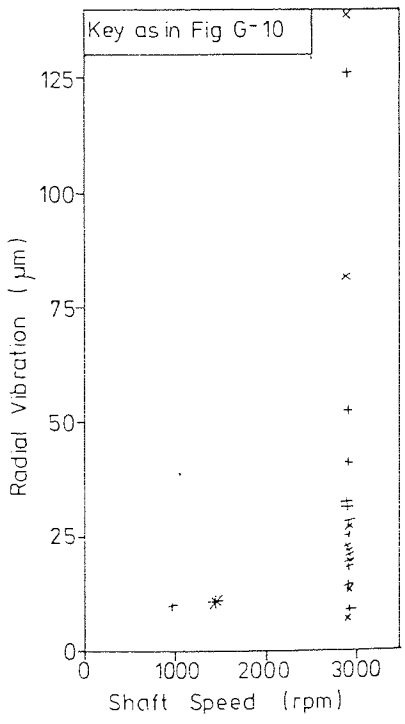

Fig G-12 Scattergraph Radial Vibration and Shaft Speed

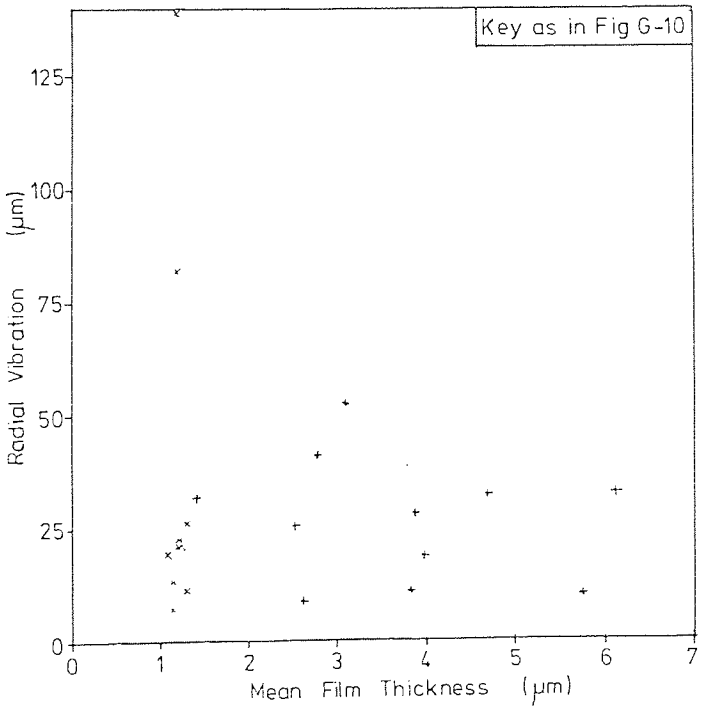

Fig G-13 Scattergraph Radial Vibration and Mean Film Thickness

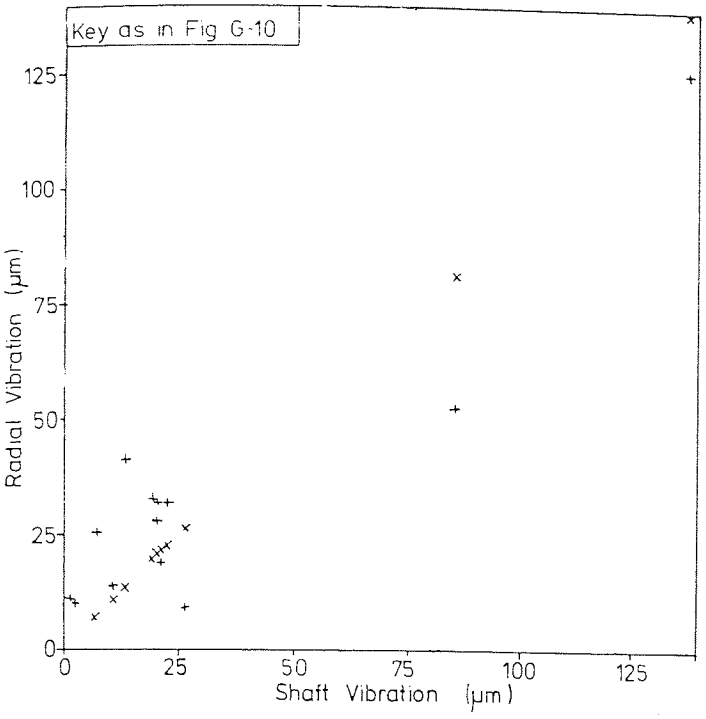

ig G-14 Scattergraph Radial and Shaft Vibration

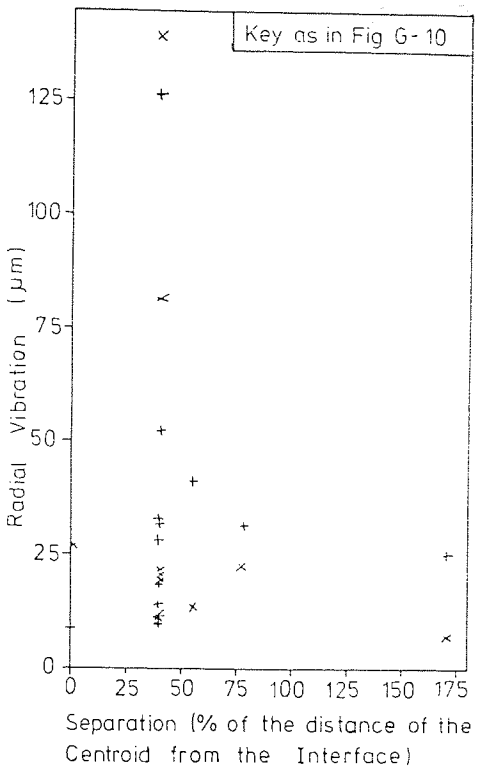

Fig G-15 Scattergraph Radial Vibration and Separation of O-Ring and Centroid

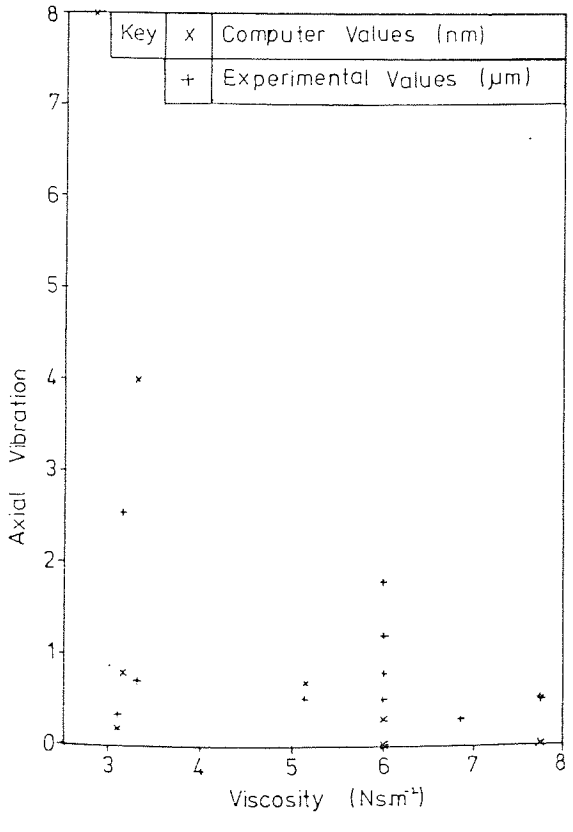

g G-16 Scattergraph Axial Vibration and Interface Fluid Viscosity

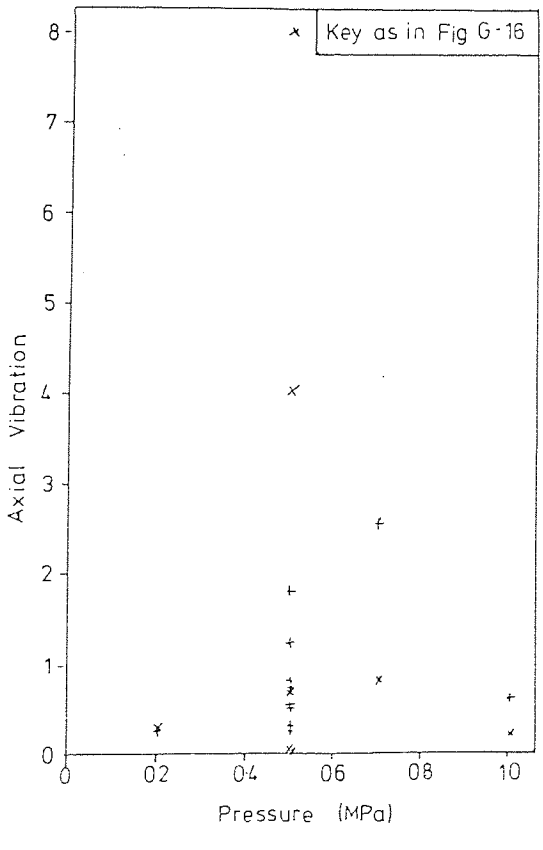

Fig G-17 Scattergraph Axial Vibration and Sealed Pressure

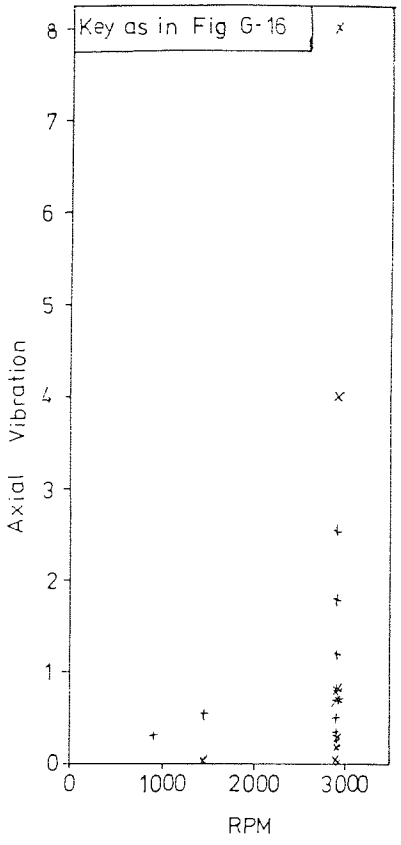

Fig G-18 Scattergraph Axial Vibration and Shaft Speed

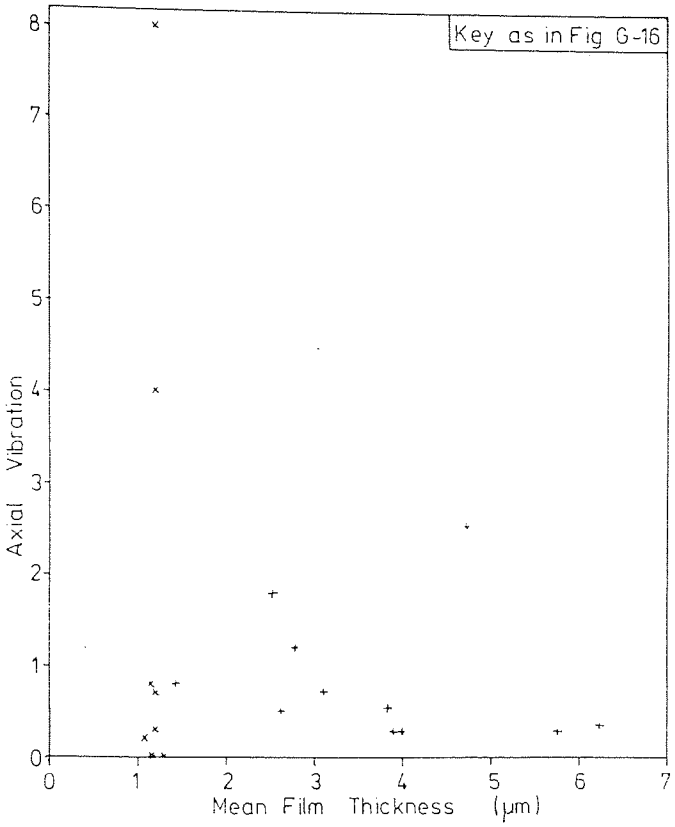

Fig G-19 Scattergraph Axial Vibration and Mean Film Thickness

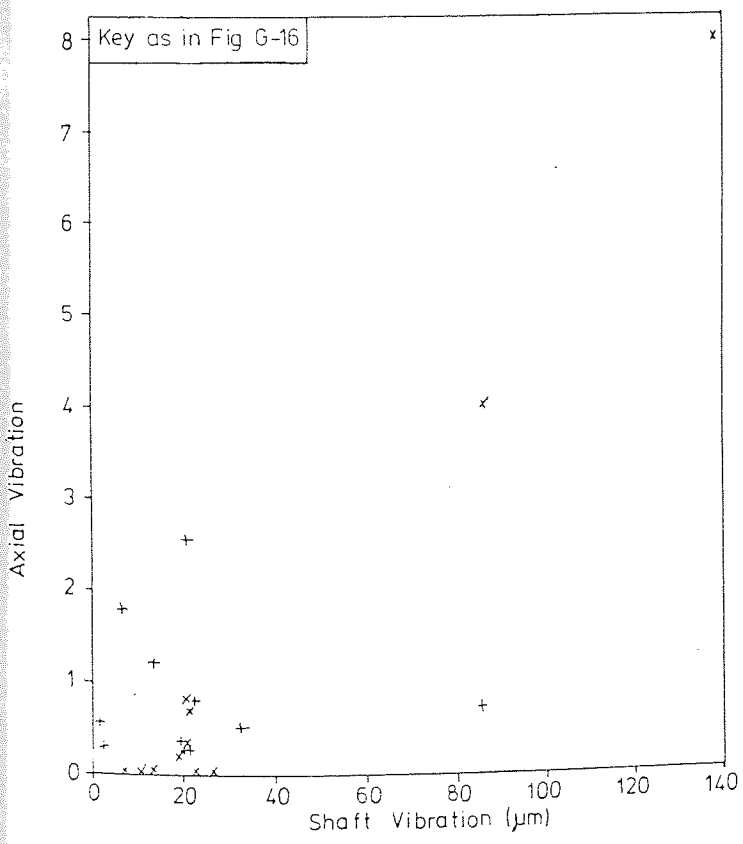

Fig G-20 Scattergraph Axial and Shaft Vibration

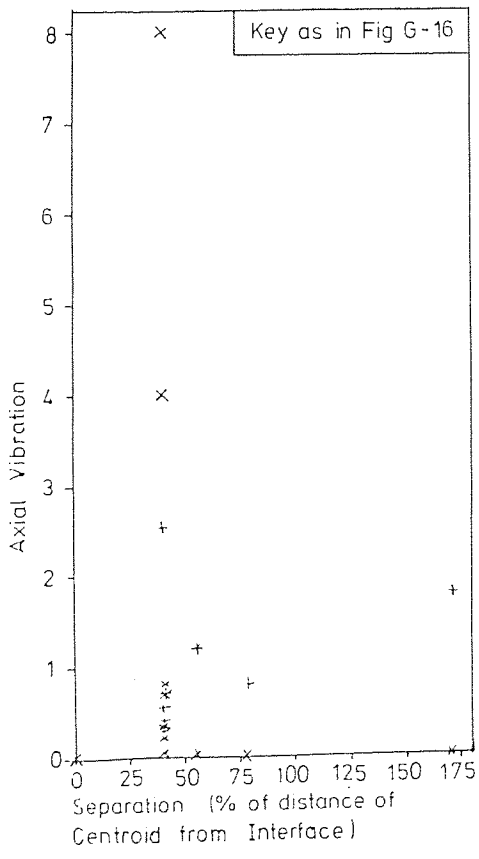

Fig G-21 Scattergraph Axial Vibration and Separation of O-Ring and Centroid

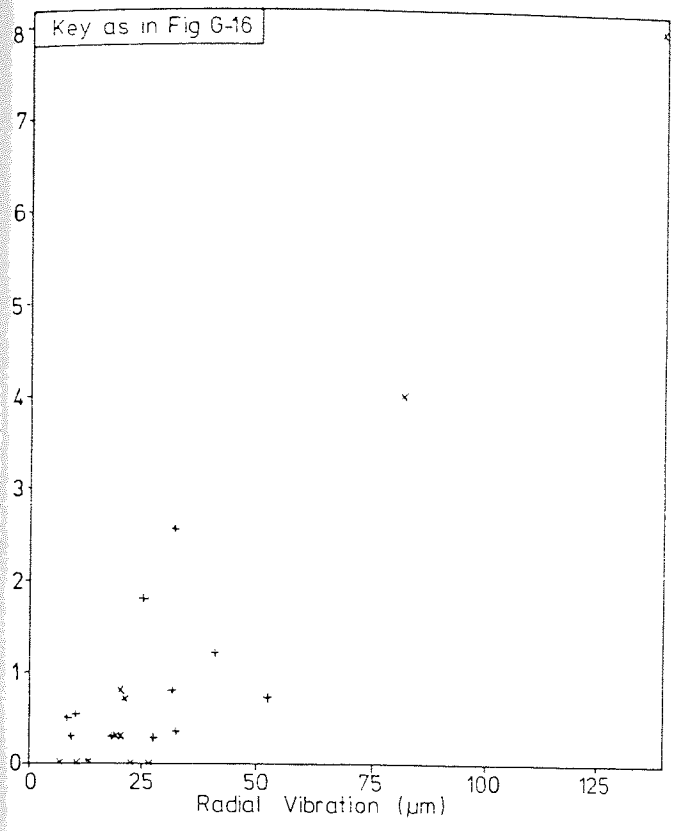

Fig G-22 Scattergraph Axial and Radial Vibration

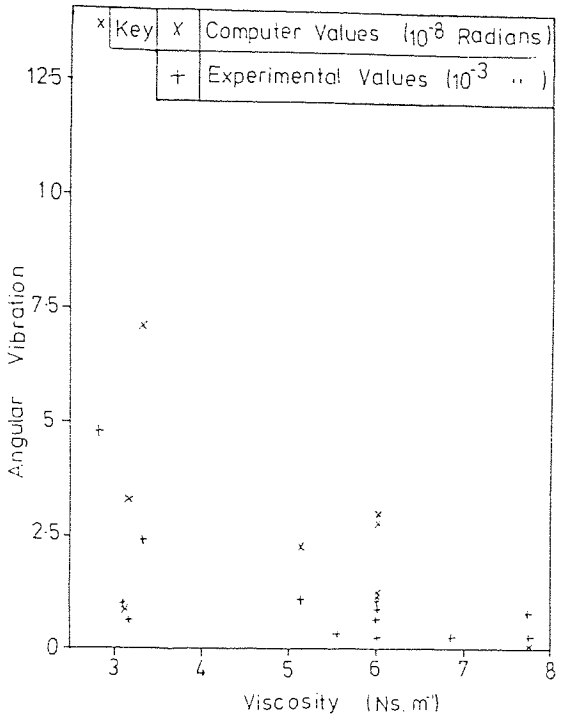

Fig G-23 Scattergraph Angular Vibration and Interface Fluid Viscosity

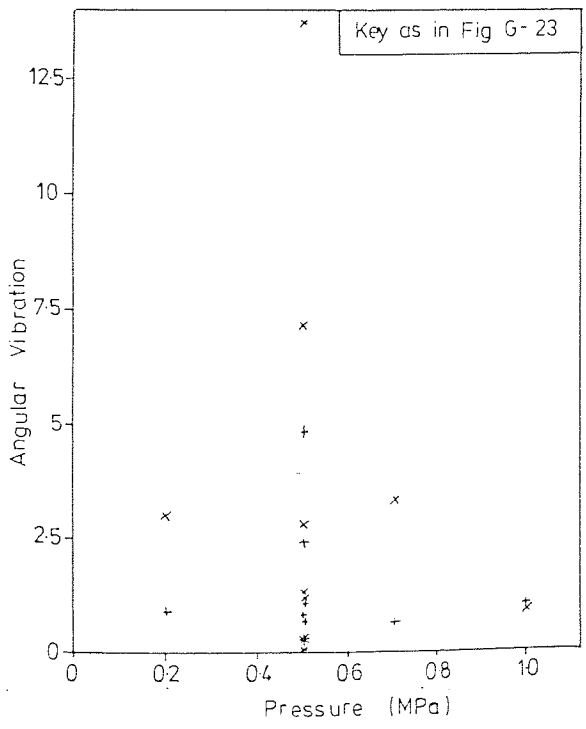

Fig G-24 Scattergraph Angular Vibration and Sealed Pressure

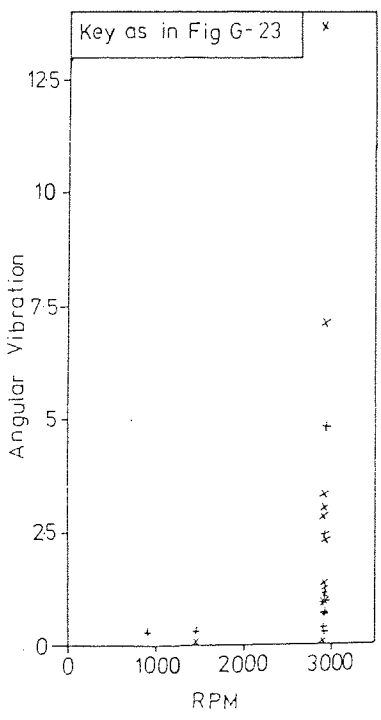

Fig G-25 Scattergraph Angular Vibration and Shaft Speed

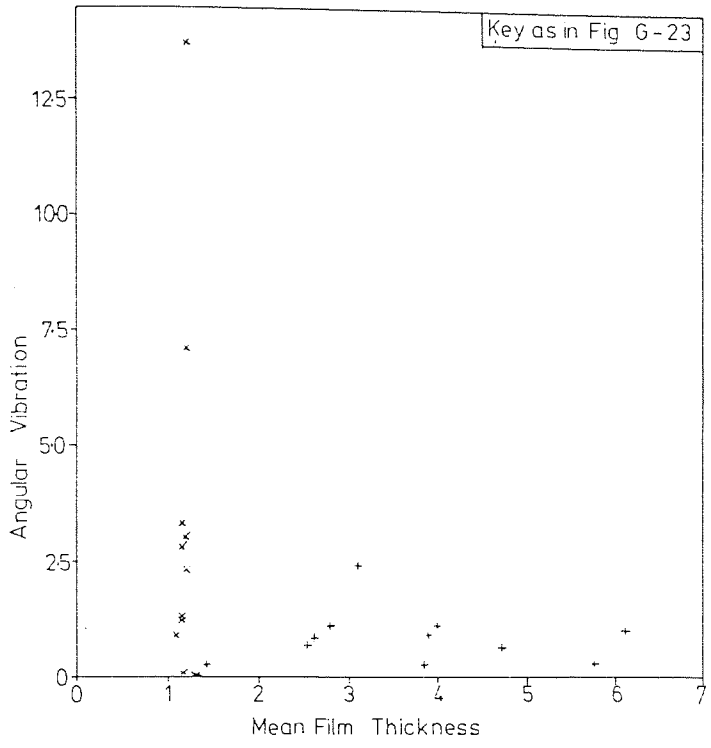

Fig G-26 Scattergraph Angular Vibration and Mean Film Thickness

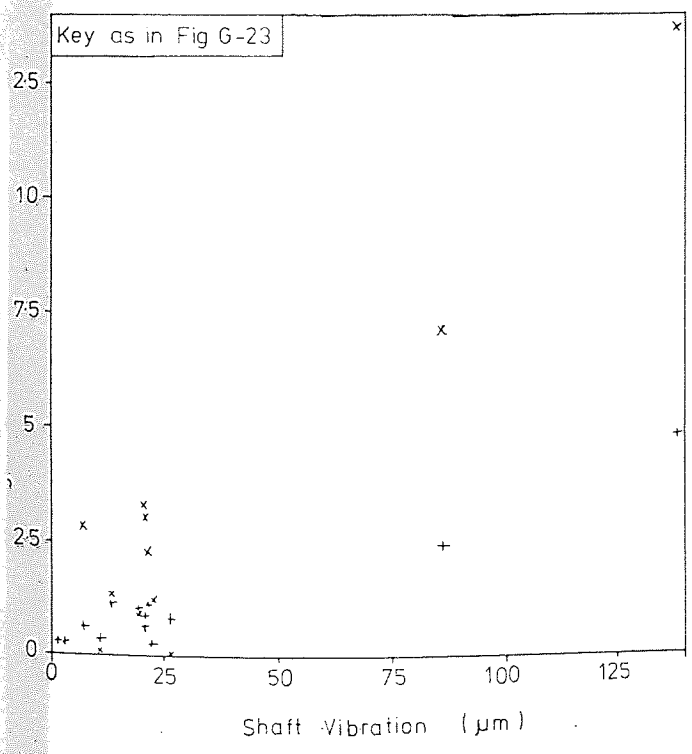

Fig G-27 Scattergraph Angular Vibration and Shaft Vibration

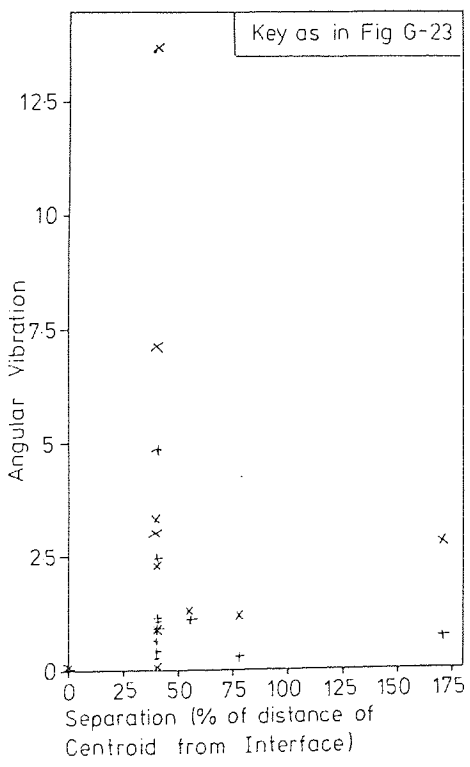

Fig G-28 Scattergraph Angular Vibration and Separation of O-Ring and Centroid

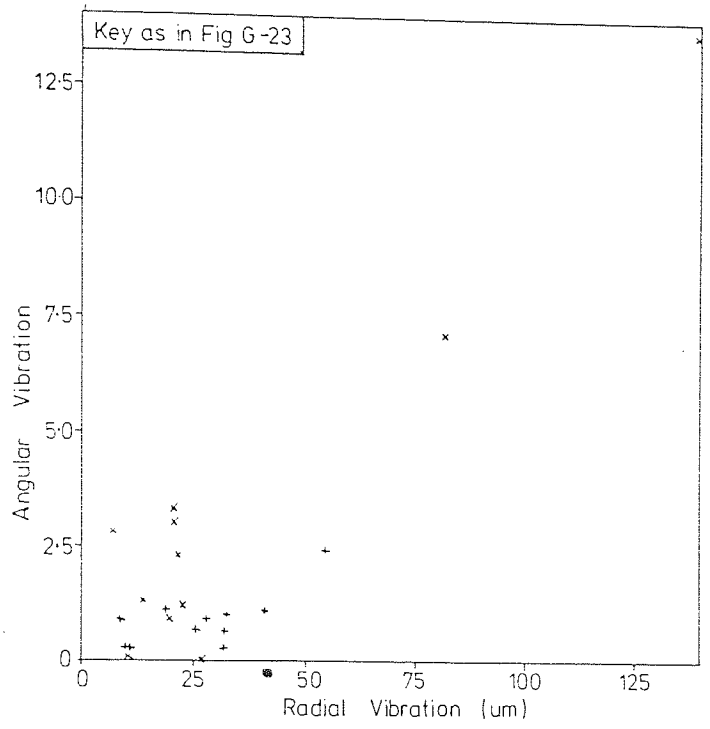

Fig G-29 Scattergraph Angular and Radial Vibration

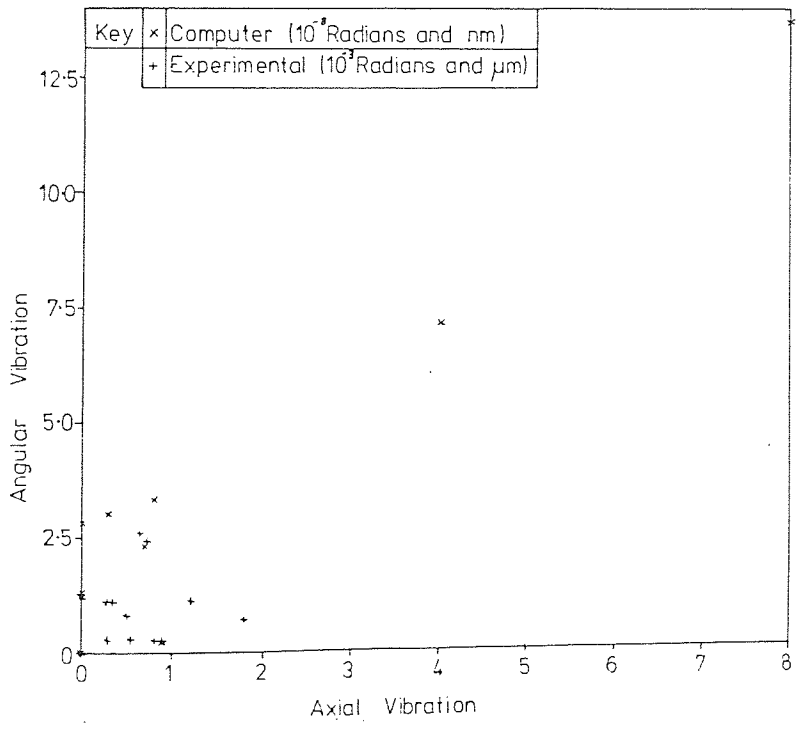

Fig G-30 Scattergraph Angular and Axial Vibration

technique assumes that the data scatter follows a normal distribution (179). However, because of the design of the experimental test programme this is not in fact the case (see for instance figs G-2 and G-3), and in consequence the correlation between some variables and the significance of the regression coefficients, are less than expected from a qualitative analysis.

There are only a small number of observations relative to the number of independent variables. For a satisfactory statistical analysis, it is usual to have at least three times as many observations as variables (180). In order to minimise the number of variables in the statistical analysis the following steps have been taken:-

(1) the number of surface profile waves has not been included as all the observations except one are for 3 waves.

(2) the mean angular misalignment has not been included as this is zero for the experimental results and thus logarithms cannot be taken.

(3) the O-ring position and the centroid position have been combined into a single variable, ie their separation parallel to the shaft axis.

(4) for the remaining variables the regressions have been carried out only for those whose correlation with the dependent variable is greater than 0.5 (Table G-3)

G.3 RESULTS

The results of the analysis are given in tables G-1 to G-3. Table G-1 gives the correlation coefficients, the variables with coefficients greater than 0.5 are summarised in table G-2. The

Independent Variable	Correlation			
	Logarithmic		Linear	
	Experimental	Computer	Experimental	Computer
Viscosity	-0.5	-0.7	-0.35	-0.7
Sealed Pressure	0.4	0.85	0.75	0.8
Shaft Speed	0.8	0.2	0.35	0.2
Mean Film Thickness	-0.4	-0.55	0.25	-0.55
Shaft Vibration	0.7	0.2	0.3	0.15
Separation*	0.05	0.15	-0.01	0.1
Radial Vibration	0.6	0.2	0.4	0.15
Axial Vibration	0.3	0.3	-0.15	0.2
Angular Vibration	0.54	0.25	0.3	0.2

(a) Leakage

Independent Variable	Correlation			
	Logarithmic		Linear	
	Experimental	Computer	Experimental	Computer
Viscosity	-0.7	-0.65	-0.7	-0.6
Sealed Pressure	0.1	-0.01	0.15	0.1
Shaft Speed	0.65	0.3	0.6	0.2
Mean Film Thickness	-0.2	0.1	-0.2	0.1
Shaft Vibration	0.6	1.0	0.7	1.0
Separation*	0.5	-0.25	0.15	-0.25

(b) Radial Floating Ring Vibration

Independent Variable	Correlation			
	Logarithmic		Linear	
	Experimental	Computer	Experimental	Computer
Viscosity	-0.25	-0.8	-0.35	-0.6
Sealed Pressure	0.3	0.01	0.2	-0.05
Shaft Speed	0.35	0.3	0.3	0.15
Mean Film Thickness	-0.35	-0.1	-0.2	0.05
Shaft Vibration	0.1	0.8	-0.05	1.0
Separation*	0.3	0.05	0.45	-0.15
Radial Vibration	0.4	0.3	0.3	1.0

(c) Axial Floating Ring Vibration

Independent Variable	Correlation			
	Logarithmic		Linear	
	Experimental	Computer	Experimental	Computer
Viscosity	-0.55	-0.7	-0.55	-0.65
Sealed Pressure	0.0	-0.1	0.01	-0.15
Shaft Speed	0.65	0.55	0.45	0.25
Mean Film Thickness	0.1	-0.55	-0.05	-0.05
Shaft Vibration	0.75	0.45	0.9	0.95
Separation*	-0.1	0.65	-0.15	-0.05
Radial Vibration	0.55	0.45	0.7	0.95
Axial Vibration	0.01	0.7	0.1	1.0

(d) Angular Floating Ring Vibration

* Separation of O-ring and floating ring centroid parallel to the shaft axis

Table 6 - 1 Correlation Coefficients

Dependent Variable	Correlation			
	Linear		Logarithmic	
	Experimental	Computer	Experimental	Computer
Leakage	Viscosity Sealed Pressure (Mean Film Thickness)*	Viscosity Sealed Pressure Mean Film Thickness	Viscosity (Sealed Pressure) (Mean Film Thickness) Shaft Speed Shaft Vibration Radial Vibration Angular Vibration	Viscosity Sealed Pressure Mean Film Thickness (Shaft Speed) (Shaft Vibration) (Radial Vibration) (Angular Vibration
Radial Vibration	Viscosity Shaft Speed Shaft Vibration	Viscosity (Shaft Speed) Shaft Vibration	Viscosity Shaft Speed Shaft Vibration Separation	Viscosity (Shaft Speed) Shaft Vibration (Separation)
Axial Vibration	(Viscosity) (Shaft Vibration) (Radial Vibration)	Viscosity Shaft Vibration Radial Vibration	(Viscosity) (Shaft Vibration) (Radial Vibration)	Viscosity Shaft Vibration Radial Vibration
Angular Vibration	Viscosity Shaft Vibration Radial Vibration (Axial Vibration)	Viscosity Shaft Vibration Radial Vibration Axial Vibration	Viscosity Shaft Speed (Mean Film Thickness) Shaft Vibration (Separation) Radial Vibration (Axial Vibration)	Viscosity Shaft Speed Mean Film Thickness (Shaft Vibration) Separation (Radial Vibration) Axial Vibration

* Variables in parentheses have correlation coefficients less than 0.5 but are included to give the same format to the regression

Table G - 2 Variables with correlation coefficients greater than 0.5

Independent Variables	Experimental Results		Computer Results	
	Coefficient	Significant?	Coefficient	Significant?
Viscosity	-0.7	no	-0.7	no
Sealed Pressure	2.0	no	1.0	yes
Mean Film Thickness	-2.0	no	3.5	no
Shaft Speed	0.1	no	0.5	yes
Shaft Vibration	0.45	no	-9.5	yes
Radial Vibration	0.3	no	9.5	yes
Angular Vibration	0.45	no	0.08	no
Type of regression	Logarithmic No Constant		Logarithmic No Constant	

(a) Leakage

Independent Variables	Experimental Results		Computer Results	
	Coefficient	Significant?	Coefficient	Significant?
Viscosity	-0.35	no	-0.002	no
Shaft Speed	0.25	no	0.007	no
Shaft Vibration	0.25	yes	1.0	yes
Separation *	0.3	yes	-0.0025	no
Type of regression	Logarithmic No Constant		Logarithmic No Constant	

(b) Floating Ring Vibration - Radial

Independent Variables	Experimental Results		Computer Results	
	Coefficient	Significant?	Coefficient	Significant?
Viscosity	0.02	no	$-0.15\ 10^{-3}$	yes
Shaft Vibration	-0.015	no	$-0.8\ 10^{-4}$	no
Radial Vibration	0.04	no	$-0.15\ 10^{-3}$	no
Type of regression	Linear No Constant		Linear No Constant	

(c) Floating Ring Vibration - Axial

Independent Variables	Experimental Results		Computer Results	
	Coefficient	Significant?	Coefficient	Significant?
Viscosity	1.0	no	1.05	no
Shaft Speed	0.1	no	5.0	yes
Mean Film Thickness	1.0	no	14.0	yes
Shaft Vibration	0.5	no	-4.5	no
Separation*	-0.04	no	1.2	yes
Radial Vibration	0.5	no	4.5	no
Axial Vibration	0.1	no	0.25	no
Constant	–	–	-46.0	yes
Type of regression	logarithmic no constant		logarithmic with constant	

(d) Floating Ring Vibration -Angular

* Separation of O-ring and floating ring centroid parallel to the shaft axis

Table C - 3 Best fit regressions for experimental and computer results with significance at a 5% level

regression results given in table G-3 have been obtained using these variables. Each pair of regressions (experimental and computer) have been calculated using the same variables (table G-2).

The significance of the individual regression coefficients is given in table G-3. Several are significant at the 5% level.

G.4 DISCUSSION AND CONCLUSIONS

G.4.1 General Significance

The low level of significance of many of the regression results reflects the unsuitablility of this type of experimental data (parameter perturbation) for a statistical analysis. Nevertheless, there is a certain measure of agreement between the experimental and computer results (Table G-2). Also, although there are large differences in the actual values, the best fit regressions (except angular vibration) take the same form. The differences between the measured and predicted angular vibration have already been discussed in Chapters 7 and 8, and this result is to be expected.

The principal use of the statistical results will be to support the comparison carried out qualitatively (Chapter 7) and hence add weight to the conclusions that have already been drawn. Whilst there are discrepancies in the comparison, there is sufficient agreement to justify retention and further development of the computer model.

G.4.2 Leakage

The computed and measured results show similar trends for correlations and regression. Thus the correlation coefficients between

measured leakage and both the mean film thickness and axial vibration have different signs for the logarithmic and linear analysis. However, the low value of the coefficients indicates the trend is not proven.

The biasing of the statistical analysis resulting from the format of the test programme is well shown by the correlation coefficients for the computer predictions. The formula used to calculate the leakage (p45) has a strong positive correlation with film thickness built in. However, the statistical analysis gives a strong negative correlation. This anomaly is a result of the small spread of mean film thickness values used and the large spread of calculated leakage rates, due to the many other parameters varied.

G.4.3 Floating Ring Vibration

The regressions give similar forms for the experimental and computer results for radial and axial vibration, but not for angular vibration.

The good agreement between the values of the correlations for viscosity demonstrates the importance of this fluid parameter. It is used in the calculation of the stiffness and damping coefficients for the fluid film, and clearly has an important effect on the resulting vibration prediction. There is however still a considerable difference in the magnitudes of the regression coefficients.

The disparity between both sets of correlation and regression results for axial vibration are to be expected from the known problems with the experimental measurements (p96).

There is good agreement between the experimental and computer correlation coefficients for angular vibration, despite the different forms of the

best fit regression lines. In particular there is good agreement between the experimental and computer values for the correlations with viscosity, shaft and radial vibration. The problems with the prediction of the angular vibration have been discussed in the main body of the thesis (section 7.1.2. and 8.3) and these probably account for the differences in the statistical analysis.

G.4.4. CONCLUSIONS

The analysis shows a measure of agreement between the experimental and computer results. The differences are, in general, those discussed in chapter 7. The regression analysis supports the contention that the computer analysis is basically sound, and reinforces the known limitations in the computer model. However, because of the small number of observations and the layout of the experimental program, this statistical analysis has its limitations, to overcome these a large number of additional tests would have to be carried out.

The low level of correlations involving the axial measurements support the conclusion that these experimental measurements were unreliable. Similarly the different forms of regression obtained for angular vibration emphasises the need to extend the computer model so that it more adequately describes the design of stator used.

It may be concluded that the regression analysis adds some weight to the qualitative conclusions drawn in the main body of the thesis despite problems due to the test program layout and the small number of observations available.

List of References

(62) ÅREDAL, T.G. 'Dynamic mechanical properties of oil extended reinforced SBR', Jnl. Applied Polymer Sci., 17, p.2823-2834 (1973)

(63) AUSTIN, R.M.
NAU, B.S. 'Unbalanced high pressure mechanical seals' BHRA, CR 1368, 26p., (Sept. 1976)

(64) BANERJEE, B.N.
BURTON, R.A. 'An instability for parallel sliding of solid surfaces separated by a viscous liquid film', Trans. ASME, Series F, 98, no.1, p.157 (1976)

(65) BANERJEE, B.N.
BURTON, R.A. 'Experimental studies on thermoelastic effects in hydrodynamically lubricated face seals', ASME Preprint 78-Lub-11, (June 1978)

(66) BARNARD, P.C.
WEIR, R.S.L. 'A theory for mechanical seal face thermodynamics', Proc. 8th Int. Conf. on Fluid Sealing, Durham, BHRA Fluid Engineering, 1, paper H1, p.H1-H8, (11-13 Sept. 1978)

(67) BILLINGTON, I.J. 'Experimental assessment of the validity of pressure measurements in the fluid film between seal faces', Proc. Second Int. Conf. on Fluid Sealing, Cranfield, BHRA, paper F3, p.F3-29 to F3-44, (Apr. 1964)

(68) BLOK, H. 'Thermal instability of flow in elasto-hydrodynamic films as a cause for cavitation collapse and scuffing', Proc. 1st Leeds-Lyon Symp. on Cavitation, Leeds, (1974)

(69) BRITISH STANDARDS INSTITUTE 'Mechanical vibration in rotating and reciprocating machinery', BS 4675, pt.1, (1976)

(70) BURTON, R.A. 'The role of insulating surface films on frictionally excited thermoelastic instability', Wear, 24, no.2, p.189, (1973)

(71) BURTON, R.A. KILAPARTI, S.R. NERLIKAR, V. 'A limiting stationary configuration with partially contacting surfaces', Wear, 24, no.2, p.199 (1973)

(72) BURTON, R.A. NERLIKAR, V. 'Large disturbance solutions for initially flat frictionally heated thermoelastically deformed surfaces', ASME, paper 74-Lub-7, (1974)

(73) CAKIROGLU, A. OZMAN, G. 'Numerical integration of forced vibration equations', Proc. ASCE, EM3, 94, p.711-730, (July 1968)

(74) CAMERON, A. 'Principles of lubrication', Longmans, (1966), p.49

(75) CAMERON, A. Op. Cit. page 230

(76) CAMERON, A. Op. Cit. page 414

(77) CANDIA, DE F.
VITTONIA, V.
'Elastic and visco-elastic behaviour of E-P co-polymer', Jnl. Applied Polymer Sci., 17, p.3243-3252 (1973)

(78) CATLIN, J.B.
'Improved maintenance of machinery through "baseline" vibration measurements', ASME paper 72-PEM-1, (Nov. 1973)

(79) CHENG, H.S.
SNAPP, R.B.
'A study of the radial film and pressure distribution of high pressure face seals', Proc. 3rd Int. Conf. on Fluid Sealing, BHRA, Cranfield, paper E3, (1967)

(80) CHENG, H.S.
SNAPP, R.B.
reply to discussion by J. Lohou (ref. 126) on 'A study of the radial film and pressure distribution of high pressure face seals', Op. Cit.

(81) CHIANG, T.
CHENG, H.S.
'Analysis of flexible seal ring vibrations', Trans. ASLE, no.11, p.204, (1968)

(82) CHIANG, T.
TESSARZIK, J.M.
BADGLEY, R.H.
'Development of procedures for calculating stiffness and damping properties of elastomers in engineering applications; Part 1 Verification of basic methods', NASA CR 120965, 110p., (31 Mar. 1972)

(83) COLE, J.A.
HUGHES, C.J.
'Visual study of film extent in dynamically loaded complete journal bearings' Conf. on Lubrication and Wear, I. Mech. E., London, (1957)

(84) CURRO, J.G.
SALAZAR, E.A.
'Mechanical behaviour of o-rings', Rubber Chemistry and Technology, 46, p.530, (1973)

(85) DENNY, D.F. 'Experiments on radial face seals', BHRA, RR 425, (1952)

(86) DENNY, D.F. 'Some measurements of fluid pressures between plane parallel thrust surfaces with special reference to the balancing of radial-face seals', BHRA, RR 613, (1959)

(87) DOMASHNEV, A.D. GAGARIN, E.M. 'Hermetization of liquids with end seals', Chemical and Petroleum Engineering, 13, no.5/6, p.401, (May/June 1977)

(88) DOWSON, D. 'Investigation of cavitation in lubricating films supporting small loads', Conf. on Lubrication and Wear, I. Mech. E., London, (1957)

(89) ECKER, R. 'Dynamic damping and Young's Modulus in the range of rubberlike elasticity', Rubber Chemistry and Technology, 27, p.859, (1954)

(90) ETSION, I. 'Nonaxisymmetric incompressible hydrostatic pressure effects in radial face seals', Trans. ASME, Jnl. of Lub. Tech., 100, p.379-385, (July 1978)

(91) ETSION, I. 'The accuracy of the narrow seal approximation in analysing radial face seals', ASLE/ASME Lubrication Conf., Minneapolis, paper 78-LC-2B-2, 8p., (24-26 Oct. 1978)

(92) ETSION, I. 'Hydrodynamic effects in a misaligned radial face seal', ASLE/ASME Lubrication Conf., Minneapolis, paper 78-Lub-12, 8p, (24-26 Oct. 1978)

(93) ETSION, I. 'Radial forces in a misaligned radial face seal', ASLE/ASME Lubrication Conf., Minneapolis, paper 78-Lub-13, 5p., (24-26 Oct. 1978)

(94) FERN, A.G. NAU, B.S. 'Seals', Engineering Design Guide, no.15, O.U.P., (1976)

(95) FERRY, J.D. 'Viscoelastic properties of polymers', 2nd ed. John Wiley & Sons, New York, (1970), p.61

(96) FERRY, J.D. Op. Cit., p.314

(97) FIELD, G.J. NAU, B.S. 'The lubrication of rectangular rubber seals under conditions of reciprocating motion, Part 3 An instrumental seal study', BHRA Fluid Engineering, RR 1200, p.62, (June 1973)

(98) FINDLAY, J.A. 'Measurements of leakage in mechanical face seals', 4th Int. Conf. on Fluid Sealing, paper 19, (1969)

(99) FLITNEY, R.K. NAU, B.S. 'Seals survey Part 1 - Mechanical seals', BHRA Fluid Engineering, (1977)

(100) FLOBERG, L. 'Experimental investigation of cavitation regions in journal bearings', Trans. Chalmers Univ. of Technology, no.233, Gothenborg, (1961)

(101) GLEW, C.A.W.
WATSON, D.
'Vibration analysis as a maintenance tool' Jnl. of Institute of Marine Engineers (Canada), (Atlantic Branch), 32, p.18-29, (1968)

(102) GRIGAN, O.A.
GRISKIN, E.N.
KARABAN, V.N.
SHTEINVOLF, V.N.
'Some problems of face seal dynamics' Dynamics and Strength of Machines, 15, Kharkov, U.S.S.R., (1972)

(103) GRISKIN, E.N.
'The effects of dynamics on fluid flow in a face seal', Proc. 7th ICFS, paper B2, p.B2-9 to B2-22, BHRA Fluid Engineering, (24-26 Sept. 1975)

(104) GUPTA, P.K.
TESSARZIK, J.M.
CZIGLENYI, L.
'Development of procedures for calculating stiffness and damping properties of elastomers in engineering applications, Part II Elastomer characteristics at constant temperature', NASA CR 134704, 125p., (26 Apr. 1974)

(105) HAARDT, R.
'Flow considerations around the cavitation area in radial face seals', Leeds-Lyon Symp. on Cavitation, Leeds, (Sept. 1974)

(106) HAARDT, R.
'Les joint d'etancheite a faces radial - les effets transitoires introduits en lubrification hydrodynamique par leur mesalignment', Ph.D. Thesis, Universitie Claude Bernard, Lyon, (1975)

(107) HAARDT, R.
Op. Cit. p.57

(108) HAUGH, E.F. 'Time temperature and linear visco-elasticity', Jnl. Applied Polymer Sci., 1, p.144-9 (1959)

(109) HERON, R.A. 'Report of the 7th meeting of Technical Panel II', BHRA Fluid Engineering, Cranfield, TP1415, p.28, (May 1977)

(110) HILL, H.H. 'Post-separation behaviour of mechanical systems subjected to harmonic excitations', Ph.D. Thesis, North Carolina State Univ., Raleigh, North Carolina, U.S.A., (1969)

(111) HIPKIN, E.L. HEIMANN, A. 'Safeguarding the health of machinery: plant condition monitoring in a chemical works', Noise Control Vibration Isolation, 9, no.4, p.129, (Apr. 1978)

(112) HUGHES, W.F. WINOWICH, N.S. DIRCHAK, M.J. KENNEDY, W.C. 'Phase change in liquid face seals', Trans. ASME Jnl. of Lub. Tech., Series F, 100, no.1, p.74, (Jan. 1978)

(113) HUHN, Dieter '75 years in shaft sealing', Gustav Huhn, (1976), p.8

(114) ISHIWATA, H. HIRABAYASHI, H. 'Friction and sealing characteristics of mechanical seals', Proc. Int. Conf. on Fluid Sealing, BHRA, Cranfield, paper D5, (1961)

(115) JAKOBSSON, B. FLOBERG, L. 'The finite journal bearing considering vaporization', Report no.3, Institute of Machine Elements, Chalmers Univ. of Technology, Gothenborg, (1957)

(116) KANETA, M.
FUKAHORI, M.
HIRANO, F.
'Dynamic characteristics of face seals', Proc. 8th Int. Conf. on Fluid Sealing, Durham, BHRA Fluid Engineering, vol. 1, paper A2, p.A2-15 to A2-28, (11-13 Sept. 1978)

(117) KHROMOV, M.K.
LAZAREVA, K.N.
'Relationship between the dynamic properties of rubbers filled with carbon black and their degree of cure', Int. Polymer Sci. and Technology, 3, no.7, p.T/59, (1976)

(118) LEBECK, A.O.
'Waviness distortion and wear in mechanical face seals', Albuquerque, New Mexico Univ., ME-64(74)NSF-271-1, PB-2343 937, (1974)

(119) LEBECK, A.O.
'Theory of thermoelastic instability of rotating rings in sliding contact with wear', Trans. ASME Jnl. Lub. Tech., Series F, 98, no.2, p.277, (1976)

(120) LEBECK, A.O.
'Causes and effects of waviness in mechanical face seals', Final Report. Tech. Report ME-68(76)NSF-271-1, Univ. of New Mexico, College of Engineering, Bureau of Engineering Research, Albuquerque, New Mexico, (1976)

(121) LEBECK, A.O.
'Elastohydrodynamic lubrication with wear and asperity contact in mechanical face seals', Bureau of Engineering Research, Univ. of New Mexico, Albuquerque, (1977) Rept. ME-76(77)ONR-414-1

(122) LEBECK, A.O. Private communication on thermoelastic instability, (1977)

(123) LEBECK, A.O. TEALE, J.L. PEARCE, R.E. 'Hydrodynamic lubrication and wear in wavy contacting face seals', Trans. ASME Jnl. Lub. Tech., Series F, 100, no.1, p.81-91 (1978)

(124) LINDSAY, R.B. 'Physical mechanics', 2nd ed, Van Nostrand Co. Ltd., New York, (1955), p.186

(125) LIPSHITZ, A. ETSION, I. 'A modified face seal for positive film stiffness', ASLE Trans., 21, no.4, p.356-360, (1978)

(126) LOHOU, J. Discussion on paper "A study of radial film and pressure distribution of high pressure face seals", by H.S. Cheng and R.B. Snapp, Proc. 3rd Int. Conf. on Fluid Sealing, BHRA, Cranfield, p.E3-25 to E3-26, (1967)

(127) LUDWIG, L.P. ALLEN, G.P. 'Face seal lubrication II - Theory of response to angular misalinement', NASA TN D-8101 (1976)

(128) MASON, P. 'Strain dependence of rubber visco-elasticity Part I Moderate strains', Trans. Faraday Soc., 55, p.1461, (1959)

(129) MASON, P. 'Strain dependence of rubber visco-elasticity Part II - Influence of carbon black', Jnl. Applied Polymer Sci., 4, p.212-218, (1960)

(130) MAYER, E. 'Leakage and wear in mechanical seals' Machine Design, 32, no.5, p.106, (3 Mar 1960)

(131) MAYER, E. 'Unbalanced mechanical seals for liquids', Proc. Int. Conf. on Fluid Sealing, paper E2, (1961)

(132) METCALFE, R. 'A fluid mechanical analysis of axisymmetric face seals on the basis of constant viscosity laminar flow', Report AECL-4073, Atomic Energy of Canada Ltd., (Dec. 1971)

(133) METCALFE, R. 'Axisymmetric distortion in face seals - mechanical and thermal', Proc. 6th Int. Conf. on Fluid Sealing, paper D1, p.D1-1 to D1-15, Cranfield, BHRA, (1973)

(134) METCALFE, R. ROTHIER, N.E. ROD, B.H. 'Diametral tilt and leakage of end face seals with convergent sealing gaps', Proc. 8th Int. Conf. on Fluid Sealing, Durham, BHRA Fluid Engineering, vol.1, paper A1, p.A1-1 to A1-14, (11-13 Sept. 1978)

(135) NAU, B.S. 'A reconsideration of pressure generation in radial-face seals', BHRA, RR 699, (1961)

(136) NAU, B.S. 'Cavitation in thin films', BHRA, TN 832, 21p., (1964)

(137) NAU, B.S. Hydrodynamic lubrication in face seals', BHRA, TN 843, 36p., (1965)

(138) NAU, B.S. 'Further experimental studies of face seal hydrodynamics', BHRA, RR 855, 15p., (Feb 1966)

(139) NAU, B.S. 'Observations of face seal flatness after use', BHRA, RR 877, (1967)

(140) NAU, B.S. 'Centripetal flow in face seals', Lubrication Engineering, 25, no.4, p.161-168, (Apr. 1968)

(141) NAU, B.S. 'Film cavitation observations in face seals', Proc. 4th Int. Conf. on Fluid Sealing, Philadelphia, BHRA, p.190-198, (1969)

(142) NAU, B.S.
ROWLES, R.T. 'Mechanical seal interface characteristics' BHRA Fluid Engineering, RR 1560, 28p., (July 1979)

(143) NETZEL, J.P. 'Application of mechanical seals to mixers and agitators', Lubrication Engineering, 34, no.2, p.67-78, (Feb. 1978)

(144) NIELSEN, L.E. 'Mechanical properties of polymers and composites', vol.2, Marcel Dekker Inc., New York, (1974), p.515

(145) OCVIRK, F.W.
DUBOIS, G.B. 'Analytical derivation and experimental evaluation of short bearing approximations of full journal bearings', NACA, Technical Report 1157, (1953)

(146) ORCUTT, F.K. 'An investigation of the operation and failure of mechanical face seals', Proc. 4th Int. Conf. on Fluid Sealing, Cranfield, BHRA Fluid Engineering, paper 22, p.205-217, (1969)

(147) PALLER, K. Confidential report on mechanical seal test work, Lucas Aerospace, (1978)

(148) PAPE, J.G. 'Fundamental aspects of radial-face seals' T.H. Delft, Netherlands, Thesis WTHD-17, (1969)

(149) PAYNE, A.R. 'Dynamic properties of carbon black loaded natural rubber vulcanizates part I and II', Jnl. Applied Polymer Sci., 6, p.57-63 and p.368-372, (1962)

(150) RATHBONE, T.C. 'Vibration tolerance', Power Plant Engineering, (Nov. 1939)

(151) ROWLES, R.T. 'Vibration monitoring on centrifugal pumps and compressors', BHRA, CR 1358 (June 1976)

(152) ROWLES, R.T. Discussion on "Diametral tilt and leakage of end face seals with convergent sealing gaps", Proc. 8th Int. Conf. on Fluid Sealing, Durham, BHRA Fluid Engineering, vol.2, (11-13 Sept. 1978)

(153) ROWLES, R.T. Discussion on "A theory for mechanical seal face thermodynamics", P.C. Barnard and R.S.L. Weir, Proc. 8th Int. Conf. on Fluid Sealing, Durham, BHRA Fluid Engineering, vol.2, (11-13 Sept. 1978)

(154) ROWLES, R.T. NAU, B.S. Discussion on "Hydrodynamic lubrication and wear in wavy contacting face seals", by A.O. Lebeck, J.L. Teale and R.E. Pierce, Trans. ASME Jnl. Lubrication Technology, 100, no.1, (1978)

(155) SAVAGE, M.D. 'Cavitation in lubrication', Jnl. Fluid Mechanics, 80, no.4, p.743-767 (23 May 1977)

(156) SCOTT, P.A. Private communication on seal performance

(157) SHTEINVOLF, V.N.
GRISKIN, E.N. 'On the problems of face seal dynamics in bottom hole motors', Machines and Oil Equipment, 10, VNIIOENG, Moscow, U.S.S.R. (1972)

(158) SIRCAR, A.K.
LAMOND, T.G. 'Strain dependent dynamic properties of carbon black reinforced vulcanizates - Part I Individual elastomers, Part II Elastomer blends', Rubber Chemistry and Technology, 48, p.79, (1975)

(159) SMALLEY, A.J.
DARLOW, M.S.
MEHTA, R.K. 'The dynamic characteristics of o-rings', ASME paper 77-DET-27, (1977)

(160) SNECK, H.J. 'The effects of geometry and inertia on face seal performance - laminar flow', Trans. ASME, Jnl. Lub. Tech., Series F, 90, no.2, p.338 (1968)

(161) SNOWDON, J.C. 'Representation of the mechanical damping possessed by rubberlike materials and structures', Jnl. of the Acoustical Soc. of America, 35, no.6, p.821-829, (June 1963)

(162) TAYLOR, R.
LEWIS, G.K.L.
'The dynamic performance of aerostatic porous thrust bearings with uniform films', 7th Int. Gas Bearing Symp., Cambridge, BHRA, paper A4, p.A4-49 to A4-66, (1976)

(163) TIMOSHENKO, S.
YOUNG, D.H.
WEAVER, J. Jnr.
'Vibration problems in engineering' 4th ed. J. Wiley & Sons, (1974), p.279

(164) TIMOSHENKO, S.
YOUNG, D.H.
WEAVER, J. Jnr.
Op. Cit. p.476

(165) TURNBULL, D.E.
NAU, B.S.
'Some effects of the elastic deformation of the sealing rings of a mechanical or radial-face seal on its sealing behaviour', BHRA, RR 644, 5p., (Feb. 1966)

(166) UNITED KINGDOM ATOMIC ENERGY AUTHORITY
'Loads to deform elastomer seals (toroidal sealing rings) in grooves and between plain flanges', AWRE Report no. O-82/66, 27p., (Oct. 1966)

(167) ULMER, J.D.
HESS, W.M.
CHIRICO, V.E.
'The effects of carbon black on rubber hysteresis', Rubber Chemistry and Technology, 47, p.729, (1974)

(168) VERNON, J.B.
'Linear vibration theory', J. Wiley & Sons Inc., New York, (1967), p.23

(169) WATSON, R.D.
'Effect of seal ring deflection on the characteristics of face-type mechanical seals in high pressure water', Atomic Energy of Canada Ltd., CRE-1176, (1963)

(170) WATSON, R.D. 'Performance testing of conical face high pressure rotary shaft seals', Atomic Energy of Canada Ltd., Report AECL-2551, (Nov. 1965)

(171) WATSON, R.D.
ROCHE, K.W. 'A comparison of the operating characteristics of flat-face and hydrodynamically lubricated rotating mechanical shaft seals in high pressure water', Atomic Energy of Canada Ltd., Report AECL-1588, (Aug. 1962)

(172) WHITTMAN, K.J. 'Pressure generation in radial face seals', BHRA, TN 578, (1958)

(173) WILLIAMS, M.L.
FERRY, J.D. 'Dynamic mechanical properties of polyvinyl acetate', Jnl. of Colloidal Sci., 9, p.48, (1954)

(174) WORSTER, H.C. Unpublished discussion "Radial forces in rotodynamic fluid machinery", I. Mech. E. Fluid Power Group, London, (19 Sept. 1977)

(175) YIN, T.P.
PARICHER, R. 'Dynamic properties of neoprene type W', Jnl. Appl. Polymer Sci., 7, p.667, (1963)

(176) YIN, T.P.
PARICHER, R. 'Dynamic mechanical properties of several elastomers and their potentialities in control applications', Jnl. Appl. Polymer Sci., 8, p.2427-2443, (1964)

(177) YANG, C.-I.
MORAN, T.J. 'Finite element solution of added mass and damping of oscillation rods in a viscous fluid', Trans. ASME Jnl. Appl. Mech., 46, p.519-523, (Sept. 1979)

(178) JENNINGS, A. 'Matrix computations for engineers and scientists', John Wiley & Sons, London, p.183, (1977)

(179) NUMERICAL ALGORITHMS GROUP. 'Nag fortran library manual', Oxford,(1978).

(180) HUSSEY, M.K. Private communication.

Bibliography

(1) ANNO, J. WALOWIT, J.A. ALLEN, C.M. 'Microasperity lubrication', Proc. 3rd Int. Conf. on Fluid Sealing, Cranfield, BHRA, paper E2, (1967)

(2) ANNO, J. WALOWIT, J.A. ALLEN, C.M. 'Load support and leakage from microasperity lubricated face seals', Proc. 4th Int. Conf. on Fluid Sealing, Philadelphia, BHRA, paper 21, (1969)

(3) AUSTIN, R.E. (et al.) 'Seal users handbook', 2nd ed., BHRA, Cranfield (1979)

(4) BARKER, J.R. 'Thermal effects in friction and wear', Dissertation St. John's College, Cambridge, (1968)

(5) BATCH, B.A. GOLDRING, B.T. WINKEY, P.E. 'An instrument for measuring the mean surface profile and seal faces', Jnl. Physics, Sec.E1, Series 2, 2, p.344, (1968)

(6) BATCH, B.A. INY, E.H. 'Pressure generation in radial face seals', Proc. 2nd Int. Conf. on Fluid Sealing, Cranfield, BHRA, paper F4, (1964)

(7) BERND 'Study of dynamic and static seals for liquid rocket engines', Final report for period Feb. 26 1963 to Nov. 30 1963 vol.12 "Studies of special topics in sealing" Appendix F, 2, "Review of dynamic face seal theory", Advanced Technology Labs. Gen. Elec. Co. (Aug 21 1964), p.235-314. Schenactady, N.Y.

(8) BERT, C.W. 'Material damping: an introductory review of mathematical models measures and experimental techniques', Jnl. of Sound and Vibration, 29, no.3, p.129-153, (1973)

(9) BLOW, C.M. 'Elastomers for seals', in 'Review and bibliography on aspects of fluid sealing', BHRA, Cranfield, England (1972)

(10) BOON, E.F. 'Some notes on seals for rotating and reciprocating shafts', De Ingenieur, 64, no.12, p.C33-C40, (1952)

(11) BRITISH RUBBER MANUFACTURERS ASSOCIATION 'Guide to elastomeric seals'

(12) BRUICH, A. 'Mechanical seals: theory and criteria for their design', Product Engineering, 21, no.4 p.85-89, (Apr. 1950)

(13) BUCKTER, H.H. 'Industrial sealing technology', John Wiley & Sons, New York, (1978)

(14) BURTON, R.A. NERLIKAR, V. 'Effect of initial surface curvature on frictionally excited thermoelastic phenomena', Wear, 27, no.2, p.195, (1974)

(15) BURTON, R.A. NERLIKAR, V. KILAPARTI, S.R. 'Thermoelastic instability in a seal-like configuration', Wear, 24, no.2, p.169, (1973)

(16) CARDEN 'The mechanical face seal, a survey of sealing theory', Univ. of Tennessee, Engng. Experimental Station, Rept. ME-5-62-T13 (1962)

(17) DABNEY, M.J.
HOLT, W.W.
'Mechanical seals effective on main line pumps', Oil and Gas Jnl., 49, no.35, (June 1951)

(18) DAVIES, M.G.
'The generation of lift by surface roughness in a radial face seal', Proc. Int. Conf. on Fluid Sealing, BHRA, Cranfield, paper E4, (1961)

(19) DENNY, D.F.
'Some measurements of fluid pressures between plane parallel thrust surfaces with special reference to radial-face seals', Wear, 4, no.1, p.64, (Jan 1961)

(20) DOW, T.A.
BURTON, R.A.
'Investigation of thermoelastic instabilities of sliding contact in the absence of wear', Wear, 19, p.315, (1972)

(21) FINDLAY, J.A.
'Inward pumping in mechanical face seals', ASME paper 67-WA/Lub-20, (1967)

(22) FISHER, M.J.
'An analysis of the deformation of the balanced ring in high pressure radial face seals', Proc. Int. Conf. on Fluid Sealing, BHRA, Cranfield, paper D4, (1961)

(23) FITZGERALD, E.R.
FERRY, J.D.
'Method for determining the dynamic mechanical behaviour of gels and solids at audio-frequencies: comparison of mechanical and electrical properties', Jnl. of Colloidal Sci., 8, no.1, p.1-34, (1953)

(24) FLITNEY, R.K. 'Rotary face seal design-application' Second review and bibliography on aspects of fluid sealing, BHRA, Cranfield, (1975)

(25) FOGG, A. 'Fluid film lubrication of parallel thrust surfaces', Proc. I. Mech. E., 155, p.49, (1946)

(26) HAARDT, R.
GODET, M. 'Axial vibration of a misaligned radial face seal under a constant closure force', ASLE preprint 74AM-7D-1 (May 1974)

(27) HAMILTON, D.B.
WALOWIT, J.A.
ALLEN, C.M. 'A theory of lubrication by microirregularities', Trans. ASME, Series D, 88, no.7, p.177, (1966)

(29) INY, E.H. 'The design of hydrodynamically lubricated seals with predictable operating characteristics', 5th Int. Conf. on Fluid Sealing, Warwick, BHRA, Cranfield, paper H1, (1971)

(30) INY, E.H. 'A theory of sealing with radial face seals', Wear, 18, no.1, p.51, (1971)

(31) KING, A.L.
NAU, B.S.
STEPHENS, H.S.
(eds.) 'Proceedings of the 3rd Int. Conf. on Fluid Sealing', BHRA, Cranfield, (1967)

(32) KING, A.L.
NAU, B.S.
STEPHENS, H.S.
(eds.) 'Proceedings of the 4th Int. Conf. on Fluid Sealing', BHRA, Cranfield, (1969)

(33) KING, A.L.
NAU, B.S.
STEPHENS, H.S.
THORNTON, M.A.
(eds) 'Proceedings of the 5th Int. Conf. on Fluid Sealing', BHRA, Cranfield, (1971)

(34) KOJABASHIAM, C. RICHARDSON, H.H. 'A micropad model for the hydrodynamic performance of carbon face seals', Proc. 3rd Int. Conf. on Fluid Sealing, BHRA, Cranfield paper E4, p.E4-41 to E4-72, (1967)

(35) KUZMA, D.C. 'Theory of the mechanism of sealing with application to face seals', Proc. 4th Int. Conf. on Fluid Sealing, BHRA, Cranfield, paper 18, p.165-173, (1969)

(36) LEBECK, A.O. 'A study of mixed lubrication in contacting mechanical face seals', 4th Leeds-Lyon Symp. on Tribology, Lyon, France, (1977)

(37) LOHOU, J. 'Hydrodynamique des joints d'etancheite du type radial', These de Docteur Ingenieur, Faculte des Sciences de l'Universite de Lyon, (June 1970)

(38) LOHOU, J. GODET, M. 'Angular misalignments and squeeze film effects in radial face seals', 6th Int. Conf. on Fluid Sealing, BHRA, Cranfield, paper D2, p.D2-15 to D2-28, (1973)

(39) LUDWIG, L.P. 'Face seal lubrication - proposed and published models', NASA TN D-8101, (1976)

(40) MAYER, E. 'Mechanical seals', 3rd ed. translation edited by B.S. Nau, Butterworths, (1977)

(41) NAU, B.S. 'An investigation into the nature of the interface film, the pressure generation, mechanism and centripetal pumping in mechanical seals', BHRA, RR 754, (1963)

(42) NAU, B.S.
STEPHENS, H.S.
TURNBULL, D.E.
'Proceedings of the 2nd Int. Conf. on Fluid Sealing', BHRA, Cranfield, (1964)

(43) NAU, B.S.
'Mechanical seals guide', BHRA, TN 904, 21p., (1967)

(44) NAU, B.S.
'A review of recent rotary face seal literature', Review and bibliography on aspects of fluid sealing, BHRA, Cranfield, (1972)

(45) NAU, B.S.
'Mechanical seal film cavitation - Cavitation and related phenomena in lubrication' ed. by D. Downs, M. Godet and C.M. Taylor, I. Mech. E., (1975)

(46) RAJAKOVICS, G.E.
'A contribution to the knowledge of the mode of operation of contact seals', Diss - Mont. Hochschule Leoben, (May 1970)

(47) RAJAKOVICS, G.E.
'On the sealing mechanism of dynamic seals' Proc. 5th Int. Conf. on Fluid Sealing, Warwick, BHRA, Cranfield, paper A6, p.A6-49 to A6-60, (1971)

(48) REINER, M.
'The centripetal pump effect in a vacuum pump', Proc. Roy. Soc. A, 247, no.1249, p.152, (1958)

(49) REINER, M.
'Cross stresses in the laminar flow of liquids', Physics of fluids, 3, no.3, p.427, (1960)

(50) SNECK, H.J. 'The misaligned eccentric face seal', Proc. 4th Int. Conf. on Fluid Sealing, BHRA, Cranfield, paper 15A, p.136-144, (1969)

(51) SNECK, H.J. 'The eccentric face seal with a tangentially varying film thickness', Op. Cit., paper 15B, p.145-152

(52) STEPHENS, H.S.
COLES, N.G.
GUY, N.G. 'Proceedings of the 7th Int. Conf. on Fluid Sealing', BHRA, Cranfield, (1975)

(53) STEPHENS, H.S.
GUY, N.G. 'Proceedings of the 8th Int. Conf. on Fluid Sealing', Durham, BHRA, Cranfield, (1978)

(54) STEPHENS, H.S.
RICHARDSON, C.A. 'Proceedings of the 6th Int. Conf. on Fluid Sealing', BHRA, Cranfield, (1973)

(55) STRANGHAM-BATCH, B.A. 'Face seal lubrication in mechanical seals', Proc. of the Tribology Convention, I. Mech. E., (1971)

(56) STROM, T.N.
LUDWIG, L.P.
HUDELSO, J.C. 'Vibration of shaft face seals and stabilising effect of viscous and friction damping', NASA TN-D-5161

(57) SUMMERS-SMITH, D. 'Laboratory investigation of the performance of a radial-face seal', Proc. Int. Conf. on Fluid Sealing, paper D1, BHRA, Cranfield, (1961)

(58) TANNER, R.I. 'The Reiner centripetal effect in face seals', Op. Cit., paper E1

(59) TAYLOR, G.I.
SAFFMAN, P.G.
'Effects of compressibility at low Reynolds' Number', Jnl. Aero. Sci., 24, no.8, p.553, (1957)

(60)
'Proceedings of the Int. Conf. on Fluid Sealing', BHRA, Cranfield, (1961)

(61) ZUK, J.
'Fundamentals of fluid sealing', NASA TN D-8151, 167p., (Mar. 1976)